

Biofabrication using recombinant spider silk proteins

Dissertation

zur Erlangung des akademischen Grades

einer Doktorin der Naturwissenschaften (Dr. rer. nat.)

im Promotionsprogramm „Polymer Science“ der

Bayreuther Graduiertenschule für Mathematik und Naturwissenschaften (BayNAT)

Universität Bayreuth

vorgelegt von

Elise DeSimone

M. Sc. Biomedical Engineering

aus Portland, Maine, USA

Bayreuth, 2018

This doctoral thesis was prepared at the department of Biomaterials at the University of Bayreuth from September, 2014 until August, 2018 and was supervised by Prof. Dr. Thomas Scheibel.

This is a full reprint of the dissertation submitted to obtain the academic degree of Doctor of Natural Sciences (Dr. rer. nat.) and approved by the Bayreuth Graduate School of Mathematical and Natural Sciences (BayNAT) of the University of Bayreuth.

Date of submission: 2018-08-29

Date of defense: 2019-03-29

Acting director: Prof. Dr. Dirk Schüler

Doctoral committee:

Prof. Dr. Thomas Scheibel (reviewer)

Prof. Dr. Hans-Werner Schmidt (reviewer)

Prof. Dr. Leonid Ionov (chairman)

Prof. Dr. Andreas Fery

*To my beloved Parents,
Who made me who I am*

*To my dear Grandfather,
Who made my education possible*

*To my wise Mentors,
Who guided the way*

*To my Friends and Family,
Who brightened my everyday*

*To my beloved Husband,
Who made this journey worthwhile*

Table of Contents

Summary	i
Zusammenfassung	iii
1. Introduction	1
1.1 Material design concepts for tissue engineering and biofabrication	2
1.1.1 Our muse for biomaterial design: The extracellular matrix (ECM).....	4
1.1.2 Biomaterial selection and design	7
1.2 Recombinant spider silk protein	12
1.2.1 Biotechnological production.....	12
1.2.2 Recombinant spider silk protein eADF4(C16)-based biomaterials.....	14
1.3 Scaffold design	16
1.3.1 Scaffold design in tissue engineering.....	16
1.3.2 Electrospinning	17
1.3.3 Hydrogels	18
1.4 Biofabrication	19
1.4.1 Biomaterials for biofabrication	21
1.4.2 3D bioprinting	22
1.4.3 Evaluating 3D bioprinted scaffolds.....	24
1.4.4 State-of-the-art in 3D bioprinting.....	26
2. Aims.....	28
3. Synopsis	29
3.1 Electrospun eADF4(C16) nonwovens from aqueous solution and aqueous post-treatment process	31
3.2 Recombinant spider silk bioinks	33
3.3 Conclusion and outlook	39
4. References.....	40
5. Publications list.....	47
6. Individual contribution to joined publications and manuscripts	48
Publications.....	51
Part 1. Recombinant spider silk-based bioinks	51
Part 2. Cations influence the cross-linking of hydrogels made of recombinant, polyanionic spider silk proteins.....	67
Part 3. Engineered 2D and 3D spider silk materials with intrinsic bacteriostatic and fungistatic properties	73
Part 4. Characterization of Hydrogels Made of a Novel Spider Silk Protein eMaSp1s and Evaluation for 3D Printing	103
Part 5. Biomedical applications of recombinant silk	119
Part 6. Biofabrication of 3D Constructs: Fabrication Technologies and Spider Silk Proteins as Bioinks.....	149
Acknowledgements	151
(Eidesstattliche) Versicherungen und Erklärungen	167

Summary

For medicine to advance such that it would be possible to regenerate tissue after illness or injury, it is necessary both to achieve a better understanding of human physiology and to apply engineering techniques. The field dedicated to these goals and this type of approach is tissue engineering. The most common approach to forming tissues *in vitro* is by creating scaffolds with specific characteristics and then seeding the surface with selected cell types. As the field of tissue engineering has progressed, and there is more evidence indicating that this approach alone is not satisfactory, more elegant tactics have arisen. Biofabrication is the simultaneous processing of biomaterials, cells and other biologically active agents to form constructs that have biological functions. However, one of the major bottlenecks for biofabrication is appropriate biomaterials, which has made biomaterial development for biofabrication of significant relevance.

Spider silk is a valuable natural resource for high-performance textiles due to its mechanical toughness and stability. More recently, it has not only been valued for its use as a textile, but for its use as a biomaterial. However, natural spider silk suffers from batch-to-batch variability, and farming of spiders is difficult as they are cannibalistic. A solution to this problem is to produce recombinant spider silk protein. The key characteristics of natural spider silk are captured in the sixteen repeats of a spider silk protein amino acid sequence, the C module, that constitute the engineered spider silk protein *Araneus diadematus* fibroin 4 (eADF4(C16)), which exhibits similar toughness to natural spider silk, hypoallergenicity and biocompatibility, and can be produced consistently in large quantities. Moreover, it can be modified with the cell binding peptide RGD to promote cell attachment onto various scaffolds produced of eADF4(C16)-RGD. For this reason, this protein was investigated for use as a cell-loaded hydrogel for 3D bioprinting, that is, as a bioink. This approach proved to be promising and inspired subsequent work with these proteins as a biomaterial for biofabrication.

The purpose of this work was to develop different biofabrication techniques using the recombinant spider silk protein eADF4(C16), in particular to develop bioinks for 3D printing and for biologically-friendly dopes for electrospinning. The motivation for combining these two approaches is that they complement each other. 3D bioprinting allows for precise deposition of cell-loaded hydrogels into complex macrostructures whereas electrospinning produces fibers in the nano- to micron- range. These two approaches together, therefore, can cover a broad spectrum of scaffold features.

Although eADF4(C16) has already been used to produce electrospun mats for fine particle filters and *in vitro* cell culture, the processing conditions have not been biocompatible. Therefore, an aqueous electrospinning dope was developed using highly concentrated eADF4(C16) solution and 400 kDa poly(ethylene oxide) (PEO) as an additive. Furthermore, the post-treatment method was modified from ethanol vapor treatment at 60 °C to water vapor treatment at 37 °C. Using green fluorescent protein (GFP) as a model for a biological active agent, it was demonstrated that GFP remained fluorescent using the all-aqueous processing route. However, fluorescence activity was diminished when added to the traditional spinning dope containing hexafluoroisopropanol (HFIP), or when post-treated by ethanol, thereby demonstrating the significance of the all-aqueous electrospinning route.

eADF4(C16) and eADF4(C16)-RGD bioinks were also developed and characterized in this work. By simple observation, it was clear that both the addition of cell culture media and the RGD peptide sequence have an effect on the final properties of the bioinks. It was found that RGD increases the stiffness and the gelation rate of the bioinks, when compared to the same concentration of eADF4(C16), however the addition of cell culture media had a more pronounced effect in terms of increasing the gelation rate and stiffness. After the bioinks were characterized based on their formulation, they were optimized for 3D cell culture. By changing the seeding regime, it was possible to have 100 % cell viability after encapsulation, and the cells were also able to proliferate in eADF4(C16)-RGD bioinks. By simply blending with a low amount of unmodified gelatin the resolution of the printed bioinks were improved, although the cells had reduced viability and proliferation post-printing.

Overall, through this work it was shown that the recombinant spider silk protein eADF4(C16) is a versatile biomaterial for biofabrication. In particular, it was successfully used for electrospinning biologically active nonwovens and as a platform for 3D cell culture. Possible future work could include using other variants of the protein to tailor the release of biologicals from electrospun nonwovens, or to promote certain cell behaviors, or to adapt bioink properties. Furthermore, these two types of processing could be used together to create composite scaffolds with variable morphologies.

Zusammenfassung

Ein besseres Verständnis der menschlichen Physiologie und die Anwendung von Ingenieurstechniken sind notwendig, um die Medizin soweit voranzutreiben, dass die Heilung von durch Krankheit oder Verletzung von geschädigtem Gewebe möglich ist. Dieses Aufgabengebiet und diese Methoden werden dem Fachbereich oder -gebiet Tissue-Engineering (TE), (z.Dt. die künstliche Herstellung biologischen Gewebes) zugewiesen. Die häufigste Herangehensweise, um Gewebe *in vitro* herzustellen, ist es dies nach spezifischen Vorgaben herzustellen und anschließender mit den gewünschten Zelltypen zu besiedeln. Die Fortschritte auf dem Gebiet des TE zeigen weisen zunehmend darauf hin, dass diese Arbeitsweise alleine nicht ausreicht, um biologisch funktionelle Materialien herzustellen. Demzufolge sind vielseitige Ansätze entstanden, um das Ziel vollständiger Geweberegenerierung zu erreichen. Ein vielversprechendes neues Verfahren ist die Biofabrikation, welche die gleichzeitige Verarbeitung von Biomaterialien, Zellen und anderen biologisch aktiven Substanzen für die Erzeugung von künstlichem Gewebe nutzt. Jedoch gibt es in der Biofabrikation bis dato wenige geeignete Biomaterialien, folglich wird der Entwicklung von Biomaterialien für die Biofabrikation eine hohe Relevanz und Bedeutung zugesprochen.

Seit Hunderten von Jahren wird natürliche Spinnenseide auf Grund der hervorragenden mechanischen Eigenschaften (Zugfestigkeit und Dehnbarkeit) als außerordentliches Material (z.B. Textilien) verwendet. . Seit Kurzem findet Spinnenseide nicht nur in der Textilbranche sondern auch als Biomaterial seine Anwendung. Natürliche Spinnenseide leidet jedoch unter Qualitätsschwankungen und die Gewinnung von natürlicher Spinnenseide gestaltet sich schwierig wegen des Kannibalismus der Tiere. Ein Lösungsansatz hierfür ist die rekombinante Produktion von Spinnenseidenproteinen. Die wichtigsten Eigenschaften der natürlichen Spinnenseide wurden in einer künstlichen Aminosäuresequenz (dem C Modul) sechzehn Mal wiederholt und das künstliche Spinnenseidenprotein „engineered“ *Araneus diadematus* Fibroin 4 (eADF4(C16)) daraus gebildet. Dieses Protein besitzt ähnliche Eigenschaften wie das natürliche Spinnenseidenprotein hinsichtlich der Zähigkeit, Biokompatibilität und Immunantwort und kann zusätzlich in konstanter Qualität in großen Mengen produziert werden. Des Weiteren kann eADF4(C16) mit der zellbindenden Aminosäuresequenz “RGD“ modifiziert werden, um die Zellanlagerung an unterschiedlichen Morphologien zu verbessern. Deshalb war es möglich lebende Zellen in Hydrogele aus diesem Protein einzubetten. Dieses Material wird “Biotinte“ genannt und für den 3-D Druck untersucht. Diese Herangehensweise erwies sich als vielversprechend und dient als Richtlinie für das weitere Arbeiten mit diesen Proteinen als Biomaterial.

Ziel dieser Arbeit war es unterschiedliche Techniken, mit besonderem Augenmerk auf Biotinten für den 3D-Druck und Spinnlösungen für biologisch kompatibles Elektrospinnen, mit dem künstlichen Spinnenseidenprotein eADF4(C16) in der Biofabrikation zu entwickeln. Die treibende Kraft hinter der Kombination dieser beiden Techniken/Verfahren ist, dass sie sich gegenseitig ergänzen. Während das 3-D-Drucken das präzise Auftragen von Biotinte zu komplexe Makrostrukturen erlaubt, bildet das Elektrospinnen Fasern im Nano- bis Mikrometerbereich. Diese zwei Methoden können demzufolge eine weite Bandbreite von Eigenschaften für Zellträger abdecken.

Obwohl elektrogewebene Vliesstoffe aus eADF4(C16) schon für Kleinpartikelfilter und *in vitro* Zellkultur verwendet wurden, waren die Verarbeitungsbedingungen bis jetzt nicht biokompatibel. In dieser Arbeit wurde eine hochkonzentrierte wässrige Spinnlösung mit 400 kDa Poly(ethylenoxid) als Zusatz entwickelt und dementsprechend die Nachbehandlungsmethode von Ethanol dampf bei 60°C durch Wasserdampf bei 37°C ersetzt. Da unter anderem mit biologisch aktiven Substanz wie zum Beispiel dem grün fluoreszierenden Protein (GFP) gearbeitet wurde, basiert der Prozess komplett auf wässriger Ebene, um die Aktivität des Fluoreszenzfarbstoffes zu erhalten. Ferner wurde gezeigt, dass die herkömmliche Spinnlösung mit Hexafluorisopropanol (HFIP) und die Nachbehandlung mit Ethanol dampf die Fluoreszenzintensität – verringert.

Zusätzlich wurden in dieser Arbeit eADF4(C16) und eADF4(C16)-RGD Biotinten weiterentwickelt und charakterisiert. Einfache Beobachtungen haben ergeben, dass das Zellkulturmedium sowie das RGD-Peptid die Eigenschaften der Biotinten beeinflussen. Es wurde festgestellt, dass das RGD-Peptid in eADF4(C16)-RGD die Steifigkeit und die Gelierungsrate im Vergleich zu eADF4(C16) in gleicher Konzentration erhöht, jedoch die Zugabe von Zellkulturmedium noch deutlichere Auswirkungen auf diese Eigenschaften zeigte. Nachdem die Zusammensetzung der Biotinten charakterisiert wurde, wurden sie für 3D-Zellkultur optimiert. Eine Änderung des Protokolls für die Zellbesiedelung ermöglichte eine 100%-ige Zellviabilität, sowie Zellproliferation nach dem Einbetten in eADF4(C16)-RGD Biotinte. Durch einfache Zugabe einer geringen Menge Gelatine konnte die Auflösung der gedruckten Biotinten verbessert werden, jedoch wiesen die Zellen reduzierte Viabilität und Proliferation nach dem 3D-Druck auf.

Insgesamt konnte durch diese Arbeit gezeigt werden, dass das rekombinante Spinnseidenprotein eADF4(C16) für die Biofabrikation ein vielseitig einsetzbares Material ist. Insbesondere konnte es erfolgreich zum Elektrosponnen von biologisch aktiven Vliesstoffen und als Trägermaterial für 3D-Zellkultur verwendet werden. Künftige Arbeiten können unter anderem unterschiedlich modifizierte Varianten des Proteins untersuchen, um die Freisetzung von biologischen Wirkstoffen aus elektrogewebenen Vliesstoffen anzupassen und ausgewähltes Zellverhalten zu fördern oder Eigenschaften von Biotinten zu regulieren. Darüber hinaus könnten diese zwei Verarbeitungsmethoden verwendet werden, um zusammengesetzte Zellträgermaterialien unterschiedlicher Morphologien zu kreieren.

1. Introduction

Ageing, illness and injury are inevitable human sorrows, and it is therefore not surprising that the search for the fountain of youth continues, albeit not in the literal sense. Rather than find the fountain of youth, modern scientists and engineers are striving to create it. In spite of the many years spent pursuing this endeavor, we are far away from vaccinating all diseases, curing cancer or achieving complete wound regeneration, however, astounding progress has been made. With modern medicine, it is possible to alleviate pain, symptoms, and to improve prognosis for many medical complications, for example, tissue injury, tissue debilitation, organ failure, cardiovascular disease, cancer, nervous system injuries, and congenital disorders. However, most available products are non-curative; primarily drugs or implants made from artificial materials. This leaves patients dependent on treatment for long periods, if not their entire life. The field of regenerative and personalized medicine has therefore emerged in attempt treat the root cause of various afflictions. Regenerative medicine, or personalized medicine, is based on the principle that, by using a scientific understanding of the pathological state as well as the capacity of the human body to generate or self-heal (e.g. heal wounds, fight diseases, form a fetus), we can engineer products that allow the body to fully recover from any ailment. As stated by Mason and Dunnill, “regenerative medicine replaces or regenerates human cells, tissue or organs, to restore or establish normal function” [1], which can be accomplished, for example, by using drugs, cell therapy, or tissue engineering. Tissue engineering is the combination of cells, biomaterials, and bioactive factors or stimuli to create tissue-like constructs with a desired functionality [2, 3]. Scaffolds are designed using either bottom-up or top-down approaches, as illustrated in [Figure 1](#).

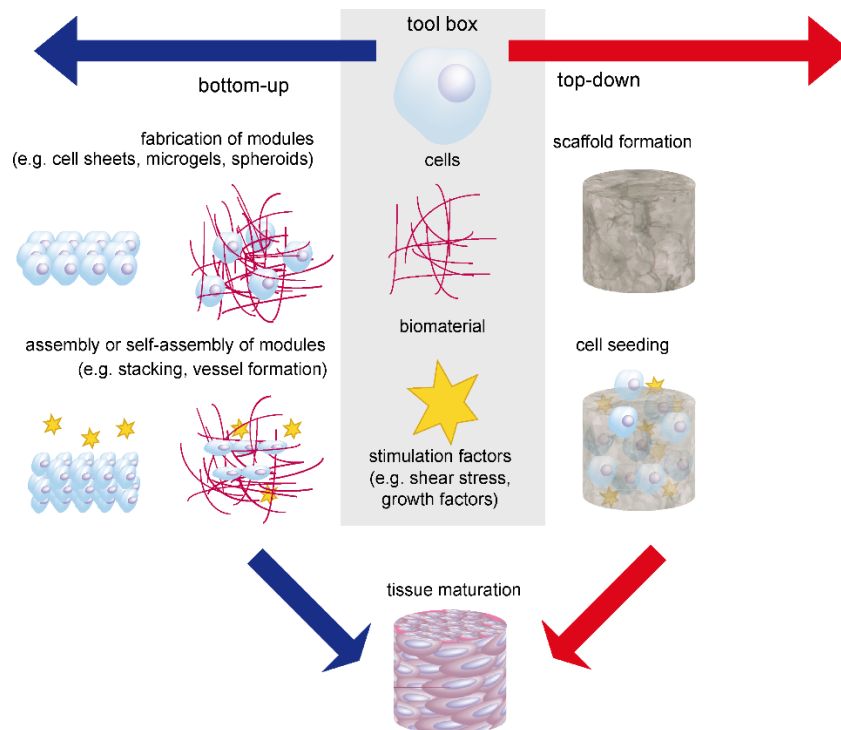


Figure 1: Tissue engineering using cells, biomaterials and stimulation factors as ‘building blocks’. Traditional tissue engineering is differentiated by top down or bottom up approach

The dogma of top-down approach is 'shape equals function', that is, the hypothesis is that controlling cell location and scaffold morphology will result in functional tissue formation. An example of this type of approach would be to form a biomaterial into the shape of blood vessel, and then seed relevant cell types in each compartment of the scaffold (intravascular, extravascular) [4]. The alternative hypothesis is that the best way to regenerate tissue is by taking a developmental biology approach. Proponents of bottom-up approach use either a developmental biology approach, or combine these two concepts. The human embryo begins as a large mass of cells that matures into the developed fetus by properly responding to complex factors; therefore, the assumption is that engineered cells cultured in the proper environment should be able to engage in this sort of behavior for wound healing. An example of this approach would be cell growth directed by mechanical stimulus from external forces or by internal stresses that occur between cells themselves [5]. Alternatively, when both models are used, first cell-laden modules are developed, and then they are assembled or self-assembled into larger structures. An example of this is making microgels loaded with cells, maturing them, and then using microfluidics to fuse them together [6]. Biofabrication, a specific subset of bottom-up approaches in tissue engineering, is the simultaneous processing of cells and biomaterials into a bioactive constructs, [Section 1.4](#). This type of fabrication imposes special requirements on biomaterials, in addition to those that are normally required. In the case of regenerative medicine, typically the objective is to make the biomaterial such that it imitates the extracellular matrix (ECM) of the tissue or tissue niche of interest in terms of the biomaterial's biochemical composition and mechanical properties. ECM is the biopolymer network (matrix) surrounding cells (extracellular) which provides mechanical support, biological cues and many other functions to the tissue [7].

1.1 Material design concepts for tissue engineering and biofabrication

Materials are classified as ceramics, metals, polymers, or composites [8]. Composite materials being combinations of the three other material classes that result in a material with unique properties. Examples of these classic engineering materials are found everywhere, [Figure 2](#). Other, more specialized material classes include semi-conductors (electrical conductivity properties between metal (conductor) and glass (insulator)) [9], smart materials (perform certain functions upon a particular stimulus) [10], and nanomaterials (nanoscale structures or fabrication) [11]. Biomaterials represent another specialized class of materials that interact with the human body to augment a tissue function or promote tissue formation, and there are examples of biomaterials in every materials classification, [Figure 2](#).

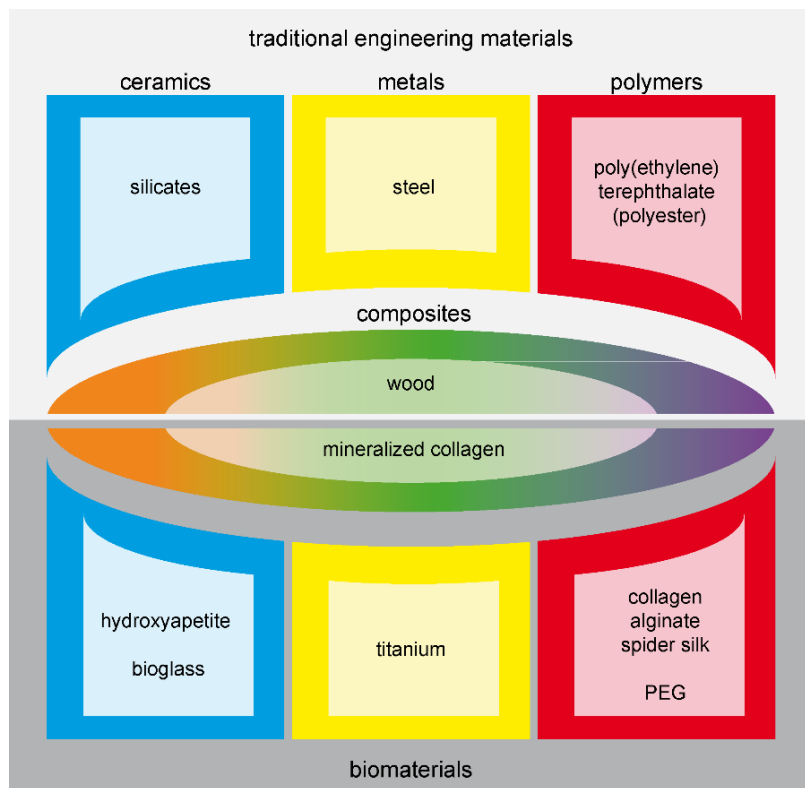


Figure 2: Well-known examples of each material class: ceramics (left, blue boxes), metals (middle, yellow boxes), polymers (right, red boxes) and composites (middle, gradient color). Examples are further separated for traditional engineering materials (top, light gray box) and biomaterials (bottom, dark gray box).

Ceramics and glasses are highly brittle materials composed of inorganic compounds that form a matrix mainly by covalent and ionic bonding. In terms of crystal structure, they can have any degree of crystallinity. For engineering, they are particularly valuable due to their electrical and thermal insulation, low friction, high mechanical strength and chemical resistance. Ceramics have therefore been traditionally used as fire-resistant utensils or parts of ovens. Modern applications for fiber reinforced ceramics include high performance composite materials (e.g. fiber-reinforced, high-performance brake pads) and thermal barrier layers (e.g. paneling on spaceships) [12, 13]. For biomedical engineering, technical ceramics are used for their low friction properties and biocompatibility as the joint for the hip implants [14], for their bone-conductive properties for bone tissue engineering (e.g. bioglass, bone graft pastes) and for dental implants [15]. Metals, on the other hand, have highly ordered atomic structure, but their electrons move freely in electron clouds. This leads to metals having a high strength to mass ratio, but also being malleable, ductile and fusible. These properties make metals ideal for load-bearing applications, for example as automotive parts [16]. Metals are usually electrically conductive, and their surfaces are chemically reactive (in particular they are sensitive to oxidization and corrosion when not pre-treated), therefore they are also used for conducting electricity, and avoided for parts which come into contact with water, salts or harsh chemicals [9, 17]. For biomedical engineering, metals have many uses, which range from relatively simple devices such as surgical tools to complex ones such as implants. For example, metals have a high strength to mass ratio as well as tensile strength, which is appropriate for the stem of hip implants [14]. Moreover, the surface reactivity of metals is useful for dental applications [18].

Unlike metals and ceramics, it is difficult to generalize the properties and behaviors of polymers, as this class of materials is large and diverse. The common definition that holds them together is that polymers are large macromolecules that are comprised of repeated monomer sequences, most commonly with covalent bonding between monomers [8]. Polymers have a broad range of uses; a few common examples are for food and water packaging [19] and for textiles [20]. Due to the broad definition and range of potential applications of polymers, they are further categorized as either natural or synthetic. Synthetic polymers are derived from petroleum and created in a laboratory setting by monomer synthesis and polymerization of the monomers [21] and natural polymers (or biopolymers) are extracted from natural resources (biosynthesized) or can be synthesized in a laboratory, and may self-assemble or may require moderators for polymerization [22]. Examples of synthetic polymers are plastics, and examples of biopolymers are polypeptides, polysaccharides, and polynucleotides. One key difference between common synthetic and natural polymers is that most natural polymers readily degrade and synthetic polymers are nearly non-degradable, although there is significant research in the field of biodegradable polymers [23]. For biomedical engineering, polymers are used for disposable, sterile parts (e.g. IV bags) [24], in implants that replace the function of normal tissue (e.g. hip implants, stents) [25] and as biomaterials for tissue engineering [26].

For the purpose of this dissertation, it is important to consider which specific materials from these classes can be used as biomaterials and why. Although a few examples were given for biomedical applications of each material class, not every example listed would actually be considered an example of a “biomaterial”. Although the definition has evolved since then, as stated in one of my co-authored reviews [27], “a biomaterial was defined by the National Institutes of Health in the 1980’s as ‘any substance (other than a drug) or combination of substances, synthetic or natural in origin, which can be used for any period of time, as a whole or as a part of a system which treats, augments, or replaces any tissue, organ, or function of the body’ [28]”. Therefore, in order to design biomaterials, it is necessary to understand the cellular and molecular level factors that underlie healthy human physiology.

1.1.1 Our muse for biomaterial design: The extracellular matrix (ECM)

As stated in the previous section, the ECM is the biopolymer network (matrix) surrounding cells (extracellular) which provides mechanical support, biological cues and many other functions to the tissue [7]. The function of ECM depends on the macromolecules that it is comprised of; for example, collagen type I provides important structural support for both cells and the tissue as a whole, and therefore the ECM of load-bearing tissues are rich in collagen type I [29]. Collagen is a fibrillar protein comprised of three protein chains wound to form a triple helix. There are nearly 30 identified forms of collagen, however the five most common types are type I (skin, bone, tendon, vasculature), type II (cartilage), type III (co-expressed with type I in reticular fibers), type IV (basal lamina) and type V (placenta). Most of these collagen types will form fibrils and fibers by parallel arrangement of the tropocollagens (the tightly wound triple helix of collagen chains). However, there are a few collagens, such as collagen IV, which form a looser triple helix, and link head-to-head instead of parallel [30]. Depending on the collagen, there are many cell-binding or molecule-binding sites. Collagen I for example has binding sites for calcium phosphate (biomineralization) [31], integrin recognitions sites for integrins $\alpha_1\beta_1$ and $\alpha_2\beta_1$ [32], and

fibronectin [33]. Excessive and disorganized production of collagen leads to poor mechanical properties of tissues, and is characteristic of fibrotic scar tissue formation [34]. Although essential, collagen alone is not sufficient to provide all structural functions of ECM, in particular due to its high stiffness. Elastin is a hydrophobic, highly stretchable protein that is highly important for recovering the shape of certain tissues after deforming them, and is abundant in skin, tendon or ear cartilage [35]. The elastin precursors, tropoelastin, include alternating blocks of hydrophilic and hydrophobic residues. Although not ascertained, most believe that elastin has high mechanical toughness due to large, aggregated elastin molecules (hydrophobic components) being surrounded by a loose, amorphous phase (hydrophilic components). When elastin is stretched, hydrophobic regions are exposed, and these regions impose constraints upon water molecules. When tension is released, the released energy from the more ordered system drives the elastin to recoil back to its original shape. Without elastin, or with poor production of elastin, skin hangs from skeletal muscle (cutis laxa) [36] and arteries can be overly stiff [37]. Another important ECM molecule for resisting mechanical forces is hyaluronic acid. Hyaluronic acid is an anionic, non-sulfated glycosaminoglycan that can bind a large quantity of water molecules [38]. For this reason, it is an important ECM molecule in skin, cartilage and muscle. The biological activity of hyaluronic acid depends on its molecular weight, where low molecular weights promote angiogenesis and result in inflammation, and high molecular weights repress angiogenesis and reduce inflammation. Cells recognize hyaluronic acid with the cell-surface protein CD44 [39, 40]. Excess production of hyaluronic acid is common for inflamed tissues and when found in tumor or cancer tissue is a sign of poor prognosis. Although structural proteins are of utmost significance to healthy tissues, proper cell adhesion, coordination, and ECM matrix formation are also critical, and mediated by proteins such as fibronectin.

Fibronectin is a protein that contains binding sites for heparin, collagen type I, fibrin and cell integrins, and is in particular “famous” for the cell-recognition peptide sequence Arginine-Glycine-Aspartic Acid (RGD) (PubChem CID: 104802) [41, 42]. The discovery of RGD in fibronectin was a great step in understanding binding of cells to ECM due to the ubiquitous recognition of different integrin classes to RGD [43]. Fibronectin is also a mediator between collagen IV and laminin in the basal lamina [44]. Therefore, fibronectin plays a major role in building organized ECM and mediating cell-ECM interactions, [Figure 3](#). For example, it was discovered that knockout of fibronectin is embryonic-lethal in mice [45]. Fibronectin is also found in a soluble form in the blood stream, and thereby performs important functions for blood clotting and wound healing, as can be inferred from its binding activity to fibrin and fibroblasts [46].

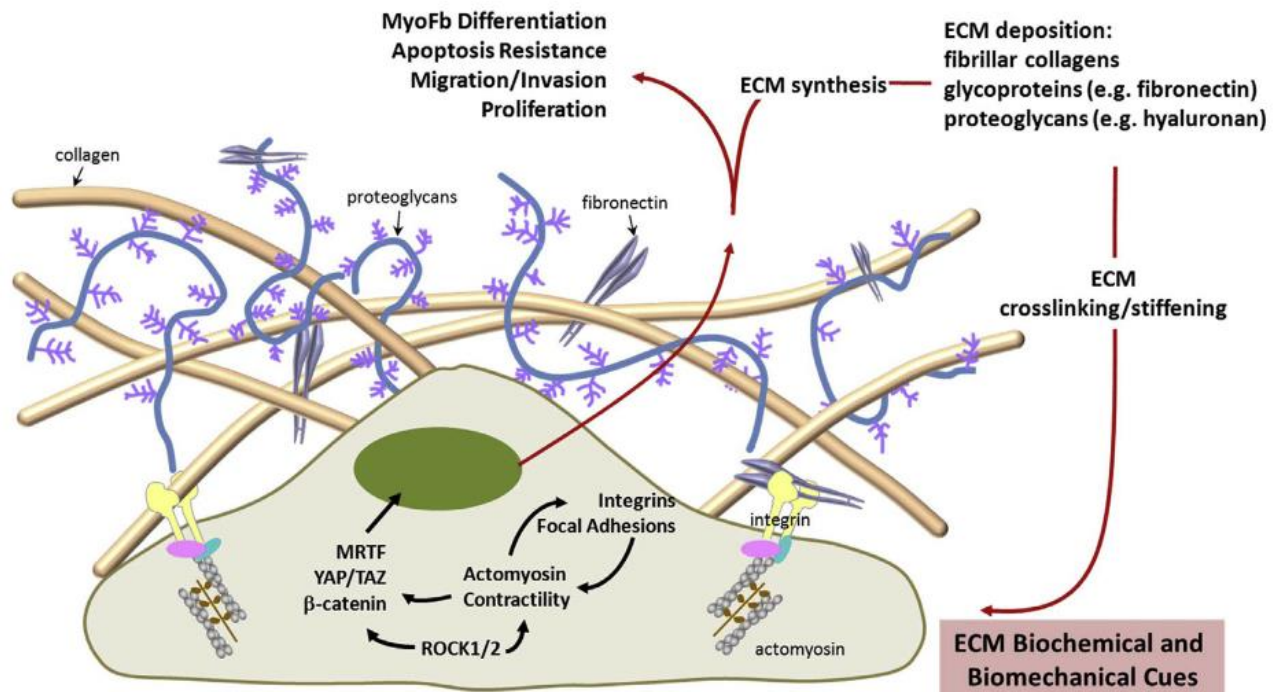


Figure 3: The molecular organization of ECM and cell-ECM interactions. A fibroblast (represented by the green ellipsoidal shape) responds to its surrounding and can alter its surrounding ECM. The classic organization of collagen, proteoglycans and fibronectin is also shown. Reprinted from *The American Journal of Pathology*, 184 Thannickal, V. J., Henke, C. A., Horowitz, J. C., Noble, P. W., Roman, J., Sime, P. J., Zhou, Y., Wells, R. G., White, E. S., Tschumperlin, D. J., *Matrix Biology of Idiopathic Pulmonary Fibrosis*, 1643-1651., 2014 with permission from Elsevier; this article is published under the terms of the Creative Commons Attribution-NonCommercial-No Derivatives License (CC BY NC ND) [47].

When designing biomaterials, the most obvious approach would be to extract this ECM from donors and use it directly, or to try to engineer exact mimics. However, there are two major problems to doing this.

(1) **Source:** Although it is possible to access and isolate human ECM, the number of donors is limited, and, depending on the ECM molecule, the yield is low, and there is possibility for batch-to-batch variation. Therefore, for the purpose of biomaterials engineering and design, it is rare that ECM is isolated from human tissue. Instead it is either isolated from an animal source which is available in larger quantities (e.g. bovine skin), a biopolymer with similar characteristics (e.g. alginate, synthetic polymers) is used instead of the native ECM or it is produced using biotechnology (e.g. recombinant collagen).

(2) **Biology:** The ECM found in the body is in homeostasis, in particular from mature donors, or, worse, in a pathological state. Therefore, the native ECM does not necessarily have the same types of cues that will promote tissue regeneration [48]. Engineers must design their biomaterials in order to promote cell behavior and thereby tissue regeneration.

By recapitulating key characteristics of the material, biomaterials can be engineered instead of being isolated from human tissue and used directly, [Table 1](#).

Table 1: Natural ECM molecules, biomolecule type and the tissues containing them.

ECM	Biomolecule Type	Key characteristics or functions	Tissues
collagen type I	protein	the most abundant protein in the human body; fibrillar collagen; contains several binding sequences (cell binding, protein binding, and mineral binding)	connective (bone) epithelial (dermis) muscle (heart)
elastin	protein	highly elastic; resistant to permanent deformation	connective epithelial (arteries)
fibronectin	glycoprotein	ECM molecular organization; contains the RGD sequence; exists in a soluble form in the bloodstream (blood clotting)	connective epithelial (basal lamina) muscle nervous
hyaluronic acid (hyaluronan, HA)	glycosaminoglycan (GAG)	Absorbs large quantities of water	connective (cartilage) epithelial (skin) muscle nervous (brain)

Table 1 should not be considered an exhaustive list of all molecules in the matrisome [49]. The table is missing many main ECM components such as laminin (forms the basal lamina of the basement membrane), heparan sulfate (found in nearly all tissues), chondroitin sulfate, keratin sulfate, tenascins, only one of twenty-nine types of collagen are listed, and vitronectin (glycoprotein important for cell attachment and homeostasis). It also contains the RGD cell-binding sequence, and is in particular known for binding to integrin $\alpha_v\beta_3$, found primarily in platelets. Further, this table does not include non-ECM proteins such as fibrinogen, or nucleic acid-based materials such as DNA or RNA, which are also sometimes utilized as biomaterials. Instead, Table 1 provides a helpful guide for some ECM molecules that are common templates for engineering biomaterials.

1.1.2 Biomaterial selection and design

Engineering design begins by creating a list of requirements and corresponding specifications, as well as weighing the relative importance of each requirement. Based on the “req-spec” chart, possible design features and materials can be selected. Biomaterial selection begins in a similar manner; however, the relative weight of importance of each requirement is different for biomedical engineering than it is for traditional engineering (e.g. mechanical or electrical engineering). For example, in traditional engineering cost assessment is usually a high priority requirement, however, in designing biomaterials cost is usually a low priority factor due to the fact that tissue engineering has a low manufacturing readiness as well as the high cost associated with medical products and research [50]. Instead, usually the first question that a researcher should ask is if the material is toxic.

Material toxicity is evaluated *in vitro* by incubating cells on biomaterial or with biomaterial in the supernatant followed by a method of evaluation such as cell staining or colorimetric assays. Some biomaterials

are non-toxic when they are intact, however become toxic when they are degraded. For this reason, the toxicity of degraded products should be tested, and it should also be determined at what concentration they are toxic. Related to this, it should be evaluated if the degraded products have a tendency to sequester in one place; that is, what is the biodistribution of the degraded products. Biodistribution is evaluated *in vivo* where an animal model, typically a small rodent, is administered a drug or biomaterial. The distribution of the different components is either monitored live by optical methods [51] or by monitoring blood concentration levels for clearance rate [52]. After a specified period of time, the animal is sacrificed and relevant tissues (e.g. injection site, liver) are examined for presence of the biomaterial [53]. If the biomaterial meets this basic requirements, more specialized functions such as inducing certain biological or physiological behaviors can be considered,

Table 2.

Table 2: Generalized requirements and specifications for tissue engineered scaffolds, and the design elements that could possibly be used to meet the requirement.

requirement	specification	design elements
carry or transmit force	1. specific Young's modulus 2. specific elastic/plastic behavior (e.g. Creep)	biomaterial , scaffold morphology
a certain biological function	1. gene expression and stability 2. single cell morphology and function 3. complex, coordinated cell function (tissue or organ function, e.g., muscle contraction)	cell type and source, biomaterial , scaffold morphology
biocompatible	1. low immunogenicity 2. no toxicity 3. no toxicity of degradation products	biomaterial , removal of processing residues (e.g. emulsion oils, crosslinking reagents)
sterile	1. must be free of all contaminants (bacteria, viruses, endotoxins or PAMPs)	processing technique, biomaterial (tolerates sterilization techniques)
specialized functions (light/electricity/sound transmission)	1. opacity, conductivity, mechanical stiffness; depends on the desired function	cell type and source, biomaterial , scaffold morphology

To summarize, a **biomaterial should be selected based-on desired physical (optical/electrical), chemical, physiochemical (hydrophobicity), biochemical, mechanical and biological properties. Important biological properties include its biocompatibility, its immunogenicity, and its toxicity. Further, the suitable morphology must be considered as well, as how the morphology is generated is partially determined by the selected biomaterial.** Overall, different material classes have different benefits based upon these basic requirements, however, as inducing certain biological/physiological responses is such an important feature to a biomaterial, metals or ceramics are rarely considered in the material selection process, [54]. A few exceptions, especially for bone tissue engineering, are titanium oxide, bone graft paste and bioglass [55]. These types of materials tend to be more popular in industry due to their more predictable behavior, practicality (fabrication, storage, sterilization) and cost-effectiveness. Implants produced from these types of materials (e.g. hip implants) can significantly improve the quality of a patient's life; however, they also have many drawbacks.

For example, most hip implants have to be replaced after 15-20 years, or, worse, there can be a critical failure of the implant due to breakage at the bone-implant interface or debris production at the artificial joint [56]. In the academic sphere, the use of metals and ceramics has significantly diminished, and most researchers concentrate on developing polymer-based implants.

Common synthetic polymers used as biomaterials are poly(caprolactone) (PCL) [57, 58], poly(lactic acid) (PLA) [59], poly(glycolic acid) (PGA) [60], poly(lactic-co-lycolide) (PLGA) [61, 62], ultra-high molecular weight polyethylene (UHMWPE) [63] and PEG-based (PEO-based) polymers and derivatives [64-66]. PLA is a unique synthetic polymer in that it is produced from renewable resources. PLA is also a popular biomaterial due to adhesion of cells and slow degradation by hydrolysis. In contrast, PGA degrades rapidly and in bulk by hydrolysis, however, its monomers are absorbable, whereas the degradation product of PLA (lactic acid) have acute toxicity. Therefore, to tailor both the degradation and decrease the potential toxicity of the PLA, the block co-polymer PGLA was developed. PGLA also exhibits erosion due to hydrolysis of the ester bond; however, this can be adjusted based upon the amount and sequence of the monomers. Nevertheless, in terms of polymers that degrade by hydrolysis, PCL has the slowest rate of biodegradation and is therefore especially well-suited for drug delivery. Further, PCL has been shown to promote collagen synthesis by mammalian cells, and is therefore appropriate for scaffolds for tissue engineering. Conversely, UHMWPE is rarely used for tissue engineering; however, due to its strength as well as low-friction properties is a popular choice for the surface of the joint for hip implants. PEG/PEO are one of the first biomaterials to be implemented; proteins do not readily adsorb to PEG, and they are biologically inert and nontoxic. PEG can be used as-is for drug delivery, or is an excellent platform to modify for special applications. For example, PEG can be produced as crosslinkers, block co-polymers, grafted with other polymers, or blended with other synthetic or natural polymers.

Of natural polymers, common protein-based biomaterials are collagen (type I or V) [67, 68], gelatin (including methylacrated gelatin (GelMA)) [69, 70], Matrigel [71] and silks [27, 72], and common polysaccharide-based are chitosan [73-75], alginate [76], hyaluronic acid [77-79], [Figure 4](#).

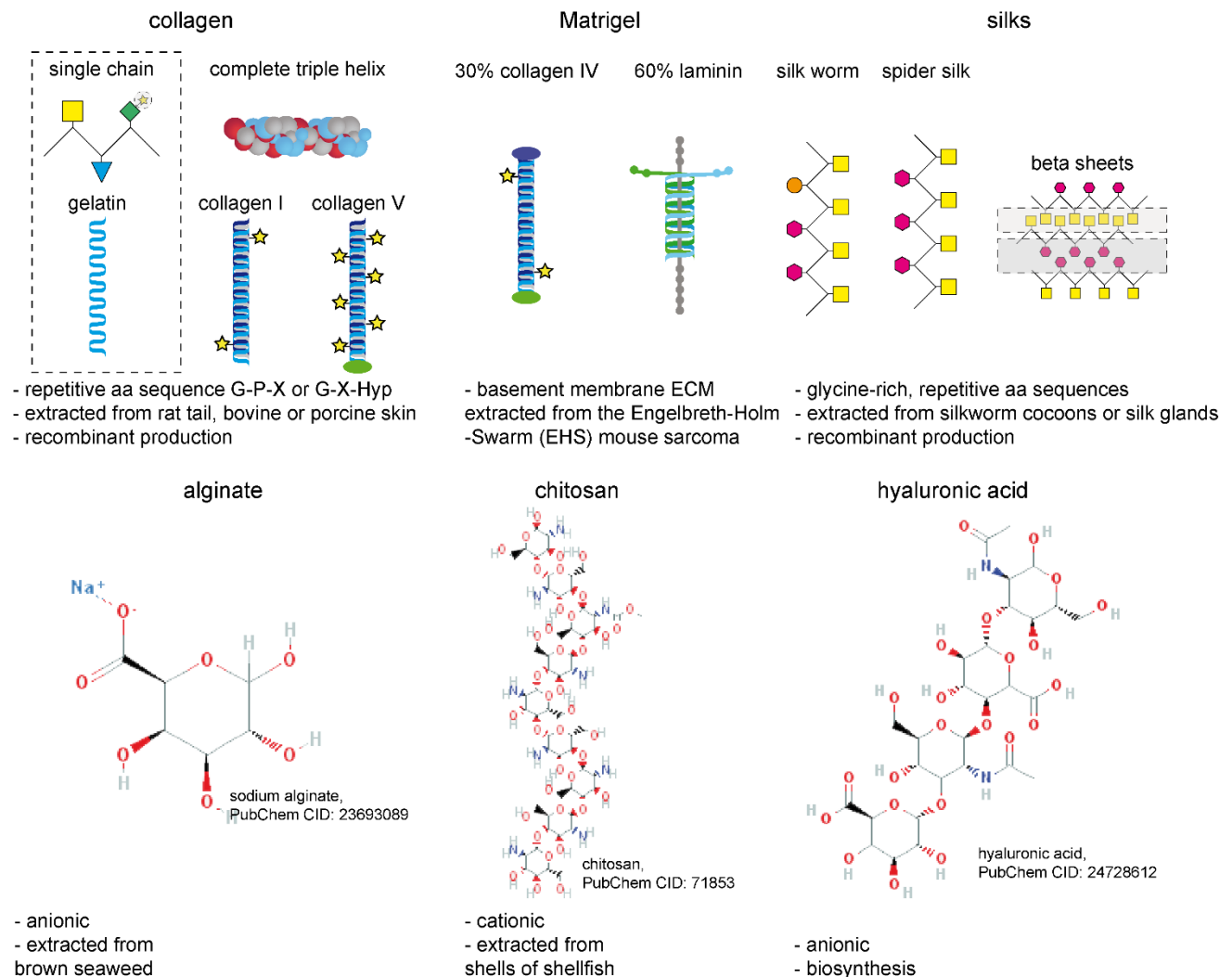


Figure 4: A comparison of common natural polymers (biopolymers) used as biomaterials. The general structure is shown, and some key properties are listed. In the top half of the figure, proteins collagen, Matrigel and silks are shown, and in the bottom half polysaccharides alginate, chitosan and hyaluronic acid are shown. The chemical structures of alginate, chitosan and hyaluronic acid are taken from the PubChem database [42].

Collagen-based biomaterials are sourced from rat-tail, bovine skin, or porcine skin, and rarely from humans; thereby, the use of native collagen has the risk for immune response or disease transmission [80]. Alternatives to using native collagen are gelatin and recombinantly produced gelatin/collagen. Gelatin, essentially a single collagen strand, has the advantage that it is far easier and cheaper to extract and produce, and is easier to functionalize or manipulate [69]. For example, it can be methylacrated to produce GelMA, which allows for rapid, cytocompatible photo-crosslinking. Furthermore, due to its additional production steps, it has nearly no problems in terms of antigenicity or sterility [70]. However it has the disadvantage that it can only be produced from collagen type I rich tissues, without modification gelatin-based hydrogels are unstable at 37 °C and will undergo a sol-gel transition [81]. Recombinant production of gelatin/collagen, on the other hand, is difficult to scale-up and, when native-like protein folding is desired, are challenging to develop [80, 82]. However, recombinant collagen/gelatin has the distinct advantage that the researcher has fine control over the end-product, as well as the ability to make any type of collagen. Another interesting, collagen-rich biomaterial is Matrigel, in particular as

it has a high collagen type IV content, as opposed to collagen type I. Matrigel is roughly composed of ~60% laminin proteins and ~30% collagen IV proteins, as it is isolated basement membrane from mouse tumors [71]. The main advantage of Matrigel is that these proteins, normally difficult to isolate, are easily obtained and promote high cell attachment and proliferation. However, due to the imprecise composition of Matrigel (contained trapped growth factors) the results achieved with Matrigel are not highly repeatable. Overall, it is clear that there are many disadvantages to harvesting ECM from animal sources. There is one ECM macromolecule that is commercially produced using biotechnology, hyaluronic acid. Hyaluronic acid is a non-sulfated, anionic glycosaminoglycan which is primarily disaccharide repeats of D-glucuronic acid (GlcUA) and N-acetylglucosamine (GlcNAc). Hyaluronic acid is biologically synthesized in the Gram-positive bacteria *Streptococcus zooepidemicus* [77]. Hyaluronic acid is useful for its high water binding activity, which helps sequester growth factors and increase mechanical stability against cyclic loading. A disadvantage is, as stated previously, low molecular weight hyaluronic acid causes inflammation, and it is therefore should be considered when selecting a molecular weight [78]. Interestingly, accumulation of low molecular weight degradation products can promote angiogenesis [79].

Although it is reasonable to use the native macromolecules found in the ECM, it is also possible to consider alternative sources of biopolymers to reduce the common risks of these molecules such as immune-rejection, disease transmission and batch-to-batch variations in the biomaterial quality. Therefore, materials such as cellulose, agarose, alginate, chitosan, silks, and non-animal collagen can be used. As stated previously, particularly popular and interesting biomaterials are alginate, chitosan and silk. Alginate is an anionic disaccharide isolated from seaweed (usually brown seaweed) that can have varying amounts of β -D-mannuronic (M-block) and α -L-guluronic acid (G-block), which plays an important role in determining its final characteristics [76]. Its properties are further determined by its production method. Alginate can be purified by precipitation with calcium (calcium alginate), or it can be purified by using an acid to form a gel, diluting the gel, and then further precipitating using sodium carbonate (sodium alginate). Alginate is advantageous in terms of its simple production and low antigenicity, however, it contains no native cell binding peptides. This, combined with its anionic nature, results in low cell adhesion to alginate. Further, as it is crosslinked by positive ions like calcium, it tends to erode in solutions containing cations [83]. Chitosan, on the other hand, is a cationic linear polysaccharide comprised of D-glucosamine (randomly acetylated or deacetylated) and sourced from exoskeleton of crustaceans [84]. Chitosan has hemostatic properties (can quickly stop blood flow) making it an excellent wound dressing. Although it has no cell-binding sites, the positive charge can promote cell attachment [73]. The positive charge also allows for complexing to negatively charged nucleic acids, making it favorable for gene delivery [74]. Major disadvantages of chitosan are that it is susceptible to seasonal availability and batch-to-batch variability, it is difficult to adapt the mechanical properties and it tends to be mechanically weak [85]. In contrast, silk-based proteins have high mechanical strength and toughness, and depending on the type of silk, how this silk is processed, or if the silk is crosslinked, several types of mechanical behaviors can be obtained [72, 86]. Silk proteins are glycine-rich polypeptides usually sourced from the cocoons of *Bombyx mori* silkworms. Different types of silk fibroins are defined primarily by differences in their repetitive core domain, and their non-repetitive termini. The mechanical toughness of silks is attributed to the combination of strong, highly ordered beta sheet crystals embedded in an amorphous, alpha-coil and coil-coil phase. Further, due to a lack of enzyme

recognition sites and resistance to hydrolysis, silks have slow biodegradation, and are particularly well-suited for applications that require slow biodegradation [87, 88]. The main disadvantage of silks is that they have also no cell binding peptides, with a few exceptions, and usually has a negative charge, leading to low cell adhesion [27]. Further, silk obtained from natural sources is also susceptible to variations.

As made apparent throughout this discussion, many common biomaterials have both advantages and disadvantages. Therefore, in order to overcome these disadvantages, or increase the number of advantages, novel biomaterials have to be produced. This can include creating biomaterial hybrids [75], functionalization of biomaterials with chemical reactive sites (e.g. for photo-crosslinking [89]) or biologically active sites (e.g. RGD [90]), or by developing new materials.

1.2 Recombinant spider silk protein

1.2.1 Biotechnological production

Spider silks are highly versatile materials that are used as a textiles or textile coatings [91, 92], for cosmetic products [93] and for biomedical products [27]. However, producing all of these spider silk-based products with natural spider silk would be difficult and time-consuming. Farming spiders requires a lot of space due to their cannibalistic behavior, and the amount of silk that can be harvested from each spider is low. Therefore, biotechnology is used to produce recombinant spider silk protein, or engineered spider silk protein, [Figure 5](#).

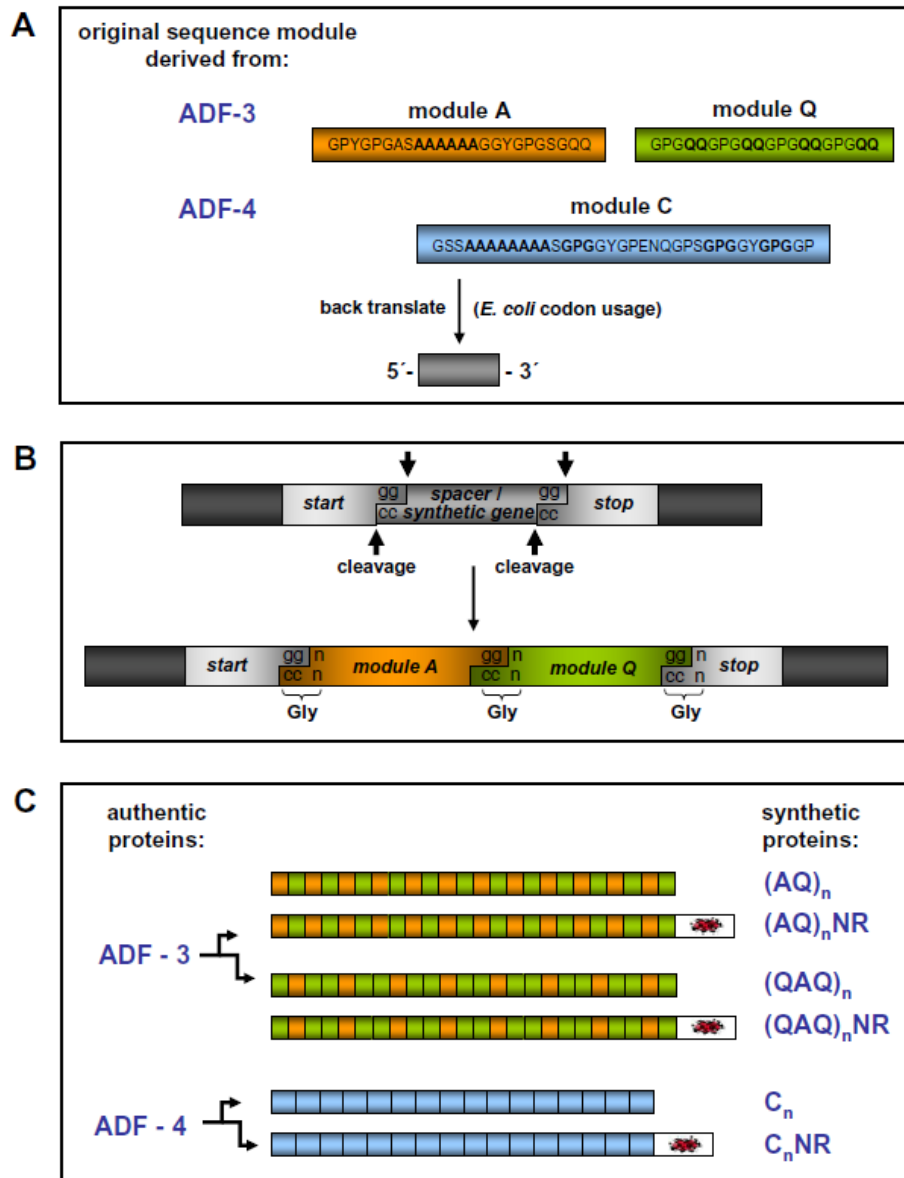


Figure 5: Biotechnological production of recombinant spider silk proteins based on ADF-4 (C module proteins, blue) and ADF-3 (A and Q module proteins, green and orange). (A) Derivation of the engineered sequence based on the natural sequence and translation to E. Coli codons (B) Insertion of consensus sequence using restricted insertion sites (C) Demonstrates the flexibility of the recombinant production; full-length or partial-length synthetic proteins, or different patterns of the modules, can be generated for better understanding of spider silk. Reprinted from *Microbial Factories*, 3, Schiebel, T., *Spider silks: recombinant synthesis, assembly, spinning, and engineering of synthetic proteins*, 2004 with permission from BioMed Central Ltd. [94]; this is an Open Access article distributed under the terms of the Creative Commons Attribution License.

To produce recombinant spider silk it was first necessary to determine the DNA sequence that encodes the protein, normally this requires extraction of the silk producing gland, followed by purification of the mRNA and conversion into complementary DNA (cDNA). For this reason, recombinant spider silk proteins are usually based-on a specific spider, type of silk, and protein. The silk genes are identified from their 5' or 3' ends, and the different DNA fragments (cDNA library) are then compared against a database of known, whole genome

sequences and mass spectrometry patterns obtained from enzymatically digested silk proteins found in silk glands. Subsequently, consensus sequences can be derived from the newly identified protein [95]. Once the natural DNA sequence is determined, a synthetic DNA can be created based on mimicking important properties of the desired product.

In spider silk, repetitive sequences found in the proteins core domain are critical for the functionality of spider silk protein within the fiber, and their secondary structures within the fiber are in turn responsible for their mechanical strength and stability. Due to host-determined limitations for producing large proteins, the natural sequence must be shortened and simplified. Therefore, to imitate the key properties of spider silks, the consensus sequence is determined, that is, most commonly found repetitive amino acid blocks are determined. The consensus sequence is then used as the template for designing the engineered consensus module.

In addition to the core domain, artificial constructs also often include the design for the highly conserved terminal domains, which are critical for the stabilization of the highly concentrated proteins in the gland and the alignment of the protein chains along fiber formation [96, 97]. The gene design method further allows for introducing specific functionalities that do not necessarily have to be derived from silk, such as cell binding motifs or biomineralization domains or domains from other structural proteins such as elastin.

The next step of recombinant protein production is to build a vector, a vehicle designed to deliver recombinant DNA. Normally vectors are plasmids, circular structures that contain the DNA sequence with other necessary components. This means that they are able to replicate independently from chromosomes, which gives them an advantage in terms of their simplicity. Plasmids include the recombinant DNA itself, an “instruction” for how many times the plasmid should be copied (a replicon), a promoter gene to turn expression on, a sequence encoding an affinity tag for purification and one encoding a cleavage site, which allows for removal of the affinity tag, and a gene encoding antibiotic-resistance for selecting properly expressing colonies (a selection marker) [98]. The plasmid is selected and the synthetic gene designed, expression vectors are first created and replicated by expansion of positively expression colonies, primarily in *Escherichia coli* (*E. coli*) [98-100]. Plasmids are then extracted and transduced into the host for final production of the recombinant protein. For unicellular (prokaryote and eukaryote) systems this is most commonly done by heat shock, which makes the host vulnerable to foreign DNA. Based on limitations or strengths of a host, the recombinant DNA or the plasmid may have to be re-designed if there is improper production of the recombinant protein. Then the transfected host culture is allowed to expand, protein expression is transduced and then later the host cells are lysed and the proteins purified.

1.2.2 Recombinant spider silk protein eADF4(C16)-based biomaterials

Recombinant spider silk engineered *Araneus diadematus* fibroin 4 with 16 repeat C-module (eADF4(C16)) is, much like other silks, an anionic biopolymer with no native attachment sites for cells [101-103]. However, eADF4(C16) outperforms most other silks (and biopolymers) in terms of its toughness [104] and low immunogenicity [105]. Further, eADF4(C16)-based materials are biocompatible [103, 105] and have slow biodegradation [88, 106], [Figure 6](#).

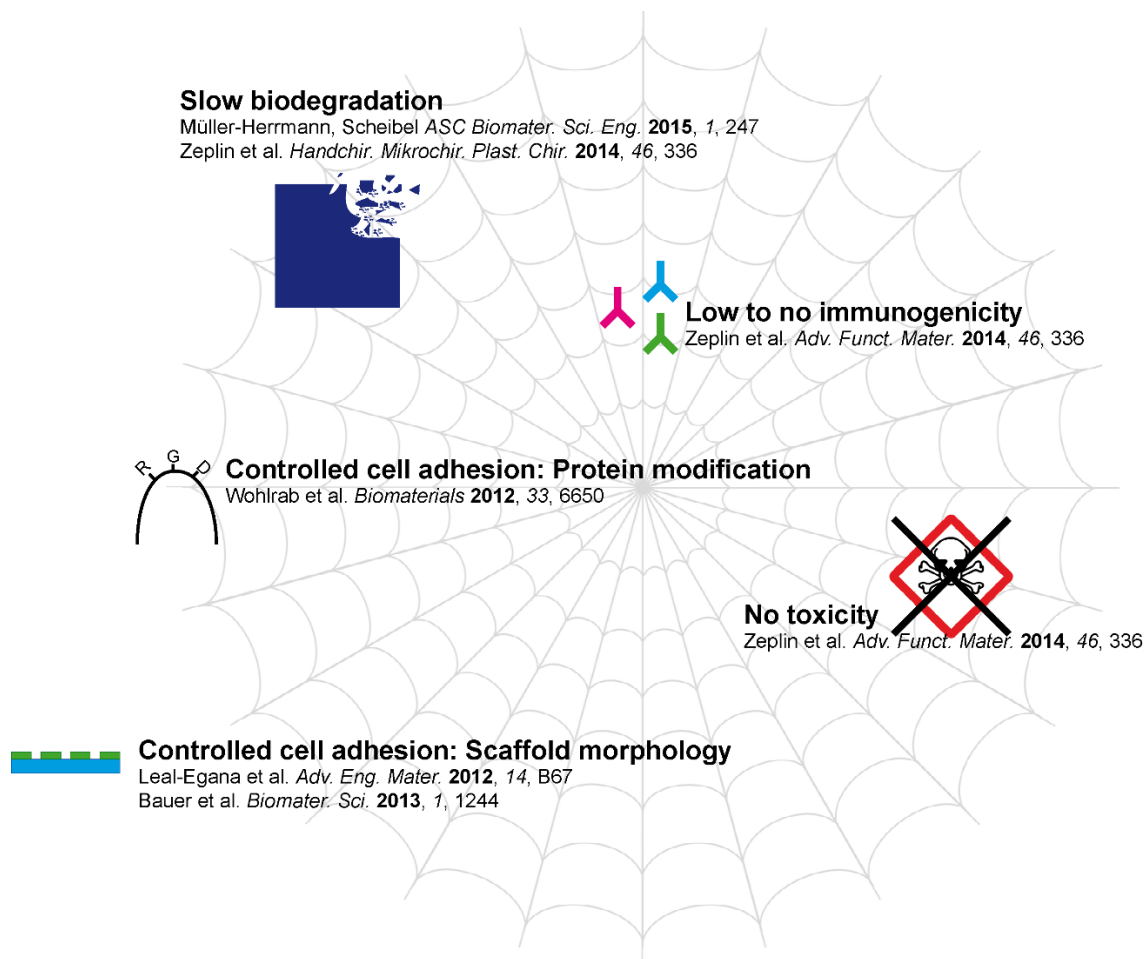


Figure 6: Key properties of recombinant spider silk eADF4(C16) as a biomaterial and corresponding citations where each property was evaluated and determined. Partially adopted from *Biotechnology and Applied Biochemistry*, 55, A. Leal-Egana, T. Scheibel, *Silk-based materials for biomedical applications*, 155-167, 2010, with permission from John Wiley and Sons [107].

Unmodified eADF4(C16) does not promote cell adhesion, which, although useful when trying to “cloak” implants from an immune response [105, 106], is typically an undesirable trait. However, due to the biotechnical production of this protein, it is simple to modify the protein to promote basic cell behavior such as attachment, spreading and proliferation. Variants of the recombinant spider silk protein eADF4(C16) which promote these cell behaviors include eADF4(C16)-RGD and, for some cell types, eADF4(κ 16). eADF4(C16)-RGD contains the RGD peptide sequence at the C-terminal end of the eADF4(C16) protein. This simple addition was shown to increase cell attachment from 75 % to 120 % (normalized to attachment on cell culture plate), as well as promote cell proliferation [103]. eADF4(κ 16), on the other hand, can promote cell adhesion, depending on the cell type, by changing the physical properties of the protein by switching glutamic acid (E) residue with lysine (K), resulting in a net positive charge (eADF4(C16) has a net negative charge) [108]. An alternative method to promoting cell attachment onto eADF4(C16) is by changing the topography, for example to channels [109] or to nonwovens [110].

1.3 Scaffold design

1.3.1 Scaffold design in tissue engineering

After a material is selected, it has to be processed into a specific morphology that will essentially be the scaffolding of the final tissue engineered product. The most common morphologies used in tissue engineering are films, foams, nanofiber meshes and hydrogels. Other common morphologies in regenerative medicine are fibers and particles, which can be used for suturing/weaving or drug delivery, respectively, [Figure 7](#).

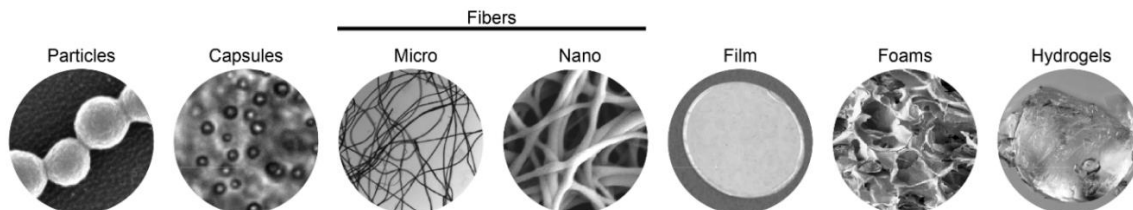


*Figure 7: Scaffold morphologies used in regenerative medicine. Partially adopted from *Advanced Materials*, 30, Aigner T., DeSimone E. and Scheibel T., *Biomedical Applications of Recombinant Silk-Based Materials*, 28, 2018, with permission from John Wiley and Sons [27].*

The different morphologies shown in [Figure 7](#) are achieved by using different processing techniques. Particles and capsules are usually produced by either mixing solution, creating an emulsion in solution, using microfluidics [111] or by emulsion/salting-out [112]. Particles are particularly useful for drug and gene delivery [113], or to modify the mechanical properties of another scaffold type (e.g. particle-reinforced hydrogels) [114]. Fibers in the range of micrometers are usually produced by wet-spinning or microfluidics, or can be isolated directly from tissue or silkworm silk cocoons, and are useful for producing nerve-grafts, vascular grafts, or tendon-replacements [115-117]. Fibers in the range of nanometers are usually produced by electrospinning for wound dressings, 2D cell culture and tissue engineering membrane tissues such cornea [118-120]. Films are produced using solution casting, dip coating, spin-coating for 2D cell culture, drug delivery and implant coatings [121, 122]. Foams are produced by cyrogelling, salt leaching, and freeze-drying and are advantageous for their resistance to compression and are utilized for bone tissue engineering or as additional mechanical support in composite scaffolds [123]. Hydrogels are produced by crosslinking a low concentration polymer solution, and are commonly used for fillers, 3D cell culture and drug delivery depots [124].

Generally, a particular morphology is selected based upon the application. For example, flat films would not be used to create a large 3D tissue such as muscle, but can be useful for thin tissues or membranes such as skin or cornea. However, certain morphologies tend to be more widely applicable than others; in particular, hydrogels can be used for almost any application, given that they are made mechanically stable either by maturation with cells *in vitro* or by being prepared as a composite with a more mechanically stable morphology like nanofibers or foams.

As hydrogels and nanofibers are the morphologies that were used for the work presented in this dissertation they will be discussed in greater detail.

1.3.2 Electrospinning

Electrospinning is the production of micro/nanofibers by applying a driving voltage to a slowly moving jet towards a collector, which usually has a voltage of the opposite charge. Ideally, generating this electrical field leads the formation of a Taylor cone, from which a jet should originate. This jet will undergo whipping instabilities, and this draws out the fiber to the point where the diameter is on the micro to nano-scale. Key parameters in electrospinning include solution concentration, solvent used, flow rate, needle length and diameter, driving voltage, working distance, collector voltage, collector geometry and substrate, air humidity, and the use of other design features such as insulation elements [125]. As an example, the set-up for the device used for this dissertation is shown, as well as key parameters that relate to electrospinning the solution, [Figure 8](#).

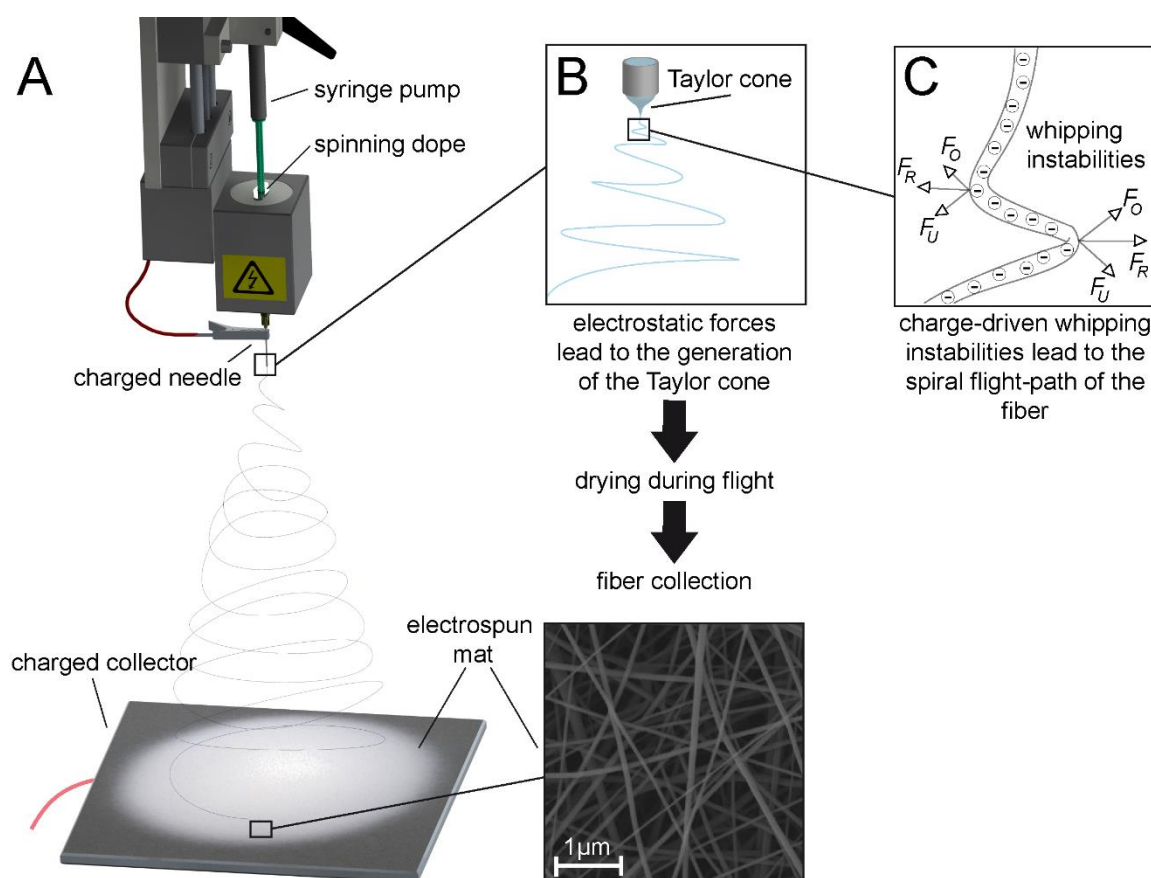


*Figure 8: The electrospinning process. A syringe is driven at a particular speed (F) and a high voltage difference is applied between the capillary tip and the collector plate, which are kept a certain distance apart (h), producing a nonwoven mesh. Translated from the dissertation of Gregor Lang, *Herstellung und Charakterisierung von Fasern aus rekombinanten Spinnenseidenproteinen und deren potentielle Applikationen*, University Bayreuth under the terms of the CC-BY 3 license [126].*

Although the idea of forming fibers from 'whipping instabilities' sounds chaotic, by fine-tuning the mentioned parameters the fiber mat production can be significantly controlled. For example, different fiber diameters can be produced by changing solution concentration [127], or aligned fibers or patterned fibers can be produced by patterning the electrical field through use of insulation elements, aligned electrodes or a rotating mandrel [128].

Nonwoven as well as aligned fiber mats are most commonly characterized by SEM and then further analyzed for fiber diameter distribution and degree of alignment [129]. Determining the mechanical properties of nonwovens is complicated due to the different scales (nano-sized fibers, millimeter sized mats), as well as the potential effect of pre-tension existing in the fibers before measurement. The most common methods used are atomic force microscopy (AFM) or nanoindentation to measure the nanoscale properties, and tensile testing of a yarn formed of the mat for the macroscale properties [130, 131].

1.3.3 Hydrogels

Hydrogels, by their simplest definition, are low concentration polymer networks containing high percentages of water. Hydrogels are fabricated by crosslinking a low concentration polymer solution; methods of crosslinking can be physical (e.g. temperature) or chemical [124], [Figure 9](#). Crosslinkers can either be added directly into the hydrogel precursor solution, or the hydrogel precursor solution can be dipped in or sprayed with crosslinker. In case of the latter, it is important to differentiate between forming a hydrogel, a coagulated fiber or a film.

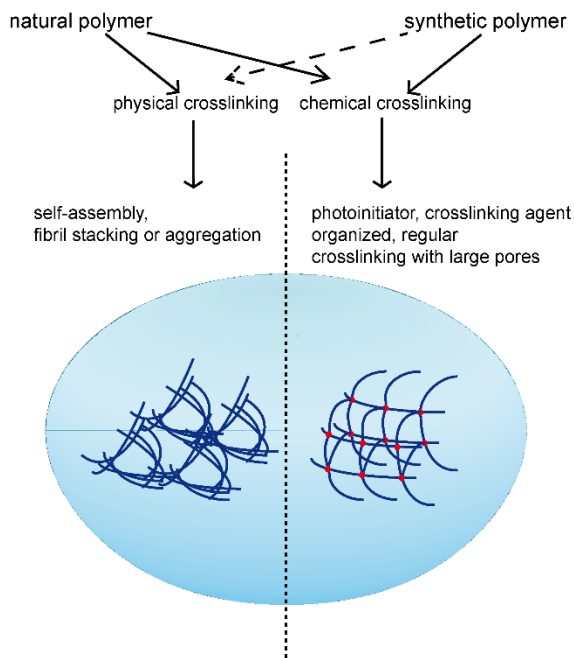


Figure 9: A generalized figure for crosslinking hydrogels and the typical properties of the polymer network. Physically crosslinked synthetic polymers (with the exception of co-block polymers) hydrogels are not common, and therefore indicated by dashed arrow.

Important properties of hydrogels to fabricate suitable scaffolds important parameters to consider include gelation rate, swelling, stiffness, porosity (mesh size), biodegradation as well as the functional response of cells to the biomaterial itself. Mesh size and degree of swelling can determine how well the hydrogel permits nutrient and waste exchange, as well as the mechanical stiffness of the hydrogels. Swelling is usually one of the simplest characteristics to observe, and is done by recording changes in weight or size before and after incubation in buffer [132]. Mesh size is most commonly determined by tracking the diffusion of different molecular weight markers through the hydrogel [132]. The degradation rate is significant parameter, and should be tailored such

that the rate of tissue regeneration and the rate of degradation matches perfectly. Degradation can be monitored by changes in weight, size, or measuring soluble polymer or protein or drug found in the supernatant, however there are other methods such as imaging or changes in stiffness that can be used [133]. Mechanical stiffness itself playing a significant role as this can determine stem cell fate and differentiation, or significantly change cell behavior. Stiffness of hydrogels is measured using rheology [134], or by compression testing [132].

Achieving a functional cell response by controlling variables in scaffold processing is a complicated issue, due to limited understanding of the biological mechanisms behind regeneration, but also due to the crude techniques used to generate the different morphologies. These methods can result in residues of cytotoxic chemical crosslinking agents, inhomogeneous cell distribution, no control over cell position and poor nutrient/waste exchange in scaffold bulk (for large, 3D constructs). Therefore, there has been a strong movement to make scaffold processing more cell-friendly, and to enhance control over scaffold generation.

1.4 Biofabrication

The term biofabrication has been around since 1994, where it was first used to describe biomineralization. Since then it has been used by many different fields, many of which have their own definition [135]. Within biomedical engineering, it was first used in 2004 to describe the use of biological materials or catalysts to aid in microfabrication. For example, using microorganisms to create nano-structure surfaces [136]. The most well-accepted use of the term today is the fabrication of materials by living organisms [135]. For the tissue engineering community, this term is used to categorize techniques where scaffolds are produced with a relatively short fabrication time and high precision, normally in the presence of living cells. These types of techniques have been used for years, for example, 3D bioprinting has publications dating back 15 years; however, the use of this term is increasing due to the increasing number of publications and interest within this field. Due to this complicated past and parallel use [137], the term “biofabrication” is confusing and often misused. A few attempts have been made to make a universal definition of biofabrication, that is, a term that is used by all fields of discipline, however the lack of consensus is likely to continue if the community continues to write independent reviews instead of meeting, for example at a conference, where terms such as biomaterials and tissue engineering were defined.

Due to these many complications, a clear definition of biofabrication that will be used for this dissertation is as follows: **Biofabrication is the simultaneous processing of biomaterials and biological materials to create constructs with a biological function.** Examples of biofabrication techniques include simple 3D cell encapsulation, modified 3D cell encapsulation using microfluidics or force-driven (e.g. dielectrophoresis-driven, magnetic-driven), biospraying, electrospinning with bioactive compounds and 3D bioprinting, [Figure 10](#).

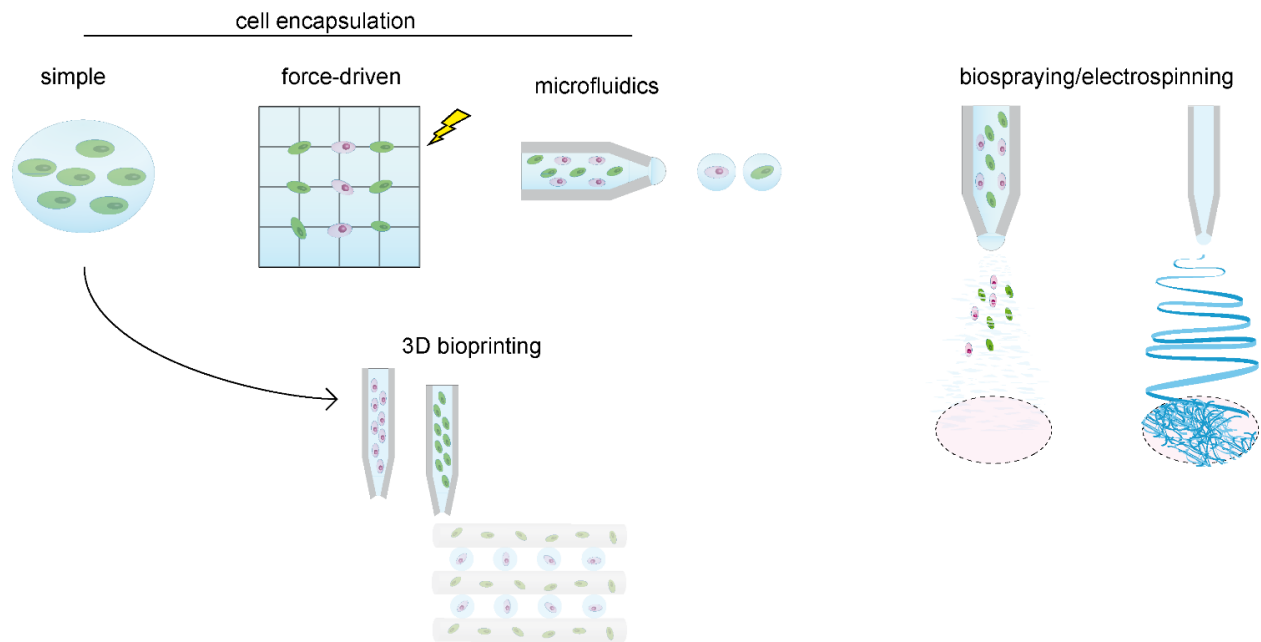


Figure 10: Generalizations of common biofabrication techniques including cell encapsulation by simple gelation, magnetic or electrically-driven positioning of cells in the matrix before encapsulation, and microfluidic-flow to produce fibers or beads before encapsulation. Cells suspended in matrix or in solution can also be delivered or patterned using biospraying, electrospinning or 3D bioprinting.

Cell encapsulation refers to the process where cells are suspended in a biomaterial solution followed by crosslinking of the solution to produce a hydrogel. Cells encapsulated in matrix are referred to generally as 3D cell culture systems; however, when they are used for 3D bioprinting they are termed bioinks [138, 139]. Cell encapsulation itself results in uncontrolled cell location, and therefore more novel biofabrication techniques include driving the cells to a particular position using similar principles to dielectrophoresis, or by driving in a magnetic field. This technique has therefore been used to pattern cells in a 3D medium and promote cell-cell interactions, one great advantage of this technique [140]. However, this technique tends to be limited in the z-direction, and therefore does not allow for the production of thick structures. Microfluidics can be used to encapsulate single cells or to produce complex composite materials. For example, single cells could be encapsulated with antibody capture beads, and could thereby be sorted and analyzed for antibody production [141]. The disadvantage to microfluidics is that, although it is relatively simple to scale-up to mass production, the produced scaffolds are too small to be used directly as a tissue replacement, and therefore the components have to be further assembled after production. Alternatively, there is bio-electrospraying, which can deliver a high number of cells to a large surface areas directly *in situ*. However, the resulting structures are 2D and not 3D, and therefore have limited use to spraying on top of scaffolds or into wound sites. 3D bioprinting, one of the most promising techniques in biofabrication, is the 3D assembly of bioinks into large 3D constructs. Although this technique can certainly be improved, most agree that the 3D bioprinters themselves are quite advanced, and that the main challenge behind producing 3D bioprinted scaffolds is the manufacture of novel biomaterials suitable for biofabrication.

1.4.1 Biomaterials for biofabrication

As implied, developing materials for biofabrication imposes additional requirements on the biomaterial that were outlined previously in [Table 2](#). Some of these additional requirements for biofabrication are general, such as all crosslinking processes must be non-cytotoxic. Others are process-dependent restrictions, for example, material used for microfluidics must undergo a sol-gel transition within seconds or minutes. Cell encapsulation in a hydrogel, on the other hand, may take a few hours without reduction in the cell viability. In the case of bioinks, it depends on the desired behavior; if the bioink is crosslinked before printing, the crosslinking process can take a few hours, whereas if the bioink is crosslinked post-printing, it must occur within seconds or minutes. Choosing between these two modes of crosslinking, before or after printing, will further have different advantages in terms of its printability.

For a bioink to be printable, it must be injectable, in other words, it must yield under process-relevant conditions. Yield stress of a material has many forms of evaluation, but two common methods are rheology (strain sweep) and by measuring the force required to eject the hydrogel from a syringe [142]. If it meets this basic requirement, then the material can then be evaluated for its “printability”. Printability refers to the quality of the fiber formation, the printing resolution and the shape fidelity [143, 144], [Figure 11](#). Fiber formation refers to the stream of material that appears after actuation, and the important characteristics include the tendency of the material to stress-relax at the tip and the flow rate. Printing resolution is usually defined as the diameter of the printed strand. Shape fidelity refers to the tendency to hold the form of the printed fiber under the forces of gravity.

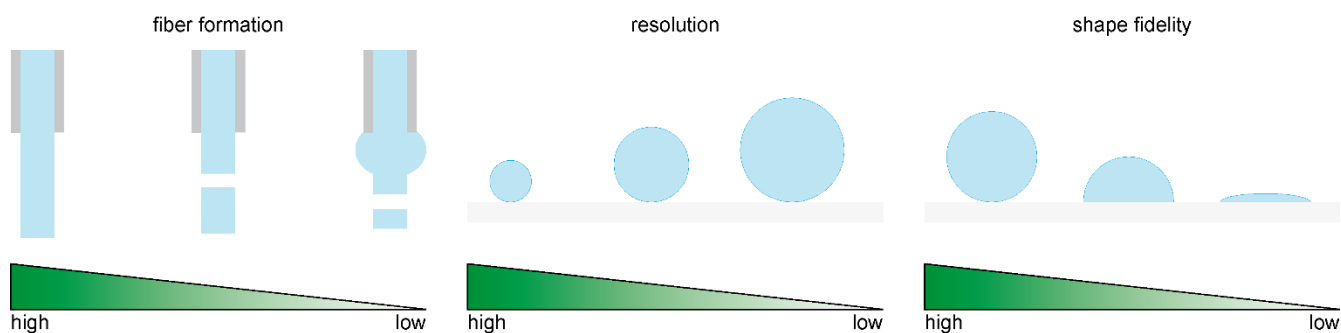


Figure 11: Characteristics of a bioink to determine its printability: fiber formation, resolution and shape fidelity. “High” on the scale indicates that this indicates high printability, and vice versa for “low” on the scale.

To understand the mechanisms which underlie printability, it is also important to clarify the dynamic mechanical behavior (shear-dependent behavior) of the material, which underlies its printability. These are usually evaluated using rheology, for example, by a shear-thinning test. In order to avoid needle clogging, however, also have high shape-fidelity, it is necessary for a material to have a high viscosity at low shear-rates, and a low viscosity at high shear rates [143]. Refer to [section 1.4.3](#) and [Figure 14](#) for more details.

Combining the characteristics of an excellent 3D culture system and a highly printable material is further complicated by the interaction between these two characteristics. For example, to have high shape fidelity usually a high elastic modulus is required, which usually translates as a dense biopolymer mesh [132]. A dense

mesh, however, is usually not beneficial for 3D cell culture due to limited nutrient/waste diffusion; it is more difficult for cells to proliferate, and it limits the ability to tune the biomaterial stiffness to the desired differentiation path of the cells. Therefore, novel materials for bioinks should have low mesh density combined with high stability [138].

Common bioinks that are particularly promising are produced from alginate, GelMA, modified hyaluronic acid (for rapid polymerization), PEG and PEG-derivatives (e.g. 8-arm PEG, Pluronic), blends with gelatin, blends with hyaluronic acid and blends with PEG or PEG crosslinkers [138, 139, 145]. Although less well-studied, peptide-based or recombinant protein-based hydrogels, such as recombinant spider silk protein, are alternatives to the more common bioinks. For example, a short peptide-based biomaterial could form mechanically stable hydrogels at low concentrations (5 mg/mL to 10 mg/mL) and there was cell spreading after two weeks [146]. GelMA, on the other hand, generally does not form stable gels at such low concentrations; however has great flexibility in terms of tuning its mechanical properties through changes in the concentration of GelMA, concentration of crosslinker, and crosslinking time [147]. Overall, in order to maintain the advantages of different bioinks and minimize the disadvantages, further materials must be engineered and studied, and likely, these materials will have to be used in combination either by synthesizing new biomaterials or by creating composites, for example by blending. Once a printable bioink is developed, other key outcomes such as maximum building volume and the fabrication time can be determined, which is also effected by the printer that is utilized.

1.4.2 3D bioprinting

3D bioprinting is the most popular biofabrication technique due to its short fabrication times, precision and the wide availability of commercial 3D bioprinters [137]. The most common types of 3D bioprinters are laser-assisted, extrusion-based, and inkjet, [Figure 12](#)

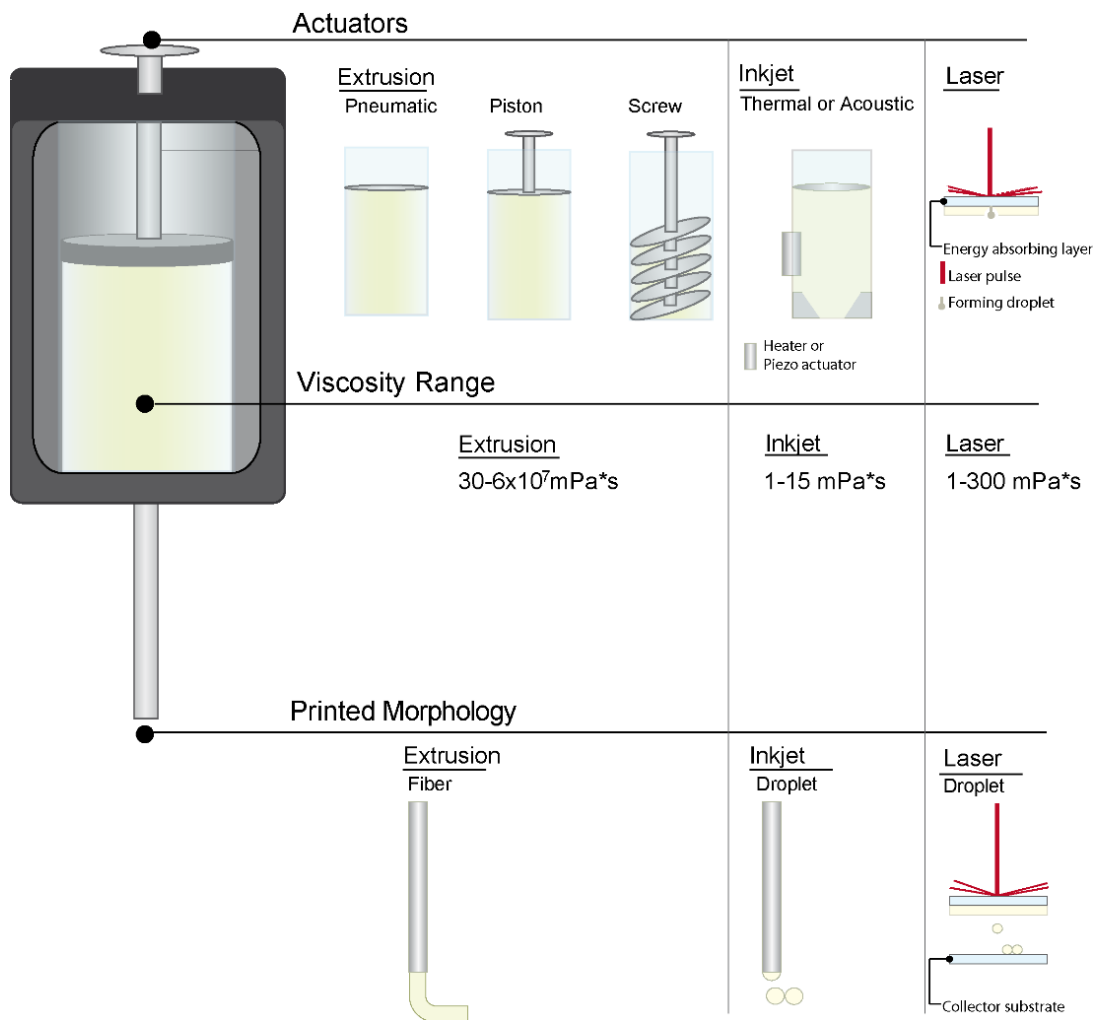


Figure 12: Types of 3D printers and their modes of actuation, the materials that can be printed based on their viscosity, and the type printed structure. Reproduced with minor corrections from *Pure and Applied Chemistry*, 87, DeSimone E, Schacht K. and Scheibel T., *Biofabrication of 3D constructs: fabrication technologies and spider silk proteins as bioinks*, 1-13, 2015, with permission from De Gruyter [139].

Extrusion bioprinting is the application of pneumatically or mechanically-drive pistons or screws to dispense fibers. This method is advantageous in its simplicity, short fabrication time and breadth of compatible materials. It is disadvantageous in terms of its low precision compared to the other printing modes [138]. Inkjet printing is useful for printing low viscosity, or cell-only solutions, with a micrometer resolution, however, cannot print high viscosity hydrogels and thick constructs [148]. Laser-induced transfer printing (LIFT) has similar advantages and disadvantages to inkjet printing; a few distinctions include that the cell viability is much higher, however, the set-up is much more complicated and the fabrication time is longer [148, 149]. Inspired by LIFT, there are also methods that use a similar approach to stereolithography, where laser energy and masks are used to create hydrogel patterns into a layer of solution [150]. This allows for generating larger constructs, but again is more limited in terms of types of bioinks that can be used. Although each method of 3D bioprinting has its advantages and disadvantages, most will use either inkjet or extrusion-based bioprinting; there is a greater variety of printers available, and they are less limited in terms of their working volume.

Extrusion-based bioprinting, due to its popularity, also has many modified forms and available products for purchase. Popular, commercially available bioprinters include 3D Bioplotter (EnvisionTEC), NovoGen MMX (Organovo), BioBot (BioBot), BioAssemblyBot (Advanced Solutions), Bioscaffolder (GeSim) and the 3D Discovery (RegenHU). Most of these printers dispense by a mechanically or pneumatically driven piston, and the higher-end printers usually also have some special modifications to this simple set-up. For example, the 3D Discover bioprinter (RegenHU), which was also the bioprinter used to complete the work presented in this dissertation, uses a magnetically-driven spring to open and close a valve, that is, the company created valve-assisted extrusion printing [Figure 13](#). This modification allows for much more precise control over viscous hydrogels.

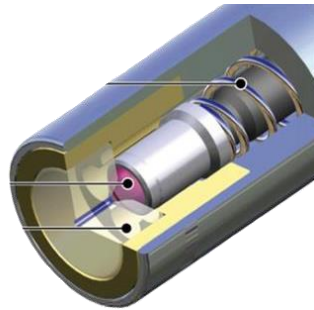


Figure 13: The microvalve used in microvalve-assisted printing from RegenHU. The ball valve is comprised of an electromagnetically-driven spring, a ball (pink) and the seat (clear with opening). Reproduced with modifications from RegenHU user manual v1.4, page 26, figure 23.

The performance of a biofabricated construct by 3D bioprinting is subject to the type of 3D bioprinter and the bioink (biomaterial and cell types) that are used. Evaluating bioprinted scaffolds is further complicated by the fact that the choice of bioprinter and bioink cannot be made independently from each other, so these variables must be tested in combination, as well as separately.

1.4.3 Evaluating 3D bioprinted scaffolds

As discussed in previous sections of this dissertation, there are several important characteristics that biomaterials must have, as well as biomaterials used for biofabrication. 3D bioprinted scaffolds should be evaluated before, during and after printing to fully understand the effect the process has on the outcome. For example, within an unprinted bioink the cells may be viable and proliferate, however, after being exposed to mechanical stress during printing the viability might be low and/or the proliferation is inhibited [151, 152]. In other words, the relationship between the bioink and the 3D bioprinter on the performance outcome must be evaluated in a time-dependent manner, [Figure 14](#).

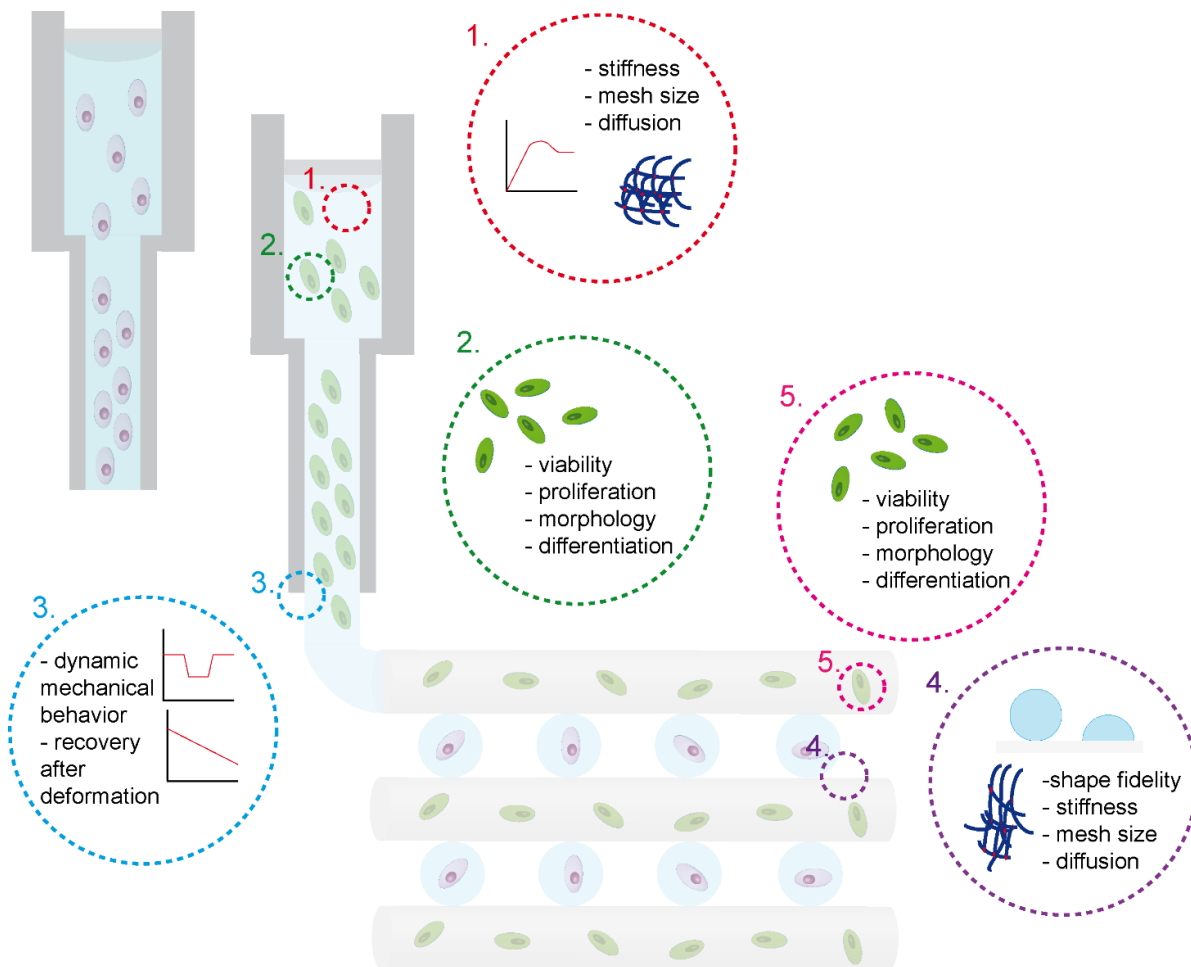


Figure 14: Evaluating 3D bioprinted scaffolds before (1,2) during (3) and after (4,5) printing. Important parameters to evaluate are materials properties (1,3,4), printability (4) and the response of cells (2,5).

Although there are many elements to the printing process that could affect the bioink, the essential variable is exposure to shear stress. The exposure to shear stress can result in changes and/or damage to the polymer network. As stated in previous sections, this will result in a change in the mechanical behavior, the degradation behavior, and the ability of molecules to diffuse through the mesh (the porosity of the mesh), which will further result in effects on the cell behavior. The shear stress can also have direct influence on the encapsulated cells; if shear stress is too high it will result in reduction in viability and in proliferation potential. The reduction in proliferation can be due to cell destruction (lower seeding density) as well as an increase in the amount of stress factors (reduces the proliferation potential of remaining viable cells) [151, 153]. However, likely due to the short exposure time to high pressure or shear stress, cells usually recover to a high viability [153, 154] and it does not typically effect cell phenotype [153]. In spite of challenges associated with 3D bioprinting, it is worth investing time and effort into optimizing a system such that it is compatible with 3D bioprinting. This is because, when the system is optimized, 3D bioprinting significantly expands the possibilities, making for some quite dazzling examples of tissue engineering.

1.4.4 State-of-the-art in 3D bioprinting

Given a suitable bioink or bioinks, 3D bioprinting can be used to generate an endless number of structures and scaffolds. Although there are many reasons why this is incredibly useful, I would propose there are two reasons why this is so relevant and significant to current research: for the development of pre-vascularized scaffolds, and to create physiologically-relevant, composite/gradient scaffolds:

The importance of pre-vascularization has been demonstrated several times as large scaffolds, without any pre-vascularization, will usually develop a necrotic core when implanted [155].

Normal adult tissues are highly complex with a hierarchy of ECM molecules, cells types and structures. Within tissues and tissue niches, these distinct microenvironments are not sharply demarcated, but rather have gradient interfaces. These gradients can include incremental changes in cell types, growth factors, ECM molecules, arrangement of ECM molecules, and so forth.

Although pre-vascularization seems like a specific topic, there are a diverse number of approaches to pre-vascularizing scaffolds using 3D bioprinting. In a study by Kolesky et al. 2014, they combined GelMA loaded with either human neonatal dermal fibroblasts (HNFs) or mouse fibroblast cell line 10T $\frac{1}{2}$, and printed sacrificial channels made of Pluronic [156]. After removing the sacrificial ink, the remaining channels were then perfused with human umbilical vein endothelial cells (HUVECs). After two days in culture, it could be demonstrated that the HUVECs lined the inner lumen, and that the scaffolds could be perfused without losing the distinct fibers of different cell types. In a further study, they were able to demonstrate the flexibility of 3D printing by printing a perfusion chamber around their scaffold [157]. By combining vascular structures with a perfusion chamber, they were able to promote the differentiation of MSCs into bone-like tissue that exceeded 1 cm in thickness. In an alternative approach, hollow channels were generated by printing using a co-axial needle set-up [158]. Using alginate- based bioink, they printed into a CaCl_2 bath as well as perfused CaCl_2 through the core of the alginate bioink, leading to rapid fabrication of hollow fibers with viable cells, which could later be perfused with media.

There are also alternative methods to developing pre-vascularized scaffolds in the early stages of development. Due to the approaches' high potential, they will also be mentioned here. One technique is to print relatively flat, 2D structures that will later fold into the vasculature in response to a stimulus (e.g. osmotic pressure, magnetic field). This combination of 3D bioprinting and origami, often referred to as "4D bioprinting", is advantageous because it eliminates the need for a sacrificial ink or media, which can potentially effect cell viability, to support the inner vascular structure until the printing process is complete. This disadvantage is that it is more difficult to directly integrate into a tissue-like scaffold, and after printing you have a free-standing vasculature which needs to be incorporated into a tissue in a second processing step. Currently, to the best of my knowledge, studies using 4D bioprinting approaches are limited to single tubes or single structures, and has yet to be used for creating a complete vascular network [159]. Another alternative to directly printing tubes is to print the "negative space" into a matrix using some sort of media or hydrogel to be removed later. In a study by Wu et al., they printed a fugitive ink into a Pluronic hydrogel-based matrix. This set-up allows for "defying

gravity”, and allowed the authors to create a free-standing, high-resolution vascular network. Although this approach was cell-free and requires quite a bit of modification to become a tissue, the method has high potential of the application to combine complex curvature with a complex hierarchy [160].

Although it is important to pre-vascularize scaffolds, as stated previously, it is not the only significant factor to consider; it is also necessary that constructs contain structural, material and growth factor gradients. For example, pore size can play a major role outside of improving the diffusion of nutrients or cell seeding efficiency. In a study by Trachtenberg et al., they examined the effect of pore size and gradient pores and their orientation, both in static conditions and under perfusion [161]. From this study they were able to demonstrate that pore size gradients and scaffold orientation relative to the flow direction, different shear stress profiles were produced, which effected not only cell viability about also cell differentiation. This being not only interesting from the perspective of tissue engineering, but also for scientific studies on cell biology.

Another interesting approach is to create composite scaffolds. In a study by Xu et al., they were able to hybridize a solvent electrospinning and inkjet bioprinting process to create scaffold for cartilage tissue engineering [162]. By hybridizing the two morphologies, they were able to improve the mechanical properties as well as improve performance of composite, cell-loaded scaffold *in vivo*. In particular, they were able to show increased production of GAGs and collagen II in cell-loaded versus cell-free scaffolds, indicating better cartilage formation. By extension, this study exemplifies the significance of bioprinting over cell-free, printed scaffolds. To the best of my knowledge, there are no other examples of bioprinting with electrospinning, although there are interesting examples of melt-electrospinning [163] and extrusion printing combined with electrospinning [164] to make cell-free scaffolds with micro and nano-sized features, which could represent potential future technologies to adapt such that they can be combined with 3D bioprinting.

There are countless examples of well-designed, multi-material bioinks [138]; however, in the examples above with modified printing techniques, almost all used “simple” bioinks. Although they represent incredible progress in the field, the “next generation” of bioinks need to be fabricated. I would propose that would be bioinks need to contain microenvironments. In a study by Du et al, they encapsulated 22 μm long, BMP-2 functionalized collagen microfibers into a GelMA-based bioink with human mesenchymal stem cells (hMSCs) [165]. Using the complete set-up, they were able to demonstrate upregulation of osteogenic markers compared to all control groups.

Although the examples presented here are quite impressive, development of bioinks and 3D bioprinting techniques need to be taken further, in particular the most novel bioprinting techniques and bioinks need to be combined into one complete system. This dissertation presents progress on the use of recombinant spider silk proteins, a powerful biomaterial platform, for use in biofabrication.

2. Aim

The **aim** of this project is to use electrospinning (ESP) and 3D bioprinting (3DBP) biofabrication techniques to create bioactive or tissue engineered constructs using recombinant spider silk protein eADF4(C16) as one of the principle biomaterials.

The main **motivations** behind this objective is to enable the production of complex scaffolds comprised of recombinant spider silk protein. All human tissues are made up of multiple materials, cell types (or sub-types), biological agents, and geometries. Recombinant spider silk proteins represent a unique tool to develop biomaterials with specific biological characteristics. Further, cells respond differently to each dimension (1D, 2D, 3D); therefore, having multiple scaffold morphologies is a powerful tool to guide cell behavior. Due to the broad range of dimensions covered between electrospinning and 3D bioprinting, they were the chosen processing techniques to develop.

Due to the breadth of this objective, it has been broken down into **three objectives**:

Objective (1) is to develop and characterize an aqueous spinning dope as well as aqueous post-treatment process of recombinant spider silk proteins in order to improve the biocompatibility of the process. In previous publications, the solvent used for electrospinning eADF4(C16) was HFIP, and the post-treatment method was 60 °C, 100 % ethanol vapor. This “toxic” method was the control for the characterization of the all-aqueous system that was developed.

Objective (2) is optimize and characterize previously established eADF4(C16) and eADF4(C16)-RGD bioinks for cell response and material properties. In particular, bioinks should be tested before and after printing for short-term cell viability, gelation-rate, rheological behavior, and long-term proliferation.

Objective (3) is to optimize the 3D bioprinting with recombinant spider silk bioinks. The printability of eADF4(C16) and eADF4(C16)-RGD based on the appearance of printed fibers and scaffolds, as well as their rheological properties.

3. Synopsis

This dissertation is comprised of two first author research publications ([publication 1](#) and [publication 2](#)), one second author research publication ([publication 4](#)), two first author review articles ([publication 5](#) and [publication 6](#)), one second author submitted research article ([publication 3](#)) and unpublished research. The publication list is found in [section 5](#); my contributions to each publication are described in [section 6](#).

Engineered *Araneus diadematus* fibroin 4 with 16 repeat C-module (eADF4(C16)) recombinant spider silk proteins, or variants thereof, were used for the research presented in this dissertation. Recombinant spider silk variants eADF4(C16), eADF4(C16)-RGD and eADF4(κ 16) are well established biomaterials for tissue engineering and regenerative medicine, even compared to other recombinant silks, as reviewed in [publication 5](#). eADF4(C16)-RGD refers to the variant of eADF4(C16) with an RGD peptide introduced at its C-terminal end, and eADF4(κ 16) where the glutamic acid (E) residue found in the C-module is switched out for a lysine (K), resulting in a net positive charge. Examples of the use of these proteins for tissue engineering include electrospinning eADF4(C16) to produce nonwovens that enhance cell attachment compared to films [110], patterning films of eADF4(C16) and eADF4(κ 16) to enhance cell attachment [109], casting films from eADF4(κ 16) alone for cardiac cell culture [108], developing foams of eADF4(C16) and eADF4(C16)-RGD to improve waste and nutrient transport to 3D cell cultures [123], and 3D bioprinting with eADF4(C16) and eADF4(C16)-RGD hydrogels [166]. Although these were successful, all except one of these examples used classical tissue engineering approaches. As previously stated, the disadvantage of this is that the fabrication time is long, and there are potentially toxic byproducts.

The aim of this work was to adapt protocols to allow for biofabrication using recombinant spider silk proteins, in particular for use in robotic dispensing and electrospinning. These two techniques were chosen because of the possibility to produce a broad range of substructures in the scaffolds from nanometers (electrospinning) to micrometers (electrospinning/3D bioprinting) to millimeters and centimeters (3D bioprinting). The adjustability of these patterns is of importance when attempting to create functional tissues or organs. The general processing of the silk proteins includes solubilization and dialysis to create the variously concentrated solutions suitable for either 3D bioprinting or electrospinning, [Figure 15](#).

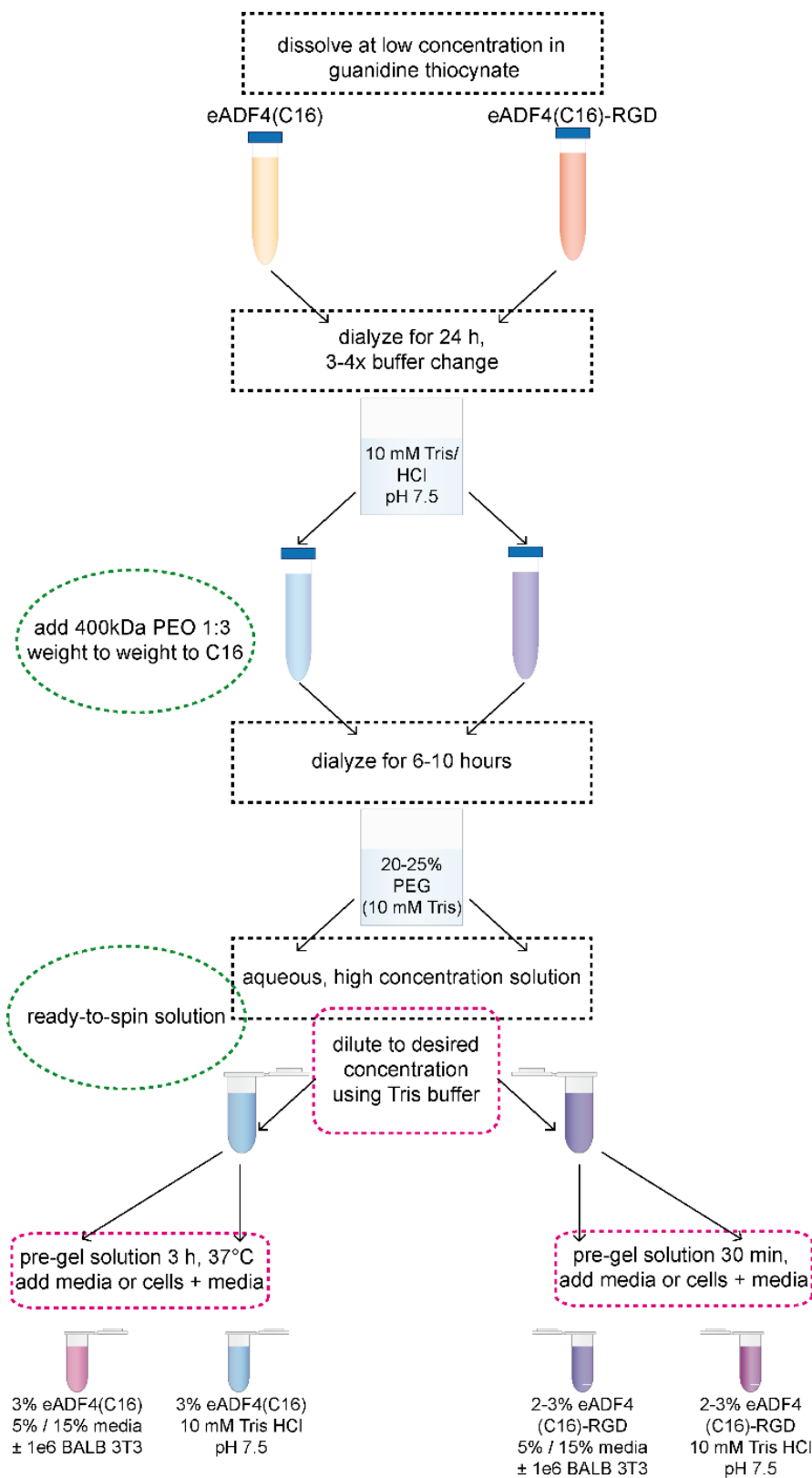


Figure 15: The processing steps to produce eADF4(C16) and eADF4(C16)-RGD solutions for the studies presented in this dissertation. Steps found in the black squares are common steps to both protocols, green circled steps are those specific to the electrospinning dope preparation, and pink rounded square steps are those specific to the bioink preparation.

eADF4(C16) had been previously used for electrospinning nonwoven mats for developing vacuum filters [92, 167] and for basic *in vitro* studies [110]. However, in these studies eADF4(C16) was dissolved in a volatile, organic solvent (Hexafluoroisopropanol, HFIP) and post-treated using 100 % ethanol (anhydrous, denatured) vapor (60 °C) to induce secondary structure formation (render water insoluble). These conditions are typically not compatible with biological activity of biomacromolecules as well viability of cells, making encapsulation of the bioactive components via *in vitro* electrospinning impossible. Further, if implanted *in vivo*, it is possible that residual HFIP inside of the fibers could damage local tissue or cause an immune response. Therefore, development of an all-aqueous electrospinning process was crucial to introduce this technique into the biofabrication field. To achieve this goal, the solvent was change to Tris buffer, and water annealing at 37 °C was used for post-treatment. This was shown to improve the fluorescence activity of green fluorescent protein (GFP) compared to the traditional method (unpublished research).

Based on pilot studies by Schacht et al. 2015 [166], which are reviewed in [publication 6](#), it was clear that there is an effect of cell culture medium as well as the RGD peptide sequence on the formation and properties of the eADF4(C16) and eADF4(C16)-RGD hydrogels. Therefore, the effect of these on hydrogel assembly was determined in [publication 2](#). Related works discusses the potential mechanisms behind the increased gelation kinetics and stiffer properties in the presence of cell culture media, as well as the difference in behavior of eADF4(C16) and eADF4(C16)-RGD hydrogels. These properties being of utmost importance, as gelation kinetics have a large impact on cell viability, mesh network and size have a large effect on cell proliferation, cell morphology, and oxygen/waste/nutrient diffusion, and mechanical properties partially determine cell differentiation. Further, change the mechanical properties can also significantly influence the printability of the bioink, which was also studied in a second author publication by comparing eADF4(C16) and engineered major ampullate spidroin 1 short (eMaSp1s) hydrogels in [publication 4](#). Using this basic information on the behavior of the bioinks, they could be optimized to overcome previous shortcomings as shown in [publication 1](#). In this study we focused on the effect printing on basic cell behavior (viability and proliferation), as well as methods to improve printability by use of gelatin in the bioink formulation. Further, in [publication 3](#) it was demonstrated that the bioink exhibits antimicrobial behavior, indicating the high potential of recombinant spider silks for biofabrication due to both their inherent properties, reviewed in [publication 5](#), as well as their flexibility for modification (e.g. addition of RGD peptide).

3.1 Electrospun eADF4(C16) nonwovens from aqueous solution and aqueous post-treatment process

Although there are many benefits to using an aqueous solution for electrospinning, as indicated in the motivation and aim of this dissertation, it is more challenging than in traditional approaches. One of the main determinates of the 'spin-ability' of a solution is its viscosity, which is ultimately determined by its concentration, molecular weight and to a minor degree the solvent it is dissolved in [168]. The aqueous solution of eADF4(C16) has a maximum concentration of 7 % (wt/vol) [86], which is close to the minimum concentration for electrospinning in HFIP (6 %) [92]. Therefore, it is not surprising that aqueous solutions comprised of eADF4(C16) alone could not be electrospun. Based on literature of silk fibroin [168, 169], PEO was chosen to use as an additive as a fiber

forming agent. Therefore, an aqueous electrospinning dope was prepared by blending PEO weight-to-weight with eADF4(C16) one to three (3 mg of eADF4(C16) to 1 mg of PEO), and, to the best of our knowledge, this is the first-time spider silk protein was electrospun from aqueous solution, [170]. The usable concentration range was determined as between 4.5 % and 5 %; concentrations below 4.5 % resulted in highly beaded fibers and above 5 %, the protein aggregated excessively or spontaneously gelled during dialysis. Due to the narrow concentration window of “spin-able” eADF4(C16) solutions, it was not possible to alter the fiber diameter, and the average fiber diameter was determined to be ~240 nm.

Generally, the spider silk scaffolds generated out of the HFIP solution (casted films, electrospun mats) contain low amounts of beta-sheets (~20 %) and high amounts of amorphous protein structures, rendering them water-soluble. Thus, post-treatment is generally applied to induce the protein folding into beta-sheet rich structures (to ~40 %) rendering scaffolds water-insoluble. There are several post-treatment methods available; usually alcohol vapors of MeOH, EtOH or i-PrOH, sometimes mixed with water, are used [126]. Alternatively, silks fibroin scaffolds could be post-treated by water vapors at increased temperature (annealing) [171, 172]. These two types of post-treatment, alcohol-based and water-based, work by opposite mechanisms. Ethanol dehydrates the proteins and induces inter- or intramolecular hydrogen bond formation whereas water annealing allows incorporation of water molecules that act as plasticizers and thereby introduce more chain flexibility. These post-treatment methods are further concomitant with increasing temperature enhancing hydrophobic effect responsible for beta-sheet formation in polyalanine regions of the protein sequence [173]. In this study we compared both methods of post-treatment, and both resulted in similar secondary structure content (~40 %), independent of the solvent system used (HFIP or 10 mM Tris buffer supplemented with PEO), as determined by FSD analysis of FTIR spectra [174]. To demonstrate the significance of this all-aqueous system in potential applications, green fluorescent protein (GFP) was incorporated into electrospinning dopes as a model of bioactive molecule, [Figure 16](#).

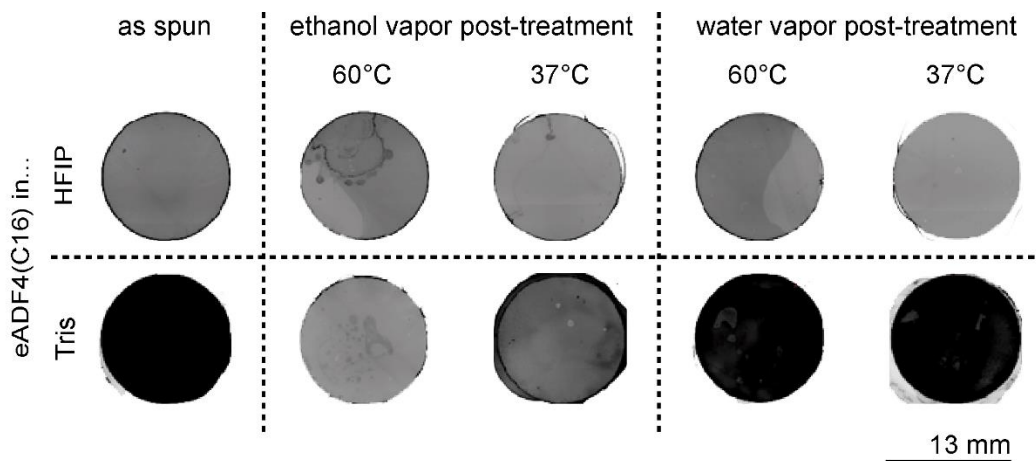


Figure 16: The bioactivity of GFP after electrospinning and after ethanol vapor or water vapor post-treatments at two different temperatures, 37 °C and 60 °C. Modified from DeSimone, E., Aigner, T., Humenik, M., Lang, G. and Scheibel T., *Aqueous electrospinning of recombinant spider silk proteins. Materials science & engineering. C, Materials for biological applications*, 2020. 106: p. 110145. [170]; as the author of this Elsevier article, I retain the right to include it in a thesis or dissertation, provided it is not published commercially.

Addition of GFP into HFIP solution of eADF4(C16) resulted in apparent loss of the fluorescence activity caused by disruption of GFP tertiary structure. Conversely, mixing the GFP into water-based eADF4(C16)/PEO dopes resulted into fluorescent nonwovens, indicating native GFP conformation. Further, the post-treatment in ethanol also had a negative effect on the fluorescent activity of GFP; the bioactivity was completely diminished after the ethanol vapor treatment. This is likely due to rapid dehydration disrupting the GFP structure. Further, the post-treatment could also be performed at 37 °C, which also improved GFP activity, and would be necessary for directly electrospinning onto cells *in vitro* or wounds *in situ*.

Overall, the significance this work in future development is utilization the all-aqueous approach for biofabrication, e.g., *in vitro* electrospinning directly on top of cells or hydrogels encapsulating cells, incorporation of growth factors or as biosensors. Another significant point is that it is possible that the all-aqueous production could influence the behavior of cells [171], and would likely influence the reaction to the nonwoven *in vivo*. Further, drug encapsulation and release studies could be done, and in order to regulate the release kinetics of the biological agents, the genetic fusions of the protein of interest with the recombinant spider silk eADF4(C16) can be used to anchor them to the eADF4(C16) based nanofibrillar scaffold [175]. The positively charged variant of the silk protein eAF4(κ 16) could be also used to prepare eADF4(C16)/(κ 16) blend nonwovens, which enable regulation of the release kinetics according to change of the biological agent.

3.2 Recombinant spider silk bioinks

In the pilot studies of 3D bioprinting with eADF4(C16) and eADF4(C16)-RGD hydrogels it was observed that cell culture media and the addition of the RGD peptide have effects on the material properties of the hydrogels. Therefore, the studies presented in [publication 2](#) concentrated on determining the effect of cell culture media on the hydrogels as well as the effect of the RGD peptide tag. The addition of cell culture media (referred to as DMEM in the publication text) to highly concentrated hydrogel precursor solutions did not change the fibril morphology of eADF4(C16) or eADF4(C16)-RGD hydrogels, as determined using transmission electron microscopy (TEM). However, there was increased gelation rate (turbidity measurements), increased the stiffness of the hydrogel (quasi-static rheology measurements) and increased the viscosity of hydrogels (flow shear ramp) in the presence of cell culture media. The increased rate of hydrogel formation, and subsequent increase in the hydrogel stiffness, could be explained by the positive ions in solution, such as Ca^{2+} , interacting the negatively charged glutamic acid residues between the protein chains [176]. To test this hypothesis, specific concentrations of CaCl_2 was added to hydrogel solutions, and a similar effect was observed, where the addition of CaCl_2 increased the stiffness of the hydrogels, implying that it is decreasing solubility and supporting ionic network formation, [Figure 17](#).

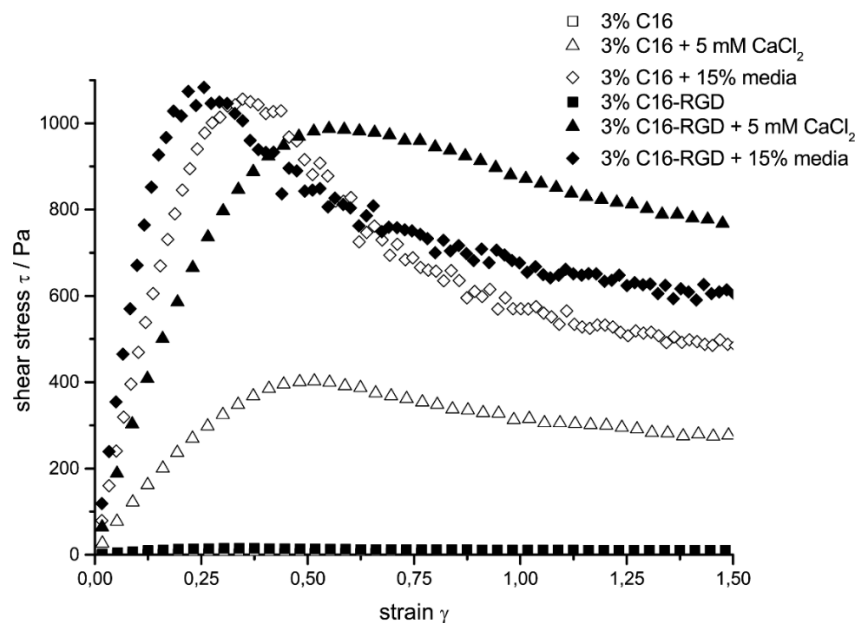


Figure 17: Rheological characterization of hydrogels made of recombinant spider silk proteins. Stress-strain curves of 3 % w/v eADF4(C16) and 3 % w/v eADF4(C16)-RGD hydrogels in the absence and presence of 5 mM CaCl_2 and DMEM (15 % v/v). Reproduced from *Materials Letters*, 183, DeSimone E., Schacht K., and Scheibel T. Cations influence the cross-linking of hydrogels made of recombinant, polyanionic spider silk proteins, 101-104, 2016 [177]; as the author of this Elsevier article, I retain the right to include it in a thesis or dissertation, provided it is not published commercially.

Addition of the RGD peptide had similar effects to cell culture media, albeit less pronounced. For example, although there was an increase in the gelation rate and the stiffness, the rheology tests conducted at higher shear rates showed that viscosity of eADF4(C16) and eADF4(C16)-RGD are identical. It is known from previous work that eADF4(C16)-RGD particles have a lower zeta potential than eADF4(C16) particles [178]. Therefore, the attraction between the proteins of the RGD variant seem to be higher, which could explain some of these differences seen in the quasi-static testing of the hydrogels. However, the increased interactions are likely weak and easily disrupted, as the stiffening effect of the RGD sequence was not observed in shear sweep tests [139, 179]. Further supporting this point is that the increase in stiffness by the RGD peptide was minimal compared to adding the cell culture media, and at the high concentrations of cell culture media there was no longer a clear effect of the RGD peptide. Overall, the studies presented in [publication 2](#) could be used to enhance the performance of bioinks in further studies presented in [publication 1](#). In the next figure captions for figures 18, 19 and 20, different experimental groups will be abbreviated as seen in the legend in [publication 1](#), provided again below.

Legend

20 mg/mL eADF4(C16) (15-% DMEM), 1x10 ⁶ BALB3T3/mL of hydrogel	2C-D15-B
30 mg/mL eADF4(C16) (15-% DMEM) 1x10 ⁶ BALB3T3/mL of hydrogel	3C-D15-B
40 mg/mL eADF4(C16) (15-% DMEM) 1x10 ⁶ BALB3T3/mL of hydrogel	4C-D15-B
30 mg/mL eADF4(C16) (15-% DMEM) 1x10 ⁶ BALB3T3/mL of hydrogel	3C-D5-B
30 mg/mL eADF4(C16) (5-% DMEM), 1x10 ⁶ BALB3T3/mL of hydrogel 0.15 mg/mL gelatin	3C-D5-g-B
20 mg/mL eADF4(C16)-RGD (15-% DMEM), 1x10 ⁶ BALB3T3/mL of hydrogel	2R-D15-B
30 mg/mL eADF4(C16)-RGD (15-% DMEM) 1x10 ⁶ BALB3T3/mL of hydrogel	3R-D15-B
20 mg/mL eADF4(C16)-RGD (5-% DMEM), 1x10 ⁶ BALB3T3/mL of hydrogel	2R-D5-B
20 mg/mL eADF4(C16)-RGD (5-% DMEM), 1x10 ⁶ BALB3T3/mL of hydrogel 0.1 mg/mL gelatin	2R-D5-g-B

An example where the data collected in [publication 2](#) informed [publication 1](#) is the gelation kinetics data, the cell seeding protocol could be optimized such that cell viability is nearly 100 % after encapsulation inside of the hydrogels. With the cell encapsulation protocol optimized, the cells were also able to proliferate in the eADF4(C16)-RGD bioinks, [Figure 18](#).

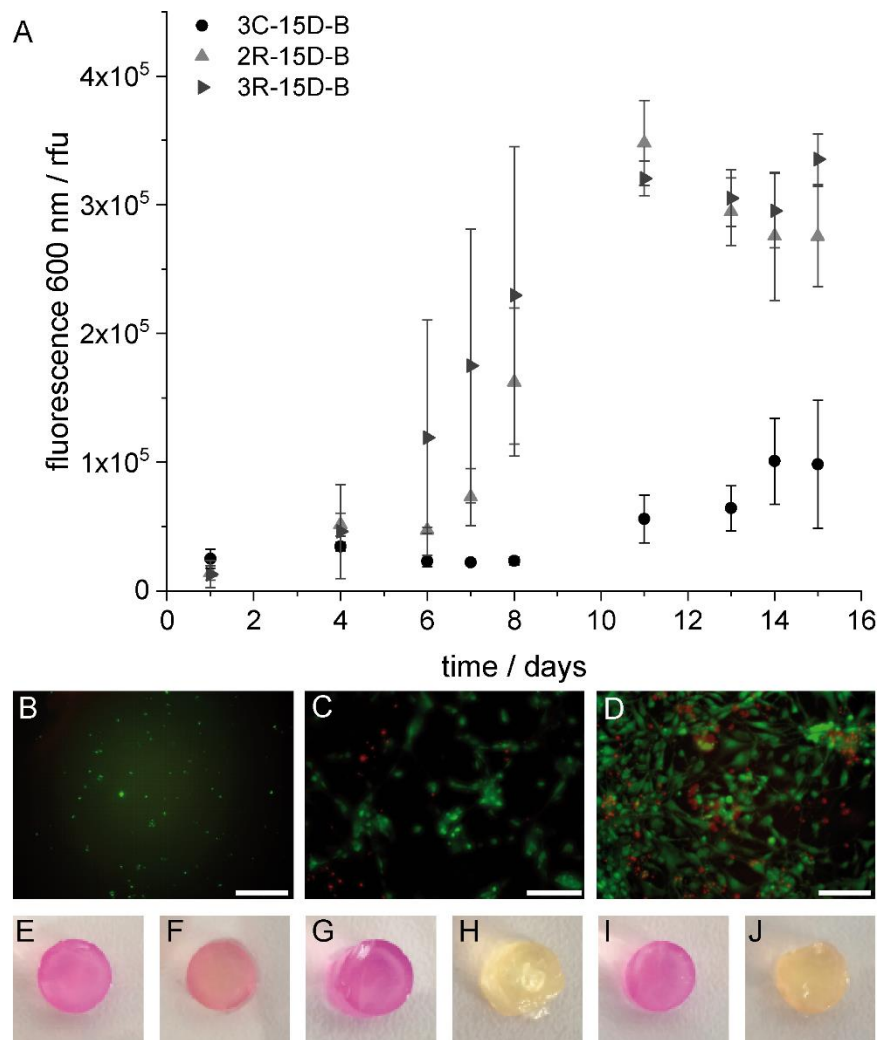


Figure 18: Proliferation of mouse fibroblasts cell line BALB3T3 in unprinted bioinks over 15 d as measured by: (A) Absorbance of cell titer blue (B-D) Fluorescence microscopy images of cells stained with calcein A/M (live cells: green) and ethidium homodimer I (dead cells: red) (scale bars = 250 μ m) and (E-J) photographs of cylinders (diameter = 0.65 cm) removed from cell culture inserts (B) 3C-15D-B, (C) 2R-15D-B, (D) 3R-15D-B, (E) 3C-15D, (F) 3C-15D-B, (G) 2R-15D, (H) 2R-15D-B, (I) 3R-15D, (J) 3R-15D-B. Three to four samples were measured per experimental group ($n = 3-4$). Standard deviation is indicated using error bars. Reproduced from *Biofabrication*, 9, DeSimone E., Schacht K., Pellert A., Scheibel T. Recombinant spider silk-based bioinks, 044104, 2017 with permission from IOP Publishing [179].

There was no difference in the proliferation of cells in 2 % and 3 % eADF4(C16)-RGD bioinks, however, due to the different protein concentrations, the mechanical stiffness for each bioink was different. Therefore, given that there was no clear difference in the proliferation of cells in 2 % and 3 % eADF4(C16)-RGD, and to match the gelation kinetics and mechanical properties, the concentration of eADF4(C16)-RGD was reduced to 2 % (20 mg/mL). The cell culture media concentration was reduced from 15 % to 5 % to improve the homogeneity of the bioink, and there was no difference found in terms of cell viability and proliferation upon this change. Gelatin was tested as an additive to improve printability, and had no significant effect on the stiffness of the hydrogels, [Figure 19](#).

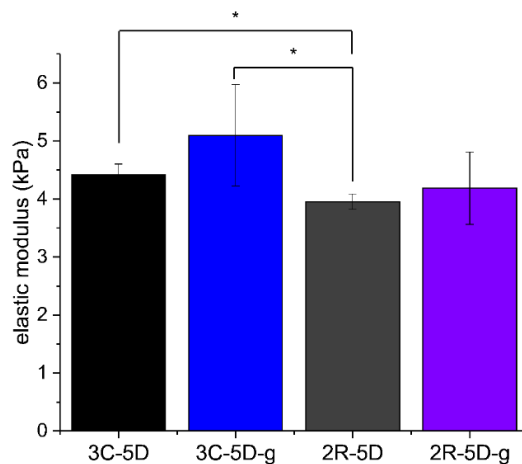


Figure 19: Young's modulus calculated using Hooke's law for 3C-5D, 3C-5D-g, 2R-5D, and 2R-5D-g. Three to four samples were measured per experimental group ($n = 3-4$). Asterisks indicate significance differences in the mean where * indicates significance level $\alpha = 0.05$. No significant difference were found using a significance level of $\alpha = 0.01$. Standard deviation is indicated using error bars. Reproduced with modifications from *Biofabrication*, 9, DeSimone E., Schacht K., Pellert A., Scheibel T. Recombinant spider silk-based bioinks, 044104, 2017 with permission from IOP Publishing [179].

BALB3T3 cells (mouse fibroblasts) cannot differentiate between a Young's modulus of 3.5 kPa and 5.5 kPa [180]. For this reason, the fact that the moduli are statistically significant different from each other was considered not important, and the bioinks were considered appropriate choices for use in further experiments.

2 % eADF4(C16)-RGD bioinks were more appropriate to compare to 3 % eADF4(C16) in terms of static 3D cell culture, however, it was found that under printing conditions the eADF4(C16)-RGD bioinks were softer and had lower printability. Further, although the resolution of eADF4(C16) bioinks could be improved by the addition of gelatin, however no clear changes were observed for the eADF4(C16)-RGD bioink, [Figure 20](#).

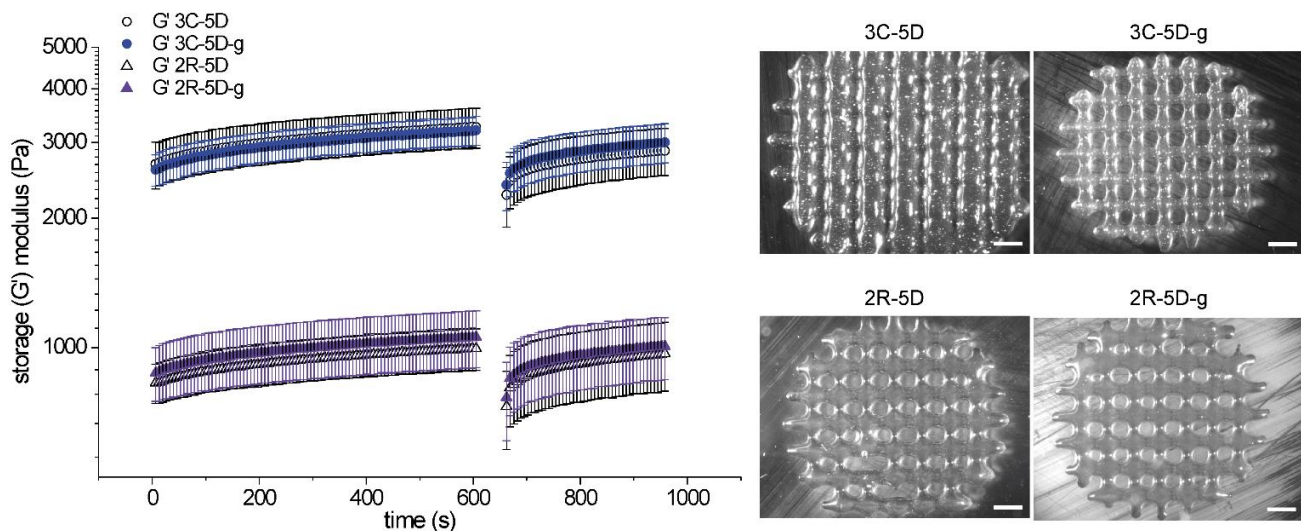


Figure 20: Recovery of bioinks after a large, non-linear deformation and printed 2-layer scaffolds. Reproduced with modifications from *Biofabrication*, 9, DeSimone E., Schacht K., Pellert A., Scheibel T. Recombinant spider silk-based bioinks, 044104, 2017 with permission from IOP Publishing [179].

The dynamic viscosity of the 2 % eADF4(C16)-RGD bioink at a higher shear rate, e.g., under printing conditions, was lower than 3 % eAD4(C16). In oscillation measurements, the 2 % eADF4(C16)-RGD bioink was much weaker (in terms of storage and loss modulus) than the 3 % eAD4(C16) bioink. However, in shear ramp data, the viscosity of the two bioinks, 2 % eADF4(C16)-RGD and 3 % eAD4(C16), was found to be nearly the same. The discrepancy between data collected from flow measurements and oscillation measurements could be explained by the fact that in the flow measurements absolute or dynamic viscosity are measured (inherent resistance to flow) whereas in oscillation measurements intramolecular forces or kinetic viscosity (density-dependent instead of force dependent) are measured. Therefore, there are fewer molecular chains or ionic bonds to break in the lower concentration bioink, however, due to the weak interactions of RGD the overall resistance to force is higher. Regardless of the mechanism, this lower storage and loss modulus led to the eADF4(C16)-RGD bioinks to have a lower resolution and shape fidelity.

Although gelatin improved the resolution of the eADf4(C16) bioink there was no clear difference in the shape fidelity, the viscosity or in the recovery behavior of the bioinks containing gelatin. This indicates that the gelatin might improve the homogeneity or stress-relaxation of the bioink, possibly acting as a plasticizer by binding more water molecules [181]. Further, both eADF4(C16) and eADF4(C16)-RGD exhibited rapid recovery to nearly original values for storage modulus, and over the course of 5 minutes had complete recovery. Although this behavior is important for printing and high shape fidelity, it is also necessary to have high storage and loss modulus to have high printability, as is evident from the 2 % eADF4(C16)-RGD bioinks. The low viscosity could explain why, although the cell viability after encapsulation in the hydrogels was improved, the post-printing cell viability was not improved in comparison to the initial study [166].

The reason behind reduced cell viability could be mechanical shear stress during the printing process, dehydration of the bioink before additional cell media could be added, or both. Although no cell proliferation was observed, the cells that survived the printing process were still viable, although they retained a round morphology, indicating that there was no cell spreading or maturation. There are a few possible explanations for this behavior. One is that the hydrogel network is too dense for the cells to spread and proliferate without degrading the matrix, however degrading the matrix is difficult with low cell number, and therefore the cells remained viable, but were caged [182, 183]. A second possible reason is that the cells that remained viable were under stress (mechanical shear from printing, exposure to debris from perished cells) and became senescent [151].

Future work for this project would be to use higher concentrations of bioinks or to add additional crosslinkers to the bioinks in order to increase the viscosity, which improves the post-printing viability, however has to be balanced with preventing reduction of cell proliferation. Further, the seeding density could be increased, which could improve the post-printing viability and proliferation.

3.3 Conclusion and outlook

Throughout these studies it was demonstrated that recombinant spider silk protein eADF4(C16) and its variant eADF4(C16)-RGD can be used for biofabrication. Highlights of this work include demonstrating the maintained bioactivity of GFP in the electrospun nonwovens prepared using the all-aqueous route, rheological studies that elucidated some possible deterministic properties of printable bioinks and the proliferation of cells encapsulated in unprinted eADF4(C16)-RGD bioinks. Interesting future improvements to the scaffolds presented here could include tailoring the release of biological agents from the nonwovens and enhancing viability and proliferation of cells within printed bioinks. Larger projects based on this work could include creating composite scaffolds with a hybridized electrospinning and bioprinting process, composite bioinks with electrospun fibers, or blended bioinks with other biopolymers to optimize the properties or towards a specific application.

4. References

1. Mason, C. and P. Dunnill, *A brief definition of regenerative medicine*. Regenerative medicine, 2008. **3**(1): p. 1-5.
2. Hubbell, J.A., *Biomaterials in Tissue Engineering*. Bio-Technology, 1995. **13**(6): p. 565-576.
3. Kaul, H. and Y. Ventikos, *On the genealogy of tissue engineering and regenerative medicine*. Tissue engineering. Part B, Reviews, 2015. **21**(2): p. 203-17.
4. Herland, A., et al., *Distinct Contributions of Astrocytes and Pericytes to Neuroinflammation Identified in a 3D Human Blood-Brain Barrier on a Chip*. PloS one, 2016. **11**(3): p. e0150360.
5. Toh, Y.C., J.W. Xing, and H.R. Yu, *Modulation of integrin and E-cadherin-mediated adhesions to spatially control heterogeneity in human pluripotent stem cell differentiation*. Biomaterials, 2015. **50**: p. 87-97.
6. Kachouie, N.N., et al., *Directed assembly of cell-laden hydrogels for engineering functional tissues*. Organogenesis, 2010. **6**(4): p. 234-44.
7. Teti, A., *Regulation of cellular functions by extracellular matrix*. Journal of the American Society of Nephrology : JASN, 1992. **2**(10 Suppl): p. S83-7.
8. Shackelford, J.F., *Introduction to Materials Science for Engineers*. 7 ed2005: Pearson International.
9. Phillips, J.C., *Bonds and Bands in Semiconductors*1973: Academic Press, INC.
10. Murphy, E.B. and F. Wudl, *The world of smart healable materials*. Progress in Polymer Science, 2010. **35**(1-2): p. 223-251.
11. Kreyling, W.G., M. Semmler-Behnke, and Q. Chaudhry, *A complementary definition of nanomaterial*. Nano Today, 2010. **5**(3): p. 165-168.
12. Cao, X.Q., R. Vassen, and D. Stoeber, *Ceramic materials for thermal barrier coatings*. Journal of the European Ceramic Society, 2004. **24**(1): p. 1-10.
13. Rosso, M., *Ceramic and metal matrix composites: Routes and properties*. Journal of Materials Processing Technology, 2006. **175**(1-3): p. 364-375.
14. Hastings, G.W., *Biomedical engineering and materials for orthopaedic implants*. Journal of physics E: Scientific instruments, 1980. **13**(6): p. 599-607.
15. Cormack, A.N. and A. Tilocca, *Structure and biological activity of glasses and ceramics*. Philosophical transactions. Series A, Mathematical, physical, and engineering sciences, 2012. **370**(1963): p. 1271-80.
16. Hirsch, J. and T. Al-Samman, *Superior light metals by texture engineering: Optimized aluminum and magnesium alloys for automotive applications*. Acta Materialia, 2013. **61**(3): p. 818-843.
17. Hendra Hermawan, D.R., Joy R. P. Djuansjah, *Metals for Biomedical Applications*, in *Precious Metals for Biomedical Applications*, T.C. Niklas Baltzer, Editor 2014, IntechOpen.
18. Feng, B., et al., *Characterization of surface oxide films on titanium and bioactivity*. Journal of Materials Science-Materials in Medicine, 2002. **13**(5): p. 457-464.
19. Siracusa, V., et al., *Biodegradable polymers for food packaging: a review*. Trends in Food Science & Technology, 2008. **19**(12): p. 634-643.
20. Adanur, S., *Wellington Sears Handbook of Industrial Textiles*1995: Technomic Publishing Company, Inc.
21. Chiellini, E. and R. Solaro, *Biodegradable polymeric materials*. Advanced Materials, 1996. **8**(4): p. 305-313.
22. Lutz, J.F., et al., *Sequence-Controlled Polymers*. Science, 2013. **341**(6146): p. 628-+.
23. Swift, G., *Directions for Environmentally Biodegradable Polymer Research*. Accounts of Chemical Research, 1993. **26**(3): p. 105-110.
24. Lee, B.K., M.J. Ellenbecker, and R. Moure-Eraso, *Analyses of the recycling potential of medical plastic wastes*. Waste Management, 2002. **22**(5): p. 461-470.
25. Teo, A.J.T., et al., *Polymeric Biomaterials for Medical Implants and Devices*. Acs Biomaterials Science & Engineering, 2016. **2**(4): p. 454-472.
26. Kim, H.N., et al., *Patterning Methods for Polymers in Cell and Tissue Engineering*. Annals of Biomedical Engineering, 2012. **40**(6): p. 1339-1355.
27. Aigner, T.B., E. DeSimone, and T. Scheibel, *Biomedical Applications of Recombinant Silk-Based Materials*. Advanced materials, 2018. **30**(19): p. e1704636.
28. Online, N.C.S. *Clinical Applications of Biomaterials*. 1982. **4**, 1-19.
29. Gelse, K., E. Poschl, and T. Aigner, *Collagens - structure, function, and biosynthesis*. Advanced Drug Delivery Reviews, 2003. **55**(12): p. 1531-1546.
30. Yurchenco, P.D. and G.C. Ruben, *Basement membrane structure in situ: evidence for lateral associations in the type IV collagen network*. The Journal of cell biology, 1987. **105**(6 Pt 1): p. 2559-68.
31. Landis, W.J., et al., *Mineral and organic matrix interaction in normally calcifying tendon visualized in*

- three dimensions by high-voltage electron microscopic tomography and graphic image reconstruction.* Journal of structural biology, 1993. **110**(1): p. 39-54.
32. Xu, Y., et al., *Multiple binding sites in collagen type I for the integrins alpha1beta1 and alpha2beta1.* The Journal of biological chemistry, 2000. **275**(50): p. 38981-9.
 33. Erat, M.C., et al., *Identification and structural analysis of type I collagen sites in complex with fibronectin fragments.* Proceedings of the National Academy of Sciences of the United States of America, 2009. **106**(11): p. 4195-200.
 34. Diegelmann, R.F. and M.C. Evans, *Wound healing: An overview of acute, fibrotic and delayed healing.* Frontiers in Bioscience-Landmark, 2004. **9**: p. 283-289.
 35. Wise, S.G., et al., *Tropoelastin: a versatile, bioactive assembly module.* Acta biomaterialia, 2014. **10**(4): p. 1532-41.
 36. Kozel, B.A., et al., *Biomechanical properties of the skin in cutis laxa.* The Journal of investigative dermatology, 2014. **134**(11): p. 2836-2838.
 37. Wagenseil, J.E. and R.P. Mecham, *Elastin in large artery stiffness and hypertension.* Journal of cardiovascular translational research, 2012. **5**(3): p. 264-73.
 38. Fraser, J.R.E., T.C. Laurent, and U.B.G. Laurent, *Hyaluronan: Its nature, distribution, functions and turnover.* Journal of Internal Medicine, 1997. **242**(1): p. 27-33.
 39. Peach, R.J., et al., *Identification of hyaluronic acid binding sites in the extracellular domain of CD44.* The Journal of cell biology, 1993. **122**(1): p. 257-64.
 40. Lam, J., N.F. Truong, and T. Segura, *Design of cell-matrix interactions in hyaluronic acid hydrogel scaffolds.* Acta biomaterialia, 2014. **10**(4): p. 1571-1580.
 41. Pankov, R. and K.M. Yamada, *Fibronectin at a glance.* Journal of Cell Science, 2002. **115**(20): p. 3861-3863.
 42. Kim, S., et al., *PubChem Substance and Compound databases.* Nucleic acids research, 2016. **44**(D1): p. D1202-13.
 43. Ruoslahti, E., *RGD and other recognition sequences for integrins.* Annual review of cell and developmental biology, 1996. **12**: p. 697-715.
 44. Laurie, G.W., et al., *Localization of binding sites for laminin, heparan sulfate proteoglycan and fibronectin on basement membrane (type IV) collagen.* Journal of molecular biology, 1986. **189**(1): p. 205-16.
 45. Mao, Y. and J.E. Schwarzbauer, *Fibronectin fibrillogenesis, a cell-mediated matrix assembly process.* Matrix biology : journal of the International Society for Matrix Biology, 2005. **24**(6): p. 389-99.
 46. Knox, P., S. Crooks, and C.S. Rimmer, *Role of fibronectin in the migration of fibroblasts into plasma clots.* The Journal of cell biology, 1986. **102**(6): p. 2318-23.
 47. Thannickal, V.J., et al., *Matrix biology of idiopathic pulmonary fibrosis: a workshop report of the national heart, lung, and blood institute.* The American journal of pathology, 2014. **184**(6): p. 1643-51.
 48. Keane, T.J. and S.F. Badylak, *The host response to allogeneic and xenogeneic biological scaffold materials.* Journal of tissue engineering and regenerative medicine, 2015. **9**(5): p. 504-11.
 49. Hynes, R.O. and A. Naba, *Overview of the matrisome--an inventory of extracellular matrix constituents and functions.* Cold Spring Harbor perspectives in biology, 2012. **4**(1): p. a004903.
 50. Wu, C., et al., *Bioprinting: an assessment based on manufacturing readiness levels.* Critical reviews in biotechnology, 2017. **37**(3): p. 333-354.
 51. Di Rocco, G., S. Baldari, and G. Toietta, *Towards Therapeutic Delivery of Extracellular Vesicles: Strategies for In Vivo Tracking and Biodistribution Analysis.* Stem cells international, 2016. **2016**: p. 5029619.
 52. Zalipsky, S., et al., *Evaluation of blood clearance rates and biodistribution of poly(2-oxazoline)-grafted liposomes.* Journal of pharmaceutical sciences, 1996. **85**(2): p. 133-7.
 53. Poursaid, A., et al., *In situ gelling silk-elastinlike protein polymer for transarterial chemoembolization.* Biomaterials, 2015. **57**: p. 142-52.
 54. Saini, M., et al., *Implant biomaterials: A comprehensive review.* World journal of clinical cases, 2015. **3**(1): p. 52-7.
 55. Stevens, M.M., *Biomaterials for bone tissue engineering.* Materials Today, 2008. **11**(5): p. 18-25.
 56. Learmonth, I.D., C. Young, and C. Rorabeck, *The operation of the century: total hip replacement.* Lancet, 2007. **370**(9597): p. 1508-1519.
 57. Sun, H.F., et al., *The in vivo degradation, absorption and excretion of PCL-based implant.* Biomaterials, 2006. **27**(9): p. 1735-1740.
 58. Li, W.J., et al., *Biological response of chondrocytes cultured in three-dimensional nanofibrous poly(epsilon-caprolactone) scaffolds.* Journal of biomedical materials research. Part A, 2003. **67**(4): p. 1105-14.

59. Tajbakhsh, S. and F. Hajiali, *A comprehensive study on the fabrication and properties of biocomposites of poly(lactic acid)/ceramics for bone tissue engineering*. Materials science & engineering. C, Materials for biological applications, 2017. **70**(Pt 1): p. 897-912.
60. Allcock, H.R., *Inorganic-Organic Polymers*. Advanced Materials, 1994. **6**(2): p. 106-115.
61. Sung, H.J., et al., *The effect of scaffold degradation rate on three-dimensional cell growth and angiogenesis*. Biomaterials, 2004. **25**(26): p. 5735-42.
62. Gentile, P., et al., *An Overview of Poly(lactic-co-glycolic) Acid (PLGA)-Based Biomaterials for Bone Tissue Engineering*. International Journal of Molecular Sciences, 2014. **15**(3): p. 3640-3659.
63. Pruitt, L.A., *Deformation, yielding, fracture and fatigue behavior of conventional and highly cross-linked ultra high molecular weight polyethylene*. Biomaterials, 2005. **26**(8): p. 905-915.
64. Buwalda, S.J., et al., *Hydrogels in a historical perspective: From simple networks to smart materials*. Journal of Controlled Release, 2014. **190**: p. 254-273.
65. Shu, X.Z., et al., *In situ crosslinkable hyaluronan hydrogels for tissue engineering*. Biomaterials, 2004. **25**(7-8): p. 1339-1348.
66. Li, J. and W.J. Kao, *Synthesis of polyethylene glycol (PEG) derivatives and PEGylated-peptide block copolymer conjugates*. Biomacromolecules, 2003. **4**(4): p. 1055-1067.
67. Parenteau-Bareil, R., R. Gauvin, and F. Berthod, *Collagen-Based Biomaterials for Tissue Engineering Applications*. Materials, 2010. **3**(3): p. 1863-1887.
68. Chattopadhyay, S. and R.T. Raines, *Review collagen-based biomaterials for wound healing*. Biopolymers, 2014. **101**(8): p. 821-33.
69. Loth, T., et al., *Gelatin-based biomaterial engineering with anhydride-containing oligomeric cross-linkers*. Biomacromolecules, 2014. **15**(6): p. 2104-18.
70. Kokol, S.G.a.V., *Collagen- vs. Gelatin-Based Biomaterials and Their Biocompatibility: Review and Perspectives*. Biomaterials Applications for Nanomedicine, ed. R. Pignatello 2011: InTech.
71. Kohen, N.T., L.E. Little, and K.E. Healy, *Characterization of Matrigel interfaces during defined human embryonic stem cell culture*. Biointerphases, 2009. **4**(4): p. 69-79.
72. Koh, L.D., et al., *Structures, mechanical properties and applications of silk fibroin materials*. Progress in Polymer Science, 2015. **46**: p. 86-110.
73. Kumar, M.N.V.R., *A review of chitin and chitosan applications*. Reactive & Functional Polymers, 2000. **46**(1): p. 1-27.
74. Mao, H.Q., et al., *Chitosan-DNA nanoparticles as gene carriers: synthesis, characterization and transfection efficiency*. Journal of Controlled Release, 2001. **70**(3): p. 399-421.
75. Madhally, S.V. and H.W. Matthew, *Porous chitosan scaffolds for tissue engineering*. Biomaterials, 1999. **20**(12): p. 1133-42.
76. Lee, K.Y. and D.J. Mooney, *Alginate: Properties and biomedical applications*. Progress in Polymer Science, 2012. **37**(1): p. 106-126.
77. Liu, L., et al., *Microbial production of hyaluronic acid: current state, challenges, and perspectives*. Microbial cell factories, 2011. **10**: p. 99.
78. Weigel, P.H., G.M. Fuller, and R.D. LeBoeuf, *A model for the role of hyaluronic acid and fibrin in the early events during the inflammatory response and wound healing*. Journal of theoretical biology, 1986. **119**(2): p. 219-34.
79. West, D.C., et al., *Angiogenesis induced by degradation products of hyaluronic acid*. Science, 1985. **228**(4705): p. 1324-6.
80. Browne, S., D.I. Zeugolis, and A. Pandit, *Collagen: finding a solution for the source*. Tissue engineering. Part A, 2013. **19**(13-14): p. 1491-4.
81. Djabourov, M. and P. Papon, *Influence of Thermal Treatments on the Structure and Stability of Gelatin Gels*. Polymer, 1983. **24**(5): p. 537-542.
82. Bulleid, N.J., D.C. John, and K.E. Kadler, *Recombinant expression systems for the production of collagen*. Biochemical Society transactions, 2000. **28**(4): p. 350-3.
83. Chan, L.W., Y. Jin, and P.W.S. Heng, *Cross-linking mechanisms of calcium and zinc in production of alginate microspheres*. International Journal of Pharmaceutics, 2002. **242**(1-2): p. 255-258.
84. Rinaudo, M., *Chitin and chitosan: Properties and applications*. Progress in Polymer Science, 2006. **31**(7): p. 603-632.
85. !!! INVALID CITATION !!!
86. Schacht, K. and T. Scheibel, *Controlled hydrogel formation of a recombinant spider silk protein*. Biomacromolecules, 2011. **12**(7): p. 2488-95.
87. Horan, R.L., et al., *In vitro degradation of silk fibroin*. Biomaterials, 2005. **26**(17): p. 3385-93.
88. Muller-Herrmann, S. and T. Scheibel, *Enzymatic Degradation of Films, Particles, and Nonwoven Meshes*

- Made of a Recombinant Spider Silk Protein*. *Acs Biomaterials Science & Engineering*, 2015. **1**(4): p. 247-259.
89. Leach, J.B., et al., *Photocrosslinked hyaluronic acid hydrogels: Natural, biodegradable tissue engineering scaffolds*. *Biotechnology and Bioengineering*, 2003. **82**(5): p. 578-589.
 90. Hersel, U., C. Dahmen, and H. Kessler, *RGD modified polymers: biomaterials for stimulated cell adhesion and beyond*. *Biomaterials*, 2003. **24**(24): p. 4385-4415.
 91. Li, G., et al., *Silk-based biomaterials in biomedical textiles and fiber-based implants*. *Advanced healthcare materials*, 2015. **4**(8): p. 1134-51.
 92. Jokisch, S., M. Neuenfeldt, and T. Scheibel, *Silk-Based Fine Dust Filters for Air Filtration*. *Advanced Sustainable Systems*, 2017. **1**(10).
 93. Fan, L.P., et al., *Vitamin C-reinforcing silk fibroin nanofibrous matrices for skin care application*. *Rsc Advances*, 2012. **2**(10): p. 4110-4119.
 94. Scheibel, T., *Spider silks: recombinant synthesis, assembly, spinning, and engineering of synthetic proteins*. *Microbial cell factories*, 2004. **3**(1): p. 14.
 95. Neuenfeldt, M. and T. Scheibel, *Sequence Identification, Recombinant Production, and Analysis of the Self-Assembly of Egg Stalk Silk Proteins from Lacewing *Chrysoperla carnea**. *Biomolecules*, 2017. **7**(2).
 96. Eisoldt, L., A. Smith, and T. Scheibel, *Decoding the secrets of spider silk*. *Materials Today*, 2011. **14**(3): p. 80-86.
 97. Bini, E., D.P. Knight, and D.L. Kaplan, *Mapping domain structures in silks from insects and spiders related to protein assembly*. *Journal of Molecular Biology*, 2004. **335**(1): p. 27-40.
 98. Rosano, G.L. and E.A. Ceccarelli, *Recombinant protein expression in *Escherichia coli*: advances and challenges*. *Frontiers in Microbiology*, 2014. **5**.
 99. Tokareva, O., et al., *Recombinant DNA production of spider silk proteins*. *Microbial Biotechnology*, 2013. **6**(6): p. 651-663.
 100. Graslund, S., et al., *Protein production and purification*. *Nature Methods*, 2008. **5**(2): p. 135-146.
 101. Huemmerich, D., et al., *Novel assembly properties of recombinant spider dragline silk proteins*. *Current Biology*, 2004. **14**(22): p. 2070-2074.
 102. Vendrely, C. and T. Scheibel, *Biotechnological production of spider-silk proteins enables new applications*. *Macromolecular Bioscience*, 2007. **7**(4): p. 401-409.
 103. Wohlrab, S., et al., *Cell adhesion and proliferation on RGD-modified recombinant spider silk proteins*. *Biomaterials*, 2012. **33**(28): p. 6650-9.
 104. Heidebrecht, A., et al., *Biomimetic fibers made of recombinant spidroins with the same toughness as natural spider silk*. *Advanced materials*, 2015. **27**(13): p. 2189-94.
 105. Zeplin, P.H., et al., *Spider Silk Coatings as a Bioshield to Reduce Periprosthetic Fibrous Capsule Formation*. *Advanced Functional Materials*, 2014. **24**(18): p. 2658-2666.
 106. Zeplin, P.H., et al., *[Improving the biocompatibility of silicone implants using spider silk coatings: immunohistochemical analysis of capsule formation]*. *Handchirurgie, Mikrochirurgie, plastische Chirurgie : Organ der Deutschsprachigen Arbeitsgemeinschaft für Handchirurgie : Organ der Deutschsprachigen Arbeitsgemeinschaft für Mikrochirurgie der Peripheren Nerven und Gefässe : Organ der V...* 2014. **46**(6): p. 336-41.
 107. Leal-Egana, A. and T. Scheibel, *Silk-based materials for biomedical applications*. *Biotechnology and applied biochemistry*, 2010. **55**(3): p. 155-67.
 108. Petzold, J., et al., *Surface Features of Recombinant Spider Silk Protein eADF4(kappa 16)-Made Materials are Well-Suited for Cardiac Tissue Engineering*. *Advanced Functional Materials*, 2017. **27**(36).
 109. Bauer, F., S. Wohlrab, and T. Scheibel, *Controllable cell adhesion, growth and orientation on layered silk protein films*. *Biomaterials Science*, 2013. **1**(12): p. 1244-1249.
 110. Leal-Egana, A., et al., *Interactions of Fibroblasts with Different Morphologies Made of an Engineered Spider Silk Protein*. *Advanced Engineering Materials*, 2012. **14**(3): p. B67-B75.
 111. Serra, C.A. and Z.Q. Chang, *Microfluidic-assisted synthesis of polymer particles*. *Chemical Engineering & Technology*, 2008. **31**(8): p. 1099-1115.
 112. Rao, J.P. and K.E. Geckeler, *Polymer nanoparticles: Preparation techniques and size-control parameters*. *Progress in Polymer Science*, 2011. **36**(7): p. 887-913.
 113. Bjornmalm, M., Y. Yan, and F. Caruso, *Engineering and evaluating drug delivery particles in microfluidic devices*. *Journal of Controlled Release*, 2014. **190**: p. 139-149.
 114. Song, F.F., et al., *Nanocomposite Hydrogels and Their Applications in Drug Delivery and Tissue Engineering*. *Journal of Biomedical Nanotechnology*, 2015. **11**(1): p. 40-52.
 115. Haynl, C., et al., *Microfluidics-Produced Collagen Fibers Show Extraordinary Mechanical Properties*. *Nano letters*, 2016. **16**(9): p. 5917-22.

116. Yaari, A., et al., *Wet Spinning and Drawing of Human Recombinant Collagen*. *Acs Biomaterials Science & Engineering*, 2016. **2**(3): p. 349-360.
117. Enomoto, S., et al., *Long-term patency of small-diameter vascular graft made from fibroin, a silk-based biodegradable material*. *Journal of Vascular Surgery*, 2010. **51**(1): p. 155-164.
118. Khil, M.S., et al., *Electrospun nanofibrous polyurethane membrane as wound dressing*. *Journal of Biomedical Materials Research Part B-Applied Biomaterials*, 2003. **67B**(2): p. 675-679.
119. Yang, F., et al., *Electrospinning of nano/micro scale poly(L-lactic acid) aligned fibers and their potential in neural tissue engineering*. *Biomaterials*, 2005. **26**(15): p. 2603-2610.
120. Yan, J., et al., *Effect of fiber alignment in electrospun scaffolds on keratocytes and corneal epithelial cells behavior*. *Journal of Biomedical Materials Research Part A*, 2012. **100A**(2): p. 527-535.
121. Scriven, L.E., *Physics and Applications of DIP Coating and Spin Coating*, in *Symposium H – Better Ceramics Through Chemistry III 1988*, Materials Research Society.
122. Vendra, V.K., Wu, L., Krishnan S., *Polymer Thin Films for Biomedical Applications in Nanomaterials for the Life Sciences Vol.5: Nanostructured Thin Films and Surfaces*, C.S.S.R. Kumar, Editor 2010, John Wiley & Sons.
123. Schacht, K., J. Vogt, and T. Scheibel, *Foams Made of Engineered Recombinant Spider Silk Proteins as 3D Scaffolds for Cell Growth*. *Acs Biomaterials Science & Engineering*, 2016. **2**(4): p. 517-525.
124. Ahmed, E.M., *Hydrogel: Preparation, characterization, and applications: A review*. *Journal of Advanced Research*, 2015. **6**(2): p. 105-121.
125. Teo, W.E. and S. Ramakrishna, *A review on electrospinning design and nanofibre assemblies*. *Nanotechnology*, 2006. **17**(14): p. R89-R106.
126. Lang, G., *Herstellung und Charakterisierung von Fasern aus rekombinanten Spinnenseidenproteinen und deren potentielle Applikationen*, in *Faculty of Engineering Science 2015*, University Bayreuth: Bayreuth. p. III, 167.
127. Fridrikh, S.V., et al., *Controlling the fiber diameter during electrospinning*. *Physical review letters*, 2003. **90**(14): p. 144502.
128. Wang, Y., et al., *Electrospun assembly: a nondestructive nanofabrication for transparent photosensors*. *Nanotechnology*, 2017. **28**(15): p. 155202.
129. Sirc, J., et al., *Controlled gentamicin release from multi-layered electrospun nanofibrous structures of various thicknesses*. *International journal of nanomedicine*, 2012. **7**: p. 5315-25.
130. Tan, E.P., S.Y. Ng, and C.T. Lim, *Tensile testing of a single ultrafine polymeric fiber*. *Biomaterials*, 2005. **26**(13): p. 1453-6.
131. Neugirg, B.R., et al., *AFM-based mechanical characterization of single nanofibres*. *Nanoscale*, 2016. **8**(16): p. 8414-26.
132. Liao, H., et al., *Influence of hydrogel mechanical properties and mesh size on vocal fold fibroblast extracellular matrix production and phenotype*. *Acta biomaterialia*, 2008. **4**(5): p. 1161-71.
133. Lee, K.Y. and D.J. Mooney, *Hydrogels for tissue engineering*. *Chemical reviews*, 2001. **101**(7): p. 1869-79.
134. Zuidema, J.M., et al., *A protocol for rheological characterization of hydrogels for tissue engineering strategies*. *Journal of biomedical materials research. Part B, Applied biomaterials*, 2014. **102**(5): p. 1063-73.
135. Groll, J., et al., *Biofabrication: reappraising the definition of an evolving field*. *Biofabrication*, 2016. **8**(1): p. 013001.
136. Ullah, M.W., et al., *Microbes as Structural Templates in Biofabrication: Study of Surface Chemistry and Applications*. *Acs Sustainable Chemistry & Engineering*, 2017. **5**(12): p. 11163-11175.
137. Moroni, L., et al., *Biofabrication: A Guide to Technology and Terminology*. *Trends in biotechnology*, 2018. **36**(4): p. 384-402.
138. Malda, J., et al., *25th Anniversary Article: Engineering Hydrogels for Biofabrication*. *Advanced Materials*, 2013. **25**(36): p. 5011-5028.
139. DeSimone, E., et al., *Biofabrication of 3D constructs: fabrication technologies and spider silk proteins as bioinks*. *Pure and Applied Chemistry*, 2015. **87**(8): p. 737-749.
140. Bajaj, P., et al., *Patterned three-dimensional encapsulation of embryonic stem cells using dielectrophoresis and stereolithography*. *Advanced healthcare materials*, 2013. **2**(3): p. 450-8.
141. Mazutis, L., et al., *Single-cell analysis and sorting using droplet-based microfluidics*. *Nature Protocols*, 2013. **8**(5): p. 870-891.
142. Cilurzo, F., et al., *Injectability evaluation: an open issue*. *AAPS PharmSciTech*, 2011. **12**(2): p. 604-9.
143. Paxton, N., et al., *Proposal to assess printability of bioinks for extrusion-based bioprinting and evaluation of rheological properties governing bioprintability*. *Biofabrication*, 2017. **9**(4): p. 044107.

144. Ribeiro, A., et al., *Assessing bioink shape fidelity to aid material development in 3D bioprinting*. Biofabrication, 2018. **10**(1).
145. Skardal, A. and A. Atala, *Biomaterials for integration with 3-D bioprinting*. Annals of biomedical engineering, 2015. **43**(3): p. 730-46.
146. Loo, Y., et al., *Peptide Bioink: Self-Assembling Nanofibrous Scaffolds for Three-Dimensional Organotypic Cultures*. Nano letters, 2015. **15**(10): p. 6919-25.
147. Schuurman, W., et al., *Gelatin-Methacrylamide Hydrogels as Potential Biomaterials for Fabrication of Tissue-Engineered Cartilage Constructs*. Macromolecular Bioscience, 2013. **13**(5): p. 551-561.
148. Murphy, S.V. and A. Atala, *3D bioprinting of tissues and organs*. Nature biotechnology, 2014. **32**(8): p. 773-85.
149. Koch, L., et al., *Laser printing of skin cells and human stem cells*. Tissue engineering. Part C, Methods, 2010. **16**(5): p. 847-54.
150. Wang, Z., et al., *A simple and high-resolution stereolithography-based 3D bioprinting system using visible light crosslinkable bioinks*. Biofabrication, 2015. **7**(4): p. 045009.
151. Fridlyanskaya, I., L. Alekseenko, and N. Nikolsky, *Senescence as a general cellular response to stress: A mini-review*. Experimental Gerontology, 2015. **72**: p. 124-128.
152. Holzl, K., et al., *Bioink properties before, during and after 3D bioprinting*. Biofabrication, 2016. **8**(3): p. 032002.
153. Blaeser, A., et al., *Controlling Shear Stress in 3D Bioprinting is a Key Factor to Balance Printing Resolution and Stem Cell Integrity*. Advanced Healthcare Materials, 2016. **5**(3): p. 326-333.
154. Chang, R. and W. Sun, *Effects of dispensing pressure and nozzle diameter on cell survival from solid freeform fabrication-based direct cell writing*. Tissue Engineering Part A, 2008. **14**(1): p. 41-48.
155. Tsigkou, O., et al., *Engineered vascularized bone grafts*. Proceedings of the National Academy of Sciences of the United States of America, 2010. **107**(8): p. 3311-3316.
156. Kolesky, D.B., et al., *3D Bioprinting of Vascularized, Heterogeneous Cell-Laden Tissue Constructs*. Advanced Materials, 2014. **26**(19): p. 3124-3130.
157. Kolesky, D.B., et al., *Three-dimensional bioprinting of thick vascularized tissues*. Proceedings of the National Academy of Sciences of the United States of America, 2016. **113**(12): p. 3179-3184.
158. Gao, Q., et al., *Coaxial nozzle-assisted 3D bioprinting with built-in microchannels for nutrients delivery*. Biomaterials, 2015. **61**: p. 203-215.
159. Gao, B., et al., *4D Bioprinting for Biomedical Applications*. Trends in Biotechnology, 2016. **34**(9): p. 746-756.
160. Wu, W., A. DeConinck, and J.A. Lewis, *Omnidirectional Printing of 3D Microvascular Networks*. Advanced Materials, 2011. **23**(24): p. H178-H183.
161. Trachtenberg, J.E., et al., *Effects of Shear Stress Gradients on Ewing Sarcoma Cells Using 3D Printed Scaffolds and Flow Perfusion*. Acs Biomaterials Science & Engineering, 2018. **4**(2): p. 347-356.
162. Xu, T., et al., *Hybrid printing of mechanically and biologically improved constructs for cartilage tissue engineering applications*. Biofabrication, 2013. **5**(1).
163. Brown, T.D., P.D. Dalton, and D.W. Hutmacher, *Direct Writing By Way of Melt Electrospinning*. Advanced Materials, 2011. **23**(47): p. 5651-+.
164. Kim, J.I. and C.S. Kim, *Nanoscale Resolution 3D Printing with Pin-Modified Electrified Inkjets for Tailorable Nano/Macrohybrid Constructs for Tissue Engineering*. Acs Applied Materials & Interfaces, 2018. **10**(15): p. 12390-12405.
165. Du, M., et al., *3D bioprinting of BMSC-laden methacrylamide gelatin scaffolds with CBD-BMP2-collagen microfibers*. Biofabrication, 2015. **7**(4): p. 044104.
166. Schacht, K., et al., *Biofabrication of Cell-Loaded 3D Spider Silk Constructs*. Angewandte Chemie-International Edition, 2015. **54**(9): p. 2816-2820.
167. Lang, G., S. Jokisch, and T. Scheibel, *Air Filter Devices Including Nonwoven Meshes of Electrospun Recombinant Spider Silk Proteins*. Jove-Journal of Visualized Experiments, 2013(75).
168. Hodgkinson, T., et al., *Rheology and electrospinning of regenerated bombyx mori silk fibroin aqueous solutions*. Biomacromolecules, 2014. **15**(4): p. 1288-98.
169. Jin, H.J., et al., *Electrospinning Bombyx mori silk with poly(ethylene oxide)*. Biomacromolecules, 2002. **3**(6): p. 1233-1239.
170. DeSimone, E., et al., *Aqueous electrospinning of recombinant spider silk proteins*. Materials science & engineering. C, Materials for biological applications, 2020. **106**: p. 110145.
171. Min, B.M., et al., *Regenerated silk fibroin nanofibers: water vapor-induced structural changes and their effects on the behavior of normal human cells*. Macromolecular bioscience, 2006. **6**(4): p. 285-92.
172. Huang, X.Y., et al., *Tunable Structures and Properties of Electrospun Regenerated Silk Fibroin Mats*

- Annealed in Water Vapor at Different Times and Temperatures*. Journal of Nanomaterials, 2014.
173. Hu, X., et al., *Regulation of Silk Material Structure by Temperature-Controlled Water Vapor Annealing*. Biomacromolecules, 2011. **12**(5): p. 1686-1696.
 174. Hu, X., D. Kaplan, and P. Cebe, *Determining beta-sheet crystallinity in fibrous proteins by thermal analysis and infrared spectroscopy*. Macromolecules, 2006. **39**(18): p. 6161-6170.
 175. Humenik, M., M. Mohrand, and T. Scheibel, *Self-Assembly of Spider Silk-Fusion Proteins Comprising Enzymatic and Fluorescence Activity*. Bioconjugate Chemistry, 2018. **29**(4): p. 898-904.
 176. Doblhofer, E. and T. Scheibel, *Engineering of Recombinant Spider Silk Proteins Allows Defined Uptake and Release of Substances*. Journal of Pharmaceutical Sciences, 2015. **104**(3): p. 988-994.
 177. DeSimone, E., K. Schacht, and T. Scheibel, *Cations influence the cross-linking of hydrogels made of recombinant, polyanionic spider silk proteins*. Materials Letters, 2016. **183**: p. 101-104.
 178. Elsner, M.B., et al., *Enhanced cellular uptake of engineered spider silk particles*. Biomaterials Science, 2015. **3**(3): p. 543-551.
 179. DeSimone, E., et al., *Recombinant spider silk-based bioinks*. Biofabrication, 2017. **9**(4): p. 044104.
 180. Solon, J., et al., *Fibroblast adaptation and stiffness matching to soft elastic substrates*. Biophysical Journal, 2007. **93**(12): p. 4453-4461.
 181. Yazawa, K., et al., *Influence of Water Content on the beta-Sheet Formation, Thermal Stability, Water Removal, and Mechanical Properties of Silk Materials*. Biomacromolecules, 2016. **17**(3): p. 1057-1066.
 182. Wozniak, M.A., et al., *Focal adhesion regulation of cell behavior*. Biochimica Et Biophysica Acta-Molecular Cell Research, 2004. **1692**(2-3): p. 103-119.
 183. Even-Ram, S. and K.M. Yamada, *Cell migration in 3D matrix*. Current Opinion in Cell Biology, 2005. **17**(5): p. 524-532.

5. Publications list

* Authors contributed equally to this work

1. **DeSimone E.**, Schacht K., Pellert A., Scheibel T. (2017). Recombinant spider silk-based bioinks. *Biofabrication* **9**, 044104. <https://doi.org/10.1088/1758-5090/aa90db>

2. **DeSimone E.***, Schacht K.* Scheibel T. (2016). Cations influence the cross-linking of hydrogels made of recombinant, polyanionic spider silk proteins. *Materials Letters* **183**, 101-104.
<https://doi.org/10.1016/j.matlet.2016.07.044>

3. Kumari S.*, Lang G.* **DeSimone E.**, Spengler C., Trossmann V., Lücker S., Hudel M., Jacobs K., Krämer N., Scheibel T. Engineered spider silk-based 2D and 3D materials prevent microbial infestation. Submitted to *Advanced Materials*, January 10 2020.

4. Thamm C., **DeSimone E.**, Scheibel T. (2017). Characterization of Hydrogels Made of a Novel Spider Silk Protein eMaSp1s and Evaluation for 3D Printing. *Macromolecular Bioscience* **17**, 1700141.
<https://doi.org/10.1002/mabi.201700141>

5. Aigner T.*, **DeSimone E.***, Scheibel T. (2018). Biomedical applications of recombinant silk. *Advanced Materials* **30**, 1704636. <https://doi.org/10.1002/adma.201704636>

6. **DeSimone E.***, Schacht K.*, Jungst T., Groll J., Scheibel T. (2015). Biofabrication of 3D Constructs: Fabrication Technologies and Spider Silk Proteins as Bioinks. *Pure and Applied Chemistry* **87**, 737-749.
<https://doi.org/10.1515/pac-2015-0106>

6. Individual contribution to joined publications and manuscripts

* Authors contributed equally to this work

1. DeSimone E., Schacht K., Pellert A., Scheibel T. (2017). Recombinant spider silk-based bioinks. *Biofabrication* **9**, 044104. <https://doi.org/10.1088/1758-5090/aa90db>

The concept for the research publication was developed by Kristin Schacht, Thomas Scheibel and myself. eADF4(C16)-RGD was produced and purified by Johannes Diehl and Andreas Schmidt. Cell culture experiments for unprinted bioinks were carried out by Alexandra Pellert, Kristin Schacht and myself. Cell culture studies for printed bioinks were conducted by Alexandra Pellert and myself. Studies on gelation kinetics, degradation, rheology and printability of bioinks were conducted by myself. The manuscript (text and figures) was created by Kristin Schacht and myself. Prof. Dr. Thomas Scheibel supervised the project, and contributed to the completion of the manuscript.

2. DeSimone E.*, Schacht K.* Scheibel T. (2016). Cations influence the cross-linking of hydrogels made of recombinant, polyanionic spider silk proteins. *Materials Letters* **183**, 101-104. <https://doi.org/10.1016/j.matlet.2016.07.044>

The concept for the research publication was developed through equal contribution of all authors. eADF4(C16)-RGD was produced and purified by Johannes Diehl and Andreas Schmidt. Production of hydrogel samples, gelation kinetics and deformation tests were completed by Kristin Schacht and myself. FTIR measurements and analysis, transmission electron microscopy (TEM), and shear rate tests were conducted by Kristin Schacht. The manuscript (text and figures) was created by Kristin Schacht and myself. Prof. Dr. Thomas Scheibel supervised the project and contributed to the completion of the manuscript.

3. Kumari S.*, Lang G.* **DeSimone E.**, Spengler C., Trossmann V., Lücker S., Hudel M., Jacobs K., Krämer N., Scheibel T. Engineered spider silk-based 2D and 3D materials prevent microbial infestation. Submitted to *Advanced Materials*, January 10 2020.

The concept for the research publication was developed by Gregor Lang, Sushma Kumari and Thomas Scheibel. Gregor Lang prepared the different 2D samples as well as performed SEM and analyzed the data. Sushma Kumari performed the in vitro bacteriostatic/fungistatic experiments and coculture experiments with *E. coli* and *P. pastoris*. The co-culture experiments were designed by myself and I did the 3D bioprinting. Vanessa Trossmann cloned and produced omega variant of engineered spider silk. Susanne Lücker, Martina Hudel and Norbert Krämer carried out *in vitro* experiments of *S. mutans* and *C. albicans*. Christian Spengler and Karin Jacobs prepared bacterial probes and performed force-distance measurements. The manuscript was prepared by Gregor Lang and Sushma Kumari, with input from Christian Spengler, Karin Jacobs and myself. Dr. Thomas Scheibel supervised the project and contributed to the completion of the manuscript.

4. Thamm C., **DeSimone E.**, Scheibel T. (2017). Characterization of Hydrogels Made of a Novel Spider Silk Protein eMaSp1s and Evaluation for 3D Printing. *Macromolecular Bioscience* **17**, 1700141. <https://doi.org/10.1002/mabi.201700141>

The concept for the publication was developed by Christopher Thamm and Prof. Dr. Thomas Scheibel. All recombinant proteins were produced, purified and prepared into samples by Christopher Thamm. SEM imaging was completed with Dr. Hendrik Bargel, TEM imaging with Tamara Aigner, and AFM with Dr. Martin Humenik. Protocols for determining rheological behavior and recovery were designed by myself, and measurements and data analysis were completed by Christopher Thamm and myself. Most of the manuscript was prepared by Christopher Thamm, and I contributed text on methods, results and discussion related to the rheological measurements. Prof. Dr. Thomas Scheibel supervised the project and contributed to the completion of the manuscript.

5. Aigner T.*, **DeSimone E.***, Scheibel T. (2018). Biomedical applications of recombinant silk. *Advanced Materials* **30**, 1704636. <https://doi.org/10.1002/adma.201704636>

The concept for the publication was developed through equal contribution of all authors. The manuscript (text and figures) was created by Tamara Aigner and myself. Thomas Scheibel contributed to the critical critique of the outlook in the field and completion of the manuscript.

6. **DeSimone E.***, Schacht K.*, Jungst T., Groll J., Scheibel T. (2015). Biofabrication of 3D Constructs: Fabrication Technologies and Spider Silk Proteins as Bioinks. *Pure and Applied Chemistry* **87**, 737-749. <https://doi.org/10.1515/pac-2015-0106>

The concept for the publication was developed by Kristin Schacht, Thomas Scheibel and myself. The manuscript (text and figures) was created by Kristin Schacht and myself. Tomasz Jungst, Prof. Dr. Jürgen Groll and Thomas Scheibel participated in scientific discussions and contributed to the completion of the manuscript.

Publications

Part 1. Recombinant spider silk-based bioinks

DeSimone E., Schacht K., Pellert A., Scheibel T.

Published in *Biofabrication*, **9**, 044104
(2017)

Reprinted with kind permission from IOP Publishing

Biofabrication



PAPER

Recombinant spider silk-based bioinks

RECEIVED
20 April 2017

REVISED
17 August 2017

ACCEPTED FOR PUBLICATION
4 October 2017

PUBLISHED
14 November 2017

Elise DeSimone, Kristin Schacht¹, Alexandra Pellert and Thomas Scheibel

Lehrstuhl Biomaterialien, Bayreuther Zentrum für Kolloide und Grenzflächen (BZKG), Bayreuther Zentrum für Bio-Makromoleküle (biomac), Bayreuther Zentrum für Molekulare Biowissenschaften (BZMB), Bayreuther Materialzentrum (BayMAT), Bayerisches Polymerinstitut (BPI) Universitätsstraße 30, Universität Bayreuth, Bayreuth D-95447, Germany

¹ Present address: AMSilk GmbH, Am Klopferspitz 19 im IZB, D-82152 Planegg/München, Germany.

E-mail: thomas.scheibel@bm.uni-bayreuth.de

Keywords: spider silk, engineered protein, recombinant protein, self-assembly, hydrogel, dispense plotting

Supplementary material for this article is available [online](#)

Abstract

Bioinks, 3D cell culture systems which can be printed, are still in the early development stages. Currently, extensive research is going into designing printers to be more accommodating to bioinks, designing scaffolds with stiff materials as support structures for the often soft bioinks, and modifying the bioinks themselves. Recombinant spider silk proteins, a potential biomaterial component for bioinks, have high biocompatibility, can be processed into several morphologies and can be modified with cell adhesion motifs to enhance their bioactivity. In this work, thermally gelled hydrogels made from recombinant spider silk protein encapsulating mouse fibroblast cell line BALB/3T3 were prepared and characterized. The bioinks were evaluated for performance *in vitro* both before and after printing, and it was observed that unprinted bioinks provided a good platform for cell spreading and proliferation, while proliferation in printed scaffolds was prohibited. To improve the properties of the printed hydrogels, gelatin was given as an additive and thereby served indirectly as a plasticizer, improving the resolution of printed strands. Taken together, recombinant spider silk proteins and hydrogels made thereof show good potential as a bioink, warranting further development.

1. Introduction

Tissue-like constructs prepared by 3D bioprinting (3DBP) are now beginning to appear in pre-clinical and clinical testing next to other products made by other particularly promising techniques such as organ decellularization and recellularization [1]. However, to achieve 3DBP for personalized medicine, the constituent components of the entire procedure, from imaging of patient to final product, require a far deeper understanding. One of the most complicated and researched steps being bioink design, characterization and implementation [2, 3].

Bioinks are cell-encapsulating biomaterials used in the 3DBP process and must therefore be suitable for both 3D cell culture and printing [4]. For 3D cell culture, no matter the final objective, encapsulated cells must be viable as well as able to attach, spread and proliferate, and there must be proper nutrient and waste exchange [5]. Bioinks should also not induce any strange, unstable or pathological phenotypes in cells. This depends not only on the selected biomaterial, but

on the chosen cell type as well: for example, in studies by Engler and colleagues comparing different cell types on the same substrates, it was shown that mesenchymal stem cells (MSCs) are extremely sensitive to tissue-level elasticity, myoblasts were less sensitive than MSCs to substrate stiffness but required specific ECM coatings to form striated myotubes, and fibroblasts in general showed the least sensitivity between the different culturing surfaces [6, 7]. In other words, for each bioink, there are specific requirements that depend on the selected cell types and the tissue that should be replicated. Some of the design attributes that must be considered, amongst others, include cell-binding peptide sequences, charge of material, mesh size, triggering of vascularization, and mechanical behavior [8]. Mechanical properties are one of the most challenging properties of a bioink to be optimized, as bioinks must both replicate tissue stiffness and also be printable. 'Printable' meaning that the material deforms under process-relevant shear stress, but upon the removal of that stress it should stop flowing [9].

In summary, there are many characteristics of bioinks which should be controlled and measured; ideally before, during, and after 3DBP. These include properties of the biomaterial (e.g. stiffness, degradation, and mesh size) as well as the cell response (e.g. attachment, proliferation, biodegradation, differentiation). In terms of physically cross-linked bioinks, one of the greatest challenges is that these tend to be softer, and usually require some additional modification to be printable. For example, in one of the first publications using a thermally gelled bioink, they used a heated gelatin bath [10]. In a more recent study, a two component bioink combining an engineered peptide with alginate was used to combine the benefits of cross-linking before and after the printing process, where it was shown that the post-printing cell viability was enhanced compared to alginate-alone [11]. Discussing the several bioinks which have already been established is out of the context of this paper, thus authors refer readers to comprehensive reviews [3, 4, 9, 12].

The recombinant spider silk protein eADF4(C16) is based on the repetitive core sequence of *Araneus diadematus* dragline silk fibroin 4 and comprises a consensus module repeated 16 times [13, 14]. eADF4(C16) was shown to be suitable for medical applications exhibiting no toxicity and low to no immunogenicity, can be formed into several morphologies, and also performs particularly well compared to other native and engineered silks [15–17]. Additionally, the protein could be modified to include integrin binding peptides, for example the –RGD peptide sequence, and thereby promoted cell attachment and proliferation [18]. In more recent work, eADF4(C16) in the form of a hydrogel was successfully employed as a bioink for 3DBP with a highlight of ~97% cell viability after printing [19]. The material properties were further characterized, in particular observing how the content of solutions carrying cations (i.e. cell culture medium) affects the properties of the hydrogels [20]. Although these studies together provide a strong foundation for the use of recombinant spider silk proteins and their variants as biomaterials for bioinks, it was also clear that the bioinks must be improved (e.g. for cell viability after encapsulation, printing strand resolution) and also more thoroughly characterized. To improve the printing resolution, gelatin was tested as an additive. Gelatin is de-natured collagen which has a slightly positive charge (depending on gelatin type and pH), thermally gels at room temperature, and is hydrophilic. Gelatin has therefore been used in other bioinks to improve the printability such as bioinks based on silk fibroin [21] and alginate [22].

The broad objective of this work was to improve and characterize the performance of recombinant spider silk-based bioinks, not to design a particular tissue. Thus a ‘work horse’ cell line, BALB/3T3 mouse fibroblasts, was chosen. The biomaterial variations included eADF4(C16) and eADF4(C16)-RGD either with or without addition of

gelatin in a weight-to-weight ratio of 200 mg of recombinant spider silk protein to 1 mg of gelatin (i.e. 200-fold excess of recombinant spider silk protein). Recombinant spider silk bioinks were characterized for the first time for long-term proliferation of mouse fibroblasts (15–18 d), the slow biodegradability of the bioink, the recovery of the hydrogel after a large strain, high shear deformation, and the printing resolution was improved to have fiber strands nearly half the diameter of previously published results. These recombinant spider silk protein-based bioinks are competitive with other hydrogel-based bioinks for the properties evaluated, and should be considered for specific applications in the future.

2. Materials and methods

There were several bioink formulations utilized for this work. Therefore, a legend was made and the abbreviations will be used throughout the rest of this text. In cases that hydrogels were prepared without cells, ‘B’ (for BALB/3T3) will not be included in the abbreviation.

Legend:

20 mg ml ⁻¹ eADF4(C16) (15% DMEM),	
1 × 10 ⁶ BALB3T3 ml ⁻¹ of hydrogel	2C-D15-B
30 mg ml ⁻¹ eADF4(C16) (15% DMEM)	
1 × 10 ⁶ BALB3T3 ml ⁻¹ of hydrogel	3C-D15-B
40 mg ml ⁻¹ eADF4(C16) (15% DMEM)	
1 × 10 ⁶ BALB3T3 ml ⁻¹ of hydrogel	4C-D15-B
30 mg ml ⁻¹ eADF4(C16) (15% DMEM)	
1 × 10 ⁶ BALB3T3 ml ⁻¹ of hydrogel	3C-D5-B
30 mg ml ⁻¹ eADF4(C16) (5% DMEM),	
1 × 10 ⁶ BALB3T3 ml ⁻¹ of hydrogel	3C-D5-g-B
0.15 mg ml ⁻¹ gelatin	
20 mg ml ⁻¹ eADF4(C16)-RGD (15% DMEM),	
1 × 10 ⁶ BALB3T3 ml ⁻¹ of hydrogel	2R-D15-B
30 mg ml ⁻¹ eADF4(C16)-RGD (15% DMEM)	
1 × 10 ⁶ BALB3T3 ml ⁻¹ of hydrogel	3R-D15-B
20 mg ml ⁻¹ eADF4(C16)-RGD (5% DMEM),	
1 × 10 ⁶ BALB3T3 ml ⁻¹ of hydrogel	2R-D5-B
20 mg ml ⁻¹ eADF4(C16)-RGD (5% DMEM),	
1 × 10 ⁶ BALB3T3 ml ⁻¹ of hydrogel	2R-D5-g-B
0.1 mg ml ⁻¹ gelatin	

2.1. Hydrogel preparation

The recombinant spider silk protein eADF4(C16) consists of 16 repeats of module C (sequence: GSSAAAAAASGPGGYGPENQGPSGGYGP GP), which mimics the repetitive core sequence of dragline silk fibroin 4 (ADF4) of the European garden spider *Araneus diadematus* [13, 14]. eADF4(C16) (MW: 47 698 g mol⁻¹) and eADF4(C16)-RGD (MW: 48 583 g mol⁻¹) were produced and purified as described previously [13, 18]. All protein variants were stored as lyophilized particles. The particles were dissolved in 6 M guanidinium thiocyanate at 4 mg ml⁻¹ and dialyzed against 10 mM Tris/HCl, pH 7.5 overnight at room temperature using dialysis

Table 1. Optimized cell-seeding protocol for different formulations of eADF4(C16) and (C16)-RGD-based bioinks. After the addition of cells, all formulations were incubated at 37 °C, 95% relative humidity overnight before adding fresh media on the next day.

Bioink	Time (h)						
	0.0	0.5	1.0	1.5	2.0	2.5	3.0
2C-D15-B				After 3 h at 37 °C, 95% r. h. add cells			
3C-D15-B				After 3 h at 37 °C, 95% r. h. add cells			
4C-D15-B		After 1.5 h at room temperature, add cells				Incubate at 37 °C, 95% r. h.	
3C-D5-B				After 3 h at 37 °C, 95% r. h. add cells			
3C-D5-g-B		After 2.5 h at 37 °C, 95% r. h. add 1.5 mg ml ⁻¹ gelatin in 10% v/v (final concentration 0.15 mg ml ⁻¹)					Further 0.5 h, add cells
2R-D15-B		After 1.5 h at 4 °C, add cells				Incubate at 37 °C, 95% r. h.	
3R-D15-B				Immediately add cells and incubate at 37 °C, 95% r. h.			
2R-D5-B			After 1.5 h at 4 °C, add cells			Incubate at 37 °C, 95% r. h.	
2R-D5-g-B		After 1 h at 4 °C, add 1 mg ml ⁻¹ gelatin in 10% v/v (final concentration 0.10 mg ml ⁻¹)		Further 0.5 h, add cells		Incubate at 37 °C, 95% r. h.	

membranes with a molecular weight cutoff of 6000–8000 Da with three buffer changes. Subsequent dialysis against 25% w/v poly(ethyleneglycol) (PEG, 35 000 g mol⁻¹), 10 mM Tris/HCl pH 7.5 with a volume extent of PEG between 50 and 400 was used to prepare high concentration protein solutions as described previously [15]. For the pre-gelling protocol, refer to table 1. Gelatin from bovine skin, Type B (~225 g Bloom, G9391, Sigma-Aldrich, Germany) was dissolved for 30 min in pre-warmed 10 mM Tris/HCl, pH 7.5 and sterile filtered before adding to the concentrated recombinant spider silk solution in a weight-to-weight ratio of 200 mg of recombinant spider silk protein to 1 mg of gelatin. Cells were added in 5%- or 15% vol/vol Dulbecco's modified eagle medium (DMEM) (Biochrom, Germany) supplemented with 10% vol/vol fetal bovine serum (Biochrom, Germany), 1% vol/vol GlutaMAX (Gibco, USA) and 0.1% vol/vol gentamicin sulphate (Sigma-Aldrich, Germany). After incubation at 37 °C, 95% relative humidity (r. h.) overnight, supplemented DMEM was added.

2.2. Transmission electron microscopy (TEM)

For TEM analysis, 3C-D5-g and 2R-D5-g hydrogels were diluted to 1 mg ml⁻¹. 5 µl of the diluted hydrogel was scattered on 100-mesh Formvar-coated copper TEM grids (Plano GmbH, Germany), incubated for 10 min, washed two times using 5 µl of double distilled water (ddH₂O), and fibrils were negatively stained using 5 µl 2% uranyl acetate solution for 2 min. Samples were allowed to dry for at least 24 h at ambient temperature before imaging. TEM imaging of dry samples was performed with a JEM-2100 transmission electron microscope (JEOL, Tokyo, Japan) operated at 80 kV and equipped with a 4000 × 4000 charge-coupled device camera (UltraScan 4000; Gatan, Pleasanton, CA).

2.3. Turbidity

To analyze the gelation kinetics of different hydrogel preparations, turbidity changes upon gelation were monitored at 570 nm using a Microplate Reader (Mithras LB 940, Berthold Technologies, Germany) in absorbance mode. Sample volume was 100 µl per well in clear-bottom 96-well plates (Nunc, Germany). A representative sample was used for 3C-5D. A sample number of 3 ($n = 3$) was used for every other experimental group.

2.4. Rheology

Stress-strain curves of different hydrogel preparations were analyzed according to a protocol established previously [15, 19, 20]. Briefly, samples were measured using an AR-G2 rheometer (TA instruments, New Castle, DE, USA) for 10 min at a constant shear rate of $3.0 \times 10^{-3} \text{ s}^{-1}$ with 25 mm plate geometry and with a modification of a 100 µm gap. Sample volumes prepared were 200 µl, and samples were allowed to equilibrate at room temperature before measurement for at least 30 min. A solvent trap with a wet sponge was used to minimize evaporation. Young's modulus, or the elastic (E) modulus, was calculated as described in a previous publication [15] according to Hooke's law using the Poisson's ratios published by Urayama *et al* 1993 [23]. A sample number of $n = 3-4$ was used for each experimental group. Additionally, as quality control, the shear-thinning behavior of hydrogels was confirmed by measuring the effect of shear rate on the viscosity using the steady state flow where the shear rate was increased from 0.01 to 500 s⁻¹. 200 µl samples were measured with 25 mm plate geometry and a 100 µm gap. One sample was measured per experimental group. Only one sample was measured per experimental group as these data have been well-established in previous works, and no abnormal results were collected for control or experimental

Table 2. Printing parameters used for production of recombinant spider silk bioink scaffolds. For every experimental group a feed rate (a velocity) of 40 mm s^{-1} was used.

Bioink	Pressure (bar)	Dosing distance (mm)	Valve opening time (μs)
3C-5D-B	2	0.12	200
3C-5D-g-B	1–2	0.10	200
2R-5D-B	0.5	0.12	175
2R-5D-g-B	0.5	0.12	150

groups [19, 20]. Samples were allowed to equilibrate at room temperature (climate controlled at 20°C) before measurement for at least 30 min, and were measured under controlled temperature (25°C).

Hydrogels were additionally evaluated for recovery by measuring the storage and loss modulus before and after a large deformation using the following protocol: the first step was to measure before deformation for 10 min (600 s) by small oscillations (10 rad s^{-1} , 0.05 strain). The linear strain value was determined by the stress–strain tests and the shear rate from data previously reported [19]. The second step was the large deformation step in a flow mode for 40 s^{-1} shear rate for 1 s. The third step was to measure the modulus after the deformation over a period of 300 s by small oscillations (10 rad s^{-1} , 0.05 strain). A sample number of $n = 3$ was used for each experimental group. Samples were allowed to equilibrate at room temperature (climate controlled at 20°C) before measurement for at least 30 min, and were measured under controlled temperature (25°C).

2.5. 3D bioprinting (3DBP)

The 3D Discovery (RegenHU, Villaz-Saint-Pierre, Switzerland) was operated according to manufacturer's instruction with the micro-valve print-head using a needle with an inner diameter of 0.33 mm. Two-layer scaffolds, layer thickness of 0.24 mm, were printed as an automatically filled 12 mm circle with 1.5 mm spacing, one layer with vertical and the other with horizontal strands. Printing parameters for each bioink formulation are summarized below in table 2.

2.6. Stereomicroscopy

A Leica M205C stereomicroscope (Wetzlar, Germany) was used to capture images of printed scaffolds. The images of hydrogels were taken using light reflected from dark field with a $0.63\times$ objective equipped with a polarization lens. One representative scaffold was imaged per group, and this same scaffold was imaged at each time point with the exception of immediately after printing, where non-sterile conditions were used.

2.7. BALB/3T3 cultivation

BALB/3T3 mouse fibroblasts (European Collection of Cell Cultures) were cultivated in DMEM (Biochrom,

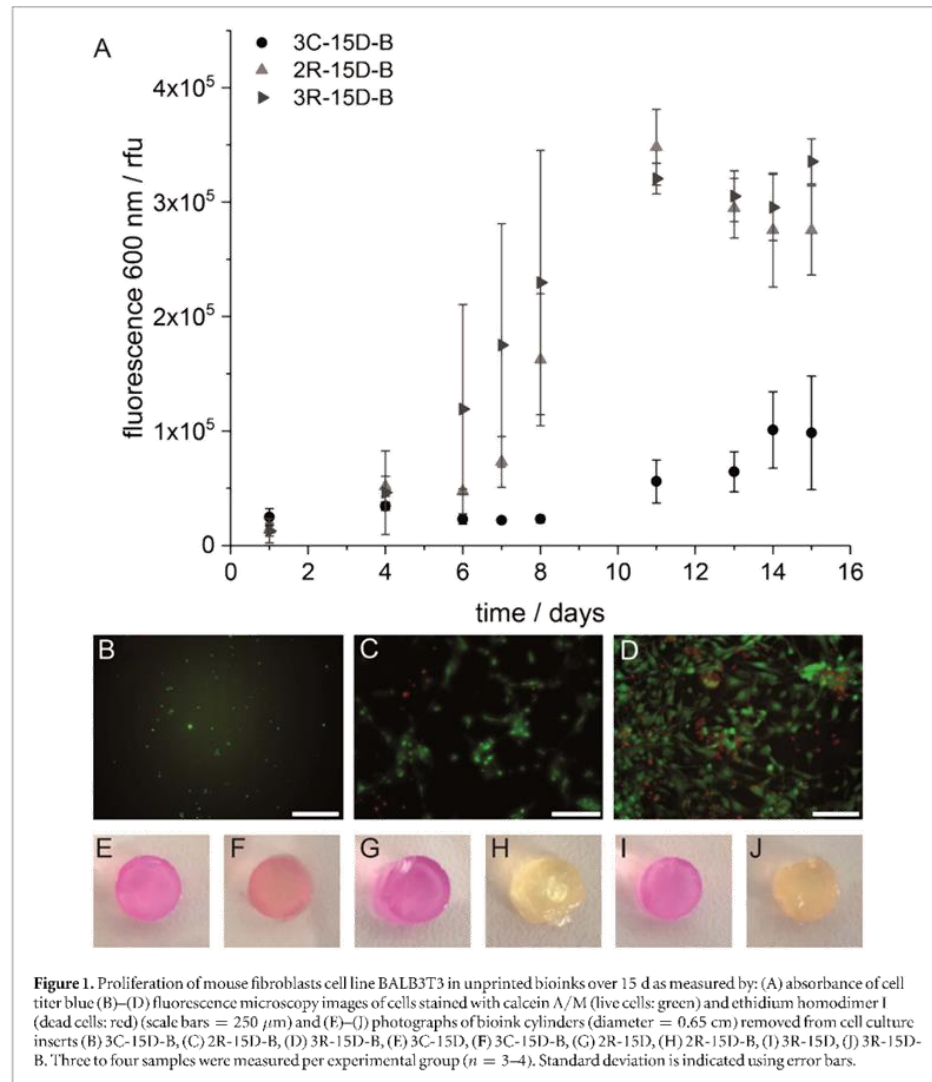
Germany) supplemented with 10% vol/vol fetal bovine serum (Biochrom, Berlin, Germany), 1% v/v GlutaMAX (Gibco, USA) and 0.1% vol/vol gentamicin sulphate (Sigma-Aldrich, Germany) in controlled atmosphere of 5% CO_2 , 95% relative humidity and 37°C . Viability and number of cells were analyzed using trypan blue (Sigma-Aldrich, UK) and a Neubauer chamber (Laboroptik, UK). 3D bioprinted scaffolds were cultured in μ -dish^{35mm,high} glass bottom (IBIDI, Germany) with 2 ml of completed DMEM.

2.8. Live/dead staining

Different bioink preparations were either pipetted into an eight-well chamber (IBIDI, Germany) or 3D bioprinted into μ -dish^{35mm,high} glass bottom (IBIDI, Germany) and cultivated under controlled atmosphere of 5% CO_2 , 95% relative humidity and 37°C for 15 or 18 d. Cell culture medium was changed every second day. For the live/dead assay cells were stained with calcein acetoxymethyl ester (calcein A/M) and ethidium homodimer-I (EthD-I) (Invitrogen, USA) after 24 h and after 15 d of incubation for unprinted bioink, or 18 d for printed bioink. A solution containing calcein A/M at a final concentration of $2 \mu\text{M}$ and EthD-I at a final concentration of $4 \mu\text{M}$ in phosphate buffered saline (PBS) was added to samples and incubated for 30–45 min at 37°C . At the end of incubation, the staining solution was removed and fresh PBS was added. Live and dead cells were visualized using a fluorescence microscope (Leica DMi8, Wetzlar, Germany) and processed using either Leica Application Suite or ImageJ.

2.9. Cell titer-blue

Unprinted bioink solutions with encapsulated BALB3T3 ($1 \times 10^6 \text{ cells ml}^{-1}$ of hydrogel) were placed in Millicell inserts with $5 \mu\text{m}$ pore diameter, and the hydrogels were formed at 37°C . For cell culturing of printed bioink, scaffolds were directly printed into μ -dish^{35mm,high} glass bottom (IBIDI, Germany). To analyze cell proliferation, different bioink preparations were incubated for 2.5 h with 10% v/v CellTiter-Blue reagent (Promega, Germany); in the case of unprinted scaffolds this was prepared fresh, and in the case of printed scaffolds, to avoid unnecessary mechanical stress from excessive pipetting, the CellTiter-blue reagent was added directly to the Petri dishes ($200 \mu\text{l}$ of reagent for 2 ml of DMEM). Cell proliferation was quantified by determining the fluorescence intensity of resorufin (ex 530 nm ; em 590 nm) by using a plate reader (Mithras LB 940, Berthold Technologies, Germany) on $100 \mu\text{l}$ samples. The scaffolds were then washed with PBS and incubated in fresh medium under controlled atmosphere until the next day. The proliferation was analyzed for 15 d (unprinted hydrogel) or 18 d (printed scaffolds), and



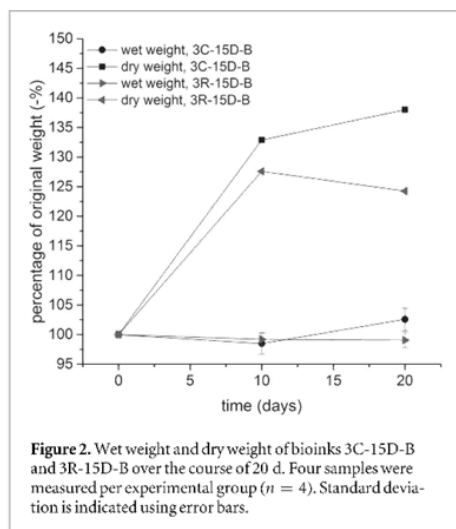
the test was repeated twice with three to four replicates per experiment ($n = 3\text{--}4$ per experimental group).

3. Results and discussion

3.1. Characterization of bioinks before printing

Recombinant spider silk protein eADF4(C16) was first prepared as hydrogels using 10% methanol as a solvent, with or without cross-linking by ammonium peroxydisulfate (APS) [24]. In a modified protocol introduced by Schacht and Scheibel (2011), a fully aqueous process was implemented to assemble the hydrogels. Rheological analysis of the hydrogels revealed that the shear elastic modulus could be tuned within the range of human tissues by altering protein concentration or by using APS as a cross-linker [15].

Therefore, due to the high biomedical potential of these proteins [16, 18] as well as relevant mechanical properties and aqueous processing of hydrogels [15], eADF4(C16) and eADF4(C16)-RGD hydrogels were recently utilized as a cell-encapsulating bioink [19]. The recombinant spider silk-based bioinks were printable, and showed high cell viability immediately after printing ($\sim 97\%$). However, the initial cell viability after encapsulation was low ($\sim 70\%$), the cells were cultured for a short period of 7 d where no proliferation was observed, and the printing resolution was reported as 654 μm (compared to average, published values of 200, or a range of 100–500 μm for other bioinks) [3, 4, 25]. The first objective of this work was to improve the cell encapsulation process, and to better characterize the bioinks before printing.



In solution, eADF4(C16) can convert from disordered structure into β -sheet rich fibrils, and this self-assembly process is triggered by temperature, kosmotropic phosphate ions and increased protein concentration [15, 26]. It was hypothesized that this initial nucleation process, as well as an extended period without an insoluble network to provide attachment sites (solution starts to gel after 4 h), were responsible for the cell death during encapsulation. Similar results were also observed in the case of a different self-assembling, beta-sheet forming peptide. In the latter case it was seen that the same population of chondrocytes had much higher viability when encapsulated in an agarose hydrogel than in the peptide-based one (~95% versus ~80% viability) [27]. Therefore, for a certain amount of time as indicated by data collected on gelation rate, (figure 3(C), [20]), the solutions were first pre-gelled without cells, and then the cells were encapsulated at a later time (table 1). The cell viability increased to nearly 100% as measured by live/dead staining, which was relatively independent of protein concentration (figure S1 is available online at stacks.iop.org/BF/9/044104/mmedia). This therefore makes the recombinant spider silk-based bioinks competitive with other, more common biomaterials for example alginate (~90%) [28], agarose (~95%) [27] and gelatin (~98%) [29]. With the cell viability optimized, cell proliferation was first tested in unprinted bioinks for 15 d (figure 1).

As expected, there was significant proliferation and spreading of BALB3T3 cells only in eADF4(C16)-RGD hydrogels [18, 19, 30]. The lack of proliferation in eADF4(C16) is also consistent with another study where primary dermal fibroblasts were encapsulated in either alginate, fibrin or fibrin-alginate hydrogels. The fibroblasts exhibited a spherical shape in alginate hydrogels, this being a good comparison as alginate is also an anionic polymer with no natural cell-binding

sequences [31]. However, interestingly, even with no spreading or proliferation, cells encapsulated in 30 mg ml^{-1} eADF4(C16) hydrogels remained viable (figure 1(B)). Although the rounded shape of the fibroblasts indicates that eADF4(C16) did not provide sites for focal adhesion, which regulate cell behaviors such as morphological changes and migration, it is possible that the network of spider silk proteins could be relatively dense, which is allowing for some kind of cell contraction and physical support [32, 33]. Compared to 2D cell culture, the speed of cell migration in a 1D or 3D environment is far less dependent on the density of cell-binding ligands; in the confined environment, usually cell contraction is responsible for cell mobility [34]. Further, this type of result has also been observed in alginate-gelatin hydrogels; after 7 d in culture there was no obvious cell spreading or proliferation, but the cells also remained viable [35].

Although there was good cell viability after 15 d, it could be clearly seen from the yellow hue of the pH indicator (phenol red) present within the DMEM that there was not efficient transport of nutrients and waste in the solid hydrogel cylinder, (figures 1(E)–(J)), which would also explain the plateau in the proliferation in the case of eADF4(C16)-RGD. Further, there was no clear degradation of the hydrogels over a 20 d period, which would also reduce the proliferation rate (figure 2).

Interestingly there was nearly no additional swelling of the hydrogel in DMEM. There seemed to be an increase in the dry weight, but this likely originated from salt or protein deposition as opposed to an increase in biomass, as there was no proliferation in eADF4(C16), and the increase in dry mass was comparable between both groups. On one side this data is surprising as it is known that encapsulated fibroblasts accelerate degradation [36], however on the other side it is expected as it is also well-known that silk tends to degrade slowly *in vitro*, even in the presence of highly concentrated protease mixtures [37–39]. In general, this data indicates that these hydrogels are more suitable for applications where slow degradation is required, such as in long-term drug release and slow regenerating tissues.

In first printing attempts of eADF4(C16) the reported resolution was $654 \mu\text{m}$ [19], which falls short of average published values of $200 \mu\text{m}$ [3, 4, 25]. The printability of the eADF4(C16) could not be significantly improved by reducing the DMEM content and altering the printing parameters (data not shown), therefore, we chose to continue with 5% DMEM content and 30 mg ml^{-1} eADF4(C16). When DMEM was added, 20 mg ml^{-1} eADF4(C16)-RGD hydrogels were found to behave nearly the same as 30 mg ml^{-1} eADF4(C16) hydrogels (figure S2). Further, in a previous study it was determined that 30 mg ml^{-1} eADF4(C16) hydrogels had a lower storage and loss modulus than 30 mg ml^{-1} eADF4(C16)-RGD hydrogels (prepared without DMEM) [19]. Therefore, 30 mg ml^{-1} eADF4

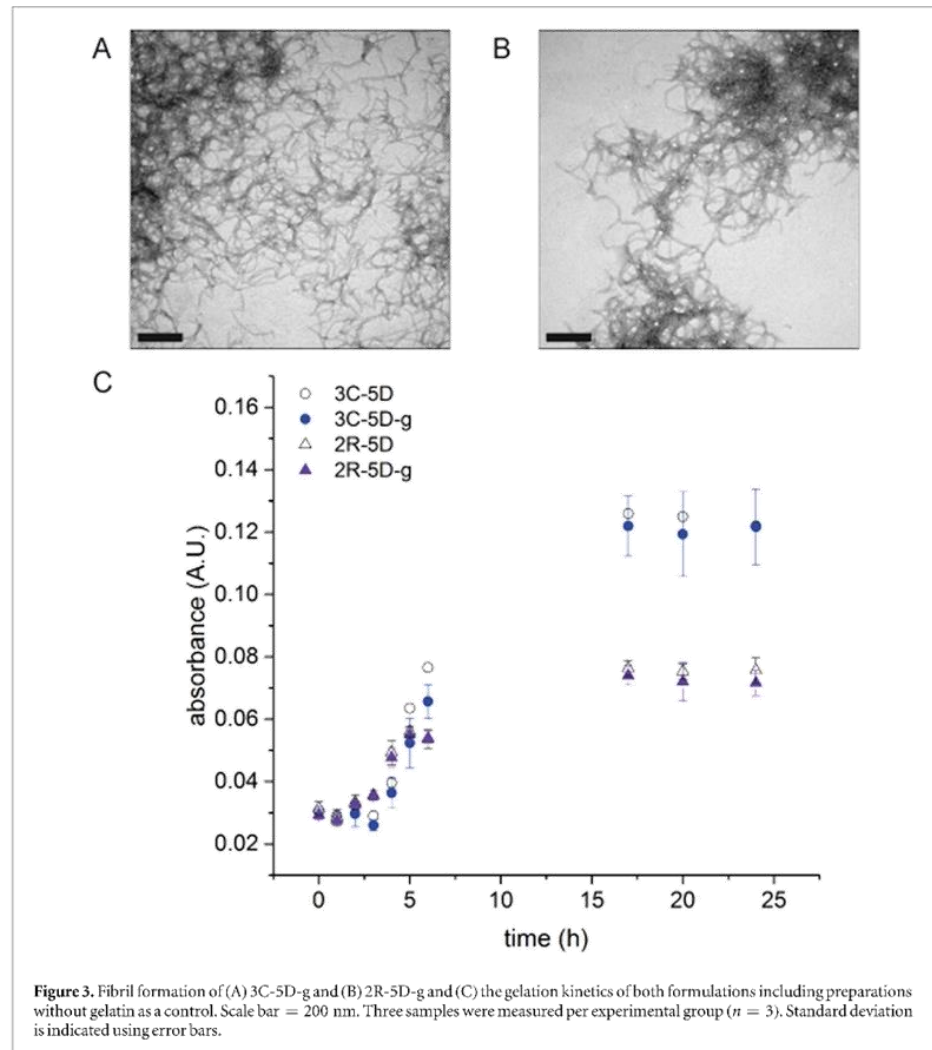


Figure 3. Fibril formation of (A) 3C-5D-g and (B) 2R-5D-g and (C) the gelation kinetics of both formulations including preparations without gelatin as a control. Scale bar = 200 nm. Three samples were measured per experimental group ($n = 3$). Standard deviation is indicated using error bars.

(C16) and 20 mg ml^{-1} eADF4(C16)-RGD were selected for use for the rest of this study, and shown to have comparable elastic moduli (figure 4). To be comparable to previous proliferation tests, 1×10^6 BALB3T3 cells ml^{-1} of hydrogel was used. In an attempt to improve the printability, there were two additional formulations where gelatin was added to the bioink in a weight-to-weight-ratio of 200:1 (200 mg of eADF4(C16) to 1 mg of gelatin). Gelatin was the chosen material due to its tendency to bind water molecules (and therefore indirectly acting as a plasticizer) and previous success when combined with silk for other applications [21, 40].

For the following experiments, 30 mg ml^{-1} eADF4(C16) containing 1×10^6 BALB3T3 cells ml^{-1} in 5% vol/vol DMEM in the absence or presence of 0.15 mg ml^{-1} gelatin, and 20 mg ml^{-1} eADF4(C16)-RGD containing 1×10^6 BALB3T3 cells ml^{-1} in 5%

vol/vol DMEM in the absence or presence of 0.1 mg ml^{-1} gelatin were evaluated for suitability as bioinks. First, using TEM, it was confirmed that gelatin does not disrupt the formation of spidroin fibrils (figures 3(A) and (B)). The fibrils were 10 nm thick in case of eADF4(C16) and 9 nm thick in case of eADF4(C16)-RGD, comparing well to previously reported values [20, 41]. It is known that the addition of DMEM does not affect fibril formation but the gelation rate [20], however, there was no apparent further changes to the gelation kinetics when gelatin was included, figure 3(C).

It seems that gelatin has no effect on fibril formation or gelation kinetics of the recombinant spider silk proteins made under the used conditions. Although it would be potentially difficult to find gelatin fibrils within the recombinant spider silk fibrils, there were no appearance of sub-unit, alpha-helical fibrils

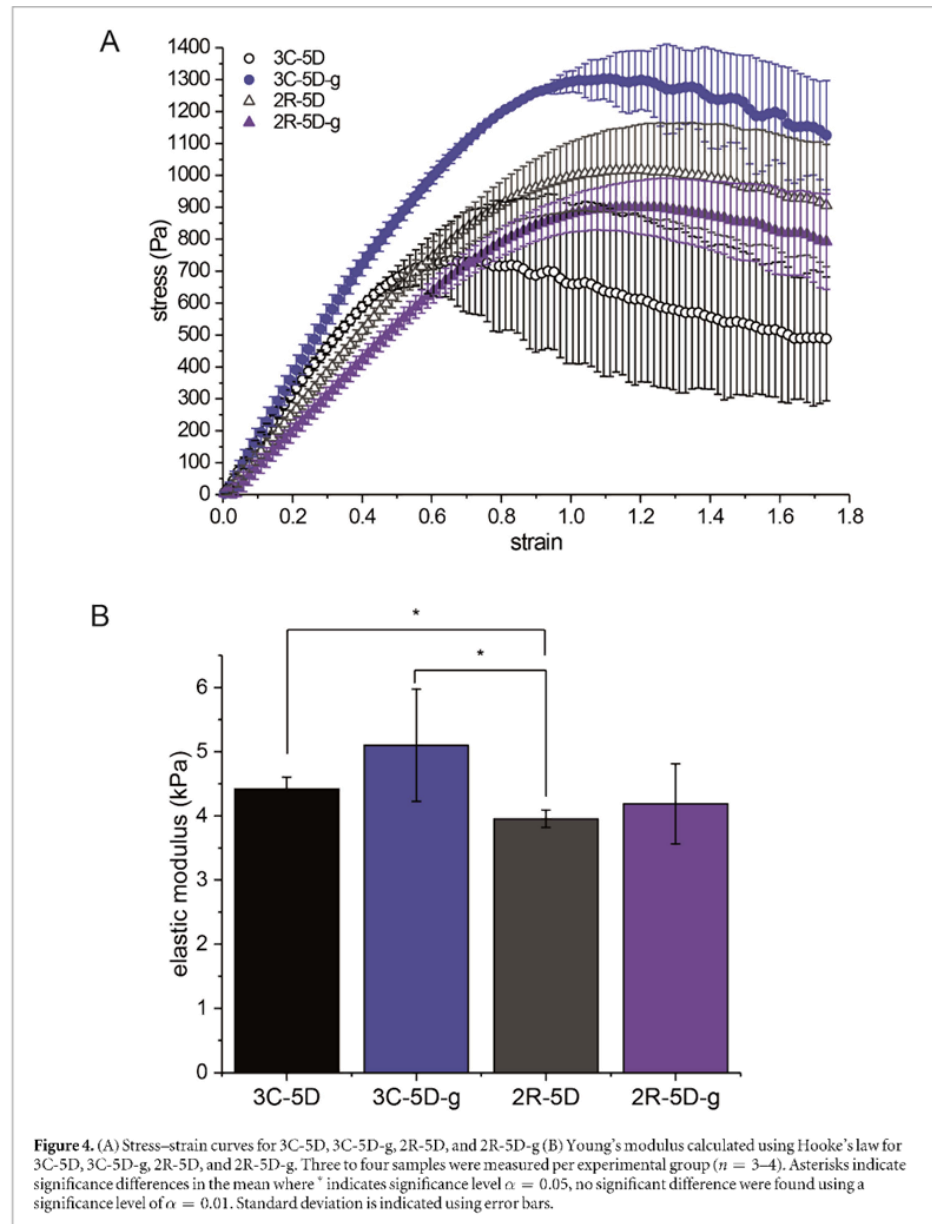
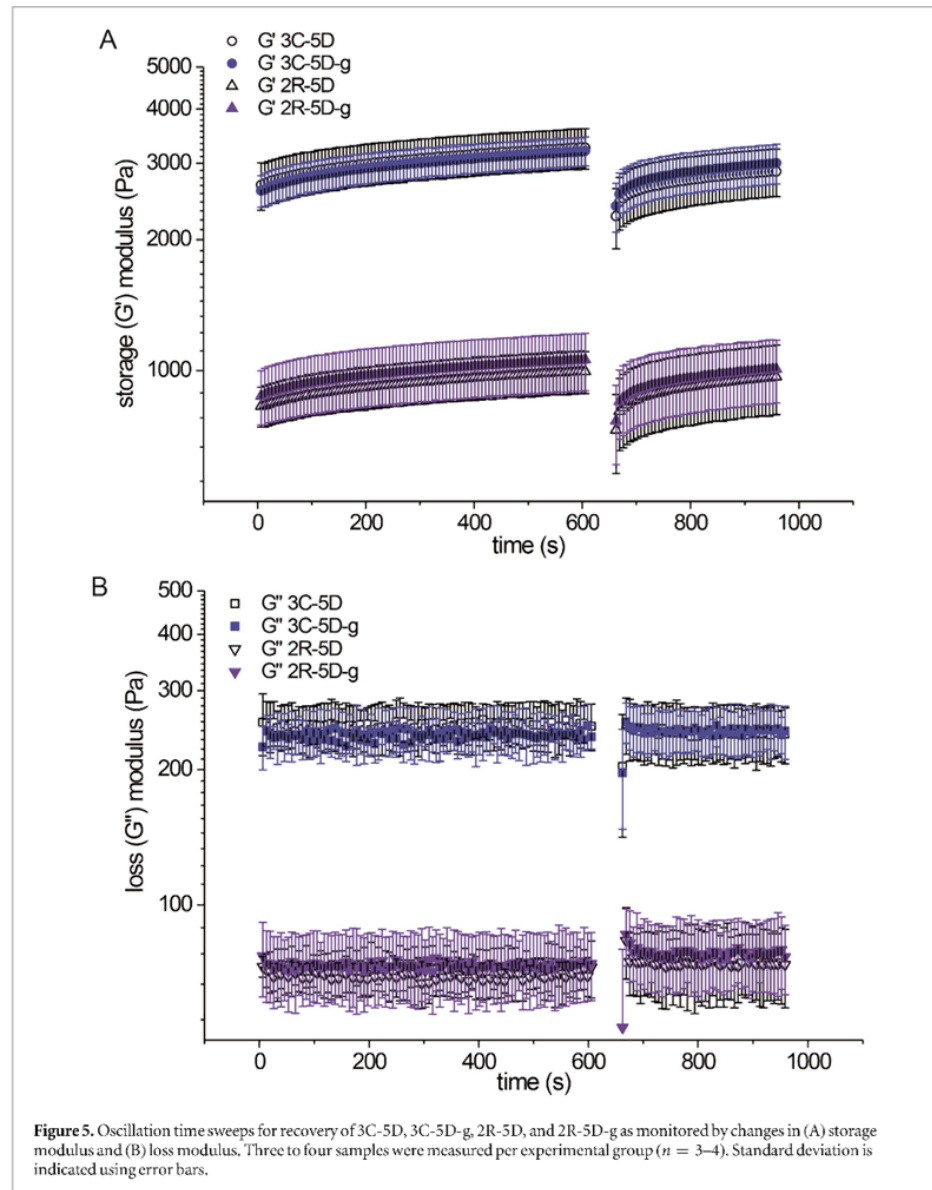


Figure 4. (A) Stress-strain curves for 3C-5D, 3C-5D-g, 2R-5D, and 2R-5D-g (B) Young's modulus calculated using Hooke's law for 3C-5D, 3C-5D-g, 2R-5D, and 2R-5D-g. Three to four samples were measured per experimental group ($n = 3-4$). Asterisks indicate significance differences in the mean where * indicates significance level $\alpha = 0.05$, no significant difference were found using a significance level of $\alpha = 0.01$. Standard deviation is indicated using error bars.

(~1.5 nm) or thicker, collagen-like fibrils (12–50 nm) in the prepared samples [42, 43]. In other works it was hypothesized that gelatin forms an interpenetrating network with silk fibroin, for example in silk-gelatin films [40], or in gelatin methacrylamide (GelMA)-silk hydrogels [37]. However, in these cases the gelatin concentration was much higher, and although difficult to confirm given this data set, it is more likely that the gelatin strands were not able to assemble triple helices in this environment and were somehow integrated into the silk fibril network. Furthermore,

unmodified gelatin is soluble at this concentration and temperature [44], and if not integrated in the network will likely simply dissolve when introduced in media, and have no effect. There was also no observable effect of gelatin on the gelation rate, indicating that the gelatin does not cause any protein aggregation or compaction, as seen in the case of DMEM. To see if there were any effects on the rheological behavior, hydrogels were measured for stress-strain behavior (figure 4).

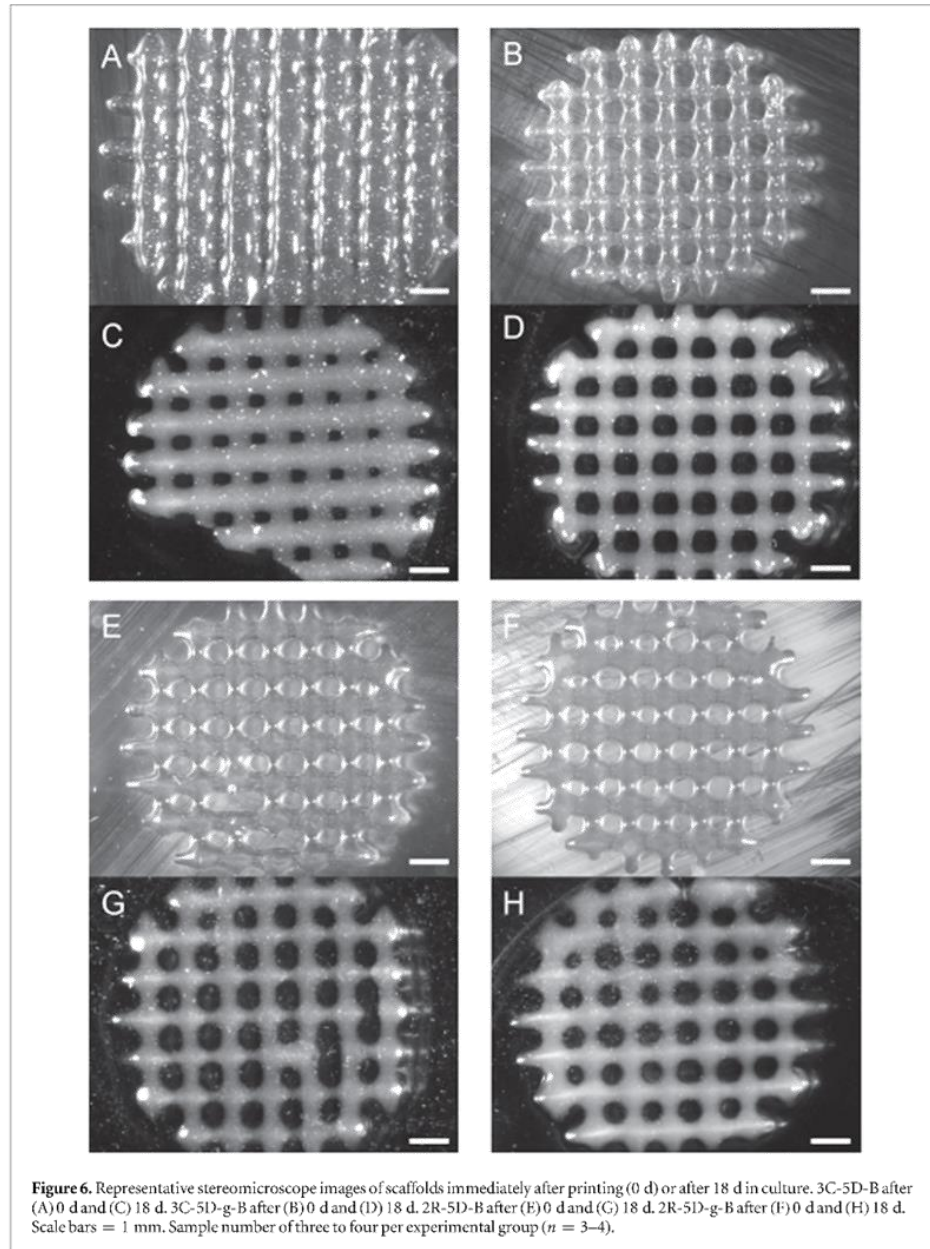
The data in figures 4(A) and S2 are in good agreement with previously reported data, where formulations



with high DMEM content have an apparent yield around 0.2 strain, and those with low content around 0.6 strain [15, 20]. This increase in elastic modulus comparing DMEM-free to those prepared with DMEM further supports the idea that there is additional cross-linking or compaction of protein due to the salt content, as strong evidence exists which correlates a decrease in optical clarity with an increase in spatial inhomogeneity, and thereby a decrease in mechanical strength in the case of hydrogels [45].

Although fibroblasts are not as sensitive as other cell lines to stiffness, it is clear that they are not

unresponsive, as seen in figures 1(C) and (D) as well as in other reports in literature [46, 47]. Therefore, another important note to the results in figure 4 is that the selected formulations have had similar stiffness. Although there was a statistically significant difference between the elastic modulus of 20 mg ml^{-1} eADF(C16)-RGD and of 30 mg ml^{-1} eADF(C16), the overall range of the moduli is within 3–5 kPa. It is not likely, based on other studies, that the fibroblasts would respond to such a range, as they rather show changes in behavior around 5 kPa and then again around 10 kPa [48]. There was no



significant difference in the elastic modulus of bioinks due to the addition of gelatin, however the apparent yield of bioinks including gelatin occurred at a much larger strain, supporting the hypothesis that the gelatin should indirectly plasticize the bioinks by binding water molecules [49, 50]. Not only could this softening improve the printing resolution, but it could possibly reduce unpredictable phase-separation events characteristic to silk proteins and hydrogels [51, 52].

3.2. Characterization of bioinks during and after 3DBP

As known from previous work, hydrogels made of cADF4(C16) and cADF4(C16)-RGD are printable without any additives [19]. To observe the behavior of the bioinks in an environment similar to printing, time sweep measurements were done before and after a large, high shear rate deformation (figure 5).

All experimental groups recovered their solid-like behavior instantaneously, and within the 5 min period

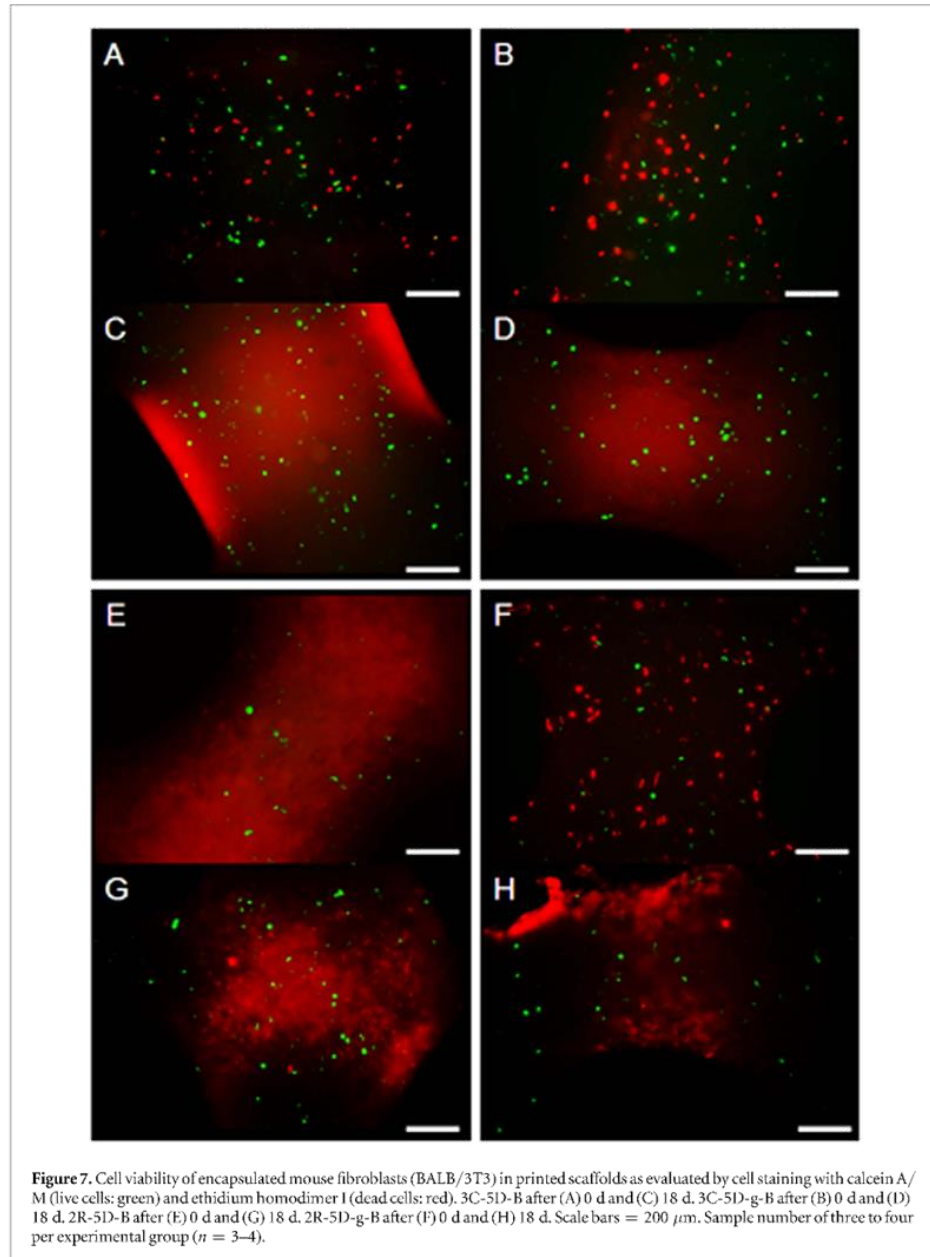


Table 3. Resolution of different bioinks immediately after printing (0 d) and after 18 d in culture.

	3C-5D-B	3C-5D-g-B	2R-5D-B	2R-5D-g-B
Resolution (μm) 0 d	628 ± 124	361 ± 18	385 ± 87	348 ± 48
Resolution (μm) 18 d	615 ± 47	387 ± 36	399 ± 45	389 ± 63

nearly recovered completely. The shear-thinning of the formulations was shown to be identical (figure S3). With clear indication that the recovery behavior is suitable in all bioinks, hydrogels were printed with cells (figures 6 and 7).

From figure 6, with printing resolution reported in table 3, it was clear that including gelatin as an additive improved the resolution and the precision of printed eADF4(C16) strands. In the case of eADF4(C16)-RGD this effect was not observed.

This result was impressive at such a low concentration of gelatin, as in the case of silk fibroin it was reported that there was a minimum of 50 mg ml^{-1} of gelatin required for the bioink to be printable, classifying the bioinks as blends [21]. Further, the largest weight-to-weight ratio used, silk to gelatin, was 2 to 1, compared to the ratio used here of 200 to 1. Further, this is impressive to most other physically cross-linked hydrogel systems, for example collagen, gelatin, and agarose [4]. Interestingly, the eADF4(C16)-RGD groups showed lower shape fidelity, and the effect of gelatin seemed to be less. This could be due to the fact that, although the stiffness's measured in quasi-static conditions were similar (figure 4), the eADF4(C16)-RGD was softer in terms of storage modulus (figure 5) and had a lower viscosity under similar conditions found in printing (figure S3). A similar result was observed for GelMA, where hyaluronic acid was blended to increase the viscosity, and the resulting shape fidelity was greatly improved [53].

The swelling data in figure 2 and the stereomicroscopy images in figure 6 were in good agreement; there is nearly no swelling and degradation of the bioink, independent of whether they are printed or not. A visible improvement when comparing printed to non-printed bioink was the small molecule transport, where phenol red dye present in DMEM was quickly and easily washed away from the printed ones with one wash, whereas several washes could not remove the dye from the solid, unprinted cylinders of bioink (figures 2(E)–(J)). The other visible difference from 1 d to 18 d was that the turbidity of the hydrogels increased. This supports the conclusion that there is some sort of salt binding as previously reported regarding cation binding during hydrogel formation [20].

There was relatively significant cell death after printing (figure 7). Interestingly, particularly obvious in the case of eADF4(C16)-RGD, the cell density seemed lower in the groups without gelatin than with gelatin. This supports the hypothesis that phase-separation might occur during the printing process. Although this contradicts the previously reported high cell viability after printing in Schacht *et al* 2015, this is likely due to the fact that the initial cell viability after encapsulation was low (~70%) compared to the nearly 100% cell viability after using the modified encapsulation protocol (table 1, figure S1) [19]. As confirmed by both CellTiter blue (data not shown) and cell viability

staining, there was minimal proliferation and spreading in the printed hydrogels, even in the case of eADF4(C16)-RGD bioinks. To be certain this was an effect of printing, and not of the batch, the test was repeated including unprinted bioinks as a control, and using 15% DMEM content as in previous experiments (data not shown). Again it was shown there was good proliferation in eADF4(C16)-RGD unprinted bioinks, and no proliferation in eADF4(C16) and printed bioinks, as already observed in figures 1 and 7. The low proliferation and spreading in printed bioinks could be due to either cell debris from initial cell death causing a stress response, or, if there is some sort of water removal, the mesh size is becoming too dense [52]. The cell viability could have also been reduced due to dehydration from water removal or due to printing in air instead of media [11]. Interestingly, although there was no proliferation, there was also no additional cell death; the cells which were viable after printing seemed to remain viable, and cell debris were completely removed at 18 d with significantly reduced dead cell staining compared to after 1 d in culture (figure 7). On the other hand, in other bioinks where cell viability is reduced after printing, such as GelMA, there is still significant proliferation [54], so it is difficult to determine if this is due to a lack of recovery of the cells from the printing process, or some change in the hydrogel itself due to the printing process.

4. Conclusion

It could be shown that recombinant spider silk proteins eADF4(C16) and eADF4(C16)-RGD can be gelled at 37°C in the presence of cells and used for 3D cell culture, and can be printed into 3D scaffolds. Although chemically cross-linked systems are used successfully [53, 54], having a thermally gelled system is advantageous in terms of cell viability after encapsulation, it circumvents cell settling in the printing cartridge, and helps to prevent cell damage during the printing process by protection against shear stress [11]. It could be said from this study that the eADF4(C16) hydrogels are permissive, but it is necessary to maximize cell viability as well as include a binding peptide in order for them to be considered promoting hydrogels [5]. Further, the printability of the eADF4(C16)-based bioinks could be improved by using gelatin as an additive, but there was no effect on those prepared from eADF4(C16)-RGD. In summary, in this study the bioinks were characterized at the foundational level, including small improvements such as initial cell viability, proliferation in unprinted hydrogels, and improvement of the printability in some cases.

Another important consideration when designing bioinks is which cells are used and how many are encapsulated in the bioink. In other studies, cell loading has been shown to play a significant role, and

therefore the cell density within the hydrogel should also be altered [55]. Further, cell–cell interactions are a significant variable in proliferation rate and tissue differentiation [56]. Additionally, an important factor to consider will be the chosen cell type to fit the slow degradation profile of eADF4(C16), or, alternatively, to somehow influence the degradation. In future work, higher concentration or addition of a thickening agent to bioinks will also be considered, due to the fact that high viscosity should improve cell viability after printing [11].

In conclusion, eADF4(C16) and its variants can be used successfully as a bioink, performing comparably to most bioinks and out-performing them in terms of long-term stability. Further improvements have to be made, but initial tests using a small amount of gelatin confirmed that these improvements should be feasible.

Acknowledgments

The authors wish to acknowledge Tamara Aigner for operating the transmission electron microscope as well as thank her for stimulating discussion about the results. The authors would also like to thank Thomas Frank, Maximilian Reinhardt and Catrin Herpich for their assistance in early work establishing the best printing conditions as well as cell culture conditions. The authors further would like to thank Eileen Lintz for her thorough proof reading and scientific discussions.

This work was funded by SFB 840 TP A8.

ORCID iDs

Thomas Scheibel  <https://orcid.org/0000-0002-0457-2423>

References

- [1] Mao A S and Mooney D J 2015 Regenerative medicine: current therapies and future directions *Proc. Natl Acad. Sci. USA* **112** 14452–9
- [2] Wu C et al 2017 Bioprinting: an assessment based on manufacturing readiness levels *Crit. Rev. Biotechnol.* **37** 333–54
- [3] Holz K et al 2016 Bioink properties before, during and after 3D bioprinting *Biofabrication* **8** 032002
- [4] Malda J et al 2013 25th Anniversary Article: Engineering hydrogels for biofabrication *Adv. Mater.* **25** 5011–28
- [5] Tibbitt M W and Anseth K S 2009 Hydrogels as extracellular matrix mimics for 3D cell culture *Biotechnol. Bioeng.* **103** 655–63
- [6] Engler A J et al 2004 Myotubes differentiate optimally on substrates with tissue-like stiffness: pathological implications for soft or stiff microenvironments *J. Cell Biol.* **166** 877–87
- [7] Engler A J et al 2006 Matrix elasticity directs stem cell lineage specification *Cell* **126** 677–89
- [8] Thiele J et al 2014 25th anniversary article: designer hydrogels for cell cultures: a materials selection guide *Adv. Mater.* **26** 125–47
- [9] Irvine S A and Venkatraman S S 2016 Bioprinting and differentiation of stem cells *Molecules* **21** 1188
- [10] Landers R et al 2002 Rapid prototyping of scaffolds derived from thermoreversible hydrogels and tailored for applications in tissue engineering *Biomaterials* **23** 4437–47
- [11] Dubbin K et al 2016 Dual-stage crosslinking of a gel-phase bioink improves cell viability and homogeneity for 3D bioprinting *Adv. Healthcare Mater.* **5** 2488–92
- [12] Jungst T et al 2016 Strategies and molecular design criteria for 3D printable hydrogels *Chem. Rev.* **116** 1496–539
- [13] Huemmerich D et al 2004 Novel assembly properties of recombinant spider dragline silk proteins *Curr. Biol.* **14** 2070–4
- [14] Vendrely C and Scheibel T 2007 Biotechnological production of spider-silk proteins enables new applications *Macromol. Biosci.* **7** 401–9
- [15] Schacht K and Scheibel T 2011 Controlled hydrogel formation of a recombinant spider silk protein *Biomacromolecules* **12** 2488–95
- [16] Zeplin P H et al 2014 Spider silk coatings as a bioshield to reduce periprosthetic fibrous capsule formation *Adv. Funct. Mater.* **24** 2658–66
- [17] Lang G, Herold H and Scheibel T 2017 Properties of engineered and fabricated silks *Sub-Cellular Biochem.* **82** 527–73
- [18] Wohlrab S et al 2012 Cell adhesion and proliferation on RGD-modified recombinant spider silk proteins *Biomaterials* **33** 6650–9
- [19] Schacht K et al 2015 Biofabrication of cell-loaded 3D spider silk constructs *Angew. Chem.* **54** 2816–20
- [20] DeSimone E, Schacht K and Scheibel T 2016 Cations influence the cross-linking of hydrogels made of recombinant, polyanionic spider silk proteins *Mater. Lett.* **183** 101–4
- [21] Rodriguez M J et al 2017 Silk based bioinks for soft tissue reconstruction using 3-dimensional (3D) printing with *in vitro* and *in vivo* assessments *Biomaterials* **117** 105–15
- [22] Chung J H Y et al 2013 Bio-ink properties and printability for extrusion printing living cells *Biomater. Sci.* **1** 763–73
- [23] Urayama K, Takigawa T and Masuda T 1993 Poisson ratio of poly(vinyl alcohol) gels *Macromolecules* **26** 3092–6
- [24] Rammensee S et al 2006 Rheological characterization of hydrogels formed by recombinantly produced spider silk *Appl. Phys. A* **82** 261–4
- [25] DeSimone E et al 2015 Biofabrication of 3D constructs: fabrication technologies and spider silk proteins as bioinks *Pure Appl. Chem.* **87** 737–49
- [26] Slotta U et al 2007 Spider silk and amyloid fibrils: a structural comparison *Macromol. Biosci.* **7** 183–8
- [27] Kisiday J et al 2002 Self-assembling peptide hydrogel fosters chondrocyte extracellular matrix production and cell division: implications for cartilage tissue repair *Proc. Natl Acad. Sci. USA* **99** 9996–10001
- [28] Jia J et al 2014 Engineering alginate as bioink for bioprinting *Acta Biomater.* **10** 4323–31
- [29] Billiet T et al 2014 The 3D printing of gelatin methacrylamide cell-laden tissue-engineered constructs with high cell viability *Biomaterials* **35** 49–62
- [30] Hersel U, Dahmen C and Kessler H 2003 RGD modified polymers: biomaterials for stimulated cell adhesion and beyond *Biomaterials* **24** 4385–415
- [31] Hwang C M et al 2013 Assessments of injectable alginate particle-embedded fibrin hydrogels for soft tissue reconstruction *Biomed. Mater.* **8** 014105
- [32] Even-Ram S and Yamada K M 2005 Cell migration in 3D matrix *Curr. Opin. Cell Biol.* **17** 524–32
- [33] Wozniak M A et al 2004 Focal adhesion regulation of cell behavior *Biochim. Biophys. Acta—Mol. Cell Res.* **1692** 103–19
- [34] Doyle A D et al 2009 One-dimensional topography underlies three-dimensional fibrillar cell migration *J. Cell Biol.* **184** 481–90
- [35] Duan B et al 2013 3D Bioprinting of heterogeneous aortic valve conduits with alginate/gelatin hydrogels *J. Biomed. Mater. Res. A* **101** 1255–64
- [36] Hunt N C et al 2010 Encapsulation of fibroblasts causes accelerated alginate hydrogel degradation *Acta Biomater.* **6**, 3649–56

- [37] Xiao W Q *et al* 2011 Synthesis and characterization of photocrosslinkable gelatin and silk fibroin interpenetrating polymer network hydrogels *Acta Biomater.* **7** 2384–93
- [38] Brown J *et al* 2015 Impact of silk biomaterial structure on proteolysis *Acta Biomater.* **11** 212–21
- [39] Schacht K, Vogt J and Scheibel T 2016 Foams made of engineered recombinant spider silk proteins as 3D scaffolds for cell growth *ACS Biomater. Sci. Eng.* **2** 517–25
- [40] Gil E S *et al* 2006 Mixed protein blends composed of gelatin and Bombyx mori silk fibroin: effects of solvent-induced crystallization and composition *Biomacromolecules* **7** 728–35
- [41] Humenik M and Scheibel T 2014 Nanomaterial building blocks based on spider silk-oligonucleotide conjugates *ACS Nano* **8** 1342–9
- [42] Kokol S G A V 2011 Collagen- vs. Gelatin-based biomaterials and their biocompatibility: review and perspectives *Biomaterials Applications for Nanomedicine* ed R Pignatello (London: InTech)
- [43] Starborg T *et al* 2013 Using transmission electron microscopy and 3View to determine collagen fibril size and three-dimensional organization *Nat. Protocols* **8** 1433–48
- [44] Mcpherson J M *et al* 1985 Collagen fibrillogenesis invitro—a characterization of fibril quality as a function of assembly conditions *Collagen Relat. Res.* **5** 119–35
- [45] Okay O 2009 *General Properties of Hydrogels (Springer Series on Chemical Sensors and Biosensors)* (Berlin: Springer)
- [46] Yeung T *et al* 2005 Effects of substrate stiffness on cell morphology, cytoskeletal structure, and adhesion *Cell Motility Cytoskeleton* **60** 24–34
- [47] Gillette B M *et al* 2008 *In situ* collagen assembly for integrating microfabricated three-dimensional cell-seeded matrices *Nat. Mater.* **7** 636–40
- [48] Solon J *et al* 2007 Fibroblast adaptation and stiffness matching to soft elastic substrates *Biophys. J.* **93** 4453–61
- [49] Lewicki P P, Busk G C and Labuza T P 1978 Measurement of gel water-binding capacity of gelatin, potato starch, and carrageenan gels by suction pressure *J. Colloid Interface Sci.* **64** 501–9
- [50] Yazawa K *et al* 2016 Influence of water content on the beta-sheet formation, thermal stability, water removal, and mechanical properties of silk materials *Biomacromolecules* **17** 1057–66
- [51] Jin H J and Kaplan D L 2003 Mechanism of silk processing in insects and spiders *Nature* **424** 1057–61
- [52] Pasqui D, De Cagna M and Barbucci R 2012 Polysaccharide-based hydrogels: the key role of water in affecting mechanical properties *Polymers* **4** 1517–34
- [53] Schuurman W *et al* 2013 Gelatin-methacrylamide hydrogels as potential biomaterials for fabrication of tissue-engineered cartilage constructs *Macromol. Biosci.* **13** 551–61
- [54] Kolesky D B *et al* 2014 3D bioprinting of vascularized, heterogeneous cell-laden tissue constructs *Adv. Mater.* **26** 3124–30
- [55] Miller J S 2014 The billion cell construct: will three-dimensional printing get us there? *PLoS Biology* **12** e1001882
- [56] Toh Y C, Xing J W and Yu H R 2015 Modulation of integrin and E-cadherin-mediated adhesions to spatially control heterogeneity in human pluripotent stem cell differentiation *Biomaterials* **50** 87–97

Part 2. Cations influence the cross-linking of hydrogels made of recombinant, polyanionic spider silk proteins

DeSimone E., Schacht K., Scheibel T.

Published in *Materials Letters*, **183**, 101-104
(2016)

Reprinted with kind permission from Elsevier



Cations influence the cross-linking of hydrogels made of recombinant, polyanionic spider silk proteins



Elise DeSimone¹, Kristin Schacht¹, Thomas Scheibel^{*}

Lehrstuhl Biomaterialien, Universität Bayreuth, Universitätsstraße 30, 95447 Bayreuth, Germany

ARTICLE INFO

Article history:
Received 23 December 2015
Received in revised form
29 June 2016
Accepted 10 July 2016
Available online 11 July 2016

Keywords:
Bioinks
Biofabrication
3D Bioprinting
Recombinant spider silk protein
Physical crosslinking
Spidroin

ABSTRACT

Hydrogels made of polyanionic recombinant spider silk proteins (spidroins) were prepared either in the presence or the absence of Dulbecco's Modified Eagle Medium (DMEM). Mono- and divalent cations present in DMEM severely affected the self-assembly process of the spidroins. Although the addition of DMEM had no apparent effect on secondary structure formation, there was a significant effect on the kinetics as well as on the hydrogel network; in the presence of DMEM, gelation occurred more rapidly. Additionally, the hydrogels were stiffer; however, the hydrogels were still shear-thinning. In summary, it can be concluded that there is a significant impact of ionic cross-linking on recombinant spidroin-based hydrogels.

© 2016 Elsevier B.V. All rights reserved.

1. Introduction

Traditional tissue engineering techniques have a significant disadvantage: the placement of different components which are used to prepare tissue-like constructs (cells, biomaterials and biochemical factors) is imprecise [1,2]. To overcome this disadvantage, researchers have developed several techniques which allow for co-processing of cells and biomaterials into specific structures; this sub-type of tissue engineering is referred to as biofabrication [3,4]. Of these techniques, one of the most promising is 3D bioprinting; layer-by-layer manufacturing of cell-encapsulating biomaterials into 3D scaffolds [5]. Natural biomaterials which have been used in 3D bioprinting are collagen, gelatin and alginate; however, all of these have some sort of disadvantage i.e. poor mechanical properties [1–3,6–14]. As an alternative to these common bioinks, the recombinant spider silk protein (spidroin) eADF4(C16) and its modified variant eADF4(C16)-RGD have been recently introduced [15].

The polyanionic spidroin eADF4(C16) consists of 16 repeats of module C (sequence: GSSAAAAAASGPGGYG PENQGPSGPG-GYGPGGP), which mimics the consensus sequence of the repetitive core of the European garden spider *Araneus diadematus* dragline silk fibroin 4 (ADF4) [16,17]. The RGD variant thereof contains an RGD integrin-binding motif introduced by genetic engineering at the

C-terminus, which was previously shown to enhance mammalian cell attachment on spider silk films [18]. These proteins can self-assemble from a disordered structure in solution into β -sheet rich fibrils [19]. Self-assembly is triggered by temperature, kosmotropic phosphate ions and increased protein concentration [20,21].

Bioinks naturally require the use of cell culture media in the fabrication process. As various ions severely affect the self-assembly process [22], the aim of this research was to characterize the material properties of the hydrogel prepared in the presence of cell culture media. Through various assays, stages of the network formation were observed: basic protein structure (FTIR), fibril morphology and association (TEM), hydrogel network formation kinetics (turbidimetry). Additionally, an effect of the formed network on a critical bulk property (i.e. mechanics) of the hydrogel was also observed (rheology).

2. Experimental

2.1. Transmission electron microscopy (TEM)

For TEM analysis, 3% w/v eADF4(C16) and 3% w/v eADF4(C16)-RGD hydrogels, in the presence or absence of 15% v/v DMEM, were diluted to 1 mg/mL. 5 μ L of the diluted hydrogel was scattered on 100-mesh Formvar-coated copper TEM grids (Plano GmbH, Germany), incubated for 10 min, washed two times using 5 μ L of double distilled water (ddH₂O), and fibrils were negatively stained

^{*} Corresponding author.

E-mail address: thomas.scheibel@bm.uni-bayreuth.de (T. Scheibel).

¹ First authors.

using 5 μ L 2% uranyl acetate solution. Samples were allowed to dry for at least 24 h at ambient temperature before imaging. TEM imaging of dry samples was performed with a JEM-2100 transmission electron microscope (JEOL, Tokyo, Japan) operated at 80 kV and equipped with a 4000 \times 4000 charge-coupled device camera (UltraScan 4000; Gatan, Pleasanton, CA).

2.2. Analysis of gelation kinetics

For gelation analysis, 100 μ L of concentrated eADF4(C16) and eADF4(C16)-RGD solutions in the presence or absence of 15% v/v Dulbecco's Modified Eagle Medium (DMEM) without phenol red (Life Technologies, USA) were added to 96-well plates (Nunc, Germany). Phenol red-free DMEM was used to prevent false measurement or background noise that might be introduced by this pH indicator. The hydrogels were incubated at 37 $^{\circ}$ C and analyzed at various time points for changes in turbidity. Turbidity changes upon gelation were monitored at 570 nm using a Microplate Reader (Mithras LB 940, Berthold Technologies, Germany) in absorbance mode. A sample number of 4 (n=4) was used for each experimental group.

2.3. Fourier-Transform Infrared (FTIR) spectroscopy

Secondary structure content of the eADF4(C16) and eADF4(C16)-RGD hydrogels in the presence or absence of 15% v/v DMEM (Biochrom, Berlin, Germany) was evaluated after freeze-drying hydrogel samples with a Bruker Tensor 27 spectrometer (Bruker, Germany). Spectra were detected by attenuated total reflection (ATR) with a resolution of 4 cm^{-1} , and 120 scans were averaged. Analysis of the amide I band (1595–1705 cm^{-1}) was performed by Fourier self-deconvolution (FSD) to determine individual secondary structure elements as described previously [23–26]. A sample number of 3 (n=3) was used for each experimental group.

2.4. Rheology

Stress-strain curves of eADF4(C16) and eADF4(C16)-RGD in the presence of different ions were measured using a flow measurement mode at the Rheometer AR-G2 (TA Instruments, New Castle, DE, USA) with a 25 mm plate-plate geometry and a 0.5 mm gap and a sample volume of 600 μ L at room temperature. The shear rate was kept constant at 3.0 $\times 10^{-3}$ 1/s. To analyze the influence of 15% v/v DMEM on the viscosity behavior of these hydrogels, the hydrogels were measured using additionally the steady state flow measurement mode. Here, the shear rate was increased from 0.1 to 100 s^{-1} . For all measurements a solvent trap with a wet sponge was used to minimize evaporation. All rheological measurements were performed with pre-formed hydrogels. The highly concentrated spider silk solutions were gelled for 24 h at 37 $^{\circ}$ C before rheological measurements. A sample number of 2–3 (n=2–3) was used for each experimental group and one representative curve shown per group.

3. Results and discussions

3.1. Concentration of relevant ions in hydrogel formulations

Dulbecco's Modified Eagle Medium (DMEM) contains numerous salts, sugars and proteins, which could influence the charge-charge interactions between the proteins. In this context, salts like CaCl_2 , NaCl and KCl have already been identified as important in the formation of spider silk threads in nature, and are therefore of particular interest for the hydrogel formation as well [27]. These ions are classified as either kosmotropic or chaotropic [28]: Ions such as Ca^{2+} , are highly chaotropic, Cl^- is neither kosmotropic of

chaotropic, and K^+ and Na^+ are kosmotropic, with K^+ being slightly more kosmotropic.

In the final formulation of the eADF4(C16) and eADF4(C16)-RGD hydrogels prepared with DMEM, the molarity is 16.43 mM for NaCl, 0.80 mM for KCl, and 0.27 mM for CaCl_2 . An example calculation for NaCl is shown below in Eq. (1). The entire value is multiplied by 0.15 to account for the fact that the final concentration of DMEM is 15% v/v.

$$6.4\text{g/L}/58.44\text{g/mol}\cdot 1000\text{mM}/1\text{M}\cdot 0.15 = 16.43\text{mM NaCl} \quad (1)$$

3.2. Structural characterization of eADF4(C16) and eADF4(C16)-RGD hydrogels

The consensus motif (C-module) comprises 35 amino acids with one (Ala)₈ stretch able to form β -sheets as well as glycine/proline rich GPGXY repeats remaining disordered or helical in solution [26,29,30]. When the protein converts from the soluble to the insoluble state, there is an increase in the amount of β -sheet rich structures [21,26]. Therefore, the gelation process of eADF4(C16) and eADF4(C16)-RGD can be characterized by the formation of nanofibrils accompanied by this change in secondary structure. Here, it was investigated if the presence of 15% v/v cell culture media influences the secondary structure of eADF4(C16) and eADF4(C16)-RGD hydrogels using FTIR spectroscopy. Fourier self-deconvolution (FSD) of the amide I band allowed assignment of individual secondary structure elements (Table 1) [23–26].

The hydrogels fabricated in the absence or presence of DMEM were indistinguishable concerning their secondary structure composition; all hydrogels showed an overall β -sheet content between 45% and 47%.

3.3. Morphological analysis of the fibrillary network

The morphology of the fibrils and fibrillary network of the 3% w/v eADF4(C16) and eADF4(C16)-RGD hydrogels in presence of cell culture media were evaluated using transmission electron microscopy (TEM) (Fig. 1A and B).

3% w/v eADF4(C16) hydrogels were organized by nanofibrils with a diameter of around 10 nm as shown previously, while 3% w/v eADF4(C16)-RGD hydrogels showed slightly thinner nanofibrils with a diameter of around 7 nm [32]. In addition, the fibrillary network of eADF4(C16)-RGD hydrogels was more densely packed in comparison to that of eADF4(C16) hydrogels. However, the presence of DMEM had no apparent influence on the gross morphology of the hydrogels; although there appeared to be a change in opacity, as confirmed by turbidity measurements, likely originating from the slightly denser packing.

Table 1
Secondary structure elements of 3% eADF4(C16) and 3% eADF4(C16)-RGD made in the absence or the presence of DMEM (15% v/v). Structural contents were calculated using Fourier self-deconvolution (FSD) of the amide I bands.

Secondary structure ^a	Wavenumber range/ cm^{-1}	Secondary structure content/%			
		3% C16	3% C16, 15% DMEM	3% C16-RGD	3% C16-RGD, 15% DMEM
α -helices	1656–1662	8.9 \pm 0.3	8.5 \pm 0.1	8.7 \pm 0.6	7.5 \pm 1.1
β -sheets	1616–1637, 1697–1703	44.7 \pm 1.3	47.1 \pm 1.8	45.1 \pm 0.8	46.1 \pm 2.5
Random coils	1638–1655	22.5 \pm 0.9	21.7 \pm 0.3	23.0 \pm 0.2	21.9 \pm 0.2
Turns	1663–1696	21.3 \pm 0.4	21.4 \pm 0.5	20.7 \pm 0.6	21.9 \pm 0.7
Side chains	1595–1615	2.6 \pm 1.1	1.3 \pm 2.2	2.5 \pm 0.4	2.6 \pm 1.0

^a Peak assignment taken from literature [23,31].

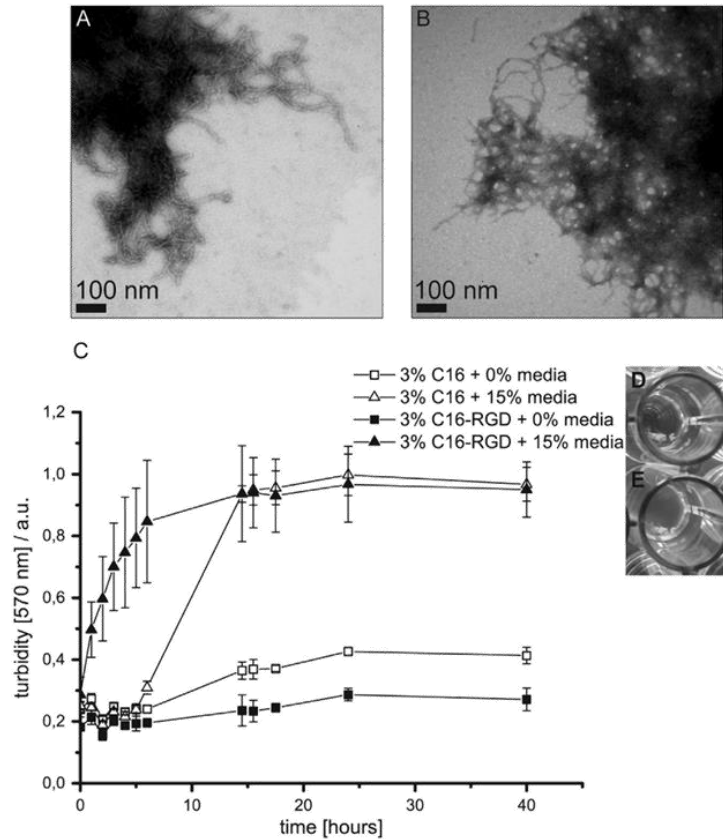


Fig. 1. (A, B) TEM images of hydrogels made of self-assembled recombinant spider silk fibrils. (A) 3% eADF4(C16), (B) 3% eADF4(C16)-RGD. (C-E) Time-dependent turbidity changes (indicative of nanofibril formation) [21] of 3% eADF4(C16) and 3% eADF4(C16)-RGD solutions in the absence and presence of DMEM (15% v/v) as indicated at 37 °C. (C) Changes in turbidity were quantified at 570 nm and normalized to the highest value. Each data point is averaged from three independent samples. 3% eADF4(C16) hydrogels in the absence of DMEM (D) and presence of DMEM (15% v/v) (E) after 2 h of incubation at 37 °C.

3.4. Effects of cell culture media on the gelation process

Physical crosslinking in recombinant spider silk protein hydrogels occurs due to the formation of inter- and intramolecular interactions among the proteins based on hydrogen bonds and hydrophobic interactions [22]. To analyze the impact of the ions and the ionic strength of the DMEM on the assembly rate of the network, the turbidity of each sample was monitored at 570 nm in a time-dependent manner (Fig. 1C).

Hydrogel formation in the presence of DMEM exhibited more rapid gelation in comparison to that without DMEM. For 3% w/v eADF4(C16)-RGD hydrogels, the gelation process began immediately after dialysis and was completed after around 10–15 h. Formation of hydrogels made of 3% eADF4(C16) had a 5 h lag-phase and took overall longer to complete. It was also observed that DMEM had a significantly greater influence on the rate of hydrogel formation of eADF4(C16)-RGD compared to that of eADF4(C16). This could be due to the additional charge residues on the RGD sequence for ionic bonding.

3.5. Rheological characterization of eADF4(C16) and eADF4(C16)-RGD hydrogels

Previously it has been shown that eADF4(C16) hydrogels demonstrate elastic moduli similar to most polymers, within the

regime of most human tissues and organs, with the exception of bone tissue [21,33–35]. To determine the effects of cations (exemplary Ca^{2+} was tested) and DMEM on the mechanical properties of spider silk hydrogels, their stiffness was determined using rheology (Fig. 2).

The addition of 5 mM CaCl_2 to 3% w/v eADF4(C16)-RGD hydrogels resulted in a $1000\times$ increase of shear stress, while the shear stress of 3% w/v eADF4(C16) hydrogels increased just $400\times$ at the same applied strain. Divalent ions decrease repulsive electrostatic interactions, and forces that favor intermolecular association reactions can prevail [36]. Additionally, COO^- ions of amino acid side chains in the spiderins by ionic interactions, and therefore result in a significant increase in the mechanical stiffness. Interestingly, the effect of DMEM was more significant than CaCl_2 alone. As DMEM is a highly complex electrolyte solution, there is most likely multiple types of ionic bonding.

Previously it was shown that hydrogels made of 3% w/v eADF4(C16) exhibit shear thinning behavior, in contrast to hydrogels made of silk fibroin [15,37]. To analyze the impact of DMEM on the shear-thinning behavior of the spider silk hydrogels, they were characterized using a steady state flow mode (Fig. 3).

All analyzed samples showed shear thinning behavior, with high viscosity at low angular frequencies and a decrease in viscosity at higher frequencies. However, the addition of DMEM lead to higher viscosities at low shear rates. Interestingly, no

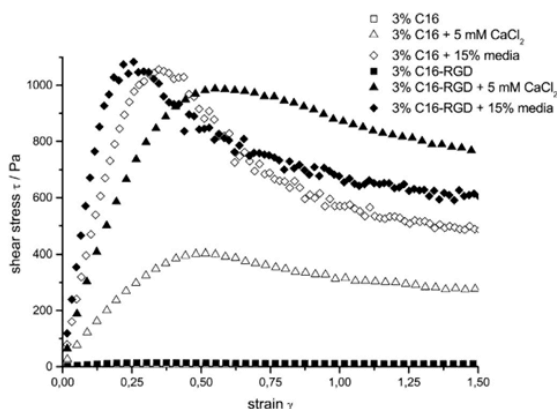


Fig. 2. Rheological characterization of hydrogels made of recombinant spider silk proteins. Stress-strain curves of 3% w/v eADF4(C16) and 3% w/v eADF4(C16)-RGD hydrogels in the absence and presence of 5 mM CaCl_2 and DMEM (15% v/v).

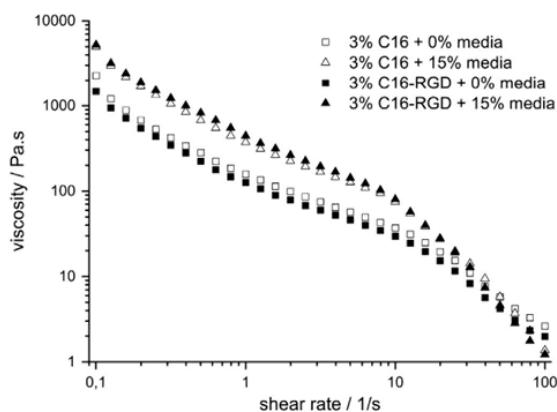


Fig. 3. Viscosity measurements with increasing shear rate of 3% w/v eADF4(C16) and 3% w/v eADF4(C16)-RGD hydrogels in the absence and presence of DMEM (15% v/v).

differences in viscosity between 3% w/v eADF4(C16) and 3% w/v eADF4(C16)-RGD was observed.

4. Conclusion

In this work, recombinant spider silk protein-based hydrogels were characterized in the presence or absence of Dulbecco's Modified Eagle Medium (DMEM). The formulation of DMEM contains many ions which are identified as important for the self-assembly process of spider silk proteins [27]. Data showed similar secondary structures and fibril formation, regardless of the addition of DMEM, and therefore differences seen in the hydrogel's stiffness, viscosity, or turbidity can be related instead to the formation of additional physical crosslinks to the presence of monovalent and bivalent cations [22,38]. However, which is an important property for 3D printing, the shear thinning behavior is maintained, this being important for applications of spider silk hydrogels as bioinks.

Acknowledgements

Funding was obtained from the Deutsche Forschungsgemeinschaft SFB 840 TP A8.

Appendix A

Hydrogel preparation: eADF4(C16) (MW: 47698 g mol⁻¹) and eADF4(C16)-RGD (MW: 48583 g mol⁻¹) were produced and purified as described previously [16,18]. Lyophilized eADF4(C16) and eADF4(C16)-RGD were dissolved in 6 M guanidinium thiocyanate at 4 mg/mL and dialyzed against 10 mM Tris/HCl, pH 7.5 overnight at room temperature using dialysis membranes with a molecular weight cutoff of 6000–8000 Da. Subsequent dialysis against 25% w/v poly(ethylene glycol) (PEG, 20,000 g mol⁻¹) with a volume extent of PEG between 50 and 400 was used to adjust 30 mg/mL (3% w/v) silk solutions as described previously [21]. Hydrogels were formed overnight at 37 °C and 95% relative humidity [21].

References

- [1] E. DeSimone, K. Schacht, T. Jungst, J. Groll, T. Scheibel, *Pure Appl. Chem.* 87 (2015) 737.
- [2] S.V. Murphy, A. Atala, *Nat. Biotechnol.* 32 (2014) 773.
- [3] J. Malda, J. Visser, F.P. Melchels, T. Jungst, W.E. Hennink, W.J. Dhert, J. Groll, D. W. Huttmacher, *Adv. Mater.* 25 (2013) 5011.
- [4] V. Mironov, T. Trusk, V. Kasyanov, S. Little, R. Swaja, R. Markwald, *Biofabrication* 1 (2009) 022001.
- [5] B. Berman, *Bus. Horiz.* 55 (2012) 155.
- [6] J. Jia, D.J. Richards, S. Pollard, Y. Tan, J. Rodriguez, R.P. Visconti, T.C. Trusk, M. J. Yost, H. Yao, R.R. Markwald, Y. Mei, *Acta Biomater.* 10 (2014) 4323.
- [7] Q.L. Loh, C. Choong, *Tissue Eng. Part B: Rev.* 19 (2013) 485.
- [8] B.S. Kim, D.J. Mooney, *Trends Biotechnol.* 16 (1998) 224.
- [9] S. Moon, S.K. Hasan, Y.S. Song, F. Xu, H.O. Keles, F. Manzur, S. Mikkilineni, J. W. Hong, J. Nagatomi, E. Haeggstrom, A. Khademhosseini, U. Demirci, *Tissue Eng. Part C: Methods* 16 (2010) 157.
- [10] X. Wang, Y. Yan, R. Zhang, *Tissue Eng. Part B: Rev.* 16 (2010) 189.
- [11] C.M. Smith, A.L. Stone, R.L. Parkhill, R.L. Stewart, M.W. Simpkins, A. M. Kachurin, W.L. Warren, S.K. Williams, *Tissue Eng.* 10 (2004) 1566.
- [12] R. Parenteau-Bareil, R. Gauvin, F. Berthod, *Materials* 3 (2010) 1863.
- [13] U. Hersel, C. Dahmen, H. Kessler, *Biomaterials* 24 (2003) 4385.
- [14] E. Hoch, T. Hirth, G.E.M. Tovar, K. Borchers, *J. Mater. Chem. B* 1 (2013) 5675.
- [15] K. Schacht, T. Jungst, M. Schweinlin, A. Ewald, J. Groll, T. Scheibel, *Angew. Chem. Int. Ed. Engl.* 54 (2015) 2816.
- [16] D. Huemmerich, C.W. Helsen, S. Quedzuweit, J. Oschmann, R. Rudolph, T. Scheibel, *Biochemistry* 43 (2004) 13604.
- [17] C. Vendrely, T. Scheibel, *Macromol. Biosci.* 7 (2007) 401.
- [18] S. Wohlrab, S. Muller, A. Schmidt, S. Neubauer, H. Kessler, A. Leal-Egana, T. Scheibel, *Biomaterials* 33 (2012) 6650.
- [19] U. Slotta, S. Hess, K. Spiess, T. Stromer, L. Serpell, T. Scheibel, *Macromol. Biosci.* 7 (2007) 183.
- [20] U.K. Slotta, S. Rammensee, S. Gorb, T. Scheibel, *Angew. Chem. Int. Ed. Engl.* 47 (2008) 4592.
- [21] K. Schacht, T. Scheibel, *Biomacromolecules* 12 (2011) 2488.
- [22] U.J. Kim, J. Park, C. Li, H.J. Jin, R. Valluzzi, D.L. Kaplan, *Biomacromolecules* 5 (2004) 786.
- [23] X. Hu, D. Kaplan, P. Cebe, *Macromolecules* 39 (2006) 6161.
- [24] A.S. Lammel, X. Hu, S.H. Park, D.L. Kaplan, T.R. Scheibel, *Biomaterials* 31 (2010) 4583.
- [25] K. Spiess, R. Ene, C.D. Keenan, J. Senker, F. Kremer, T. Scheibel, *J. Mater. Chem.* 21 (2011) 13594.
- [26] M. Humenik, M. Drechsler, T. Scheibel, *Nano Lett.* 14 (2014) 3999.
- [27] L. Eisdold, C. Thamm, T. Scheibel, *Biopolymers* 97 (2012) 355.
- [28] J.J. Grigsby, H.W. Blanch, J.M. Prausnitz, *Biophys. Chem.* 91 (2001) 231.
- [29] K. Spiess, A. Lammel, T. Scheibel, *Macromol. Biosci.* 10 (2010) 998.
- [30] T. Lefevre, S. Boudreaux, C. Cloutier, M. Pezolet, *J. Mol. Biol.* 405 (2011) 238.
- [31] A. Nova, S. Keten, N.M. Pugno, A. Redaelli, M.J. Buehler, *Nano Lett.* 10 (2010) 2626.
- [32] M. Humenik, T. Scheibel, *ACS Nano* 8 (2014) 1342.
- [33] A. Leal-Egana, T. Scheibel, *Biotechnol. Appl. Biochem.* 55 (2010) 155.
- [34] F.C. MacKintosh, J. Kas, P.A. Janmey, *Phys. Rev. Lett.* 75 (1995) 4425.
- [35] A.J. Engler, S. Sen, H.L. Sweeney, D.E. Discher, *Cell* 126 (2006) 677.
- [36] K. Klement, K. Wieligmann, J. Meinhardt, P. Hortschansky, W. Richter, M. Fandrich, *J. Mol. Biol.* 373 (2007) 1321.
- [37] T. Jungst, W. Smolan, K. Schacht, T. Scheibel, J. Groll, *Chem. Rev.* (2015).
- [38] A. Ochi, K.S. Hossain, J. Magoshi, N. Nemoto, *Biomacromolecules* 3 (2002) 1187.

Part 3. Engineered spider silk-based 2D and 3D materials prevent microbial infestation.

Kumari S.*, Lang G.*, **DeSimone E.**, Spengler C., Trossmann, V., Lücker S., Hudel M., Jacobs K., Krämer N., Scheibel T.

Submitted to *Advanced Materials*
(2020)

Submitted to John Wiley and Sons

Engineered spider silk-based 2D and 3D materials prevent microbial infestation

*Sushma Kumari,[†] Gregor Lang,[†] Elise DeSimone, Christian Spengler, Vanessa T. Trossmann, Susanne Lücker, Martina Hudel, Karin Jacobs, Norbert Krämer and Thomas Scheibel**

Dr. S. Kumari, Dr. E. DeSimone, V. T. Trossmann, Prof. T. Scheibel,
Department of Biomaterials,
Faculty of Engineering Science,
University of Bayreuth,
Prof.-Rüdiger-Bormann-Str. 1, 95447 Bayreuth, Germany

Prof. G. Lang
Biopolymer Processing Group,
Department of Biomaterials,
Faculty of Engineering Science,
University of Bayreuth,
Ludwig-Thoma-Str 36A, 95447 Bayreuth, Germany

Dr. C. Spengler, Prof. K. Jacobs
Department of Experimental Physics,
Saarland University,
66123 Saarbrücken, Germany

Dr. S. Lücker, Prof. N. Krämer
Medical Center for Dentistry,
Department of Paediatric Dentistry,
Medical Center Gießen and Marburg,
Justus-Liebig University Gießen,
Schlagenzahl 14, 35392 Gießen, Germany

M. Hudel,
Institute of Medical Microbiology,
Justus-Liebig University Gießen,
Schubertstraße 81, 35392 Gießen, Germany

Prof. T. Scheibel
Bayreuth Center for Material Science and Engineering (BayMAT),
Bavarian Polymer Institute (BPI),
Bayreuth Center for Colloids and Interfaces (BZKG),

Bayreuth Center for Molecular Biosciences (BZMB),
University of Bayreuth,
Universitätsstraße 30, 95447 Bayreuth, Germany
E-mail: thomas.scheibel@bm.uni-bayreuth.de

†These authors contributed equally to this work.

Keywords: microbe adhesion, hydrogels, patterned films, bio-selective surface, engineered spider silk proteins

Abstract

Antimicrobial-resistant microbial strains are a major problem in health care and are increasing in number at an alarming rate due to the overuse of antimicrobial agents. Therefore, there is a great interest in developing advanced materials that are selectively inhibiting microbial growth (i.e. their adhesion) without actively killing microbes and simultaneously promoting mammalian cell growth (i.e. by promoting adhesion and proliferation). Microbe repellence is a specific feature of some natural spider silks. To unravel how microbe repellence can be achieved in man-processed materials, different recombinant spider silk proteins based on the consensus sequences of *Araneus diadematus* dragline silk proteins (fibroin 3 and 4) were processed into 2D-patterned films and 3D-hydrogels. Strikingly, protein structure characteristics on the nanoscale are the basis for the detected microbe-repellence. Designed spider silk materials promoted mammalian cell attachment and proliferation while inhibiting microbial infestation, indicating the great potential of these engineered spider silk-based materials as bio-selective microbial-resistant coatings in biomedical and technical applications as well as for hydrogel-based tissue regeneration.

1. Introduction

Pathogenic microbial contaminations of surfaces, when exposed to patients, significantly increase the risk of infection and represent a severe problem in the public health care sector.^[1,2] Biofilm formation on biomedical devices, such as prosthetics, medical implants, contact lenses, and catheters, not only limits their functionality and lifetime but can also cause life-threatening infections.^[3,4] Consequently, microbial biofilm generation and nosocomial infection during conventional medical therapy have significantly increased mortality as well as healthcare costs worldwide in the last decade. Outside of the clinical setting, diseases associated with food contamination as well as biofouling of material surfaces in contact with water supply systems are considered major health issues.^[5] There are several interacting parameters that have ultimately led to this problem, however, the most critical is the evolution of antimicrobial-resistant (or even multi-drug resistant)^[6] microbes due to the overuse of antibiotics.^[7,8] Furthermore, microbial colonization can subsequently lead to formation of almost irremovable biofilms, hardly accessible for antibiotics as, after becoming a dense colony, the microbes secrete a protective coating, making it much more difficult to eradicate biofilms in contrast to isolated microbes.^[9,10] One example of a “superbug” is methicillin-resistant *Staphylococcus aureus*, a major cause of community-acquired infections resulting in high morbidity and mortality rates in hospital-acquired infections.^[11] Concerning treatment of these infections, glycopeptide antibiotics (GPAs) targeting the acyl-D-alanyl-D-alanine (D-Ala-D-Ala) terminus of the growing peptidoglycans on the outer surface of the Gram-positive bacteria’s cytoplasmic membrane are considered the last, non-antibiotic resort for medical treatment.^[12] Nevertheless, glycopeptide-resistant organisms cause new problems, as they significantly reduce antibiotic affinity by replacing the D-Ala-D-Ala terminus with D-alanyl-D-lactate (D-Ala-D-Lac) or D-alanyl-D-serine (D-Ala-D-Ser), prompting the search for second generation drugs and new strategies to inhibit spreading of such pathogens by new hygiene standards and for materials with explicit repelling surfaces.^[13] In this context, biomaterials with inherent non-fouling properties would provide new opportunities of long-term protection, especially when they can be used as surface coating materials for already existing products. However, one draw-back of such surfaces is that they often repel any kind of cells, even human ones, making it difficult to employ them in applications such as tissue engineering.^[14]

As one critical step in biofilm formation is the initial adherence of pathogenic microbes onto a material’s surface,^[9] inhibiting microbial attachment is a favorable approach to develop material surfaces resistant to biofilm formation.^[15,16] There are two main approaches for inhibiting surface attachment, referred to as either active or passive resistance. While passively resistant surfaces are typically made of super hydrophilic or hydrophobic as well as zwitterionic or other synthetic polymers,^[17-19] actively resistant ones are often “contact killing” materials, such as cationic polymers, amphiphilic polymers, antimicrobial peptides and polymeric/composite materials loaded with antimicrobial agents.^[20-25] Although these approaches can combat microbial infection by inhibiting mechanisms of persistence and adaptation, several drawbacks exist, such as instability under physiological conditions, cytotoxicity to mammalian cells, inflammatory responses, a narrow antimicrobial spectrum, and implications for transmitting multidrug resistance.^[26] Further, antimicrobial activity has been mostly investigated in terms of its effectiveness against bacteria, although fungal infections also contribute significantly to patient morbidity and mortality. Moreover, fungal infections can readily form polymicrobial biofilms with enhanced resistance to antifungal drugs, further limiting therapeutic options.^[27] Therefore, efficient mitigation of microbial

infection associated with both bacteria and fungi is required for the future development of broad-range multifunctional material coatings.

Spider silk exhibits extraordinary mechanical properties, surpassing the toughness of other polymer fibers, and further displays excellent biocompatibility useful for biomedical applications.^[28,29] Remarkably, most spider silk webs withstand microbial omnipresence and remain resistant to microbial decomposition for years, irrespective of environmental impacts such as humidity, temperature, and location, though being composed of proteins and therefore of amino acids, which would be a valuable source of nutrition for microbes. Only few studies have been published examining microbe-repelling effects of natural spider silk,^[30] and so far, the underlying mechanism remains ambiguous. This is because the surface of silk fibers consists of varying mixtures of spidroins, glycoproteins and lipids, and the composition of the surface further depends on the spider species as well as environmental conditions.^[31] In some cases, even antimicrobial peptides might be implemented recombinantly to the spider silk coatings.^[32,33] Consequently, the resistance of spider silk fibers against microbial infestation has so far only been macroscopically described, but not assigned to single material components such as lipids, glycoproteins, silk proteins or material features of these composite materials. Recently published results indicate that bacterial infestation and decomposition of spider silk is inhibited by bacteriostatic activity rather than by anti-bacterial means.^[34,35] The authors further hypothesized, that the complex network of interconnected crystalline and non-crystalline structures might prevent accessibility of nitrogen, which is necessary for bacterial growth. Here, 2D and 3D scaffolds based on explicit individual recombinant spider silk proteins, based on sequences of the dragline silk of the European garden spider *Araneus diadematus*, were found to withstand microbial infestation depending on the structural features of the material's surfaces. Two engineered *Araneus diadematus* fibroins eADF3 and eADF4 and variants thereof were utilized, based on consensus sequences of the core domains of the naturally occurring fibroins 3 and 4.^[36,37] Materials made thereof polyanionic eADF4(C16), the best investigated of these variants, display absence of toxicity, lack of immune reactivity and slow biodegradation.^[38,39] As eADF4(C16) lacks cell binding motifs, like most so far identified spider silk proteins, eADF4(C16)-coated implants and catheters display a significantly reduced adhesion and proliferation of mammalian cells as compared to non-treated ones.^[40,41] When transplanted *in vivo* in rats, eADF4(C16)-coated silicone implants exhibited a substantial reduction in capsular fibrosis.^[40] However, cell attachment to eADF4-based materials could be promoted by generating defined surface topographies, such as surface-structured films or non-woven mats, on both of which good cell adhesion and proliferation could be detected due to the precisely controlled topography, dimensions and its increased surface area^[42,43]. As a second approach, genetically modifying eADF4(C16) with the cell-binding motif RGD (Arginine-Glycine-Aspartate) promoted mammalian cell adhesion and proliferation with good cell viability in 2D and 3D materials.^[44,45] Interestingly, even without sterilization, surfaces of materials based on the used recombinant spider silk protein eADF4(C16) were commonly free of microbes.^[46,34]

To systematically analyze microbe repellence, an extensive study was performed applying a diverse selection of different biofilm forming microbes, representing pathogenic bacteria (*S. mutans*, *S. aureus*, *E. coli*) and fungi (*C. albicans*, *P. pastoris*) (**Figure 1A**). Unlike the complex mixture/composite of natural spider silk fibers, recombinant technologies provide pure and perfectly defined proteins and materials made thereof, which are intrinsically non-toxic. Consequently, it was hypothesized, that anti-fouling effects of spider silk surfaces might

not be attributed to toxic effects or explicit amino acid sequences, but to nano-structural features. Numerous technical^[47,48] as well as natural^[49,50] examples have shown the achievement of anti-fouling properties by nano-scaled topographies (**Figure 1B**).^[51] Here, biotechnological design and recombinant production of different spider silk proteins was applied as a platform technology to systematically study the impact of the β -sheet structure-based nano-crystallites concerning anti-fouling performance (**Figure 1C**). To test the hypothesis of nano-topographical effects leading to microbe-repellence, we investigated the impact of the bio-functionalization with a cell-binding motif (RGD), which doesn't change the basic crystallite-structural features of eADF4(C16) and has the potential of bio-selective mammalian cell growth with simultaneous microbe repellence (**Figure 1C: a1, a3**). To evaluate the impact of molecular weight as well as terminal domains, eADF4(C32NR4) was included within this study as its non-repetitive terminal domain causes dimerization resulting in an apparent MW of 208 kDa (**Figure 1C: a2**). As no structural differences between the core-domains of these proteins and that of eADF4(C16) could be detected,^[36] anti-fouling properties were expected to be the same.

On the other hand, structural changes and thus changed microbe-repellent properties were predicted to be induced by varying charges or different amino acid sequence motifs. To analyze the impact of charge, all negatively charged glutamic acid residues (E) in the consensus sequence of eADF4(C16) were replaced by uncharged glutamine residues (Q), resulting in the so far not examined neutral recombinant spider silk variant eADF4(Q16) (**Figure 1C: a4**). We predicted, that loss of electrostatic repulsion would impact the homogeneous crystalline distribution as found in the eADF4(C16) structure leading to rather heterogenous packing, clustering and distribution of β -sheet structures in eADF4(Q16)-based materials. Although, the fibroin 3-based protein variant eADF3(AQ)₁₂ is also uncharged, the amino acid sequence significantly differs in length of the polyalanine as well as glycine-rich sequence motif with direct implications on β -sheet size/crystallite size as well as amorphous regions (**Figure 1C: b1**). It could be expected that the larger amorphous regions in eADF3(AQ)₁₂ sterically separate the crystal parts, leading to a more homogeneous distribution of crystals similar to those found in eADF4(C16), which are based on electrostatic repulsion (**Figure 1C: b1**).

Importantly, recombinant spider silk proteins can be processed into solid morphologies such as films (representing the potential use as coatings of medical devices or bio-plastic foils as packaging materials)^[41,52,53] or soft hydrogels (which are highly relevant in the fields of tissue engineering and biofabrication).^[54-56] Thus, the experimental design included the use of smooth and structured films as well as hydrogels. For comparison, regenerated *B. mori* fibroin was included representing a non-spider silk type with a significantly different amino acid sequence and respective slightly different structural features and therefore crystal size, poly(caprolactone) (PCL) as a broadly applied biopolymer and gelatin, a protein-based material which is often used in the context of biofabrication (i.e. 3D-bioprinting together with cells). To explicitly analyze their suitability in the field of biofabrication and tissue engineering, the bio-selectivity of 2D and 3D materials made of recombinant spider silk proteins was tested in co-culture experiments including microbes and fibroblasts.

2. Results

Bacteriostatic and fungistatic properties of recombinant spider silk films

To systematically investigate the absence of microbes and the putative bacteriostatic and fungistatic properties of distinct spider silk surfaces, films of the negatively charged recombinant spider silk proteins eADF4(C16) and eADF4(C32NR4) and the uncharged eADF4(Q16) and eADF3((AQ)12) were fabricated to test the influence of

the primary structure, molecular weight, net charge and the presence of a terminal assembly domain (**Table S1**, Supporting Information) on microbial adhesion.

At first, we investigated the single bacterial adhesion forces in contact with 2D spider silk surfaces. The forces involved in bacterial adhesion were quantified by atomic force microscopy (AFM) in force spectroscopy mode using single cell bacterial probes.^[57,58] Methicillin-resistant *Staphylococcus aureus* strain (MRSA) is a widespread problem in hospitals and is a highly infectious pathogen responsible for numerous fatalities worldwide. A single *S. aureus* cell was immobilized on a tipless AFM cantilever and pressed with a maximum force of 300 pN onto silanized glass slides coated with eADF4(C16), eADF4(C32NR4), eADF4(Q16), eADF3((AQ)12), *B. mori* fibroin, and PCL, the latter two acting as controls. Direct contact was allowed for some microseconds (termed 0 s in the following) or additional 5 s of surface delay time before the single bacterium was lifted and the adhesion force F_{ad} was measured. Then, the forces were normalized ($F_{ad} (bacteria) /$ adhesion force on uncoated silanized glass $F_{ad} (glass)$), and the statistically weighted mean adhesion force was determined. Thereby, the microbe-repellent properties of recombinant spider silk films of eADF4(C16), eADF4(C32NR4), and eADF3((AQ)12), yielded an extremely low bacterial adhesion force (**Figure 2A**). The initial adhesive force at 0 s was slightly, but significantly higher on eADF4(Q16) (factor ~4.5) and even higher on surfaces of *B. mori* fibroin (factor ~28) and of PCL (factor ~168) in comparison to that of eADF4(C16). At a surface delay time of 5 s, the adhesive forces increased in all cases, but still adhesion forces on the three recombinant spider silk protein-based films (eADF4(C16), eADF4(C32NR4), and eADF3(AQ)12,) were significantly lower than on the control materials (*B. mori* fibroin and PCL). To the best of our knowledge, this bacteriostatic and fungistatic properties of materials made of recombinant spider silk are unique, as materials prepared from regenerated *B. mori* fibroin, which resemble to some extent the composition and properties of spider silk proteins but not the amino acid sequence, do not show such behavior.

Next, we investigated biofilm formation on 2D-surfaces using *E. coli* and *P. pastoris*, this time also including an RGD-modified variant of eADF4(C16). Microbial viability was quantified using the CellTiter-Blue assay. The negligible adhesion of *E. coli* and *P. pastoris* on eADF4(C16), eADF4(C32NR4), and eADF3((AQ)₁₂) as well as eADF4(C16)-RGD films resulted in low fluorescence intensity in comparison to that of consolidated biofilm formation on eADF4(Q16), *B. mori* fibroin and PCL films with much higher microbial viability (**Figure 2B**). These results clearly indicated that explicit spider silk surfaces do not allow efficient adhesion of *E. coli* and *P. pastoris*, an observation that is complementary to the previous quantitative adhesion force measurements using *S. aureus*.

This finding is intriguing, since the amino acid building blocks between the different silk proteins are similar with only slight differences. However, these differences are the basis of distinct structural features with significant impact on protein folding and self assembly. The microbe-repellent properties of these different silks seem to be directly based on these structural features. To confirm that microbe-repellance is based on structural but not topographical features, flat spider silk films were compared to micro-patterned ones (2 μm wide grooves, 1 μm wide and 4 μm high ridges) concerning microbial adhesion. The surface topography of spider silk films has previously been shown to influence mammalian cell attachment and proliferation making this experiment important.^[42] Suspended cariogenic *Streptococcus mutans* (*S. mutans*) as well as pathogenic *Candida albicans* (*C. albicans*) were seeded on top of all smooth and patterned films for 12 h at 37 °C. After washing to remove

non-adherent pathogens, films were air dried for microscopic analysis of microbial growth. Scanning electron microscope (SEM) images clearly showed that both smooth and patterned eADF films substantially restricted the attachment, growth and microbial colonization of *S. mutans* as well as *C. albicans*, and confirmed the superior repellence of spider silk 2D films (exemplarily shown are eADF4(C16) films) as compared to PCL ones (**Figure 2, C-F**). This finding confirmed the strict dependence of microbe adhesion to protein-structural surface pattern but not on surface topography, which was surprising since the grooves were expected to provide optimal niches for bacterial and fungal physical attachment, being thought to provide at least some impact on microbe adhesion. The microbe-repellence structural features were overruling any effect that the topography would normally have, which was also exhibited in the control groups. This property could have far-reaching impact on future applications, as *C. albicans* is an opportunistic, common fungal pathogen found in hospitals and is known to be highly infectious and life threatening. Additionally, *E. coli* and *P. pastoris* cells were tested concerning their adhesion to all recombinant spider silk protein-based films and could not attach to either smooth and patterned films (**Figure S1**, Supporting Information).

Next, it was investigated whether this protein structure-based bacteriostatic and fungistatic properties are restricted to the surface of explicit spider silk films or if they are generic, that is, the feature is retained when other spider silk morphologies (with identical protein structures) are prepared, such as hydrogels. Spider silk proteins can be processed into shear thinning hydrogels which can be 3D printed,^[45] and one possible application is their use as scaffolds in tissue regeneration. Therefore, bacteriostatic and fungistatic properties would complement other interesting features such as non-toxicity and biodegradability of recombinant spider silk hydrogels.^[53,38,39] These properties, in combination with a controllable adhesion of mammalian cells, would boost their applicability in various biomedical applications.

Bacteriostatic and fungistatic properties of spider silk hydrogels

To monitor their bacteriostatic and fungistatic properties, spider silk hydrogels were incubated with *E. coli* and *P. pastoris* for 24 h at 37 °C. As a control, hydrogels of regenerated *B. mori* fibroin^[59] and gelatin^[60] as a further commonly used biomaterial were incubated in an identical manner. Subsequently, all hydrogels were washed carefully to remove non-adherent bacteria, and an alamar blue viability assay was used to determine *E. coli* and *P. pastoris*. Spider silk hydrogels with microbes showed little alamar blue fluorescence, exemplarily shown for eADF4(C16) and eADF4(C16)-RGD (**Figure 3A**). SEM images of lyophilized hydrogels clearly indicated that bacteria and fungi were not adhering and growing on and within recombinant spider silk hydrogels (**Figure 3, B (i-ii) and C (i-ii)**) even upon incubation for 10 days (**Figure S2**, Supporting Information). Importantly, in this study, adhesion of microbial cells to eADF4(Q16) hydrogels endorsed the microbe-repellence structural features of spider silk in 3D surfaces as well to some extent (**Figure 3, A, D (i-ii)**). However, it can be clearly seen that *B. mori* fibroin and gelatin hydrogels enabled *E. coli* and *P. pastoris* cells to adhere and colonize, (**Figure 3, A, E (i-ii) and F (i-ii)**). On and within both *B. mori* fibroin and gelatin hydrogels, microbial biofilms could be easily detected.

Bio-selective properties of spider silk films and hydrogels

Since the identified bacteriostatic and fungistatic properties of distinct spider silk materials can be distinguished from the previously determined topography-dependent adhesion of mammalian cells, we wanted to elucidate whether it is possible to trigger a bio-selective behavior, which represses the growth of microbes but enhances

mammalian cell attachment and proliferation. To improve mammalian cell adhesion, we used eADF4(C16)-RGD known to interact with integrin receptors to promote mammalian cell attachment.^[44,45,55] Importantly, all other physicochemical characteristics of this variant are indistinguishable to that of eADF4(C16) including pronounced bacteriostatic and fungistatic properties to resist biofilm formation as shown above.

Hydrogels made of eADF4(C16) and eADF4(C16)-RGD were used to encapsulate BALB/3T3 fibroblasts, and these were seeded with *E. coli* and *P. pastoris* for 6 h to mimic a situation similar to that of a post-operative infection (**Figure S3**, Supporting Information). After 6 h of incubation, hydrogels were washed carefully to remove non-adherent cells (mammalian as well as microbial), and the hydrogels were further incubated with fresh cell culture media. Viability of microbes and fibroblasts was evaluated by microscopy and live/dead staining after 3, 6, and 10 days of incubation (**Figure 4, (A-i) – (A-iii), (B-i) – (B-iii), (C-i) – (C-iii), and (D-i) – (D-iii)**). Encapsulated fibroblasts showed good viability within the hydrogels made of eADF4(C16) and eADF4(C16)-RGD over a culture period of 10 days (**Figure 4E**), while no bacterial and fungi growth/contamination could be detected during the entire cultivation period (**Figure 4F and G**), since the microbes could not adhere to start colony formation and did not manifest a biofilm. As expected, introduction of the RGD-sequence stimulated the proliferation of BALB/3T3 fibroblasts in contrast to eADF4(C16) hydrogels in which very little proliferation was observed.

3. Discussion

Microbial adhesion tests with different pathogenic microorganisms using both bacteria (*S. mutans*, *S. aureus*, and *E. coli*) and fungi (*C. albicans*, and *P. pastoris*) demonstrated microbe repellence of distinct recombinant spider silk materials. None of the tested microbes could manifest biofilms on selected recombinant spider silk films, hydrogel surfaces or within hydrogels. The inherent property of bacteriostatic and fungistatic performance of distinct spider silk materials was speculated to be related to the structural features of the underlying proteins responsible for the formation of hydrophobic patches.^[61] The used protein platform technology (**Figure 5I**), confirmed the correlation of adhesion of microorganisms with the arrangement of protein secondary structures (i.e. hydrophobic patches) (**Figure 5II, and III**). As shown schematically, based on the primary sequence, the size and homogeneous distribution of hydrophobic patches can be controlled due to either intermolecular charge-charge repulsion as in eADF4(C16) and eADF4(C32NR4) or volume effect of the amorphous region in eADF3(AQ)12. In contrast, the absence of charge in eADF4(Q16) was hypothesized to induce a denser and less homogeneous packing of nano β -crystallites, creating large-enough anchoring sites for microbes. On the mesoscale, microbial cell attachment most readily occurs on surfaces which are rougher, more hydrophobic and positively charged. Distinct silk proteins, such as spider silk and silkworm silks, feature structural differences e.g. concerning the β -sheet crystallite size (spider silk: ~ 7 nm, *B. mori* fibroin ~ 14 -200 nm) and crystallite orientation,^[43,44] both influencing the dimensions of the respective hydrophobic patches. Our study demonstrated that 2D and 3D surfaces of *B. mori* fibroin with larger hydrophobic patches than that of spider silk are easily accessible for microbial manifestation. RGD-modified spider silk with homogeneous hydrophobic patches allowed selective mammalian cell adhesion and proliferation, with concomitant repellence of microbes. In comparison to natural spider silk with its composite surface layer. It is highly interesting that no additional components such as glycoproteins, lipids or antimicrobial agents but only the structural features of individual recombinant spider silk proteins are necessary to generate a microbe-repelling spider silk surface. To the best of

our knowledge, this is a completely new finding which opens the door for novel applications of spider silk materials, e.g., as bioselective coatings in various biomedical applications.

Acronyms

eADF4	engineered <i>Araneus diadematus</i> Fibroin 4
<i>B. mori</i>	<i>Bombyx mori</i>
PCL	poly(caprolactone)
<i>S. aureus</i>	<i>Staphylococcus aureus</i>
<i>E. coli</i>	<i>Escherichia coli</i>
<i>P. pastoris</i>	<i>Pichia pastoris</i>
<i>C. albicans</i>	<i>Candida albicans</i>
<i>S. mutans</i>	<i>Streptococcus mutans</i>
AFM	atomic force microscopy

Experimental Section

Protein design and production of recombinant spider silk proteins: eADF4(C16) was purchased from AMSilk GmbH (Planegg, Germany). The recombinant spider silk proteins eADF4(C16)-RGD, eADF4(C32NR4) and eADF3(AQ)12 were produced and purified as described previously.^[36,44] To generate the uncharged eADF4(Q16) variant, the glutamic acid residues (E) of the consensus sequence of eADF4(C16) were exchanged with glutamine (Q) ones. The recombinant spider silk protein eADF4(Q16) was produced in *E. coli* BL21 gold (DE3) and purified following a protocol as described previously.^[36] Briefly, after cell disruption eADF4(Q16) was purified using a heat step and an ammonium sulfate precipitation.

***Bombyx mori* (*B. mori*) fibroin protein:** Regenerated fibroin solutions were prepared as described previously^[59] by dissolving degummed (boiled for 30 min in 0.02M sodium carbonate) silk fibres in 9.3 M LiBr solution, dialysis against ultrapure water (Milli-Q) for 2 d at 4 °C, centrifugation at 8500 rpm for 45 min at 4 °C, and collection of the supernatant. The *B. mori* fibroin solutions had a final concentration of ~6% w/v and were stored at 4 °C until use. For the production of flat and patterned films, solutions were freeze-dried and processed in the same way as spider silk and PCL.

Production of flat and patterned films: All flat and patterned films of proteins and polycaprolactone (PCL; Perstorp AB) were produced by film casting onto patterned polydimethylsiloxane (PDMS; Sylgard 184 Silicone Elastomer, Dow Corning) substrates. PDMS stamps were produced by casting of a 10:1 mixture of PDMS pre-polymer and curing agent (degassed for 20 min) on a photo-lithographically patterned wafer to generate the desired geometry (12 x 12 mm area with 2 µm wide grooves, ridges with a width of 1 µm and a height of 4 µm). After curing at 80 °C for 90 min, the stamps were solidified and could be easily peeled off. To produce patterned films, proteins and PCL were dissolved in 1,1,1,3,3,3,-hexafluoro-2-propanol (HFIP; Alpha Aesar) at a concentration of 100 mg/mL (room temperature, overnight). To generate films with a thickness of 10-15 µm, 250 µL of solution (corresponding to 25 mg of protein/polymer) were poured into the stamp, and the solvent was subsequently evaporated at room temperature. The dried patterned films were removed and post-treated with 100% ethanol for 1 h to render the silk protein water insoluble upon induction of β-sheet structures. To ensure that only material properties determined the results of microbial growth experiments, all samples (including PCL films) were treated the same way. After post-treatment, the samples were stored sterile in 70 % ethanol at 4 °C.

Bacteria and yeast culture on films: (a) *Streptococcus mutans* (DSMZ 20523, Braunschweig) and *Candida albicans* (patient isolate), stored at -80 °C, were thawed at RT, fractionally spread on Columbia blood agar (PB 5039A, oxoid, Wesel) and incubated for 48 h at 37 °C and 5 % CO₂. Afterwards, an overnight culture was prepared in BBLTM Schaedler Broth medium (Becton Dickinson, Sparks MD, USA), and then the culture was diluted (1:10) with Schaedler Broth medium. (b) *Escherichia coli* BL21(DE3)-gold (Novagen, Merck, Darmstadt, Germany), stored at -80 °C, was thawed at RT and inoculated in Luria–Bertani medium (LB), at 37 °C with constant shaking at 150 rpm until an optical density (OD₆₀₀) between 0.8 and 1 was reached (corresponding to a viable count of approx. 10⁷–10⁸ CFU mL⁻¹). The *E. coli* culture was diluted (1:10) with LB medium. (c) *Pichia pastoris* X33 (wild type, Invitrogen, Germany) was inoculated in YPD-media and allowed to grow for 24 h at 30 °C with constant shaking at 150 rpm. The *P. pastoris* culture was diluted (1:10) with YPD medium. Silk and polymer films were taken out of 70 % ethanol, subsequently washed with PBS (8.18 g NaCl, 0.2 g KCl, 0.24 g anhydrous KH₂PO₄, 1.78 g Na₂HPO₄ x 2H₂O, 1 L distilled water, pH 7.4, Sigma Aldrich, St. Louis, Missouri, USA), and incubated in 5 mL of diluted microbial solution (as described above) in petri dishes (Ø 5 cm) for 60 h (5 % CO₂, 37 °C). Then, the films were removed and carefully washed with PBS to remove non-adherent bacteria and yeast cells and dried at room temperature for subsequent SEM imaging. (d) For adhesion force measurements, *Staphylococcus aureus* (strain SA113), stored at -20 °C, was thawed and cultured for three days at 37 °C on blood agar plates. Then, one colony from a plate was transferred into 5 mL of sterile tryptic soy broth (TSB) and cultured overnight at 37 °C, 150 rpm agitation. For each experiment, 40 µL of the culture were transferred into 4 mL fresh TSB and cultured for another 2.5 h at 37 °C. The bacterial culture was washed three times with sterile phosphate buffered saline (PBS). The final suspension of bacteria in PBS was stored at 4 °C and used no longer than 6 hours.

Adhesion force measurements: Single *S. aureus* cells were attached to a tipless AFM cantilever (MLCT-0 with a nominal spring constant of 0.03 N/m from Bruker Nano, Santa Barbara, Ca, USA) coated with polydopamine that were calibrated before each set of experiments.^[57,58] Force-distance measurements were performed using a Bioscope Catalyst from Bruker-Nano in PBS at room temperature. The maximum force with which the cells were pressed onto the surfaces was set to 300 pN. On each surface, 25 force-distance curves were performed for 0 s and 5 s of additional surface delay time with one and the same cell, the total number of individual cells being twelve. The results obtained from three of these cells were not used for the analysis as their adhesion forces were less than 5 % of the mean adhesion force of the remaining cells indicating that the adhesive strengths of these cells were not representative for the totality of *S. aureus* cells used. Nine more cells were tested on eADF4(C16), *B. mori* fibroin, and PCL with identical parameters under the same conditions. Approaching speed towards the surfaces was set to 800 nm/s for 0 s of surface delay time and 100 nm/s for 5 s of surface delay time. Retraction speed was 800 nm/s. To test the results of adhesion measurements for statistical significance, all adhesion force distributions were analyzed in pairs by a Man-Whitney-U-test with the software Matlab.

Bacterial and yeast cell viability: Adhesion of *E. coli* and *P. pastoris* to silk and polymer films or hydrogels after culturing for 24 h at 37 °C was measured by analysis of cell vitality using the CellTiter-Blue assay. Samples incubated with bacterial and yeast cells were washed with phosphate buffered saline (PBS; Sigma-Aldrich) three

times, and then incubated with 10 % CellTiter-Blue (Promega) in PBS for 3 h at 37 °C. Transformation of the blue fluorescent dye resazurin into red fluorescent resorufin ($\lambda_{\text{ex}} = 530 \text{ nm}$; $\lambda_{\text{em}} = 590 \text{ nm}$) was measured using a plate reader (Mithras LB 940, Berthold, Bad Wildbad) with counting time of 0.5 s.

Preparation of eADF4(C16), eADF4(C16)-RGD and eADF4(Q16) hydrogels: Lyophilized eADF4(C16) and eADF4(C16)-RGD were dissolved in 6 M guanidinium thiocyanate (GdmSCN) at 5 mg/mL and dialyzed against 10 mM Tris/HCl, pH 7.5 overnight at room temperature using dialysis membranes with a molecular weight cutoff of 6–8 kDa. Subsequent dialysis against 20 % w/v poly (ethylene glycol) (PEG, 20,000 g/mol) at a volume ratio of PEG/eADF4(C16) solution of 100:1 was used to remove water by osmotic pressure and to adjust 30 mg/mL (3 % w/v) spider silk solutions. Hydrogels were self-assembled after an overnight incubation at 37 °C. For the preparation of eADF4(Q16) hydrogels, all steps were carried out at 4 °C, and hydrogels were prepared at concentration of 20 mg/mL (2 % w/v) eADF4(Q16).

For co-culture experiments, 1×10^6 BALB/3T3 fibroblasts were added to 3 % w/v eADF4(C16) and eADF4(C16)-RGD spider silk solutions before gelation in an incubator at 37 °C.

Preparation of B. mori fibroin hydrogels: *B. mori* fibroin hydrogels were prepared using sonication induced gelation, as previously reported.^[59] In brief, 4 % (w/v) aqueous silk fibroin solution in a 15 mL conical tube was ultra-sonicated (Ultrasonic Homogenizers HD 3100, BANDELIN) at 50 % amplitude (21 W) for 30 s, and overnight incubation at 37 °C induced gelation.

Preparation of gelatin hydrogels: GelMA was produced upon reacting gelatin solutions (gelatin from bovine skin, Type B, ~225g Bloom, Sigma-Aldrich) with methacrylic anhydride (Sigma-Aldrich) following previously described protocols.^[60] After the dissolution of 10 % (w/v) gelatin in 0.1M CB buffer (3.18 g sodium carbonate and 5.86 g sodium bicarbonate in 1L distilled water) at 60 °C, one sixth of 1 % (v/v) methacrylic anhydride was added dropwise every 30 min for 3 h. The solution was vigorously stirred for another 1 h, diluted with 0.1M CB, and dialyzed for 2 days against ultrapure (Milli-Q) water at 37 °C. The solution was then freeze-dried in a lyophilizer to obtain methacrylamide-modified gelatin as a dry white powder.

Methacrylamide-modified gelatin hydrogel was obtained by UV exposure of 5 % (w/v) GelMA solution in 24 well cell culture vessels at 365 nm using an ultraviolet lamp (Benda, type NU -4 KL) for 15 min in the presence of 0.5 mg/mL of the photoinitiator 2-hydroxy-4'-(2-hydroxyethoxy)-2-methylpropiophenone (Irgacure- 2959, Sigma-Aldrich).

Bacteria and yeast culture with hydrogels: Hydrogels were incubated with 1 mL of diluted liquid cultures of *E. coli* and *P. pastoris* for 12 h at 37 °C. Hydrogels were washed with phosphate buffered saline (PBS; Sigma-Aldrich) three times to remove non-adherent bacteria and yeast cells and then lyophilized.

Microbial adhesion: The anti-adherence activity of eADF4(C16) and eADF4(C16)-RGD hydrogels concerning *E. coli* and *P. pastoris* was measured by inoculating the supernatant (100 μL) of the microbe-treated hydrogels (after washing) in fresh media and culturing for additional 12 h at 37 °C. Optical density at 600 nm (OD_{600} ; OD_{600} DiluPhotometer™, IMPLEN) was measured to monitor microbial growth/infection.

BALB/3T3 cultivation: BALB/3T3 mouse fibroblasts (European Collection of Cell Cultures) were cultured in Dulbecco's Modified Eagle Medium (DMEM, Biochrom) supplemented with 10 % fetal bovine serum (Biochrom) and 1 % (v/v) GlutaMAX (Gibco) in a controlled atmosphere of 5 % CO₂, 95 % humidity and at 37 °C. Viability and number of cells were analyzed using trypan blue (Sigma-Aldrich) in a Neubauer chamber (Laboroptik, UK).

Co-culture experiments with hydrogels: eADF4(C16) and eADF4(C16)-RGD hydrogels with encapsulated BALB/3T3 mouse fibroblasts (i.e. bioinks) were prepared in hanging cell culture inserts using 24-well plates (Merck Millipore) and then exposed to diluted (1:10, corresponding to OD 0.25) bacterial and yeast cells prepared in DMEM for 6 h at 37 °C with 80 % relative humidity. Hydrogels were washed three times to remove non-adherent microbes and incubated with fresh DMEM media and cultivated for 10 days under identical conditions. Cell culture medium was changed every 24 h. The cell viability of BALB/3T3 mouse fibroblasts was analyzed using the Live/Dead assay after 3, 6 and 10 days.

Live/Dead assay: Films and hydrogels of eADF4(C16) and eADF4(C16)-RGD were washed with PBS and stained with Calcein acetoxymethylester (Calcein A/M, Invitrogen) and Ethidium Homodimer-1 (EthD-1, Invitrogen) in cell culture medium for the detection of live and dead cells, respectively. Calcein A/M was added to the medium at a final concentration of 0.3 µM, and Ethidium Homodimer-1 was added to the medium at a final concentration of 0.1 µM and incubated for 30 min. After staining, the solution was removed, and fresh PBS was added for imaging. Live and dead cells were visualized and analyzed using a fluorescence microscope (Leica DMI8, Wetzlar) and processed using either Leica Application Suite or Image J.

Scanning electron microscopy (SEM): To analyze the morphological structure using SEM, hydrogels were lyophilized and fixed to SEM stubs using conductive carbon cement solution (Leit-C, PLANO GmbH). Samples were sputter-coated with 2 nm platinum (Sputter Coater 208 HR with 268 MTM 20, Cressington, Watford, U.K.) and then imaged at an accelerating voltage of 2.5 kV using a scanning electron microscope 270 Zeiss Sigma VP 300 (Zeiss, Oberkochen, Germany) and Field Emission Gun (FEG; Apreo VS, ThermoFisher Scientific/FEI, Germany).

Supporting Information

Supporting Information is available from the Wiley Online Library or from the author.

Acknowledgements

S.K. and G.L. contributed equally to this work. The authors thank Dr. Hendrik Bargel for SEM imaging. This project has been funded by the Deutsche Forschungsgemeinschaft (DFG, German Research Foundation)-project number 326998133–TRR225 (funded subprojects and PIs: A07: G.L.; and C01: T.S.).

Received: ((will be filled in by the editorial staff))

Revised: ((will be filled in by the editorial staff))

Published online: ((will be filled in by the editorial staff))

References

- [1] L. L. Leape, T. A. Brennan, N. Laird, A. G. Lawthers, A. R. Localio, B. A. Barnes, L. Hebert, J. P. Newhouse, P. C. Weiler, H. Hiatt, *N. Engl. J. Med.* **1991**, 324, 377.
- [2] V. Russotto, A. Cortegiani, S. M. Raineri, A. Giarratano, *J. Intensive Care* **2015**, 3, 54.
- [3] A. Gristina, *Science* **1987**, 237, 1588.
- [4] E. Barth, Q. M. Myrvik, W. Wagner, A. G. Gristina, *Biomaterials* **1989**, 10, 325.
- [5] B. Carpentier, O. Cerf, *J. Appl. Bacteriol.* **1993**, 75, 499.
- [6] S. B. Levy, B. Marshall, *Nat. Med.* **2004**, 10, S122.
- [7] D. Davies, *Nat. Rev. Drug Discov.* **2003**, 2, 114.
- [8] G. D. Wright, *Nat. Rev. Microbiol.* **2007**, 5, 175.
- [9] J. W. Costerton, P. S. Stewart, E. P. Greenberg, *Science* **1999**, 284, 1318.
- [10] P. S. Stewart, J. William Costerton, *The Lancet* **2001**, 358, 135.
- [11] T. J. Foster, *J. Clin. Invest.* **2004**, 114, 1693.
- [12] E. Binda, F. Marinelli, G. L. Marcone, *Antibiotics* **2014**, 3, 572.
- [13] J. Pootoolal, J. Neu, G. D. Wright, *Annu. Rev. Pharmacol. Toxicol.* **2002**, 42, 381.
- [14] J. Hasan, R. J. Crawford, E. P. Ivanova, *Trends Biotechnol.* **2013**, 31, 295.
- [15] D. Campoccia, L. Montanaro, C. R. Arciola, *Biomaterials* **2013**, 34, 8018.
- [16] D. Campoccia, L. Montanaro, C. R. Arciola, *Biomaterials* **2013**, 34, 8533.
- [17] S. Chen, L. Li, C. Zhao, J. Zheng, *Polymer* **2010**, 51, 5283.
- [18] S. Krishnan, C. J. Weinman, C. K. Ober, *J. Mater. Chem.* **2008**, 18, 3405.
- [19] E.-R. Kenawy, S. D. Worley, R. Broughton, *Biomacromolecules* **2007**, 8, 1359.
- [20] M. R. E. Santos, A. C. Fonseca, P. V. Mendonça, R. Branco, A. C. Serra, P. V. Morais, J. F. J. Coelho, *Materials* **2016**, 9, 599.
- [21] Y. Yang, Z. Cai, Z. Huang, X. Tang, X. Zhang, *Polym. J.* **2018**, 50, 33.
- [22] M. Zasloff, *Nature* **2002**, 415, 389.
- [23] E. M. Hetrick, M. H. Schoenfish, *Chem. Soc. Rev.* **2006**, 35, 780.
- [24] K. P. Miller, L. Wang, B. C. Benicewicz, A. W. Decho, *Chem. Soc. Rev.* **2015**, 44, 7787.
- [25] Y. Liu, L. Shi, L. Su, H. C. van der Mei, P. C. Jutte, Y. Ren, H. J. Busscher, *Chem. Soc. Rev.* **2019**, 48, 428.
- [26] D. Campoccia, L. Montanaro, P. Speziale, C. R. Arciola, *Biomaterials* **2010**, 31, 6363.
- [27] M. M. Harriott, M. C. Noverr, *Antimicrob. Agents Chemother.* **2009**, 53, 3914.
- [28] L. Eisoldt, A. Smith, T. Scheibel, *Mater. Today* **2011**, 14, 80.
- [29] J. A. Kluge, O. Rabotyagova, G. G. Leisk, D. L. Kaplan, *Trends Biotechnol.* **2008**, 26, 244.
- [30] S. Wright, S. L. Goodacre, *BMC Research Notes* **2012**, 5, 326.
- [31] A. Sponner, W. Vater, S. Monajembashi, E. Unger, F. Grosse, K. Weisshart, *PLOS ONE* **2007**, 2, e998.
- [32] A. R. Franco, E. M. Fernandes, M. T. Rodrigues, F. J. Rodrigues, M. E. Gomes, I. B. Leonor, D. L. Kaplan, R. L. Reis, *Acta Biomater.* **2019**, 99, 236.
- [33] L. Nilebäck, J. Hedin, M. Widhe, L. S. Floderus, A. Krona, H. Bysell, M. Hedhammar,

- Biomacromolecules* **2017**, *18*, 846-854.
- [34] R. H. Zha, P. Delparastan, T. D. Fink, J. Bauer, T. Scheibel, P. B. Messersmith, *Biomater. Sci.* **2019**, *7*, 683.
- [35] S. Zhang, D. Piorkowski, W.-R. Lin, Y.-R. Lee, C.-P. Liao, P.-H. Wang, I. M. Tso, *J. Exp. Biol.* **2019**, *222*, jeb214981.
- [36] D. Huemmerich, C. W. Helsen, S. Quedzuweit, J. Oschmann, R. Rudolph, T. Scheibel, *Biochemistry* **2004**, *43*, 13604.
- [37] C. Vendrely, T. Scheibel, *Macromol. Biosci.* **2007**, *7*, 401.
- [38] A. Leal-Egaña, T. Scheibel, *Biotechnol. Appl. Biochem.* **2010**, *55*, 155.
- [39] S. Müller-Herrmann, T. Scheibel, *ACS Biomater. Sci. Eng.* **2015**, *1*, 247.
- [40] P. H. Zeplin, N. C. Maksimovikj, M. C. Jordan, J. Nickel, G. Lang, A. H. Leimer, L. Römer, T. Scheibel, *Adv. Funct. Mater.* **2014**, *24*, 2658.
- [41] C. B. Borkner, S. Wohlrab, E. Möller, G. Lang, T. Scheibel, *ACS Biomater. Sci. Eng.* **2017**, *3*, 767.
- [42] F. Bauer, S. Wohlrab, T. Scheibel, *Biomater. Sci.* **2013**, *1*, 1244.
- [43] A. Leal-Egana, G. Lang, C. Mauerer, J. Wickinghoff, M. Weber, S. Geimer, T. Scheibel, *Adv. Eng. Mater.* **2012**, *14*, B67.
- [44] S. Wohlrab, S. Müller, A. Schmidt, S. Neubauer, H. Kessler, A. Leal-Egaña, T. Scheibel, *Biomaterials* **2012**, *33*, 6650.
- [45] K. Schacht, T. Jüngst, M. Schweinlin, A. Ewald, J. Groll, T. Scheibel, *Angew. Chem.* **2015**, *127*, 2858; *Angew. Chem. Int. Ed.* **2015**, *54*, 2816.
- [46] K. Schacht, U. Slotta, M. Suhre, *sofwjournal* **2017**, *143*, 04.
- [47] M. V. Graham, N. C. Cady, *Coatings*, **2014**, *4*, 37.
- [48] X. Khoo, M. W. Grinstaff, *MRS Bulletin* **2011**, *36*, 357.
- [49] A. Tripathy, P. Sen, B. Su, W. H. Briscoe, *Adv. Colloid Interface Sci.* **2017**, *248*, 85.
- [50] S. Erramilli, J. Genzer, *Soft Matter* **2019**, *15*, 4045.
- [51] Y. Cheng, G. Feng, C. I. Moraru, *Front. Microbiol.* **2019**, *10*, 191.
- [52] S. Wohlrab, K. Spieß, T. Scheibel, *J. Mater. Chem.* **2012**, *22*, 22050.
- [53] K. Spiess, A. Lammel, T. Scheibel, *Macromol. Biosci.* **2010**, *10*, 998.
- [54] S. Kumari, H. Barga, M. U. Anby, D. Lafargue, T. Scheibel, *ACS Biomater. Sci. Eng.* **2018**, *4*, 1750.
- [55] D. Elise, S. Kristin, P. Alexandra, S. Thomas, *Biofabrication* **2017**, *9*, 044104.
- [56] C. Thamm, E. DeSimone, T. Scheibel, *Macromol. Biosci.* **2017**, *17*, 1700141.
- [57] N. Thewes, P. Loskill, C. Spengler, S. Humbert, M. Bischoff, K. Jacobs, *Eur. Phys. J. E* **2015**, *38*, 140.
- [58] N. Thewes, A. Thewes, P. Loskill, H. Peisker, M. Bischoff, M. Herrmann, L. Santen, K. Jacobs, *Soft matter* **2015**, *11*, 8913.
- [59] D. N. Rockwood, R. C. Preda, T. Yucel, X. Wang, M. L. Lovett, D. L. Kaplan, *Nat. Protoc.* **2011**, *6*, 1612.
- [60] H. Shirahama, B. H. Lee, L. P. Tan, N.-J. Cho, *Sci. Rep.* **2016**, *6*, 31036.
- [61] C. B. Borkner, S. Lentz, M. Müller, A. Fery, T. Scheibel, *ACS Appl. Polym. Mater.* **2019**, DOI 10.1021/acsapm.9b00792.

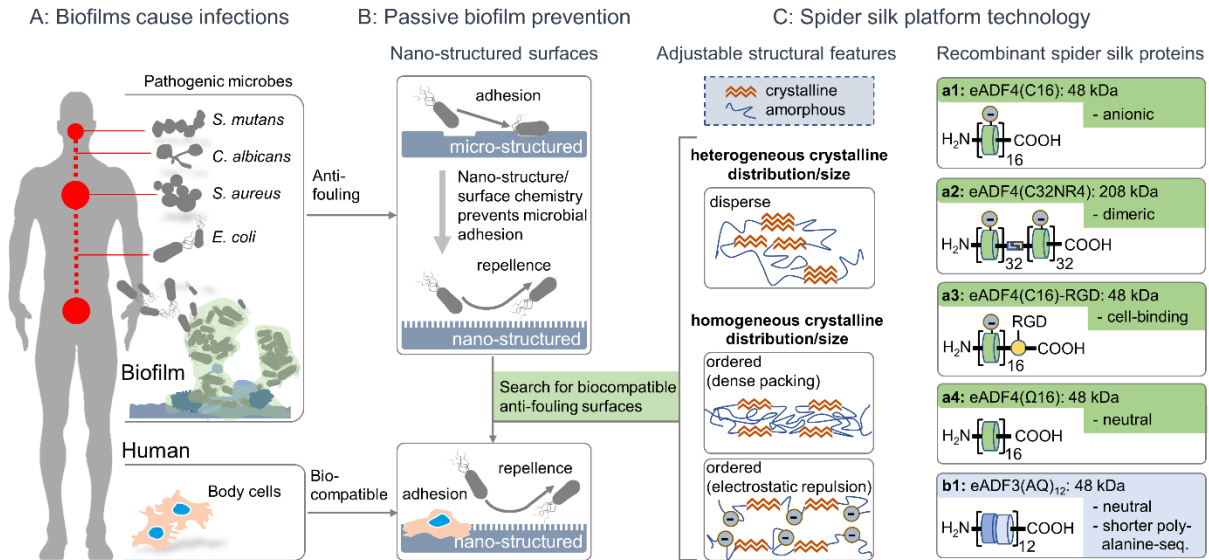


Figure 1. Schematic overview of the conceptual strategy to prevent biofilm formation using spider silk materials. Various biofilm-forming microbes representing pathogenic bacteria and fungi (A) as well as *P. pastoris* (model system) were chosen to verify previously established concepts of passive biofilm prevention by nano-structured surfaces (B) using the engineered recombinant spider silk platform technology (C). It is predicted that particularly the charge and the amino acid sequence contributes to the homogeneity of crystallite size and distribution. Biotechnological engineering allows for systematic adaption of e.g. molecular weight (a1 vs. a2) and bio-functionality (a1 vs. a3) not affecting the crystallite properties of the underlying silk proteins. On the other hand, changes such as charge (a1 vs. a4) or amino acid sequence (a1 vs. b1) are expected to impact crystallite size and distribution. Combining microbe-repellant structural features with the ability to modify the intrinsically bio-compatible spider silk proteins with cell-adhesion motifs (a3) resulted in distinct bio-selective 2D and 3D spider silk materials.

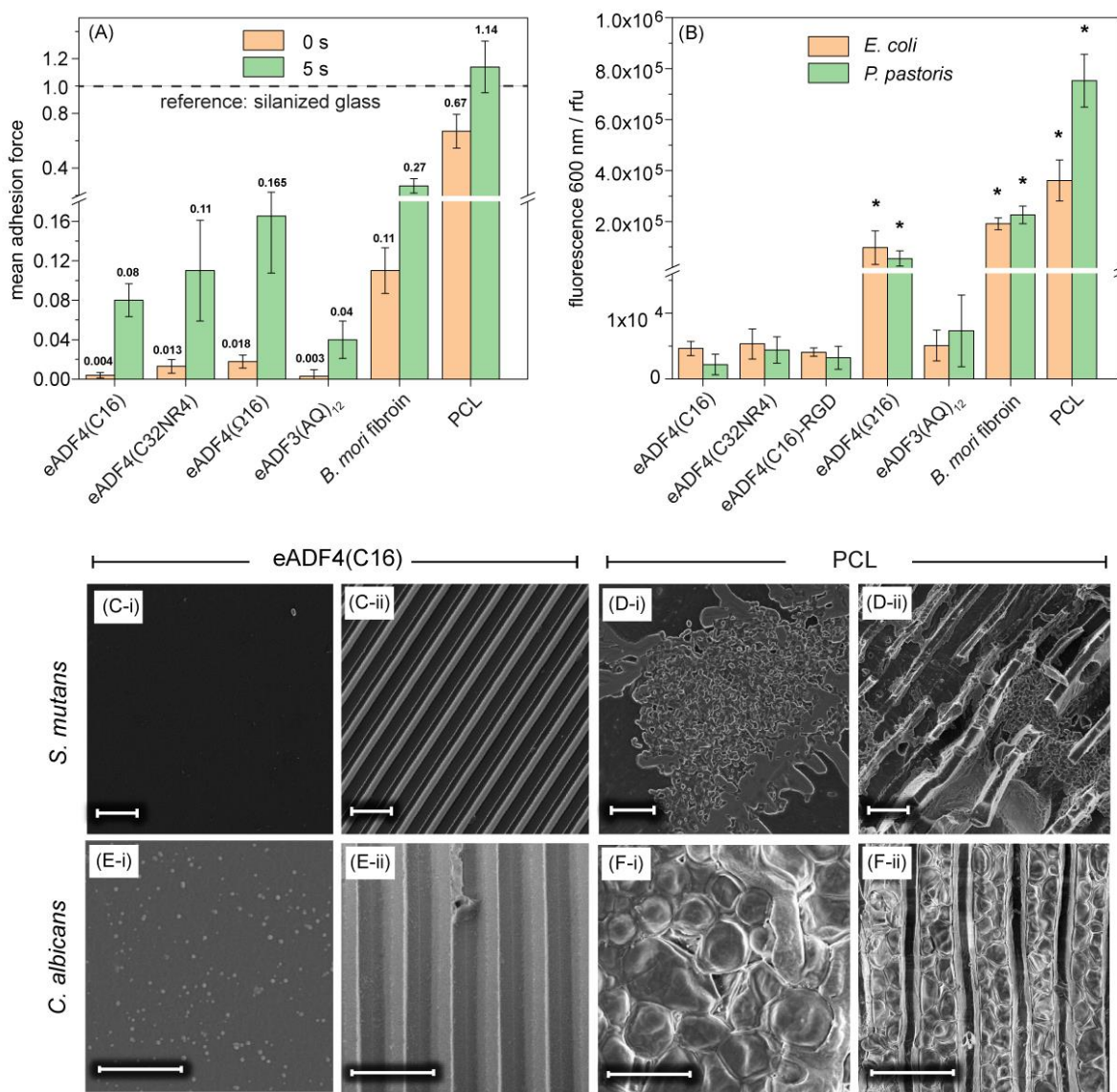


Figure 2. Bacteriostatic and fungistatic properties of 2D scaffolds made of recombinant spider silk proteins. (A) Adhesion force measurements using single *S. aureus* probes on silanized glass coated with eADF4(C16), eADF4(C32NR4), eADF4(Q16), eADF3((AQ)₁₂), *B. mori* fibroin, and PCL, the latter two serving as controls. Representative normalized mean adhesion forces were obtained from 25 force-distance curves performed on each surface for 0 s (brown) as well as 5 s (green) surface delay time using one and the same cell immobilized on a cantilever with a nominal spring constant of 0.03 N m⁻¹. Forces were referred to the values measured on uncoated silanized glass (4.8 ± 2.4 nN). It was detected that all distributions of adhesion forces were significantly different with p values below 0.001. (B) Viability of *E. coli* and *P. pastoris* cells on films of eADF4(C16), eADF4(C32NR4), eADF4(C16)-RGD, eADF3((AQ)₁₂), *B. mori* fibroin, and PCL, after incubation for 24 h at 37 °C. Microbial viability was quantified using the CellTiter-Blue assay by measuring the transformation of the blue fluorescent dye resazurin into red fluorescent resorufin using 530 nm excitation and 600 nm emission filters in a microplate reader. Each result is an average of five experiments, and the error bars designate the standard deviations. Student's t-test was performed for statistical analysis, *indicates significant difference to eADF4(C16) (p < 0.05). Exemplarily SEM images showing (i) plane and (ii) micro-patterned surfaces of (C & E)

eADF4(C16) and (D & F) PCL after 12 h of incubation with (C & D) *S. mutans* and (E & F) *C. albicans* at 37 °C. Scale bars = 5 µm.

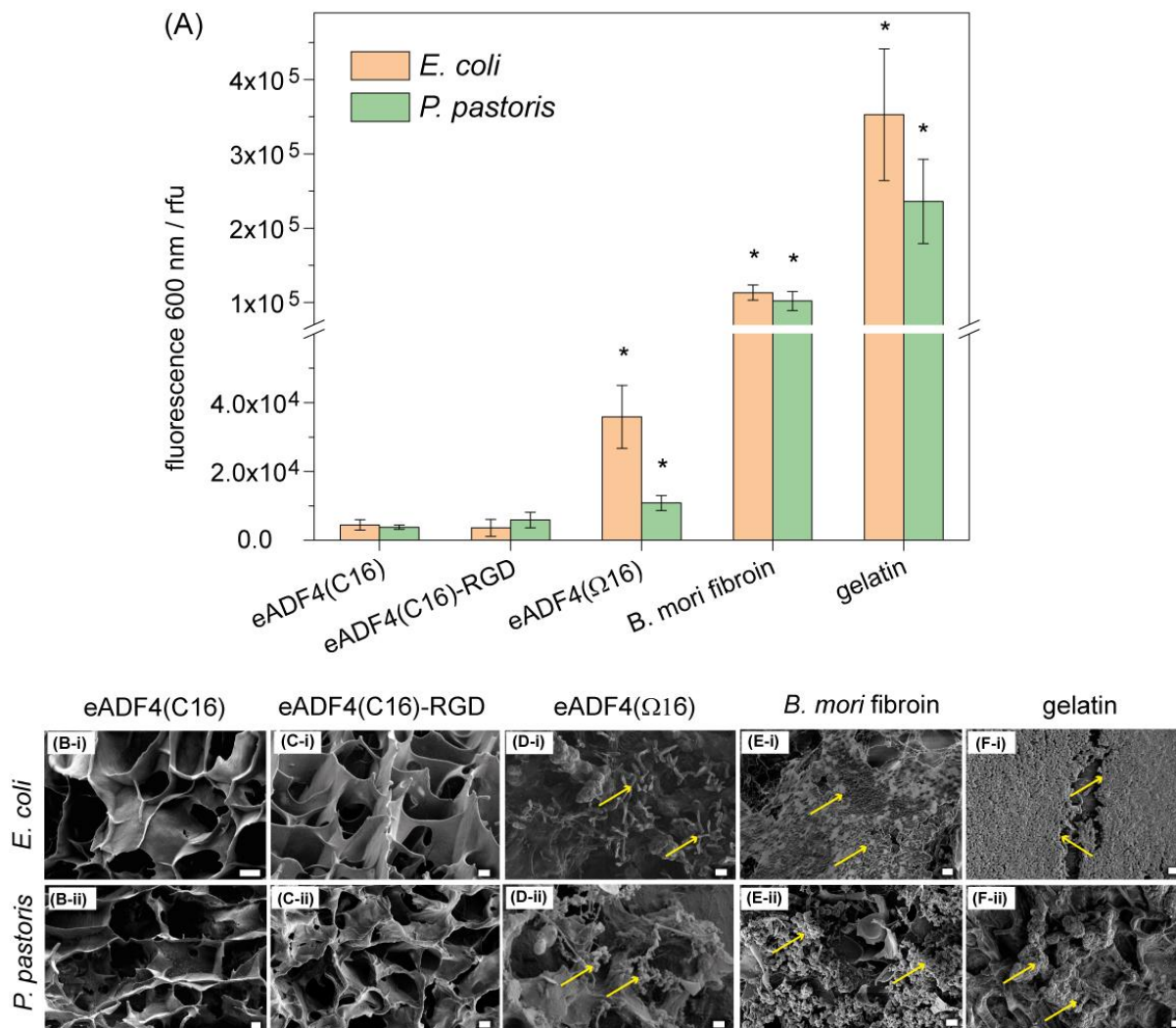


Figure 3. Bacteriostatic and fungistatic properties of spider silk hydrogels made of eADF4(C16). (A) Viability of microbial cells on hydrogels made of eADF4(C16), eADF4(C16)-RGD, eADF4(Ω16), *B. mori* fibroin and gelatin after 24 h incubation with *E. coli* and *P. pastoris* at 37 °C. Microbial viability was quantified using the alamar blue assay by measuring the transformation of the blue fluorescent dye resazurin into red fluorescent resorufin with 530 nm excitation and 600 nm emission filters in a microplate reader. Minimal adhesion of *E. coli* and *P. pastoris* on eADF4(C16) and eADF4(C16)-RGD hydrogels resulted in low fluorescence intensity in comparison to adhesion on eADF4(Ω16), *B. mori* fibroin and gelatin hydrogels with higher microbial viability. Each result is an average of three experiments, and the error bars designate the standard deviations. Student's t-test was performed for statistical analysis, *indicates significant difference to eADF4(C16) (p < 0.05). SEM images of hydrogels prepared from (B) eADF4(C16), (C) eADF4(C16)-RGD, (D) eADF4(Ω16), (E) *B. mori* fibroin and (F) gelatin after 24 h of incubation with (i) *E. coli* and (ii) *P. pastoris*. Arrows show biofilm or microbial cells on hydrogels. Scale bars = 2 µm.

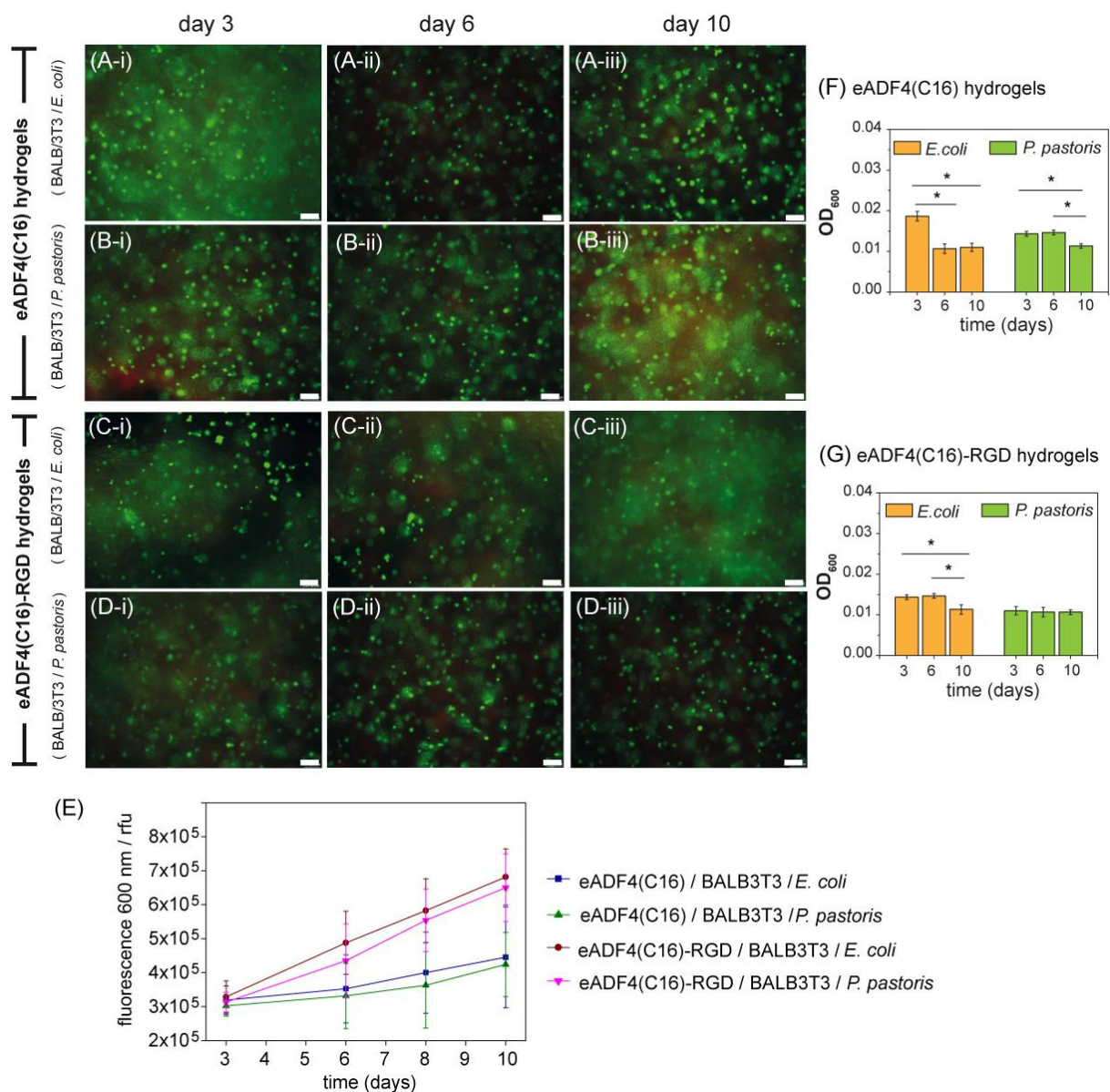


Figure 4. Bacteriostatic and fungistatic properties of 3D scaffolds made of eADF4(C16) in co-culture of microbes and mammalian cells. Fluorescence images of (A and B) eADF4(C16) and (C and D) eADF4(C16)-RGD hydrogels with encapsulated BALB/3T3 fibroblasts and co-cultured with (A and C) *E. coli* and (B and D) *P. pastoris* for (i) 3 days, (ii) 6 days, and (iii) 10 days. Scale bars = 100 μ m. The cells were stained with calcein A/M (live cells: green) and ethidium homo dimer I (dead cells: red). Ethidium homodimer I also stained the hydrogels yielding an unspecific red background fluorescence (A–D). Proliferation of mouse fibroblasts (BALB/3T3) in coculture over 10 days was measured using (E) the absorbance of cell titer blue. Microbial growth of *E. coli* and *P. pastoris* in fresh media was measured using (F and G) optical density at 600 nm (OD₆₀₀) with microbial inoculated hydrogels (after washing) and after incubation for 12 h at 37 °C. Each result is an average of three experiments, and the error bars designate the standard deviation. Student's t-test was performed for statistical analysis, *p < 0.05.

I. Protein platform technology II. β -sheet induced hydrophobic patches III. Interaction of surfaces with microbial/mammalian cells

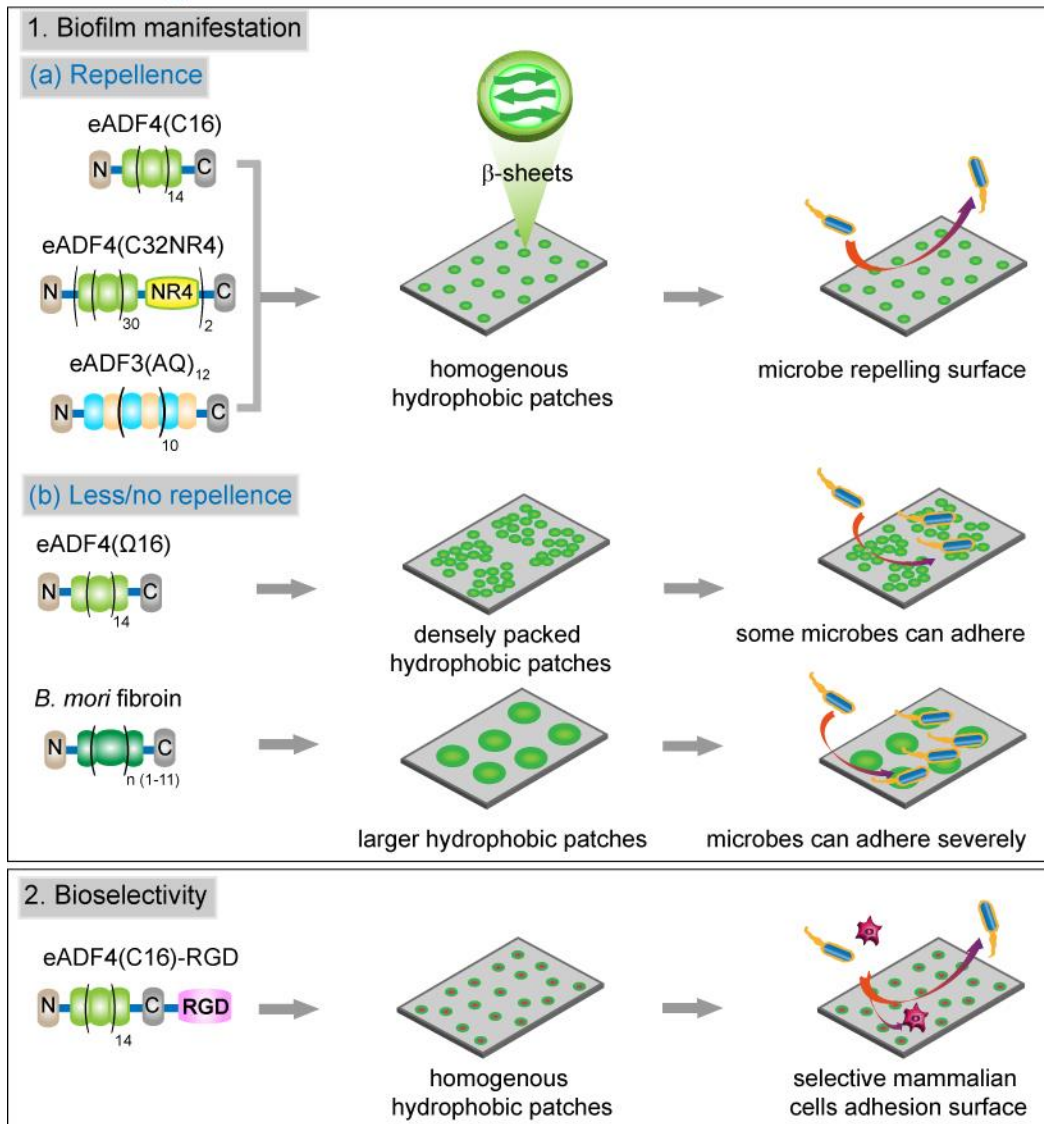


Figure 5. Schematic illustration of the microbial behaviour on the hydrophobic patches of silk with (1) repellent / non-repellent and (2) bioselective surfaces. (I) Recombinant spider silk variant / silk worm silk, (II) β -sheet formation yields hydrophobic surface patches with unique distribution and dimensions. (III) Homogeneous hydrophobic patch distribution of eADF4(C16), dimeric eADF4(C32NR4), and eADF3((AQ)₁₂) shows microbe repellence characteristics. The absence of charge-charge repulsion or steric effects in eADF4(Q16) leads to the dense packing of hydrophobic patches or structured larger hydrophobic patches in *B. mori* fibroin favouring the attachment of microbial cells. eADF4(C16)-RGD allows selective mammalian cell attachment with simultaneous microbe repellence.

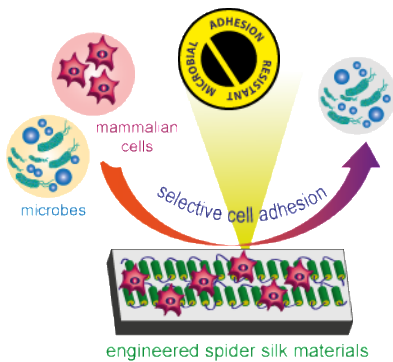
TOC

Materials based on engineered spider silk proteins are resistant to attachment of pathogenic bacteria and fungi, and efficiently inhibit biofilm formation. Films and hydrogels made of a RGD-modified spider silk variant allow for selective attachment and proliferation of mammalian cells in co-culture with microbes, while the microbes are non-adherent and easily washed off.

Keywords: microbe adhesion, hydrogels, patterned films, bio-selective surface, engineered spider silk proteins

Sushma Kumari,[†] Gregor Lang,[†] Elise DeSimone, Christian Spengler, Vanessa T. Trossmann, Susanne Lücker, Martina Hudel, Karin Jacobs, Norbert Krämer and Thomas Scheibel*

Title: Engineered spider silk-based 2D and 3D materials prevent microbial infestation



Supporting Information

Engineered spider silk-based 2D and 3D materials prevent microbial infestation

*Sushma Kumari,[†] Gregor Lang,[†] Elise DeSimone, Christian Spengler, Vanessa T. Trossmann, Susanne Lücker, Martina Hudel, Karin Jacobs, Norbert Krämer and Thomas Scheibel**

Dr. S. Kumari, Dr. E. DeSimone, V. T. Trossmann, Prof. T. Scheibel,
Department of Biomaterials,
Faculty of Engineering Science,
University of Bayreuth,
Prof.-Rüdiger-Bormann-Str. 1, 95447 Bayreuth, Germany

Prof. G. Lang
Biopolymer Processing Group,
Department of Biomaterials,
Faculty of Engineering Science,
University of Bayreuth,
Ludwig-Thoma-Str 36A, 95447 Bayreuth, Germany

Dr. C. Spengler, Prof. K. Jacobs
Department of Experimental Physics,
Saarland University,
66123 Saarbrücken, Germany

Dr. S. Lücker, Prof. N. Krämer
Medical Center for Dentistry,
Department of Paediatric Dentistry,
Medical Center Gießen and Marburg,
Justus-Liebig University Gießen,
Schlagenzahl 14, 35392 Gießen, Germany

M. Hudel,
Institute of Medical Microbiology,
Justus-Liebig University Gießen,
Schubertstraße 81, 35392 Gießen, Germany

Prof. T. Scheibel
Bayreuth Center for Material Science and Engineering (BayMAT),

Bavarian Polymer Institute (BPI),
Bayreuth Center for Colloids and Interfaces (BZKG),
Bayreuth Center for Molecular Biosciences (BZMB),
University of Bayreuth,
Universitätsstraße 30, 95447 Bayreuth, Germany
E-mail: thomas.scheibel@bm.uni-bayreuth.de

†These authors contributed equally to this work.

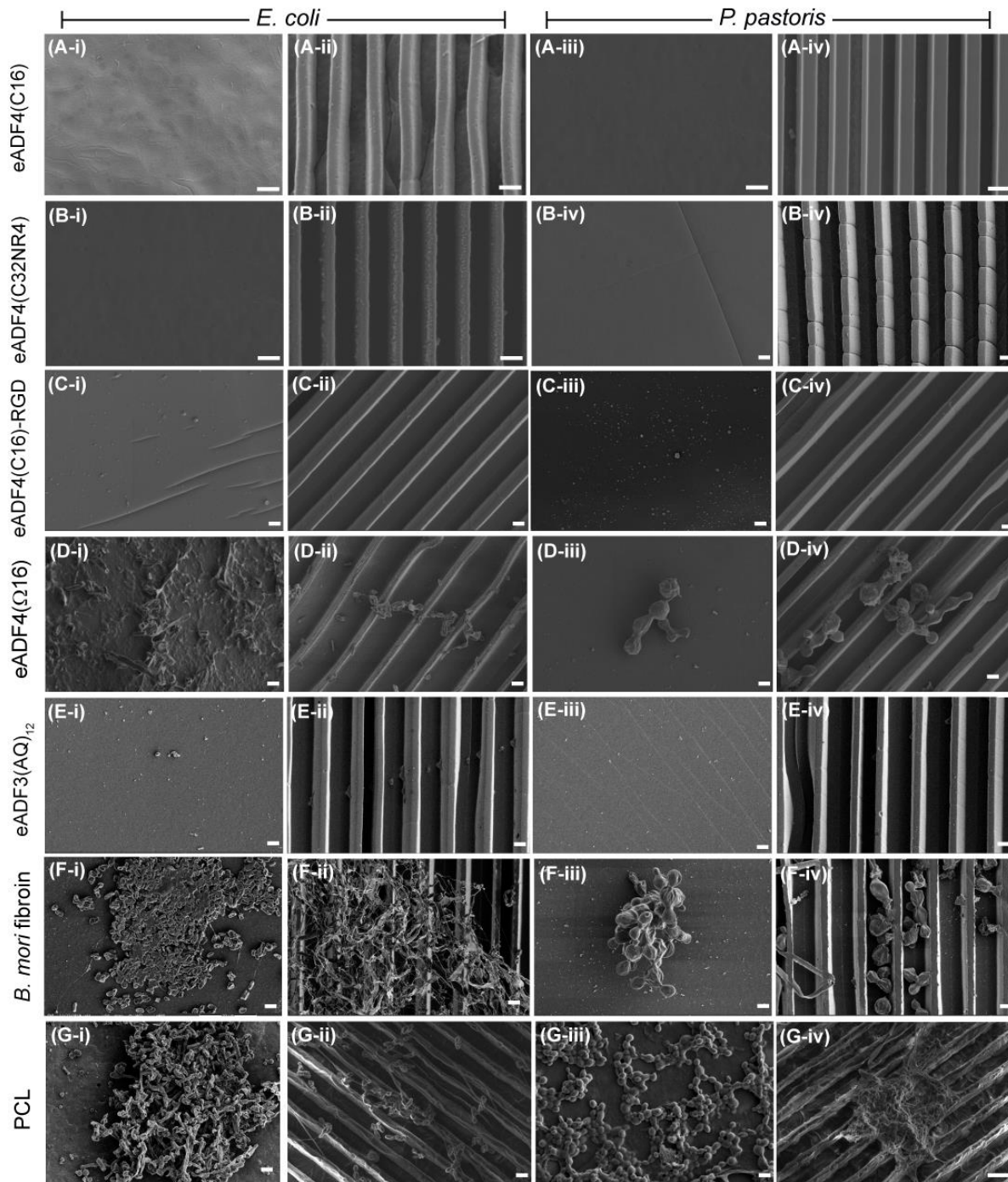


Figure S1. Bacteriostatic and fungistatic properties of films made of eADF4(C16). SEM images showing (i & iii) plane and (ii & iv) micro-patterned surfaces of films made of (A) eADF4(C16), (B) eADF4(C32NR4), (C) eADF4(C16)-RGD, (D) eADF4(Q16), (E) eADF3(AQ)₁₂, (F) *B. mori* fibroin and (G) PCL after 12 h of incubation with (i & ii) *E. coli* and (iii & iv) *P. pastoris* at 37 °C. Scale bars = 2 μm.

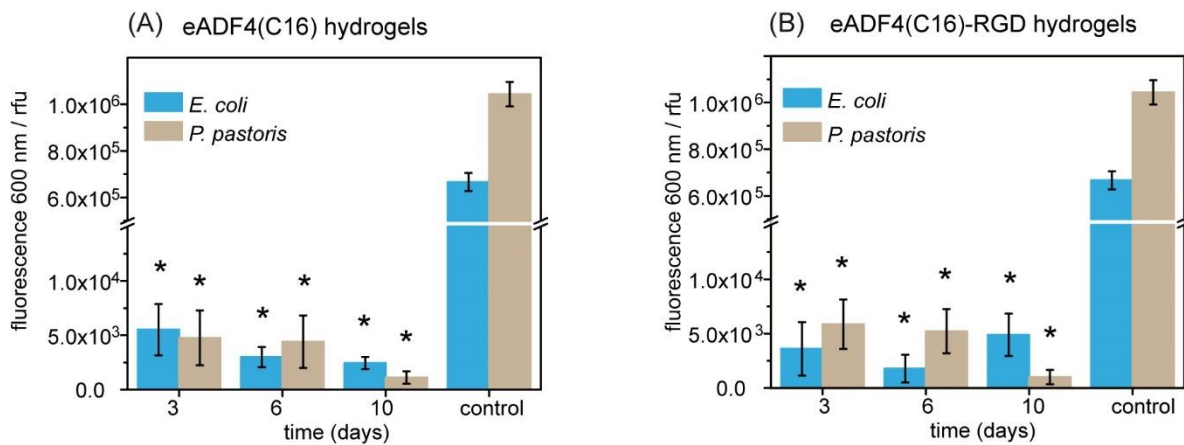


Figure S2. Bacteriostatic and fungistatic properties of hydrogels made of spider silk variants. Viability of *E. coli* and *P. pastoris* cells on hydrogels of (A) eADF4(C16) and (B) eADF4(C16)-RGD over 10 days was quantified using the CellTiter-Blue assay by measuring the transformation of the blue fluorescent dye resazurin into red fluorescent resorufin using 530 nm excitation and 600 nm emission filters in a microplate reader. Cell culture treated plates without coating were used as control. Each result is an average of five experiments, and the error bars designate the standard deviations. Student's t-test was performed for statistical analysis, *p < 0.05.

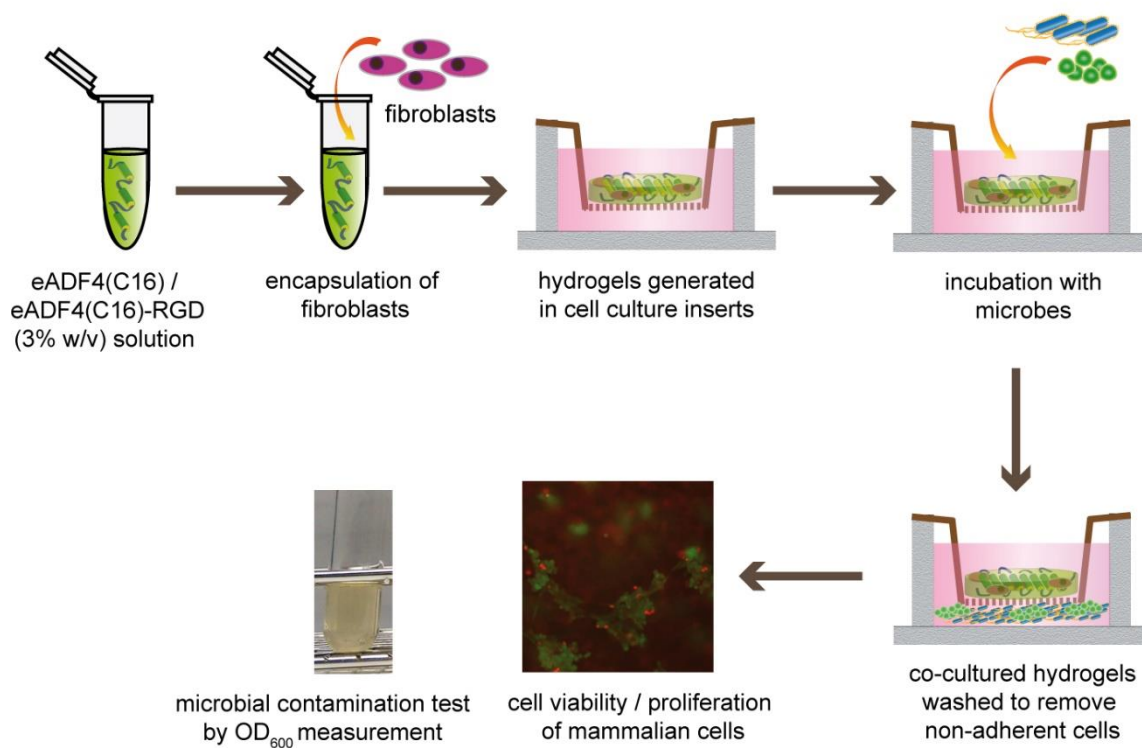


Figure S3. Schematic illustration demonstrating the co-culture of microbes (*E. coli* and *P. pastoris*) and mammalian cells (BALB/3T3) within hydrogels of eADF4(C16) and eADF4(C16)-RGD. The cell viability of mouse fibroblasts (BALB/3T3) in co-culture with microbes was evaluated by cell staining with calcein A/M (live cells: green) and ethidium homodimer I (dead cells: red), and microbial growth of *E. coli* and *P. pastoris* in fresh media was measured using the optical density at 600 nm (OD₆₀₀).

Table S1. Properties of recombinant spider silk proteins

Recombinant spider silk protein	M _w (kDa)	No. of charged amino acid residues at neutral pH (positive/negative)	pI
eADF4(C16)	47.7	0/16	3.5
eADF4(C32NR4)	104.1	2/34	3.5
eADF4(C16)-RGD	48.5	1/17	3.6
eADF4(Q16)	48.0	0/0	7.8
eADF3(AQ) ₁₂	48.0	0/0	5.5

Charged amino acid residues refer to silk sequences only; the T7 tag, present in all constructs, comprises an additional arginine residue.

Part 4. Characterization of Hydrogels Made of a Novel Spider Silk Protein eMaSp1s and Evaluation for 3D Printing

Thamm C., **DeSimone E.**, Scheibel T.

Published in *Macromolecular Bioscience*, **17**, 1700141
(2017)

Reprinted with kind permission from John Wiley and Sons

Characterization of Hydrogels Made of a Novel Spider Silk Protein eMaSp1s and Evaluation for 3D Printing

Christopher Thamm, Elise DeSimone, and Thomas Scheibel*

Recombinantly produced spider silk proteins have high potential for bio-engineering and various biomedical applications because of their biocompatibility, biodegradability, and low immunogenicity. Here, the recently described small spider silk protein eMaSp1s is assembled into hydrogels, which can be 3D printed into scaffolds. Further, blending with a recombinantly produced MaSp2 derivative eADF4(C16) alters the mechanical properties of the resulting hydrogels. Different spider silk hydrogels also show a distinct recovery after a high shear stress deformation, exhibiting the tunability of their features for selected applications.

1. Introduction

Orb-weaver spiders can produce up to seven different silk types in specific glands for applications such as offspring protection, prey wrapping or building the spider web.^[1–3] The most frequently investigated silk type is the dragline silk (MA: major ampullate silk), which forms the frame and radii of an orb web.^[4–7] Some of the notable characteristics of MA silk are its high toughness, biocompatibility, and low immunogenicity.^[7–11] MA silk is typically composed of two classes of spider silk proteins (i.e. spidroins), major ampullate spidroin 1 and 2

(MaSp1 and MaSp2), each exhibiting a large repetitive core domain, flanked by nonrepetitive amino- and carboxyterminal domains.^[12–15] Core domains comprise polyalanine motifs, which form β -sheet crystals and are responsible for the high tensile strength of spider silk fibers. In addition, glycine-rich motifs form an amorphous matrix, which surrounds the β -sheet crystals, and this matrix is responsible for the good elasticity.^[16–18] The spidroins contain terminal domains needed for proper storage and assembly, which have α -helical structure.^[19–23]

Large scale production of spider silk by farming is not feasible due to the cannibalistic behavior of most spider species.^[24] Therefore, spidroins have to be recombinantly produced in host organisms like *Escherichia coli* to have appropriate amounts for processing into fibers and other morphologies.^[25,26] In particular, developing cost-effective methods for producing 3D morphologies of recombinant spider silk is an important endeavor for this field.^[27] Recently, a short MaSp1 (MaSp1s) derivative has been described, expanding the list of major ampullate spidroin classes.^[28] This protein comprises only 439 amino acids in total, consisting of a small nonrepetitive core and two flanking terminal domains. An engineered variant thereof, eMaSp1s, could be successfully recombinantly produced and spun into fibers, and the resulting fibers had good mechanical properties.^[29]

In addition to fiber assembly, other morphologies were investigated to expand the applicability of this protein. Among these non-native morphologies are hydrogels, which are 3D polymer networks absorbing water in excess of over 95% (w/w).^[30–32] Hydrogels made of recombinant spidroins have been successfully produced in the past, and properties thereof can be controlled by adjusting protein concentration, pH, temperature, ion composition, and ion concentration.^[33–36] They assemble upon concentration-dependent gelation in which β -sheet rich silk fibrils form a stable physically cross-linked 3D network.^[33,34,37] The structure, the rheological properties (i.e., a shear thinning behavior), and the biocompatibility of spider silk hydrogels make them promising candidates for biomedical applications.^[38,39] One particularly interesting use of hydrogels is in 3D printing to develop biologically functional constructs. To the best of the authors' knowledge, there is only one case where recombinant silk proteins were used in an extrusion printing process to produce biofabricated scaffolds.^[35] Conversely, there are many interesting examples of using silk fibroin of silkworms for 3D printing. However, a disadvantage of extrusion printing of silk fibroin is that blending with other

C. Thamm, E. DeSimone, Prof. T. Scheibel

Lehrstuhl Biomaterialien

Fakultät für Ingenieurwissenschaften

Universität Bayreuth

Universitätsstraße 30, 95440 Bayreuth, Germany

E-mail: thomas.scheibel@bm.uni-bayreuth.de

Prof. T. Scheibel

Bayreuther Zentrum für Kolloide und Grenzflächen (BZKG)

Universität Bayreuth

Universitätsstraße 30, 95440 Bayreuth, Germany

Prof. T. Scheibel

Bayerisches Polymerinstitut (BPI)

Universitätsstraße 30, 95440 Bayreuth, Germany

Prof. T. Scheibel

Bayreuther Zentrum für Molekulare Biowissenschaften (BZMB)

Universität Bayreuth

Universitätsstraße 30, 95440 Bayreuth, Germany

Prof. T. Scheibel

Institut für Bio-Makromoleküle (bio-mac)

Universität Bayreuth

Universitätsstraße 30, 95440 Bayreuth, Germany

Prof. T. Scheibel

Bayreuther Materialzentrum (BayMAT)

Universität Bayreuth

Universitätsstraße 30, 95440 Bayreuth, Germany

DOI: 10.1002/mabi.201700141



biomaterials such as gelatin and hydroxyapatite is required for the hydrogels to be printable.^[40,41] Further, silk fibroin has also been utilized in inkjet printing, a process where the precursor solution is printed instead of the preformed hydrogel, and which works by similar principles to an inkjet printer. This technique allows higher resolution than extrusion printing, but yields smaller constructs.^[38] Although inkjet printing is not effective for tissue engineering, it is much more appropriate for other applications, for example, silk fibroin was used as an ink for effective development of biosensor arrays.^[42]

In this study, we successfully produced hydrogels of eMaSp1s and performed a rheological and structural analysis. Strikingly, blending with an engineered MaSp2 variant eADF4(C16) significantly altered the mechanical properties of the hydrogels.

2. Experimental Section

All chemicals used in this study were of analytical grade and performed a rheological and structural analysis. Strikingly, blending with an engineered MaSp2 variant eADF4(C16) significantly altered the mechanical properties of the hydrogels.

2.1. Recombinant Production and Purification of Spidroins

The engineered protein MaSp1s (eMaSp1s) consists of a small core domain, flanked by nonrepetitive termini and has a molecular weight of 43 kDa. eMaSp1s was produced recombinantly in *E. coli* and purified using affinity chromatography steps and ammonium sulfate precipitation as described previously.^[29]

The recombinant spidroin eADF4(C16) was produced and purified as previously described.^[25]

2.2. Hydrogel Formation

Hydrogels were produced following the protocol reported previously.^[33] Briefly, lyophilized proteins were solved in 6 M guanidinium thiocyanate and then dialyzed against 10×10^{-3} M Tris/HCl, pH 7.5 overnight at room temperature using dialysis membranes with a molecular weight cutoff of 6000–8000 Da. Subsequent dialysis against 25% (w/v) poly(ethylene glycol) (PEG) (35 kDa) removed water by osmotic stress, allowing protein concentrations of up to 70 mg mL⁻¹.^[43,44] Final concentrations of the protein solutions were determined photometrically after PEG-dialysis. Since gelation is faster at higher temperatures,^[33] solutions were gelled at 37 °C for 60 h and hydrogels were stored at 4 °C for 24 h before analysis.

2.3. Analysis of Gelation Kinetics

For gelation analysis, 150 μ L of concentrated protein solutions were added to Nunc 96-well plates (Thermo Fisher Scientific, Darmstadt, Germany), incubated at 37 °C and analyzed at various time points for changes in turbidity. Turbidity changes upon gelation of the protein solution were monitored at 570 nm using a Microplate Reader (Mithras LB 940, Berthold

Technologies, Bad Wildbad, Germany) in absorbance mode. For each protein concentration four samples ($n = 4$) were analyzed.

2.4. Fourier Transform Infrared (FTIR) and Circular Dichroism (CD) Spectroscopy

FTIR measurements were recorded in absorbance mode using a Bruker Tensor 27 IR spectrometer (Bruker, Rheinstetten, Germany). Lyophilized hydrogel and protein samples were placed on an attenuated total reflection (ATR)-crystal and pressed with a stamp. Each measurement comprised a 60-scan interferogram with a 2 cm⁻¹ resolution between 4000 and 800 cm⁻¹ and atmospheric compensation. The amide I region (1590–1720 cm⁻¹) was analyzed by Fourier self-deconvolution (FSD) using OPUS software (version 6.5). Signals were assigned to protein secondary structure elements according to Hu et al.^[45]

Far-ultraviolet (UV) CD measurements were performed using a Jasco J-715 spectropolarimeter (Jasco, Groß-Umstadt, Germany). Protein concentrations were adjusted to 0.2 mg mL⁻¹ using 10×10^{-3} M sodium phosphate buffer, pH 7.5, and cuvettes were used with a path length of 0.1 cm.

2.5. Rheological Properties

Stress–strain curves of eMaSp1s hydrogels were measured according to a protocol established previously.^[33,35] Briefly, the deformation curves of various hydrogels were monitored for 10 min using a flow measurement mode at an AR-G2 rheometer (TA instruments, New Castle, DE, USA) at a constant shear rate of 3.0×10^{-3} s⁻¹ with 25 mm plate geometry and a 100 μ m gap. To analyze the viscosity behavior of the hydrogels, steady state flow measurements were performed with shear rates increasing from 0.01 to 500 s⁻¹. In all measurements a solvent trap with a wet sponge was used to reduce evaporation. Shear (G) and elastic (E) moduli were calculated as described in one of the previous publications^[33] according to Hooke's law using the Poisson's ratios published by Urayama et al.^[46] Three samples ($n = 3$) were measured for each experimental group, and one representative curve is shown per group.

Hydrogels were additionally evaluated for recovery by measuring the storage and loss modulus before and after a large deformation which induces either “fluid-like” viscosity (40 s⁻¹ shear rate) or “soft solid-like” viscosity (0.2 s⁻¹ shear rate). This was conducted by taking the hydrogels through a three step analysis: the first step was a measurement before deformation for 10 min (600 s) by small oscillations (10 rad s⁻¹, 0.5% strain). The oscillation program and rate was based on protocols previously written.^[47–49] The linear strain value was determined by the analysis of the stress–strain curves and the shear rate from data as previously established.^[33,35] The second step was a large deformation step in a flow mode for either 40 s⁻¹ shear rate for 1 s or 0.2 s⁻¹ shear rate for 10 s. The third step was to measure the modulus after deformation over a period of 5 min (300 s) by small oscillations (10 rad s⁻¹, 0.5% strain) to see if there is any recovery. Three samples ($n = 3$) were measured for each experimental group, and one representative curve is shown per group.

2.6. Congo Red (CR) and Thioflavin T (ThT) Binding Experiments

2.6.1. CR

Soluble protein and solubilized hydrogels were diluted to a protein concentration of 0.2 mg mL⁻¹ and mixed with 4 × 10⁻⁶ M CR in 10 × 10⁻³ M Tris/HCl, pH 7.5. Ultraviolet-visible (UV-vis) spectrometry was performed using a Cary 50 Bio spectrometer (Varian, Darmstadt, Germany) after 30 min of incubation time. Baselines without CR were recorded at the same protein concentration to correct the spectra for light scattering.

2.6.2. ThT

Soluble protein and solubilized hydrogels were diluted to a protein concentration of 1.0 mg mL⁻¹ and mixed with 15 × 10⁻⁶ M ThT for 10 min in 10 × 10⁻³ M Tris/HCl, pH 7.5. Fluorescence spectra were recorded using a Jasco FP-6500 fluorescence spectrometer with a 3 mm path length at an excitation wavelength of 450 nm (Jasco, Groß-Umstadt, Germany).

2.7. Transmission Electron Microscopy (TEM) Imaging

For TEM analysis, eMaSp1s hydrogels were resolubilized manually by harsh mixing in ddH₂O, followed by centrifugation at 17 700 g for 30 min, and 5 μL of the resulting protein solution (1.0 mg mL⁻¹) were spotted on supports (Piloform 100-mesh copper grids and Formvar 200-mesh copper grids (Plano GmbH, Wetzlar, Germany)), incubated for 2 min, washed two times with 5 μL ddH₂O, and stained using 5 μL of 2% uranyl acetate solution. For atomic force microscopy (AFM) analysis, 30 μL of protein solution (1.0 mg mL⁻¹) was spotted on freshly cleaved mica plates (Ø 10 mm, V1 grade, Plano GmbH, Wetzlar, Germany). TEM samples were dried for at least 20 h at 20 °C before imaging. TEM imaging of solubilized hydrogel samples was performed with a JEM-2100 transmission electron microscope (JEOL GmbH, Freising, Germany) operated at 80 kV. Images were recorded using a 4000 × 4000 charge-coupled device camera (UltraScan 4000, Gatan, Pleasanton, CA, USA) and Gatan Digital Micrograph software (version 1.83.842).

2.8. AFM Imaging

For AFM analysis, eMaSp1s hydrogels were prepared in solution identically as for TEM, and 30 μL protein solution (1.0 mg mL⁻¹) were spotted on freshly cleaved mica plates (Ø 10 mm, V1 grade, Plano GmbH, Wetzlar, Germany). AFM samples were dried for at least 20 h at 20 °C before imaging. AFM scanning of dried samples was done using

a DimensionTM 3100 device equipped with a NanoScope V controller (Veeco Instruments Inc., Plainview, NY, USA) using Si₃N₄ cantilevers (OMCLAC160TS, Olympus, spring constant of 42 N m⁻¹, resonance frequency of 300 kHz, tip radius less than 7 nm) and operating in Tapping-Mode. AFM scans were processed using NanoScope Analysis software version 1.40r3 (Bruker, Santa Barbara, CA, USA).

2.9. Scanning Electron Microscopy (SEM) Imaging

To analyze morphological structure via SEM, hydrogels were chemically fixed using a fixation buffer (2.5% (v/v) glutaraldehyde, 80 × 10⁻³ M HEPES, 3 × 10⁻³ M CaCl₂, pH 7.3) at room temperature followed by incubation for 4 h at 4 °C. Then, samples were washed with water four times, frozen at -80 °C and freeze dried. SEM pictures of dry platinum sputtered samples (2 nm platinum coating; Cressington sputter coater 108auto, Watford, United Kingdom) were taken at an accelerating voltage of 2.5 kV, using a scanning microscope Leo 1530 Gemini (Carl Zeiss, Oberkochen, Germany).

2.10. Optical Imaging

Visualization of hydrogel fibrils was performed after adding ThT, using an inverted optical microscope (Leica DMi8) with an excitation wavelength of 480 nm using the software Leica V4.3 (Leica Microsystems, Wetzlar, Germany).

2.11. Differential Scanning Calorimetry (DSC)

DSC of freshly produced hydrogels was conducted using a DSC1 (Mettler Toledo, Columbus, OH, USA) by applying between 14 and 16 mg of hydrogel under nitrogen-atmosphere conditions and a heating rate of 20 °C min⁻¹.

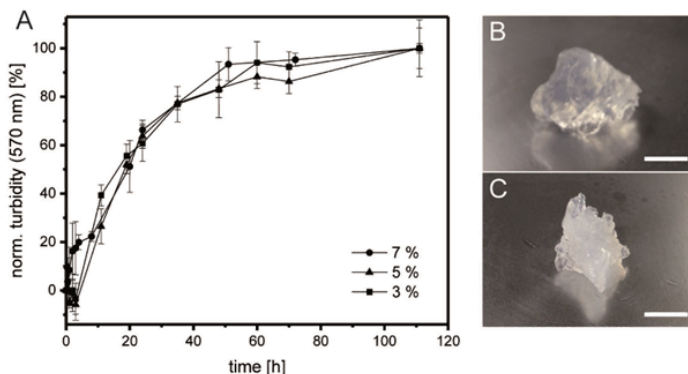


Figure 1. A) Turbidity changes of 3%, 5%, and 7% (w/v) eMaSp1s solutions over time incubated at 37 °C. Changes in turbidity were monitored at 570 nm and reflect the rate of hydrogel formation. Each data point was averaged from three independent samples ($n = 3$), and standard deviations are indicated for each time point. Photographs of B) 3% (w/v) and C) 7% (w/v) eMaSp1s hydrogels. Scale bars: 0.5 cm.

2.12. Dispense-Plotting

Robotic dispensing was performed using a 3D Discovery (regenHU) in a laminar-flow hood. The print head (DD-135N, print head for contact dispensing) operated in the y,z -plane and the collector along the x -axis. Printing was conducted at room temperature in a pressurized 3cc syringe (regenHU). Dispensing was achieved by pneumatic-driven piston driving hydrogel through a needle with an inner diameter of 0.33 mm. The flow was regulated by pressure (0.5 bar), and the printing velocity was 20 mm s^{-1} . The printed constructs were imaged using a stereo microscope (Leica M205C, Leica Microsystems, Wetzlar, Germany).

2.13. Stereomicroscopy

The Leica M205C stereomicroscope (Wetzlar, Germany) was used to capture images of printed scaffolds. The images of hydrogels were taken on light reflected from dark field using a $0.63\times$ objective with a polarization lens. One representative scaffold was imaged per experimental group.

3. Results and Discussion

3.1. Assembly of eMaSp1s Hydrogels

It has been previously shown that the recombinantly produced spider silk protein eADF4(C16) (a 48 kDa MaSp2 derivative, consisting of 16 repetitive consensus sequence modules of the core domain of *Araneus diadematus* fibroin 4 (ADF4), containing polyalanine stretches (A) and glycine/proline-rich areas (Q), (Figure S1, Supporting Information)) can spontaneously self-assemble into hydrogels at concentrations between 5 and 70 mg mL^{-1} .^[33,50] Similarly, eMaSp1s self-assembled into hydrogels at concentrations between 20 and 70 mg mL^{-1} .

The produced eMaSp1s hydrogels exhibited good storage stability, remaining intact when water or buffer was added. With this successful processing into hydrogels, eMaSp1s is one of the few recombinantly produced spider silk proteins, which are able to form both wet-spun solid fibers^[29] and stable hydrogels.

The influence of protein concentration on the rate of gelation was analyzed by turbidity measurements at 570 nm for five consecutive days (Figure 1A). Gelation began after a few hours and was almost complete after 60 h; notably, the gelation rate was almost independent of protein concentration. Although the gelation rate was comparable, 7% (w/v) eMaSp1s hydrogels showed a slightly increased turbidity in the assembled hydrogel in comparison to lower protein concentrations, which could be confirmed visually (Figure 1B,C). As also described by Schacht et al.^[33] for a different recombinant spider silk protein, the gelation process was highly reproducible at all eMaSp1s concentrations.

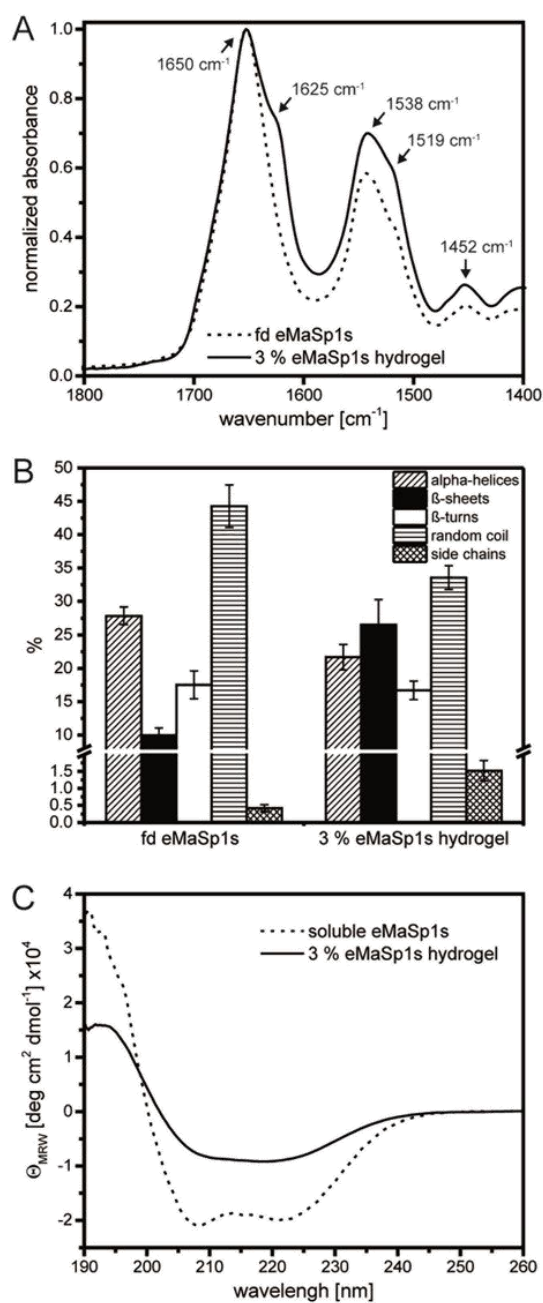


Figure 2. FT-IR spectroscopy showing (A: amide I and II region) B) secondary structure distribution based on FTIR spectra of a 3% (w/v) eMaSp1s hydrogel in comparison to freeze-dried (fd) eMaSp1s. C) CD spectra of soluble eMaSp1s (0.2 mg mL^{-1}) versus hydrogels made thereof.

3.2. Structural Analysis of eMaSp1s in Solution and in Hydrogels

It was recently shown that eMaSp1s has α -helical secondary structure in aqueous solution, dominated by its helically folded terminal domains. However, during hydrogel formation, spider silk proteins structurally convert into β -sheet rich structures.^[33,51]

Therefore, resuspended hydrogels were analyzed using FTIR and CD spectroscopy to determine their secondary structure content (Figure 2A; Table S1, Supporting Information). In FTIR spectra, the absorbance maxima at 1625 and 1519 cm^{-1} indicated the presence of β -sheets. FSD of the amide I band (Figure 2B) showed that the overall β -sheet content increased from 9% to 27%, the α -helical content decreased from 28% to 22% and the random coil content decreased from 44% to 35% upon hydrogel formation. All hydrogels showed a maximum at 963 cm^{-1} , indicating that the polyaniline regions were in β -sheet conformation (data not shown).^[52] These findings also suggested that β -sheet formation occurred preliminary in the previously unfolded core domain of MaSp1s while the folded termini mainly retained their helical structure during hydrogel formation.

CD spectroscopy confirmed the FTIR data, showing a change in ellipticity which indicated the additional formation of β -sheet structures, lowering the overall signal intensities (Figure 2C).

3.3. β -Fibrillization During eMaSp1s Hydrogel Formation

Hydrogels were resuspended in buffer and analyzed by TEM, AFM, CR staining, and ThT staining (Figure 3A,B).^[53,54]

TEM as well as AFM revealed fibrillar structures (Figure 3A,B), exhibiting a length of around 200–500 nm, average diameters of 15 nm (Figure 3A), and heights in the range of 1.0–1.3 nm (Figure 3B). Length and diameter of eMaSp1s fibrils is consistent with values reported earlier for recombinant spider silk fibrils.^[55,56]

The absorbance spectrum of CR redshifted upon binding to the β -sheets within the nanofibrils (Figure 3B), and ThT fluorescence significantly increased at 482 nm (Figure 3C), both confirming the formation of β -sheet containing fibrils during eMaSp1s hydrogel formation.

3.4. Rheological Characterization of eMaSp1s Hydrogels

Previously described recombinant spider silk hydrogels made from eADF4(C16) showed elastic moduli in a range of 1–30 kPa.^[33,57] The mechanical properties of eMaSp1s hydrogels were determined using rheology (Figure 4). All eMaSp1s

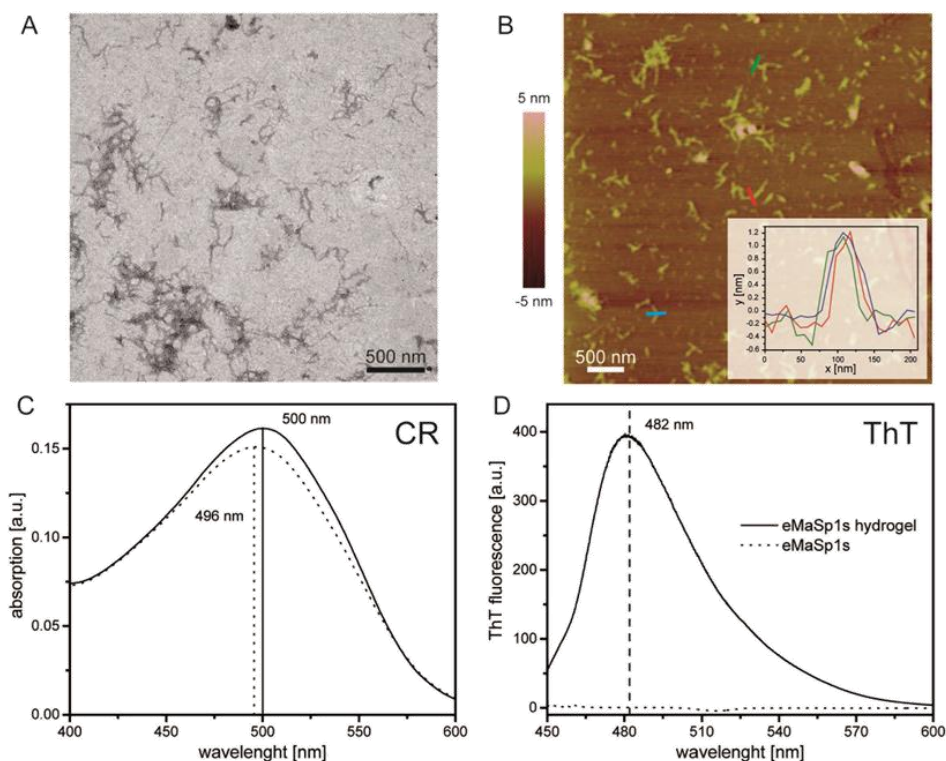


Figure 3. Identification and morphology of β -sheet fibrils in 3% (w/v) eMaSp1s hydrogels. A) TEM image and B) AFM image of eMaSp1s fibrils. The color bar on the left side of the AFM image presents heights from -5 nm (dark brown) to 5 nm (white). The inset shows height profiles of three randomly selected eMaSp1s fibrils. C) CR and D) ThT spectra of samples gained from eMaSp1s hydrogels and freshly purified eMaSp1s in solution.

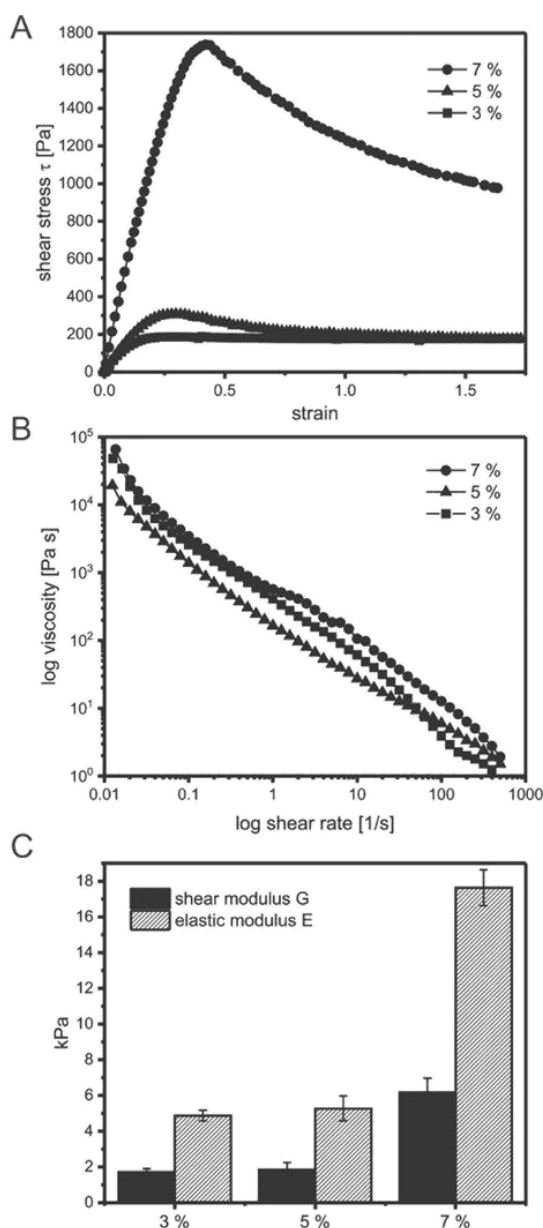


Figure 4. Rheological measurements (stress–strain and flow curves) of 3%, 5%, and 7% (w/v) eMaSp1s hydrogels at 20 °C. Each hydrogel was measured in a single experiment, and representative curves are shown. A) Stress–strain and B) flow curves of eMaSp1s hydrogels at different protein concentrations. C) Shear moduli and elastic moduli of eMaSp1s hydrogels.

hydrogels showed slightly inferior values in maximum shear stress compared to that of previously determined eADF4(C16) hydrogels at the same concentration (Figure 4A).^[33,56,58] Shear

and elastic moduli increased with increasing protein concentration; this is likely due to less eMaSp1s nanofibril mobility in highly concentrated solutions, causing higher mechanical stiffness of the hydrogels (Figure 4C).^[59]

To analyze whether the hydrogels also showed shear thinning behavior as previously shown for hydrogels made of eADF4(C16),^[60] eMaSp1s hydrogels were characterized using a steady state flow mode and exhibited shear thinning at these conditions (Figure 4B).

Taken together, the mechanical properties of eMaSp1s hydrogels are in the same regime in comparison to that of eADF4(C16) hydrogels.

Something notable about Figure 4A,C is that there is a sharp increase in the stiffness of the hydrogels from 5% to 7% (w/v), a behavior that was also observed for eADF4(C16) hydrogels.^[33] Although the studies here are not sufficient to explain this behavior, the authors would speculate this is because working with higher concentration within the starting solution triggers aggregation, resulting in a mixture of fibrillar network formation with protein aggregation. It was decided from this point that only 3% (w/v) hydrogels would be tested; the desired future application of these hydrogels is soft tissue engineering or drug delivery, and as 3% and 5% (w/v) had nearly the same modulus, it was sensible to use the formulation which requires less protein and which also yields slightly larger pore sizes.

Next, concentrated eADF4(C16) and eMaSp1s solutions were mixed and then assembled into hydrogels. Surprisingly, mixed hydrogels made of equal amounts of both proteins showed a significantly increased shear stress in comparison to those made of only a single protein (Figure 5A).

To analyze the basis of this unexpected behavior, samples were freeze dried and investigated by SEM. Hydrogels made of eADF4(C16) showed sheet-like morphology with sheet-like pores around 100 μm (Figure 5C).^[33] By contrast, eMaSp1s hydrogels revealed a morphology with predominantly round pores at a smaller size range of 20–40 μm (Figure 5B). Blend hydrogels appeared to be composed of a mixture of both morphologies (Figure 5C).

Next, the thermal stability was characterized by DSC (Figure 5E). After initial water removal, all hydrogels were stable upon ≈ 150 °C. DSC measurements showed a main endothermic peak of eMaSp1s at 281 °C, of eADF4(C16) at 330 °C and of the 1:1 blend hydrogel at 311 °C. In summary, although there is a special structure which results from the blending, the thermal stability of the blend was not noticeably increased but was in between that of the single protein hydrogels, indicating a blend with likely phase-separated eADF4(C16) and eMaSp1s areas (i.e., reflecting an interpenetrating network). Therefore, it was not a molecular interaction between both proteins, but rather the interpenetration, yielding the increased mechanical properties.

3.5. 3D Printing and Oscillation Experiments

eMaSp1s, eMaSp1s blend, and eADF4(C16) hydrogels as a control were examined for printability using similar parameters as those reported previously for eADF4(C16) hydrogels.^[35]

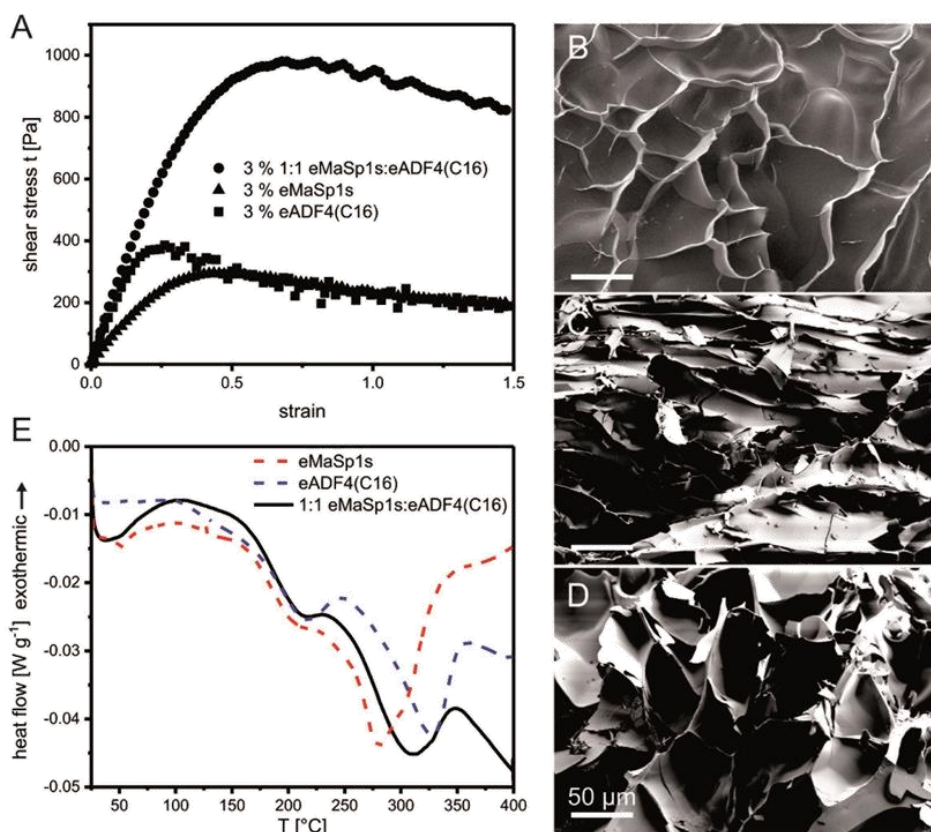


Figure 5. A) Rheological, B–D) SEM, and E) DSC analysis of 3% (w/v) blend hydrogels made of eMaSp1s and eADF4(C16) in a 1:1 (w/w) ratio compared to single-protein hydrogels. SEM images show hydrogels made of B) eMaSp1s, C) eADF4(C16), and D) 1:1 (w/w) blend hydrogel.

Dispense plotted hydrogels of eMaSp1s were not as form stable as those made of eADF4(C16) (Figure 6). This was not expected considering the shear thinning behavior of the protein combined with a higher modulus as determined by stress-strain measurements (Figure 4). To identify the origin of this behavior, oscillation experiments were conducted to evaluate the shear modulus before and after a large deformation with an experimental set-up and parameter determination similar to protocols previously reported.^{147–49]}

Based on the change in the shear storage modulus of the different hydrogels before and after “fluid-like” viscosity deformation, MaSp1s and the blend were not able to completely recover their mechanical properties after deformation (Figure 7A). On the other hand, eADF4(C16) experienced a permanent increase in the loss modulus (Figure 7C). This shear rate resulted in the hydrogel exhibiting a “fluid-like” behavior with viscosities less than 10 Pa s (Figure S2, Supporting Information). In the case of the “soft solid-like” behavior, the blend and eADF4(C16) seemed to recover instantaneously at viscosities greater than 100 Pa s (Figure S2, Supporting Information), but the eMaSp1s hydrogel did not recover

at all. eADF4(C16) showed a slight, irreversible increase in the loss modulus, and in this case the blend did as well (Figure 7D).

These results were confirmed by observing the apparent yield stress using stress-strain measurements. Directly after printing, the apparent yield stress decreased significantly in the case of hydrogels made of eADF4(C16), eMaSp1s, and the blend (Figure S3, Supporting Information). Interestingly however, in this case, the eMaSp1s hydrogels also recovered their original apparent yield stress, although with a much slower recovery time.

4. Conclusion

Hydrogels of the spider silk protein eMaSp1s were assembled and characterized. Hydrogels showed a fibrillar morphology with increased β -sheet content and shear thinning properties as well as shear and elastic moduli different to that of previously produced recombinant spider silk hydrogels based on MaSp2 derivatives eADF4(C16).

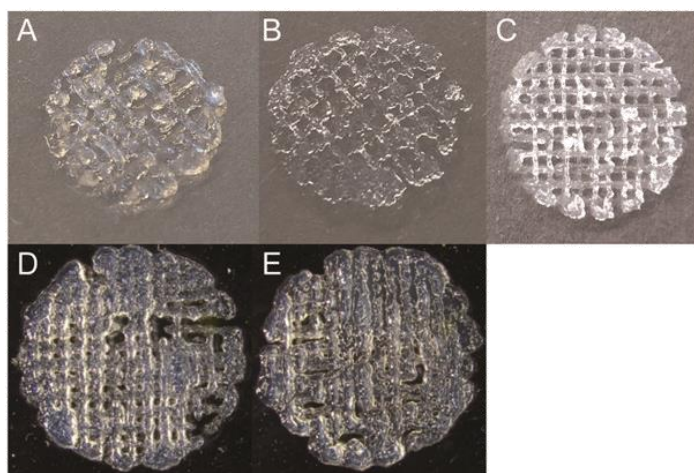


Figure 6. Photographs of 3D dispense plotted scaffolds: A) 3% (w/v) 1:1 eADF4(C16):eMaSp1s blend, B) 3% (w/v) eMaSp1s, and C) 3% (w/v) eADF4(C16). Additionally, stereomicroscopic images of D) 3% (w/v) 1:1 eADF4(C16):eMaSp1s blend and E) 3% (w/v) eMaSp1s were taken. The two-layer scaffolds had a diameter of either (A–C) 1.0 or (D,E) 1.8 cm.

Further, the hydrogels were strengthened by blending with eADF4(C16). However, under high shear rates, the eMaSp1s hydrogels and hydrogel blends were not able to recover within minutes, unlike eADF4(C16). Therefore, although the eMaSp1s hydrogels are not suitable for 3D printing, they could be envisioned for other applications such as injectable drug delivery reservoirs, which will be investigated in the future.

Supporting Information

Supporting Information is available from the Wiley Online Library or from the author.

Acknowledgements

This work was supported by the European Union, Project ID 123 ("green bio-based polymers"). The authors thank Dr. Hendrik Bargel for SEM imaging, Dr. Martin Humenik for assistance with AFM measurements, and Tamara Aigner for TEM imaging.

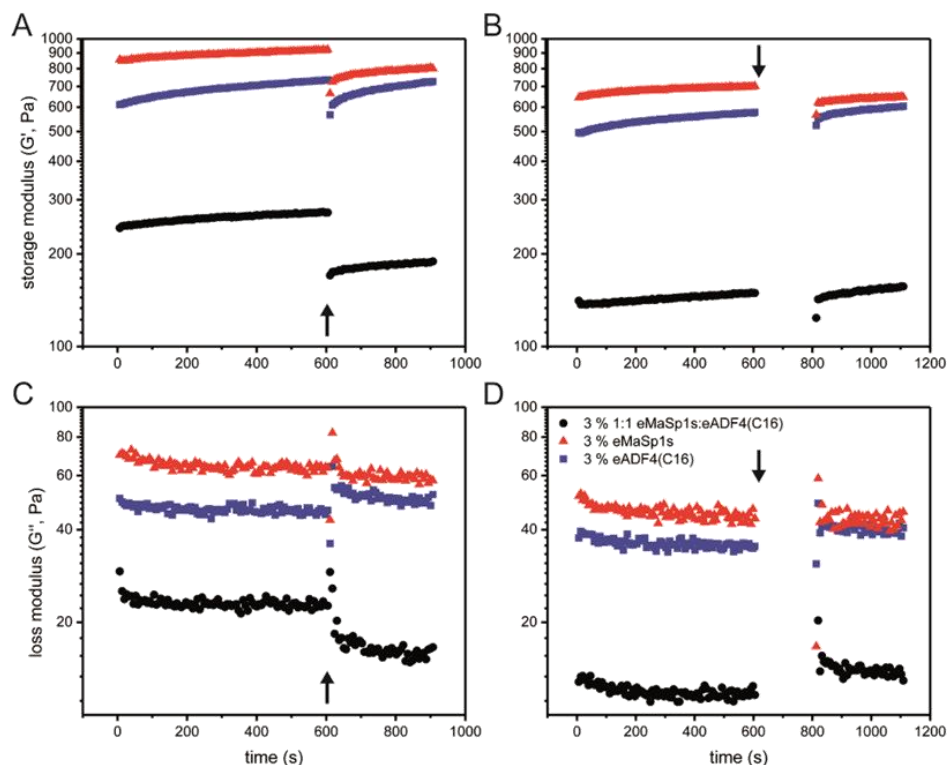


Figure 7. Time sweep experiments showing the recovery behavior of hydrogels after large strain deformations at A,C) 0.2 s^{-1} or B,D) 40 s^{-1} shear rate as measured by changes in (A,B) shear storage modulus and (C,D) shear loss modulus. Hydrogels were measured before deformation for 10 min (600 s) and after deformation for 5 min (300 s) by small oscillations within the linear behavior of the hydrogel as determined by previous hydrogel tests (10 rad s^{-1} , 0.5% strain). The x-axis label is shared for (A) and (C) and (B) and (D), and the y-axis label is shared for (A) and (B) and (C) and (D). Each curve is one representative sample, and an arrow indicates the start of the deformation phase.

Conflict of Interest

The authors declare no conflict of interest.

Keywords

biopolymers, circular dichroism, FTIR, hydrogels, major ampullate spideroin, rheology

Received: April 19, 2017

Revised: June 26, 2017

Published online:

- [1] A. Rising, H. Nimmervoll, S. Grip, A. Fernandez-Arias, E. Storckenfeldt, D. P. Knight, F. Vollrath, W. Engstrom, *Zool. Sci.* **2005**, *22*, 273.
- [2] S. L. Stauffer, S. L. Coguill, R. V. Lewis, *J. Arachnol.* **1994**, *22*, 5.
- [3] F. Vollrath, *J. Biotechnol.* **2000**, *74*, 67.
- [4] T. A. Blackledge, C. Y. Hayashi, *J. Exp. Biol.* **2006**, *209*, 2452.
- [5] M. Andersson, L. Holm, Y. Ridderstrale, J. Johansson, A. Rising, *Biomacromolecules* **2013**, *14*, 2945.
- [6] M. Denny, *J. Exp. Biol.* **1976**, *65*, 483.
- [7] M. Heim, D. Keerl, T. Scheibel, *Angew. Chem., Int. Ed. Engl.* **2009**, *48*, 3584.
- [8] F. Vollrath, P. Barth, A. Basedow, W. Engstrom, H. List, *In Vivo* **2002**, *16*, 229.
- [9] G. H. Altman, F. Diaz, C. Jakuba, T. Calabro, R. L. Horan, J. Chen, H. Lu, J. Richmond, D. L. Kaplan, *Biomaterials* **2003**, *24*, 401.
- [10] J. M. Gosline, P. A. Guerette, C. S. Ortlepp, K. N. Savage, *J. Exp. Biol.* **1999**, *202*, 3295.
- [11] L. Römer, T. Scheibel, *Chem. Unserer Zeit* **2007**, *41*, 306.
- [12] N. A. Ayoub, J. E. Garb, R. M. Tinghitella, M. A. Collin, C. Y. Hayashi, *PLoS One* **2007**, *2*, e514.
- [13] M. Humenik, T. Scheibel, A. Smith, *Prog. Mol. Biol. Transl. Sci.* **2011**, *103*, 131.
- [14] P. A. Guerette, D. G. Ginzinger, B. H. Weber, J. M. Gosline, *Science* **1996**, *272*, 112.
- [15] C. Y. Hayashi, T. A. Blackledge, R. V. Lewis, *Mol. Biol. Evol.* **2004**, *21*, 1950.
- [16] A. H. Simmons, C. A. Michal, L. W. Jelinski, *Science* **1996**, *271*, 84.
- [17] S. R. Fahnstocck, S. L. Irwin, *Appl. Microbiol. Biotechnol.* **1997**, *47*, 23.
- [18] M. Heim, L. Roemer, T. Scheibel, *Chem. Soc. Rev.* **2010**, *39*, 156.
- [19] F. Hagn, L. Eisdoldt, J. G. Hardy, C. Vendrely, M. Coles, T. Scheibel, H. Kessler, *Nature* **2010**, *465*, 239.
- [20] F. Hagn, C. Thamm, T. Scheibel, H. Kessler, *Angew. Chem., Int. Ed. Engl.* **2011**, *50*, 310.
- [21] G. Askarieh, M. Hedhammar, K. Nordling, A. Saenz, C. Casals, A. Rising, J. Johansson, S. D. Knight, *Nature* **2010**, *465*, 236.
- [22] J. Bauer, D. Schaal, L. Eisdoldt, K. Schweimer, S. Schwarzingler, T. Scheibel, *Sci. Rep.* **2016**, *6*, 34442.
- [23] L. Eisdoldt, J. G. Hardy, M. Heim, T. R. Scheibel, *J. Struct. Biol.* **2010**, *170*, 413.
- [24] L. R. Fox, *Annu. Rev. Ecol. Syst.* **1975**, *6*, 87.
- [25] D. Huemmerich, C. W. Helsen, S. Quedzuweit, J. Oschmann, R. Rudolph, T. Scheibel, *Biochemistry* **2004**, *43*, 13604.
- [26] C. Vendrely, T. Scheibel, *Macromol. Biosci.* **2007**, *7*, 401.
- [27] J. A. Jones, T. I. Harris, C. L. Tucker, K. R. Berg, S. Y. Christy, B. A. Day, D. A. Gaztambide, N. J. C. Needham, A. L. Ruben, P. F. Oliveira, R. E. Decker, R. V. Lewis, *Biomacromolecules* **2015**, *16*, 1418.
- [28] L. Han, L. Zhang, T. Zhao, Y. Wang, M. Nakagaki, *Int. J. Biol. Macromol.* **2013**, *56*, 156.
- [29] C. Thamm, T. Scheibel, *Biomacromolecules* **2017**, *18*, 1365.
- [30] D. P. Knight, L. Nash, X. W. Hu, J. Haffegge, M. W. Ho, J. *Biomed. Mater. Res.* **1998**, *41*, 185.
- [31] H. Shin, S. Jo, A. G. Mikos, *Biomaterials* **2003**, *24*, 4353.
- [32] H. Yan, A. Saiani, J. E. Gough, A. F. Miller, *Biomacromolecules* **2006**, *7*, 2776.
- [33] K. Schacht, T. Scheibel, *Biomacromolecules* **2011**, *12*, 2488.
- [34] S. Rammensee, D. Huemmerich, K. D. Hermanson, T. Scheibel, A. R. Bausch, *Appl. Phys. A* **2006**, *82*, 261.
- [35] K. Schacht, T. Jungst, M. Schweinlin, A. Ewald, J. Groll, T. Scheibel, *Angew. Chem., Int. Ed. Engl.* **2015**, *54*, 2816.
- [36] C. Vepari, D. L. Kaplan, *Prog. Polym. Sci.* **2007**, *32*, 991.
- [37] X. Hu, Q. Lu, L. Sun, P. Cebe, X. Wang, X. Zhang, D. L. Kaplan, *Biomacromolecules* **2010**, *11*, 3178.
- [38] S. V. Murphy, A. Atala, *Nat. Biotechnol.* **2014**, *32*, 773.
- [39] S. Kapoor, S. C. Kundu, *Acta Biomater.* **2016**, *31*, 17.
- [40] M. J. Rodriguez, J. Brown, J. Giordano, S. J. Lin, F. G. Omenetto, D. L. Kaplan, *Biomaterials* **2017**, *117*, 105.
- [41] L. Sun, S. T. Parker, D. Syoji, X. Wang, J. A. Lewis, D. L. Kaplan, *Adv. Healthcare Mater.* **2012**, *1*, 729.
- [42] R. Suntivich, I. Drachuk, R. Calabrese, D. L. Kaplan, V. V. Tsukruk, *Biomacromolecules* **2014**, *15*, 1428.
- [43] U. J. Kim, J. Park, C. Li, H. J. Jin, R. Valluzzi, D. L. Kaplan, *Biomacromolecules* **2004**, *5*, 786.
- [44] V. A. Parsegian, R. P. Rand, N. L. Fuller, D. C. Rau, *Methods Enzymol.* **1986**, *127*, 400.
- [45] X. Hu, D. Kaplan, P. Cebe, *Macromolecules* **2006**, *39*, 6161.
- [46] K. Urayama, T. Takigawa, T. Masuda, *Macromolecules* **1993**, *26*, 3092.
- [47] J. M. Zuidema, C. J. Rivet, R. J. Gilbert, F. A. Morrison, *J. Biomed. Mater. Res., Part B* **2014**, *102*, 1063.
- [48] E. L. Bakota, Y. Wang, F. R. Danesh, J. D. Hartgerink, *Biomacromolecules* **2011**, *12*, 1651.
- [49] L. Li, B. Yan, J. Yang, L. Chen, H. Zeng, *Adv. Mater.* **2015**, *27*, 1294.
- [50] D. Huemmerich, U. Slotta, T. Scheibel, *Appl. Phys. A* **2006**, *82*, 219.
- [51] M. Humenik, M. Drechsler, T. Scheibel, *Nano Lett.* **2014**, *14*, 3999.
- [52] A. Barth, *Prog. Biophys. Mol. Biol.* **2000**, *74*, 141.
- [53] U. Slotta, S. Hess, K. Spiess, T. Stromer, L. Serpell, T. Scheibel, *Macromol. Biosci.* **2007**, *7*, 183.
- [54] M. Groenning, *J. Chem. Biol.* **2010**, *3*, 1.
- [55] M. Humenik, M. Magdeburg, T. Scheibel, *J. Struct. Biol.* **2014**, *186*, 431.
- [56] E. DeSimone, K. Schacht, T. Scheibel, *Mater. Lett.* **2016**, *183*, 101.
- [57] A. Leal-Egana, T. Scheibel, *Biotechnol. Appl. Biochem.* **2010**, *55*, 155.
- [58] F. C. Mackintosh, J. Kas, P. A. Janmey, *Phys. Rev. Lett.* **1995**, *75*, 4425.
- [59] A. Martinez-Ruvalcaba, E. Chornet, D. Rodrigue, *Carbohydr. Polym.* **2007**, *67*, 586.
- [60] T. Jungst, W. Smolan, K. Schacht, T. Scheibel, J. Groll, *Chem. Rev.* **2016**, *116*, 1496.



Supporting Information

for *Macromol. Biosci.*, DOI: 10.1002/mabi.201700141

Characterization of Hydrogels Made of a Novel Spider Silk
Protein eMaSp1s and Evaluation for 3D Printing

Christopher Thamm, Elise DeSimone, and Thomas Scheibel*

Supporting Information

for *Macromol. Biosci.*, DOI: 10.1002/mabi.201700141

Characterization of hydrogels made of a novel spider silk protein eMaSp1s and evaluation for 3D printing

Christopher Thamm, Elise DeSimone and Thomas Scheibel*

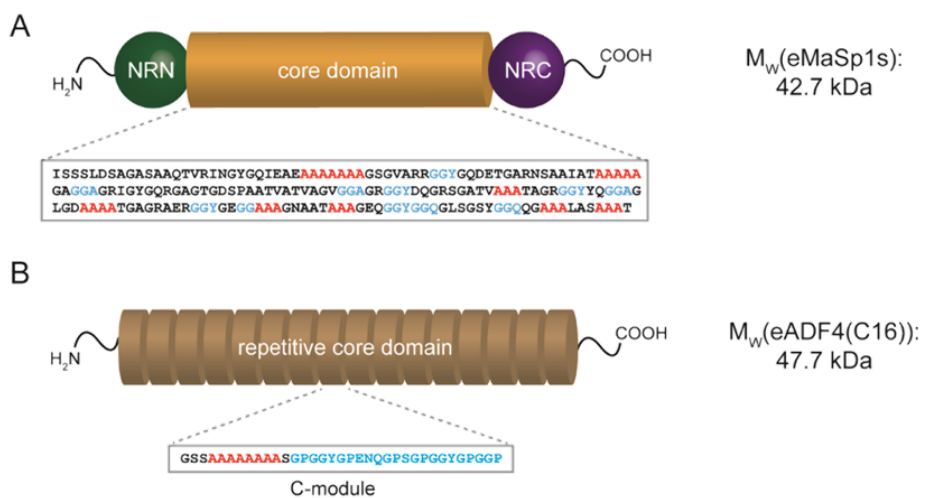


Figure S1: Scheme and sequence of eMaSp1s and eADF4(C16). Specific motifs are highlighted in red (poly-A) and blue (glycine-rich). The theoretical molecular weights (M_w) of both proteins were calculated using ProtParam tool: <http://web.expasy.org/protparam>.

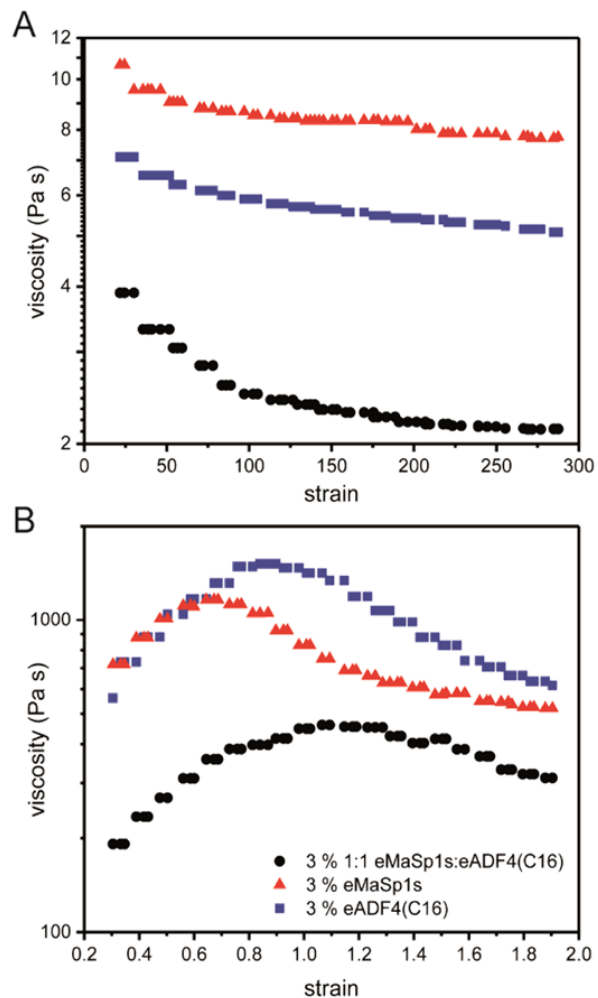


Figure S2: Viscosity measurements of hydrogels during the deformation phase at time sweep recovery measurements (see also figure 6). Hydrogels were either deformed at a shear rate of 40 s^{-1} for 1 second (A) or 0.2 s^{-1} for 10 seconds (B).

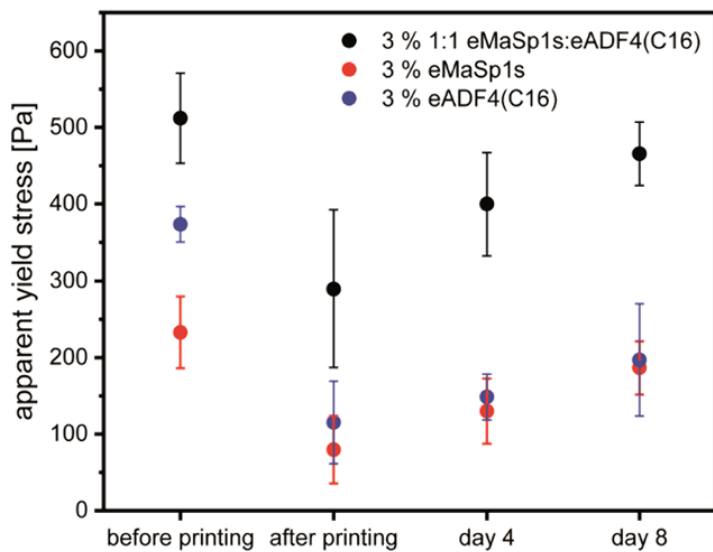


Figure S3: Changes in the apparent yield stress of 3 % (w/v) eMaSp1s, eADF4(C16) and blended hydrogels before printing, immediately after printing, 4 days after printing and 8 days after printing. Apparent yield stress was defined as the maximum stress experienced by the sample before yielding. Between measurements, hydrogels were stored at 4 °C and 100 % RH. Three samples were measured per group (n = 3).

Table S1: Secondary structure content of MaSp1s hydrogels and blended hydrogels with eADF4(C16) as determined by FSD of FTIR spectra.

	α -helices	β -sheets	β -turns	random coil	side chains
3 % (w/v) MaSp1s	21.7	26.6	16.7	33.6	1.5
7 % (w/v) MaSp1s	12.0	25.3	23.9	34.2	4.6
3 % (w/v) 1:1 eADF4(C16): eMaSp1s Blend	10.6	33.4	33.4	31.3	2.8

Part 5. Biomedical applications of recombinant silk

Aigner T.*, **DeSimone E.***, Scheibel T.

Published in *Advanced Materials*, **30**, 1704636
(2018)

Reprinted with kind permission from John Wiley and Sons

Biomedical Applications of Recombinant Silk-Based Materials

Tamara Bernadette Aigner, Elise DeSimone, and Thomas Scheibel*

Silk is mostly known as a luxurious textile, which originates from silkworms first cultivated in China. A deeper look into the variety of silk reveals that it can be used for much more, in nature and by humanity. For medical purposes, natural silks were recognized early as a potential biomaterial for surgical threads or wound dressings; however, as biomedical engineering advances, the demand for high-performance, naturally derived biomaterials becomes more pressing and stringent. A common problem of natural materials is their large batch-to-batch variation, the quantity available, their potentially high immunogenicity, and their fast biodegradation. Some of these common problems also apply to silk; therefore, recombinant approaches for producing silk proteins have been developed. There are several research groups which study and utilize various recombinantly produced silk proteins, and many of these have also investigated their products for biomedical applications. This review gives a critical overview over the results for applications of recombinant silk proteins in biomedical engineering.

1. Prologue

The purpose of this review is to summarize the use of recombinant silk proteins in biomedical engineering and the most beneficial characteristics of recombinant silks for these types of applications. Readers will also be given substantial amounts of background information on silks as well as important sub-fields in biomedical engineering, in hopes of making this review accommodating to specialists from different fields. The motivation is to provide a broad picture of a class of interesting biopolymers which are not as well-known as, for example, collagen, for biomedical engineering.

T. B. Aigner, E. DeSimone
University Bayreuth, Lehrstuhl Biomaterialien
Universitätsstr. 30, 95447 Bayreuth, Germany
Prof. T. Scheibel
Bayreuther Zentrum für Kolloide und Grenzflächen (BZKG)
Bayreuther Zentrum für Bio-Makromoleküle (bio-mac)
Bayreuther Zentrum für Molekulare Biowissenschaften (BZMB)
Bayreuther Materialzentrum (BayMAT)
Bayerisches Polymerinstitut (BPI)
University Bayreuth
Universitätsstr. 30, 95447 Bayreuth, Germany
E-mail: thomas.scheibel@brn.uni-bayreuth.de

 The ORCID identification number(s) for the author(s) of this article can be found under <https://doi.org/10.1002/adma.201704636>.

DOI: 10.1002/adma.201704636

2. Biomedical Engineering

Biomedical engineering (BME) is the practice of applying engineering principles to medical problems in order to improve the quality of health care. It encompasses everything from patient data collection, to medical machine design (e.g., magnetic resonance imaging), to pregnancy tests, to contributing to basic science, to tissue engineering.^[1] It seeks not only to increase lifespan but also to improve the quality of life for people afflicted with injury or disease. Generally speaking, there are four major patient populations which are in need: the elderly, the diseased or injured, those infected with “super bugs,” and those in third world countries.

The population world-wide is growing larger due to an increase in successful birth rate and life expectancy.^[2] The aging population is particularly problematic in terms of medical costs, as they are at increased risk for disease, injury, and tissue dysfunction.^[3] Common ailments of the elderly include dilapidation of joints through arthritis^[4] and failure of the heart and blood vessels through various heart diseases.^[5] Although there are many existing treatments, these are only able to alleviate the ailment, and not treat it. For example, hip implants for joint replacement are made from hard, inorganic materials. This results in improper integration with the host tissue, and there is no restoration of the original tissue. The most successful existing therapy is organs replacement.^[6] However, in this case, there is still no proper tissue integration because the organ is considered foreign by the immune system, requiring use of immune-repressive drugs and thereby increasing the patient's risk of infection. Further, the demand of organs is much greater than the supply, and the associated costs are quite high.^[7] There are also diseases which effect this population and are currently untreatable such as Alzheimer's.^[8]

A larger, broader patient demographic is those who have had nonfatal, accidental injuries (according to statistics reported by Center for Disease Control and Prevention (CDC)^[9]), for example bone fracture, anterior crucial ligament tear, peripheral nerve damage, skeletal muscle damage, and burns. Although treatments are relatively advanced for these types of injuries, there is still scarring and incomplete restoration of tissue function.^[10] More complicated injuries are those caused by disease or tissue pathology, for example osteoarthritis in the knee joint. This is particularly complicated because it requires both treatment of the disease and replacement of the damaged tissue.

Current solutions usually involve disease management through collagen injections, surgery, physical therapy, and in extreme cases joint replacement.^[11]

Another significant problem in modern medicine is that hospitals are notorious for high occurrence of transmitted diseases. In a survey from 183 hospitals in 2011 in the United States, it was found that 4% of patients contracted a healthcare-associated infection (HAIs).^[12] Of these incidents, the most predominant types were pneumonia (21.8%), surgical-site infections (21.8%), and gastrointestinal infections (17.1%). Infections in hospitals also tend to be more serious than those contracted elsewhere, as there is greater risk of antibiotic-resistant strains of bacteria. In a separate study in 2010, it was shown that nearly 20% of pathogens reported from all HAIs had multidrug-resistant phenotypes (e.g., methicillin-resistant *Staphylococcus aureus* (8.5%), vancomycin-resistant *Enterococcus* (3%)).^[13] The most common way to deal with this is through preventative medicine by sanitary protocols. However, no matter how good the sanitary protocols, infections will happen. Infections are usually handled through antibiotics, and in extreme cases the patient(s) will also be quarantined. Additionally, the overuse of antibiotics and antibiotic soaps in sanitary protocols has resulted in antibiotic resistant strains which cannot be treated by available drugs.^[14]

A last short-coming of modern medicine worth mentioning is the lack of remedies available to those in third world countries or with lower incomes. Although there are movements to improve this situation occurring in several sectors, for example, by improving water quality, providing household energy and education, and developing vaccines for vector-borne diseases (e.g., malaria), there is still much work left to do (according to Health and Environment Linkages Initiative (HELI) division of the World Health Organization (WHO)^[15]).

There are several new trends to meet these current medical problems in the BME field. Interesting examples include smart wear technology, primarily to be used for at-home patient monitoring,^[16] technology for mapping and stimulating the brain achieved through recent pushes by the BRAIN initiative as well as its internationalization,^[17] soft robotics for interaction with soft tissues,^[18] in vitro modeling for research to clinic translation for basic research and drug toxicology screening (e.g., liver on a chip),^[19] biomaterial coatings (active or passive) which physically disrupt bacteria with or without use of antibiotics to prevent disease transmission,^[20] or biofabrication for regenerative medicine.^[21] Although all of these products are novel and exciting, there are still drawbacks to even the most cutting edge designs such as poor translation from research to use in the clinic^[22] and the manufacturing readiness of the technology is low.^[23] Although there are many complicated reasons for this, one major step toward producing clinically viable products is to develop novel, suitable biomaterials. Among the suitable candidates, a particularly interesting biomaterial is the one derived from silks, due to its highly unique, inherent properties. For example, it has slow biodegradation^[24] and it is hypoallergenic.^[25] Originally, among a multiplicity of silks, only silkworm silk could be used for biomedical engineering, due to the difficulty of collecting silk from other animals and the challenges in biotechnological production. However,



Tamara Bernadette Aigner graduated from the double degree Bachelor's and joint Master's program for biological chemistry at the Johannes Kepler University (Austria, Linz) and the University of South Bohemia (Czech Republic, České Budějovice). She is currently a

Ph.D. candidate at University of Bayreuth (Germany) under the supervision of Thomas Scheibel and her research focuses on using recombinant spider silk proteins as a biomaterial for heart muscle and nerve regeneration.



Elise DeSimone received her Bachelor's degree in biomedical engineering from Rensselaer Polytechnic Institute (Troy, New York) and Master's degree in biomedical engineering from Tufts University (Medford, Massachusetts). She is currently a Ph.D. candidate at University of Bayreuth (Germany) under the

supervision of Thomas Scheibel and her current research focuses on the use of recombinant spider silk proteins as a biomaterial for biofabrication.



Thomas Scheibel has been full professor at the department of biomaterials at the Universität Bayreuth in Germany since 2007. He received both his Diploma of Biochemistry (1994) and a Dr. rer. nat. (1998) from the Universität Regensburg in Germany. After his postdoc at the University of Chicago

(1998–2001), he received his habilitation (2007) from the Technische Universität München in Germany. His research focuses on biotechnological production and processing of structural proteins, as well as their biomedical and technical application.

over the past 15 years, the recombinant production of silk proteins has been optimized to the extent that it can even be manufactured.^[26] Therefore, considering its favorable properties for biomedical applications and its recently realized availability, we believe and will try to present the case in this review that recombinant silk proteins could be one of these new biomaterials.

3. Silk

3.1. Natural Silk—What Is Silk?

Silks have a long history as a natural resource; silk from the silkworm *Bombyx mori* (*B. mori*) was used for weaving precious textiles in China, and was a greatly sought after product by the Europeans, with attempts to smuggle worms on the silk road.^[27] Natural silk even played a role in the early developments of the modern medicine, being identified as biocompatible and hypoallergenic, as well as suitable for direct use as wound dressing or surgical thread.^[28]

Craig defined silk as follows: “Silks are fibrous proteins containing highly repetitive sequences of amino acids and are stored in the animal as a liquid and configure into fibers when sheared or “spun” at secretion.”^[29] The most notable part of this definition is that silks are fibrous proteins, unlike glues, which are processed directly out of a highly concentrated solution, which is a process unlike that for other fibrous proteins such as collagen.^[29] Silks have evolved in many organisms independently, and some of their general characteristics are presented in Figure 1.

Silks are mainly composed of structural proteins, and their functionality can be traced back to their primary amino acid

sequences, which is rich in alanine, serine, and/or glycine. Although several different silk structures are possible, from β -sheets over α -helices to coiled-coil to collagen/polyglycine families, usually silk materials, depending on their equilibrium state, have either a high content of β -sheets or α -helices. When a solid silk morphology has high β -sheet content, usually these β -sheet structures resemble crystallites. Normally this would result in a material which is strong and brittle, however, silk is not brittle; silk is tough. This is because the β -sheets are surrounded by α -helices and coils, which act as a matrix phase. In other words, silks processed into water-insoluble fibers are semi-crystalline biopolymers and it follows that silk fibers with higher crystalline content are usually stronger or tougher.^[30]

Due to the significance of secondary structures to material properties, and as will be later shown to the response of cells, they are usually characterized every time a new silk protein is produced, or a different processing technique is used. To determine secondary structure content, commonly circular dichroism (CD) spectroscopy or Fourier-transform infrared (FTIR) spectroscopy in solid or liquid phase are performed. In interpreting CD measurements, core domains of silk proteins in solution at room temperature typically show random coil, polyproline II-like conformations or α -helical structures. The

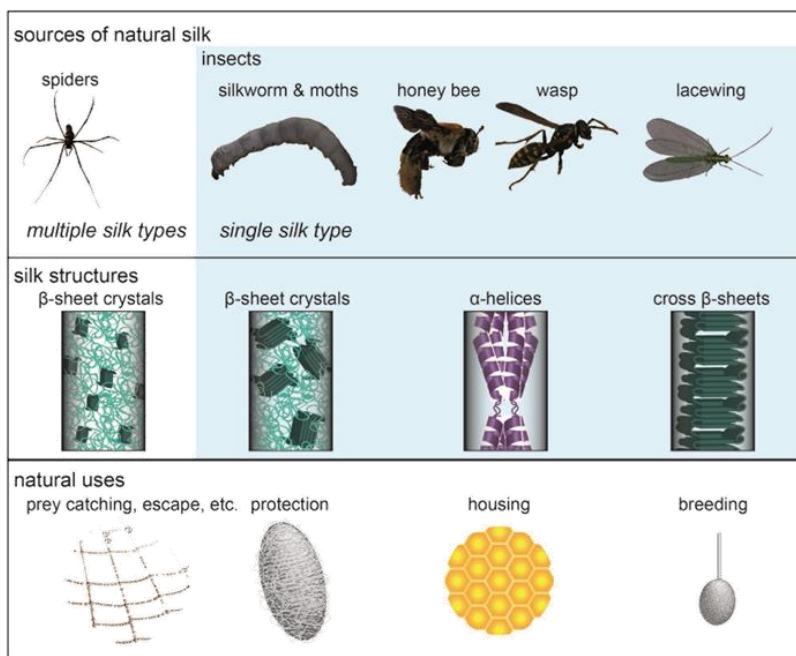


Figure 1. Natural silks. Natural silks of spiders, silkworms, moths, bees, wasps, and lacewings were used as an inspiration for the recombinant production of silk proteins to be used for biomedical applications. Spider and silkworm silk consist of β -sheet crystals embedded in an amorphous matrix. The huge difference in these two silk types is that these crystals in spider silks are much smaller and perfectly aligned along the fiber axis. Honey bee and wasp silk mainly consist of coiled-coil structures. Lacewing silk is composed of cross- β -sheet structures allowing a high bending stiffness. These secondary structural features evolved due to the desired function, e.g., a spider silk web has to withstand the force of a flying prey being caught without breaking, and the egg stalk should be able to carry an egg and protect it from predators. Silk worm, honey bee and wasp photos were taken and modified from open source images found on Pexels or Pixabay.

terminal domains in spider silk proteins, in contrast, often show α -helical structures, revealing α -helix bundles. When the protein solution is heated, conformational changes occur in the core domain forming β -sheet and/or β -turn structures.^[31] In FTIR spectroscopy the sum of these C=O stretching vibrations is found in the broad amide I band located between 1705 and 1595 cm^{-1} . Several methods were developed to retrieve information about the secondary structure content from the amide I band. To estimate the single bands which form the broad and undefined amide I band, Fourier self-deconvolution (FSD) is applied as described in Hu et al.^[32] Each of the single bands can then be assigned to a secondary structure motif, and thereby the percentage of each structural element can be calculated. The secondary structure content of solid silk samples differs remarkably between the species and the treatment of the material, for example, recombinant honey-bee silk mainly consists of coiled-coil structure (60%), whereas recombinant spider silk can reach a β -sheet content of about 40%.^[31,33]

Silks are produced in many arthropods and are important for survival and reproduction. Interestingly, different silks and their glands have evolved independently, which is the basis of some key differences in the silks between different animals. In insects, silk is produced in Malpighian tubules, labial, or dermal glands. Silks produced in the labial glands of different animals show all five known silk protein structures (coiled-coil, extended β -sheet, cross- β -sheet, collagen triple helix, polyglycine II) as they are used for various functions. In dermal glands silks only adopt β -sheet structure, and Malpighian tubule silks form either cross- β or α -helical structures.^[30]

In contrast to most insects, which can produce one silk type only,^[30] orb weaving spiders are able to produce up to seven different silks, each in a separate gland.^[34] However, dragline silk, the silk which spiders use for escaping danger and creating the strong frame of their webs, usually receives the most attention. These dragline fibers comprise primarily two protein classes, major ampullate spidroin 1 and 2 (MaSp1 and MaSp2).^[35] The main difference between MaSp1 and MaSp2 is that MaSp1 is almost proline-free, while MaSp2 contains about 15% proline residues.^[36]

3.2. Recombinant Silk—Why Go Recombinant?

There are many drawbacks to harvesting from natural biomaterial sources, these include batch-to-batch variation, impurities, risk for disease transmission, risk for rejection by immune response, and gathering in substantial (useable) quantities.^[37] In the case of silks, the main drawback of harvesting the material, with the exception of *B. mori* silk, is that large scale farming of most of the animals is not possible or harvesting the material is complicated (e.g., lacewing silk). Spiders are particularly difficult to domesticate, as most species are territorial and cannibalistic.^[38] Nevertheless, efforts have been made to harvest native silk from *Nephila* spiders and combine it with decellularized, porcine veins to prepare nerve guidance conduits.^[39] Insects such as lacewing flies or bees are easier to farm, however they produce minuscule amounts of silk, and harvesting these silks would not only be tedious, but would severely limit their applications due to the limited amount of material.^[40] Consequently,

in terms of sourcing, silk is less accessible unlike other natural materials such as collagens, which are abundant, however are at higher risk for an undesirable response upon implantation. Collagen has been associated with product impurities, disease transmission, and increased likelihood of bacterial infection.^[41]

To create an alternative source of biomaterials, biotechnological solutions have been developed to produce larger amounts of protein with more consistent quality and greater biological safety. Although this was a challenging endeavor, over the course of 15 years recombinant silk protein production has become well-established, and some variants are even available commercially.^[26] To continue with the previous comparison, collagen is also favorable for protein engineering in that it has a repetitive amino acid sequence. In the case of collagen, this repetitive sequence is characterized by motif Gly-X-Y where Y is most commonly hydroxylated proline.^[42] Hydroxylation of the proline is a highly complex process requiring special enzymes. Therefore, in spite of its repetitive amino acid sequence, collagen cannot be produced by most expression systems due to its need for extensive post-translational modification.^[41] In this respect, recombinant silk proteins could be considered more ready than recombinant collagen proteins.

For a more in depth discussion on the challenges of recombinant silk production, the authors refer readers to in-depth reviews on this subject.^[43]

Several steps are required to design and produce a recombinant protein. They can be roughly divided by natural DNA sequence determination, recombinant DNA design based on natural sequence, vector cloning, host organism transformation, induction, and purification of the protein.^[44] When engineering recombinant protein, it is often advantageous to engineer the sequence to be produced more efficiently, while maintaining its key functions. Although a demanding task, this offers huge advantage in terms of studying these proteins, and further allows for hybridizing or functionalizing recombinant silk protein (Figure 2). The most often used host organism for recombinant silk protein production is *Escherichia coli* (*E. coli*), and therefore, the process will be explained from this perspective, although other hosts are also available and have been recently reviewed.^[43c,d]

Recombinantly produced silk proteins have been in general shown to be versatile in terms of being able to form several, tailorable morphologies. They can be formed into films, capsules, particles, foams, hydrogels, micrometer-fibers and nanofibers (Figure 3). This allows a wide range of applications in different fields.

3.3. Nomenclature

The authors would also like to make a few direct comments regarding nomenclature, as this is sometimes challenging in the field of recombinant silk proteins, especially with spider silks. This is because spider silk can be characterized by species, silk type (e.g., dragline or flagelliform silk) and/or protein type (e.g., MaSp1 vs MaSp2). Further, there is sometimes confusion between silk proteins produced by insects (fibroins) versus silks produced by spiders (spidroins), and spider silk proteins are often referred to as both (fibroin

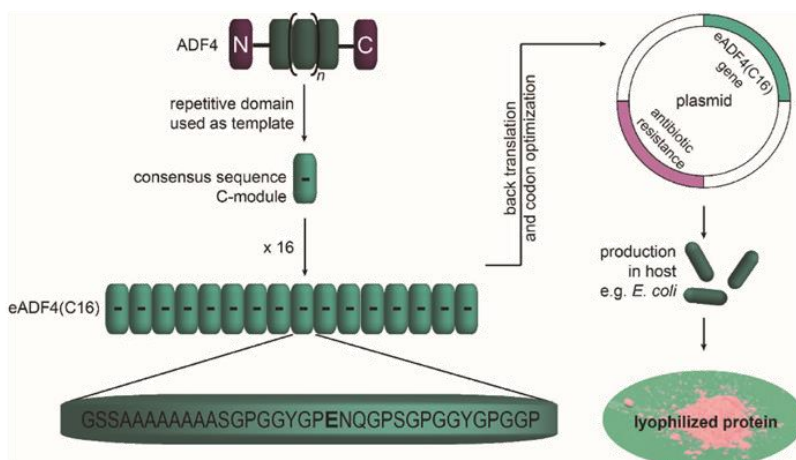


Figure 2. Development of recombinant silk protein using eADF4(C16) as an example. The repetitive core of *Araneus diadematus* fibroin 4 (ADF4) was identified and used as a template for the C-module. This C-module was then repeated 16 times to create the engineered AFD4 (eADF4(C16)). The amino acid sequence was back translated and codon optimized for the host organism (here *E. coli*). A plasmid containing the silk gene and a gene for antibiotic resistance to allow selection was created. The host was then transfected and protein production triggered. After several purification steps protein powder was obtained, which can be further processed into different morphologies.

or spidroin), whereas silkworm and insect silk proteins are referred to exclusively as silk fibroin.

Most recombinant spider silk proteins are based on *Nephila clavipes* sequences and refer to their spidroins as MaSp1 and MaSp2, depending on their proline content (MaSp1 low, MaSp2 high). Other recombinant spider silk proteins are based

on *Araneus diadematus*, which has two identified proteins in dragline silk named as fibroins 3 and 4 (ADF3–ADF4), however both are MaSp2 proteins.^[45] In most other cases, even though the recombinant spider silk protein is based on a different spider than *Nephila clavipes*, the protein will be referred to as MaSp1 or MaSp2. Another way researchers name their recombinant

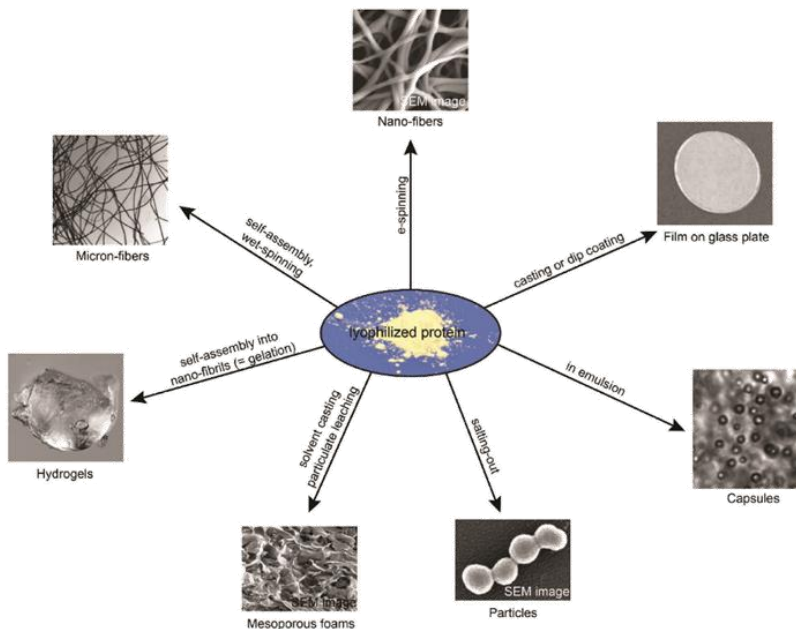


Figure 3. Processing routes for recombinant silk proteins to prepare different morphologies.

proteins is based on their molecular arrangement, or based on the number of consensus modules in the sequence.

As a further complication, throughout the course of their research, some groups will change their naming system of their proteins, making it difficult to differentiate between a newly designed recombinant protein or a variation or optimization of an earlier recombinant protein. Although the decision to rename an existing protein is often justified, it can be difficult to follow throughout the literature. A few examples in which researchers change the name of their recombinant protein is for "15mer"^[31a] also called MS1,^[46] eADF4(C16) which was originally ADF4(C16)^[47] or C₁₆,^[48] and rS1/9^[49] which is also called 1F9.^[50]

To provide a guide for the reader for this review, recombinant silk proteins used in BME are summarized in **Table 1**.

4. Regenerative Medicine

Damaged human tissues or organs are rarely able to completely regenerate, the regenerative capability depending directly on the tissue type and the severity of the damage. Regenerative medicine is the field dedicated to creating tissue or organ-like implants in order to heal or replace damaged tissues or organs.^[64] The important concepts and definitions will be presented here; however, the authors encourage interested readers to explore other reviews and opinion pieces, which delve into the topic of regenerative medicine and importantly touch on critical points as well as scientific debate in the field.^[65]

The largest subfield of regenerative medicine is tissue engineering, which is the selection and spatial arrangement of cells and biomaterials for artificial tissue design. The approach used is typically characterized as bottom-up or top-down, where bottom-up refers to modular assembly of building units into tissue-like constructs, and top-down refers to simply combining the components and allowing them to self-form structures.^[66] Which type of method is used, bottom up or top down, usually depends on the problem which must be solved. For example, there are some cases where a fully matured tissue must be implanted because the implant must function immediately, such as in heart or heart tissue replacement. On the other hand, there are tissues which can benefit from a slow healing process, for example in neurological tissues where there is a nerve gap. Regardless of the technique, the "building blocks" for implants made based on regenerative medicine principles are biomaterials, cells, soluble bioactive factors, and specialized, *in vitro* culturing conditions (e.g., mechanical stimulation through liquid flow) (reported by nibib online^[64b]). It is important to note that not all these "building blocks" must be used in one construct, and it is widely debated which of these components are truly necessary for regenerative medicine.

In this review, the tissue engineering design element focused on is biomaterials based on silk proteins. As defined by the National Institutes of Health in the 1980s a biomaterial is "any substance (other than a drug) or combination of substances, synthetic or natural in origin, which can be used for any period of time, as a whole or as a part of a system which treats, augments, or replaces any tissue, organ, or function of the body."^[67] Biomaterials are not to be confused with

biogenic materials, which are defined as materials produced *in nature*.

Due to its principle role in tissue function, researchers often try to recapitulate properties of the extracellular matrix (ECM) by altering the morphology of the biomaterial, introducing gradients of biomaterials, and so on. One of the most significant design elements of a biomaterials scaffold is dimension that the cells are cultured in (1D, 2D, or 3D); in 1D cells form elongated shapes, which polarizes the cells (e.g., cortical neurons), in 2D cells tend to form monolayers as in the case of membrane tissues (e.g., endothelial cells), and in 3D cells tend to form irregular shapes with many filopodia, and this is the environment which most cells are exposed to.^[68]

4.1. Micrometer-Fibers Made of Recombinant Silk Proteins

"Micrometer-fiber" is a term which will be used by the authors to describe fibers which have diameters in the micrometer-range. In terms of silk proteins, the most classic example of producing these fibers is by biomimetic or wet spinning, the latter being the extrusion of a spinning dope into a coagulation bath.^[69] However, to the best of the authors' knowledge, there are only limited number of papers using wet-spinning to investigate for the potential for use of silk-based micrometer-fibers for tissue engineering applications (e.g., suture materials).^[70] This is unexpected in that wet-spun fibers usually provide the best mechanical properties out of all fiber production methods (raw extracted, electrospinning, microfluidics), as well as the excellent control of fiber diameter.^[70] That this technique is used less often than other techniques is likely due to the fact that the fibers cannot be produced as quickly or in the same quantity as in the other production methods. Therefore, wet-spinning will not be extensively discussed in this review.

Micrometer-fibers have also been further processed by braiding, weaving, chopping, and combining into nonwoven meshes.^[31b,59,71]

4.1.1. Micrometer-Sized, Recombinant Silk Fibers, Fiber Meshes, or Fiber Knits in Tissue Engineering

Self-assembled 4RepCT fibers were evaluated concerning toxicity and immunogenicity by subcutaneous implantation in rats.^[72] No toxicity was detected, and the immunogenicity was low as determined by the presence of infiltrated immune cells, and the formation of fibrous capsule or granulation tissue. A particularly important point of this study was the removal of endotoxins, a common problematic by-product of recombinant proteins produced in *E. coli*. Next, it was shown that the self-assembled micrometer-fibers could be sterilized without negative effects on the fiber properties, **Figure 4**.^[73] This is a clear benefit of this particular protein variant toward tissue engineering, as endotoxin-free, sterile materials are necessary to qualify for Food and Drug Administration (FDA)-approval.

After pilot studies were complete, fiber meshes were produced from 4RepCT self-assembled fibers, and compared to films and foams for promoting growth of primary fibroblasts as well as maintenance of differentiation state (as measured by

Table 1. Recombinant silk proteins used in biomedical engineering applications, not including information on modified versions (e.g., with RGD sequence).

Origin species	Natural protein	Recombinant protein	Host	Molecular weight (recombinant protein)	Unique features of the recombinant protein primary sequence	Reference
<i>Anshrasa pernyi</i> (moth)	Fibroin	EAEFN ₅₇₁₀	<i>E. coli</i> strain BL21	≈11.4 kDa, ≈22.9 kDa	G-rich, poly-A repeat, repetitive unit repeated 5 or 10 times	[31d]
<i>Apis mellifera</i> (honey bee)	AmelF1-4	Recombinant AmelF1, AmelF2, AmelF3, AmelF4	<i>E. coli</i> strain Rosetta 2 (DE3) competent cells	32 kDa	29–33% alanine, amino acid sequence of recombinant protein exactly the same as natural protein	[51]
<i>Bombyx mori</i> (silkworm)	Heavy chain (H-chain)	Transgenic silk fibroin	Transgenic silkworm, <i>B. mori</i>	N/A—Variable; Natural silk fibroin = 100–400 kDa, usually ≈300	Natural silk fibroin characterized by silk fibroin block (GAGAGS)	[52]
<i>Bombyx mori</i> (silkworm)	Light chain (L-chain)	L-RGDSx2 fibroin (LRF)	Transgenic silkworm, <i>B. mori</i>	N/A—Variable; Natural silk usually ≈26 kDa	Natural silk fibroin light chain modified with RGD binding sequence	[53]
<i>Bombyx mori</i> (silkworm)	Crystalline	[(AGSGAG) ₄ E ₈ AS] ₄	Transgenic silkworm, <i>B. mori</i> and <i>E. coli</i>	19.9 kDa (theoretical 19.7 kDa)	Polyglutamic acid for calcium binding	[54]
<i>Bombyx mori</i> (silkworm) and “mammalian”	Silk fibroin and elastin	SELP-47K and SELP-815K	<i>E. coli</i> strain HB101	SELP-815K ≈65 kDa SELP-47K ≈70 kDa	Silk fibroin block (GAGAGS) and mammalian elastin-like block (GVGVVP) either with silk 4 times and elastin 7 times (SELP-47K) or with silk 8 times and elastin 15 times (SELP-815K)	[55]
<i>Chrysopa carnea</i> (lacewing)	MalXB2	N[AS] ₈ C	<i>E. coli</i> strain BL21 (DE3)	53 kDa	AS module repeated 8 times	[33b,56]
<i>Vespa simillima</i> (hornet)	Vssilk1-4	Recombinant Vssilk1-4	<i>E. coli</i> strain BL21	30–70 kDa	Relatively low number of repetitive sequences, amino acid sequence of recombinant protein exactly the same as natural protein	[57]
<i>Avaneus diadematus</i> (spider)	ADF-4 (MaSp2)	eADF4(C16), eADF4(x16)	<i>E. coli</i> strain BL21	48 kDa	GPGXX-rich with poly-A sequence, module is repeated 16 times	[58]
<i>Euprosthenops australis</i> (spider)	MaSp1	4RepCT	<i>E. coli</i> strain BL21	23.4 kDa	G-rich, poly-A repetitive unit repeated 4 times	[31b,59]
<i>Nephila clavipes</i> (spider)	MaSp1	6mer, 15mer	<i>E. coli</i> strain or RY-3041, a mutant BLR (DE3) defective in the expression of SlyD protein	16–22 kDa, 40–50 kDa	G-rich, poly-A monomer	[31a,60]
<i>Nephila clavipes</i> (spider)	MaSp1	1F9 and rS1/9	<i>Pichia pastoris</i> (yeast) or <i>Saccharomyces cerevisiae</i> (yeast)	94 kDa	9 monomer repeats, monomer contains consensus primary repeats	[49,50,61]
<i>Nephila clavipes</i> (spider)	MaSp1, MaSp2	rMaSp1, rMaSp2	Transgenic goats	65–120 kDa	not defined	[62]
<i>Nephila clavipes</i> (spider)	MaSp1	MS1 (15mer)	<i>E. coli</i> BLR (DE3)	MS1: 39 kDa	MS1: G-rich, poly-A, repetitive unit repeated 15 times	[46,63]
	MaSp2	MS2 (9mer)		MS2: 28.15 kDa	MS2: G-rich, poly-A, 4x Q, repetitive unit repeated 9 times	

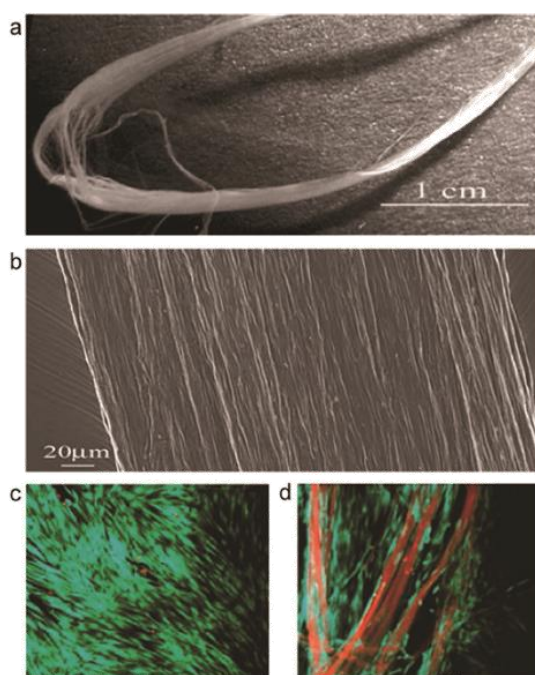


Figure 4. Sterilized, self-assembled 4RepCT micrometer-fibers as visualized by a) photography and b) SEM. Fibroblast attachment and proliferation for 7 d on c) tissue culture plastic (TCP) as a control and d) sterilized 4RepCT micrometer-fibers as evaluated by LIVE (green)/DEAD (red) staining. Micrometer-fibers were also nonspecifically stained red by the staining solution. The micrometer-fibers showed cell attachment comparable to the TCP control, and the lack of dead cells indicated there was no cytotoxicity. Reproduced with permission.^[73] Copyright 2010, American Chemical Society.

collagen I production).^[71] As in the case for most silks, it was clear that inclusion of a cell-binding peptide would be necessary for proper cell attachment, and variants modified with either the tri-peptide RGD (Arg-Gly-Asp), RGE (Arg-Gly-Glu, negative control for RGD), the penta-peptides IKVAV (Ile-Lys-Val-Ala-Val), or YIGSR (Tyr-Ile-Gly-Ser-Arg) were also tested.^[74] There was no challenge or observed changes in the self-assembly of fibers made of 4RepCT modified with cell binding peptides, however cell attachment was significantly enhanced on films made thereof. 4RepCT has also been modified with several other binding sequences, as well as antibiotics to repress bacterial growth.^[75]

The potential of self-assembling fibers 4RepCT for specific applications was introduced in Johansson et al., where the performance of 4RepCT as a biomaterial for pancreatic islet formation was evaluated. The authors compared the performance of films, foams, and meshes made of self-assembled fibers. Pancreatic donors were collected either from C57Bl/6J mice or from human islets of diseased patients. The islets were evaluated for cell viability and attachment, as well as insulin production and the amount of intracellular calcium. The best performance was on RGD functionalized 4RepCT

assembled into foams, and the details of these results are therefore described in the foams section of this review.^[76]

When silkworms build their cocoons, these consist of one long, winding thread with a protein core surrounded by sericin gum. To remove the sericin, or to “degum” the fibers, cocoons or cocoon pieces are boiled, and the remaining product is intact silk fibroin threads, usually referred to as regenerated silk fibroin (RSF). These fibers can then be used as single strands, bundled into yarns, or woven into a knit structure.^[77] In a preliminary study, wild-type and transgenic worm RSFs modified with adhesive collagen sequence were used to prepare small-diameter vascular grafts.^[77a] The grafts were created by winding onto a tube template (1.5 mm diameter, 10 mm long) using a 16-bobbin braiding machine. The grafts were further coated with aqueous RSF solution, post-treated with 50% ethanol, and then removed from the template. Male Sprague–Dawley rats were used as an animal model for implantation in the abdominal aorta. After 12 months there was significantly high patency in wild-type silk fibroin compared to poly(tetrafluoroethylene) grafts, and there was infiltration of cell types as well as structured vessel formation after 4–12 weeks. At this stage, the recombinant silk fibroin production is still needed to be optimized, and therefore only an *in vitro* examination was conducted, and showed enhanced attachment of endothelial cells.

In further work, the transgenic worms were modified to produce silk fibroin, which includes vascular endothelial growth factor (VEGF) or RGD sequences in the heavy chain.^[77c] The successful production was confirmed using western blotting and antibody staining, however there was no quantification of the ratio of modified and unmodified heavy chains. Human umbilical vein endothelial cells showed enhanced cell attachment proliferation on the modified variants. Further, the grafts were tested for attachment of serum proteins, as attachment of serum proteins results in a closing of the graft to blood flow. In this study, the attachment of platelets was evaluated *in vitro* as well as patency *in vivo*. *In vitro*, it was found that both VEGF and RGD modified silk fibroin showed enhanced attachment of platelets compared to materials made of the unmodified silk fibroin. However, materials of the RGD variant showed far less patency *in vivo* compared to that of both unmodified silk and VEGF modified variants, and the authors hypothesized this was due to thrombosis.

In conclusion, VEGF modified silk fibroin-based materials not only showed the best patency, but showed the best tissue infiltration and new vessel formation, making this variant particularly promising for future application.^[77c] Furthermore, there seemed to be a clear benefit of fibers which were fixed into some kind of morphology (braided, mesh) over free-floating fibers, implying that, although it was important to test the fibers independently, practically micrometer-fibers need to be reformed to be useful in application.

4.2. Sub-Micrometer and Nanofibers

Sub-micrometer and nanofibers are used in regenerative medicine due to the size relevance of such fibers to many natural structures found in tissues.^[78] When used alone and not in composite scaffolds, the most common tissue engineering

applications of such fibers are in the context of membrane tissues and/or hollow tubes such as vascular grafts,^[79] nerve guides,^[80] skin grafts, or wound dressings.^[81] One common technique to produce sub-micrometer and nanofibers is electrospinning.

Electrospinning is the formation of fibers in the micrometer to nanometer range by electrically charging a slowly extruded solution.^[82] First, a droplet forms at the tip of the needle, and, if the parameters are set correctly, the force of the electrical charge overcomes the tension of the droplet, and a jet is formed. Eventually, the jet undergoes whipping instabilities, thereby stretching the jet, in the ideal case, into an ultrathin fiber which forms the mat.^[82,83] The main advantages of electrospinning are that it requires low working volumes to produce large amounts of scaffold, and there is relatively fine control over what is produced. However, the disadvantage is that mats produced from electrospinning are generally 2D, although it is technically possible to produce 3D scaffolds.^[84] Further, low molecular weight (i.e., most recombinant proteins) polymers or proteins are often difficult to use in electrospinning, although this can usually be overcome by increasing the concentration.^[85] Another disadvantage to electrospinning solutions is that they are commonly produced by dissolving the solute in toxic, fast evaporating solvents. This, combined with the extreme electrical voltage, makes the process less friendly to biological agents exposed to the process, and can also be considered dangerous from a regulatory point of view.

4.2.1. Recombinant Silks Processed into Nonwoven Fiber Mats for Tissue Engineering

In an evaluation of Balb/3T3 mouse fibroblast adhesion of films, hydrogels, and nonwoven mats produced from recombinant spider silk eADF4(C16), one of the most interesting results was that, without introduction of an RGD sequence, cells were able to attach to nonwoven meshes. This was surprising, since the flat films prepared by the same recombinant protein resulted in low cell adhesion. Interestingly, there was a strong dependence of the cell attachment on the fiber diameter.^[33a] Through these studies it was shown that the bioactivity of cells on recombinant spider silk materials can also be enhanced by changing the morphology, and in this study it was assumed that the fiber diameter primarily determines the success of cell attachment. However, it is difficult to say if the negative space or the fibers themselves contributed to the cell attachment, as both the architecture of the fibers as well as the porosity play a significant role in this process.^[86]

In a similar study, attachment of primary green fluorescent protein (GFP)-expressing fibroblasts from rabbits to AmelF3 (recombinant honey bee silk, Table 1) nonwoven meshes was evaluated.^[51b] In this case, an aqueous solvent was used for electrospinning, but poly(ethylene oxide) was added as a fiber forming agent. It was shown that there was fibroblast monolayer formation in 7 d, without any modification to the protein, as in the case of eADF4(C16). However, in this case, there were no films cast as a further control, and no citations or previous work are available showing cell culture on films made of the recombinant honey bee silk protein. Therefore, it is not

possible to definitively conclude if the attachment of cells on this recombinant silk is due to its biochemical or physical character, or if it was due to the use of this morphology.

A more complex example of using nonwoven mats produced from recombinant spider silk proteins was exhibited in Zhu et al., using MaSp1/MaSp2 blended with collagen. The spinning dopes were at concentrations of 100 mg mL⁻¹ and comprised of either collagen type I, 4:1 MaSp1/MaSp2, or a blend of the two. Here, human decidua perietalis placental stem cells were cultured on the nonwoven mats and tested for proliferation and neural differentiation.^[87] MaSp-based nonwoven meshes had the advantage that they resisted degradation in Dulbecco's Modified Eagle Medium and were mechanically stronger (Young's modulus <1 GPa for collagen-based and ~4.5 GPa for MaSp-based fibers). On the other hand, the collagen-based nonwoven mats were more biologically active with increased attachment as well as increased expression of β -tubulin III, a structural protein found in the axons of neurons. To try to achieve both of these properties, they experimented with the ratios of collagen and recombinant spider silk protein in the spinning dope, and it was found that the fibers produced from 30% MaSp content seemed to be the best balance between the two properties, mechanical stability, and bioactivity, showing resistance to degradation as well as significant differentiation of the stem cells. However, these nonwoven meshes were only cultured for 7 d, and neural cell differentiation and maturation is a much longer process, and perhaps it would have been more advantageous to use less collagen and allow for longer growth periods.^[19b] Another possible route for this would be instead to use mixtures of recombinant protein variants, which have collagen-associated cell-binding peptides, or other neuronal growth factors. Thereby, the mechanical stability of silk would not be compromised by blending.

In summary, fiber mats are an interesting morphology bridging the gap between flat films and complex 3D networks like hydrogels. It was shown that sub-micrometer fiber morphologies can enhance the cell attachment. However, there seems to be further benefits of including cell-recognition sites, which should be considered in terms of producing functional tissue, but have not been thoroughly analyzed so far.

4.3. Films

Films are the morphology of choice for screening the response of cells to the biochemical features (e.g., cell-binding sites), cytocompatibility, and physical (e.g., charge) character of the biomaterial. The small amount of material required, the ability to control the effects of topology and mechanical stiffness, as well as the ease and simplicity for high-throughput experiments, makes films a particularly powerful tool for initial characterization of the material. Especially in terms of recombinant proteins, this can be a crucial point due to the low amount of available material before the production is optimized. Films have been produced by recombinant silk proteins 4RepCT, eADF4(C16), N[AS]₅C, 6/15mer, MaSp1/MaSp2 (transgenic goats), Vssilks, EAEPN_n, transgenic fibroins and variants thereof.

4.3.1. Recombinant Silks Processed into Films

Silk films are usually produced by casting a silk solution within various solvents like 1,1,1,3,3,3-hexafluoro-2-propanol (HFIP), formic acid, aqueous buffers, or mixtures thereof. Due to the rapid evaporation of HFIP after casting, the proteins remain in the same equilibrium state of secondary structures as if they were in solution, and films must be post-treated to be rendered water insoluble. The post-treatment step usually is incubation in primary alcohols like methanol or ethanol at various percentages ranging from 70% to anhydrous.^[31a,33a,d,57b,88] One exception is that, if cast out of formic acid, the proteins tend to immediately convert into β -sheet rich structures, and therefore post-treatment is not necessarily required.^[33b,e] Films out of aqueous solutions were sometimes post-treated with alcohol,^[31c,57a,60b,89] and sometimes used as obtained.^[71,74–76,90]

The surface characteristics of silk films such as surface topography, roughness, and composition are commonly investigated by various microscopy techniques such as atomic force microscopy (AFM),^[89a,91] light microscopy, and scanning electron microscopy (SEM).^[89c,92] These types of assays have shown that generally silk films are smooth. Surface hydrophobicity is typically studied on films using contact angle measurements, which have revealed that recombinant silk films tend to be slightly hydrophilic (contact angle between 55° and 90°).^[53a,57b,88a,89a] Given how similar recombinant silk films seem in materials characterization tests, the results in cell culture were surprisingly different.

One of the most common ways to evaluate recombinant silk proteins films is by determining cell attachment and proliferation. 4RepCT films were incubated with human fibroblasts, and although no cell recognition sites were present, cells adhered, proliferated, and produced collagen I.^[72] Several cell binding motifs—RGD, IKVAV, YIGSR, and RGE as negative control—were generated. Primary human fibroblasts, keratinocytes, endothelial, and Schwann cells were seeded on silk films with the different binding motifs. Focal adhesions of fibroblasts, keratinocytes, and endothelial cells were best on films of the RGD variant, whereby Schwann cells seemed to prefer films made of the IKVAV variant.^[74] Films of different silk variants bearing a fibronectin motif, with RGD being presented in a loop similar to native ECM, were incubated with human primary cells, which showed an increased attachment, spreading stress fiber formation and focal adhesion points compared to RGD-4RepCT. Moreover, human dermal microvascular endothelial cells (HDMEC), human mesenchymal stem cells (hMSC), and human epidermal keratinocytes (NHEK) were able to attach and proliferate, and NHEK could be directed to migrate into a wound area.^[93] By contrast, eADF4(C16) films resulted in low cell adhesion and proliferation of Balb/3T3 mouse fibroblasts, likely due to the fact that this protein lacks specific domains for cell adhesion, has a net negative charge, and the films have a smooth surface.^[33a] An RGD tag was covalently bound to the C-terminus by introducing the encoding sequence directly into the recombinant DNA sequence, or via chemical coupling of a cyclic RGD-peptide to the N-terminus; both variants tremendously improved Balb/3T3 adhesion compared to that on the RGE-modified control.^[89a]

In Kambe et al., the attachment of chondrocytes isolated from white rabbits was tested on films produced from fibroins with different numbers of RGD motifs per recombinant protein. Indeed, it was shown that primary chondrocytes exhibited a spread morphology on films of the L-RGDSx2 after 12 h, which was not found on films of native fibroin. A modified cantilever was used to determine the adhesive force and demonstrated an increase in adhesive strength on the RGD modified fibroin surface. Further, real-time polymerase chain reaction (qPCR) measurements revealed that this increased cell adhesive strength did not occur at the expense of down-regulating the chondrocyte-specific phenotype. Thus, films of the L-RGDSx2 fibroin containing two RGD motifs in the fibroin light chain were determined to be a promising substrate for primary chondrocytes.^[53b] Films made of four recombinant silk proteins of *Vespa simillima* hornets were also investigated. It was shown that Vssilk1 and Vssilk2 film surfaces are positively charged at physiological pH and were rather hydrophobic with water contact angles between 85° and 90°. It was therefore not surprising that there was a significant higher cell adhesion on films made of Vssilk1 and 2 than of Vssilk3 and 4. It was proposed that this effect comes from a cell–substrate interaction mediated by adsorbed negatively charged ECM proteins, for instance collagen I or fibronectin.^[57b] In a further study, an RGD motif was added to Vssilk1, which improved NIH3T3 fibroblast adhesion.^[57a]

Independent of cell-binding motifs, it was also shown that by structuring films of different eADF4(C16) variants and the lacewing egg stalk mimic N[AS]₆C, the attachment of Balb/3T3 fibroblasts and C2C12 myoblasts can be improved. Moreover, the cells aligned in the grooves of the structured films, independent of the silk proteins and variants used, and myoblasts even formed myotubes.^[33b] Films of transgenic silkworm silk have also been analyzed by several groups. In Yanagisawa et al., a collagen or an RGD motif was added to the light chain of fibroin in an attempt to improve cell adhesion. Tests using Balb/3T3 fibroblasts showed that on films of both constructs adhesion could be improved compared to that on films of native fibroin, whereby RGD modified silks resulted in the best performance.^[52c]

Recombinant silk films have also been used as screening tools for more specific applications. On 4RepCT films, mouse and human pancreatic islets were studied. The cells were investigated in terms of viability and function by their Ca²⁺ and insulin release as well as the islet morphology and immunohistochemistry were assessed.^[76] Lewicka et al. investigated neural stem cells (NSCs) on 4RepCT films and showed that before differentiation cells could proliferate and after differentiation with ciliary neurotrophic factor matured into astrocytes and after differentiation with bone morphogenetic protein matured into neurons. However, differentiation with the thyroid hormone T3 into oligodendrocytes resulted in a lower success rate compared to the positive control (poly-L-ornithine and fibronectin coated plates). These results suggest the applicability of 4RepCT films in combination with NSCs for drug screening and in the future for cell therapy-based treatments of neurological disorders like Parkinson's disease or traumatic spinal cord injuries.^[90a] In the study by An et al. MaSp1 and MaSp2 films were compared to *B. mori* silk films, and it

was shown that cortical neurons grow on MaSp1 films only. The hypothesized reason for this behavior is that MaSp1 films are not only stiffer, but also inherently positively charged at neutral pH. Thus, the neural cell adhesion molecule (NCAM), which is negatively charged, preferably attaches to this silk film. A significant increase in NCAM protein level was determined by qRT-PCR. Additionally, they found a GRGGL (Gly-Arg-Gly-Leu) motif in MaSp1, also found in brain aggrecan core protein, which seems to support neural growth.^[88b]

MaSp1 derivatives 15mer and 15mer conjugated with the RGD cell binding motif films were evaluated for the attachment of hMSCs, as well as the tendency of the MSCs to biomineralize the scaffold. Interestingly, a higher amount of calcium as well as a higher proliferation was obtained on films of the 15mer without the RGD tag. Although experimentally unconfirmed, it was speculated that the RGD motif was not accessible on the surface.^[31a] To remedy the problem, the silaffin derived R5 tag, which is responsible for silica mineralization in *Cylindrotheca fusiformis*, was tagged onto 15mer. hMSCs were grown on films with and without silica nanoparticles (SNPs) and on both a comparable cell growth and morphology was shown in comparison to growth on plain tissue culture plates. However, an up-regulation of osteogenic genes (alkaline phosphatase and bone sialoprotein (BSP)) was found mainly in SNP containing samples.^[92] In a later study, the 6mer was genetically coupled with BSP to induce bone mineralization in vitro. Calcium phosphate deposition was confirmed after 6 h incubation in accelerated calcification solution, and after 7 d in osteogenic culture media. Such films also showed a higher hMSC attachment and proliferation rate as in native 6mer, likely due to the fact that BSP contains triple RGD (Figure 5).^[89c] In the presence of calcium a higher stiffness of films of the 6mer with BSP than without BSP was found. Additionally, 6mer films treated with BSP had a much higher Young's modulus than of those which were not treated, as determined by AFM measurements. This might be due to the fact that, when calcium is present, supramolecular networks can be formed, and these

have the ability to dissipate energy in response to applied force. This is a highly promising property for bone plasticity, and therefore it was suggested to use this protein as organic glue for synthetic nanoscale composites.^[89b] Another interesting recombinant silk is the silk moth derivative EAEFN_n (*n* = 5 or 10) from *Antheraea pernyi*. On EAEFN₁₀ films, an osteoblast cell line showed an increased adhesion compared to that on *B. mori* fibroin films. Further, differentiated cells after 14 and 21 d deposited more calcium phosphate onto EAEFN₁₀ films than *B. mori* fibroin films, however, the positive control resulted in the greatest degree of biomineralization by the osteoblasts.^[31d]

In a separate study, 6mer was coupled to the antibacterial peptides, namely human neutrophil defensin 2 and 4 and hepcidin. Paper discs were immersed in these different protein solutions and placed on LB plates with gram-negative or gram-positive bacteria which resulted in clear inhibition zones for antibiotic-loaded films.^[60b] Further, films of the 6mer, 6mer with hepcidin, poly(lactic-co-glycolic acid) film, or no film were implanted into the subcutaneous pocket in mice. Flow cytometry and histology showed that there was a mild inflammatory response in all implants after two weeks. Fewer and more localized responses to scaffolds were noted after six weeks.^[89d] In their last study a tag-free purification approach of plain 6mer and 15mer was developed and shown to be noncytotoxic.^[60a]

In Petzold et al., the response of primary cardiac cells from 3-day-old Sprague–Dawley rats was evaluated on films prepared from eADF4(κ16), a positively charged variant of eADF4(C16). Cardiomyocytes cultured on eADF4(κ16) formed a healthy monolayer with clear cell–cell communication, and furthermore the monolayer was shown to contract (Figure 6). Cardiomyocytes on eADF4(κ16) films showed no hypertrophic effect, reacted to pro-proliferative stimuli, and the contractions were synchronized between cells. Therefore, eADF4(κ16) not only performs with comparable success to fibronectin, but also offers other advantages, such as no induction of hypertrophy, the possibility to be transferred into different morphologies, and it can be produced in much larger quantities.^[33c]

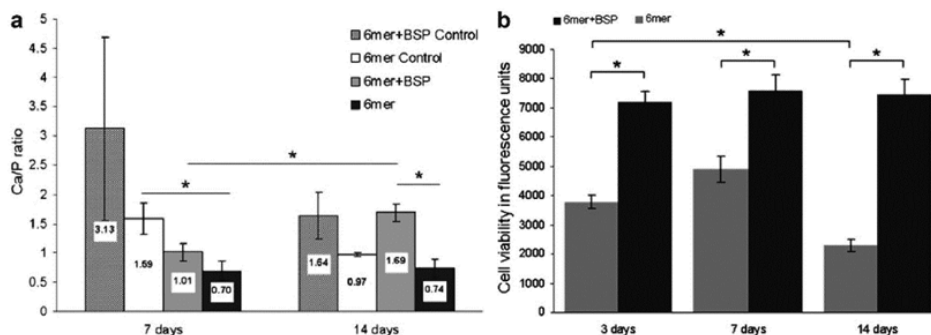


Figure 5. a) Ca/P ratios found on 6mer and 6mer+BSP films with and without (control) cells were determined using energy dispersive spectroscopy. hMSC were seeded onto silk films, and after reaching 80–90 % confluence osteogenic differentiation was induced. Controls were incubated in osteogenic medium only. The higher ratios found on 6mer+BSP samples can be explained by the affinity of the BPS domain for calcium ions. Remarkably, the ratios found after 14 d closely resemble ratios found in tricalcium phosphate (1.50) and hydroxyapatite (1.67). b) hMSC viability was investigated on 6mer and 6mer+BSP films and determined using an alamarBlue assay. Here, a higher cell viability/proliferation was found for cells on 6mer-BSP films than on plain 6mer films, probably due to the BPS binding domain, which contains three RGD sequences (**p* < 0.05). Reproduced with permission.^[89c] Copyright 2011, Royal Society of Chemistry.

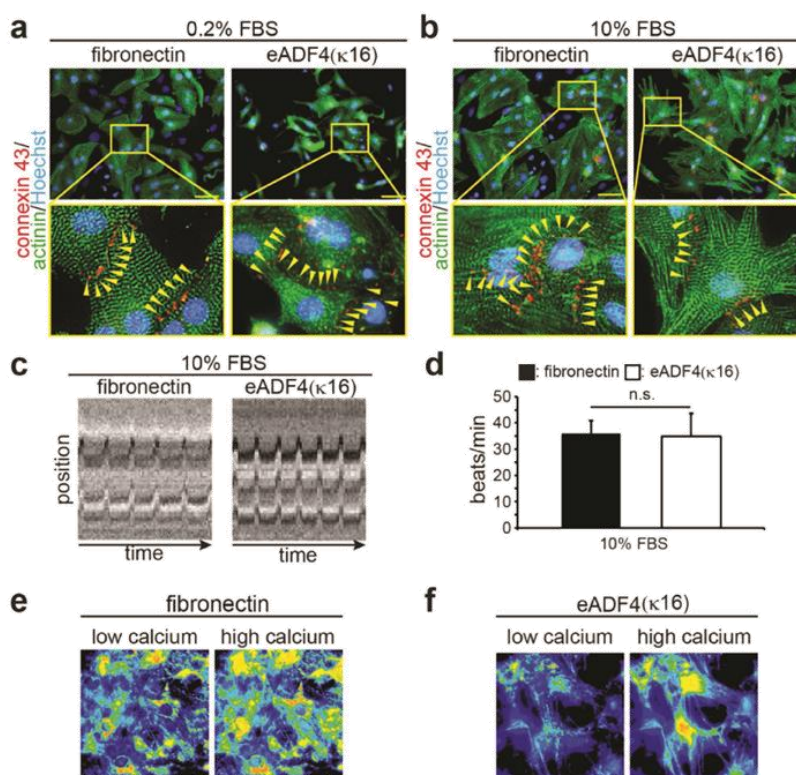


Figure 6. Cardiomyocytes cultured on fibronectin and eADF4(κ16) films. a,b) Heart muscle cells on fibronectin and eADF4(κ16) stimulated with 0.2% or 10% fetal bovine serum (FBS), stained for sarcomeric-α-actinin (green), connexin 43 (red), and DNA (blue). In order to allow contractility, cardiomyocytes must exhibit well-differentiated sarcomers, which can be seen in cells seeded on both materials (green stacked lines). Further, electrical coupling between the cells plays a significant role in efficient contraction. The efficient coupling in cardiomyocytes on both film types was shown by staining for the gap junction protein connexin 43 (marked with yellow arrows), where an enhancement could be achieved by stimulation with FBS. Additionally, FBS stimulation lead to an induction of hypertrophy in heart muscle cells cultivated on silk films. Scale bar: 50 μm. c) Kymograph analysis showing contractions and d) its quantitative analysis. Neonatal cardiomyocytes spontaneously show contractile activity, which was recorded and analyzed via Kymograph analysis software, confirming that cells beat with the same frequency on both film types. e,f) Calcium imaging representing intracellular change in calcium concentration during contraction. Therefore, the matrices were loaded with a calcium sensitive dye to investigate the effects on the calcium homeostasis. It was found that neither the number of contractions nor the contraction frequency showed a significant difference between the two film materials.^[33e]

In conclusion it can be said that many different recombinant silks from different origin were investigated as materials of film scaffolds giving an insight into the basic response of various cell types. Unfortunately, some studies did not characterize the surface before seeding cells on it,^[52c] or did not show any microscopy images to confirm their cell culture data.^[52c,60b] Further should be mentioned that many groups use immortalized cell lines to test the performance of their silk films, which is helpful for understanding how cells might react on a basic level, but are also insensitive to more specific culture conditions.^[94] As more and more special cell binding motifs are added to the silk variants, it would be desirable that in future studies a focus is laid on primary or stem cells specific for these motifs. Nevertheless, there were some preliminary tests for use in neural, bone, and cardiac tissue engineering. Unfortunately,

bone tissue engineering showed less promising results compared to established control materials, but results were particularly interesting for cardiac tissue engineering.

4.4. Mesoporous Foams

Mesoporous foams are 3D structures comprised of 3D arranged, thin-walled pores. One of the most critical parameters is pore size, where large pores (>100 μm) might prevent vascularization of the artificial tissue, as endothelial cells are not able to bridge pores which are larger than a cell diameter,^[95] but small pores (<100 nm) will limit the diffusion of nutrients, metabolic waste products, and gases.^[96]

There are several approaches for creating foams which are used, the most common being salt-leaching, freeze-drying,

and gas foaming. In the case of gas foaming, the polymer is saturated with a gas, such as CO₂, at high pressure. Then, the pressure is slowly released to atmospheric pressure, which reduces the solubility of the gas in the polymer and thereby gas bubbles are formed.^[97] In solvent-casting particulate leaching, salt particles are homogeneously dispersed in a polymer solution and the solvent is evaporated. The salt is leached out of the scaffold in a water bath, which leaves behind a porous foam structure.^[96] Salt leaching is the most common technique for producing foams from recombinant silk proteins.

To create a scaffold by freeze-drying, the most simple method is to freeze an aqueous polymer solution, which results in crystal formation by the solvent, and then to remove the solvent by sublimation, leading to a porous foam.^[99] Here, the pore size can be controlled by changing the pH or freezing rate.^[100] Alternatively, the pore size can also be controlled by use of emulsion freeze-drying, where an aqueous phase is mixed with a water-miscible organic solvent and subsequently frozen.^[101] To avoid the necessity of post-treatment, an alternative is to use cryogelation. In this case, a polymerizing agent is added to the polymer solution, and due to the formation of ice crystals, and hence indirect removal of solvent, the polymer solution and crosslinking agent concentration become so high that it results in matrix formation, leading to a stable foam which requires no further processing.^[102] Pore direction can also be controlled by cyrostructuring. Cryostructuring, or the directional growth of solvent crystals, occurs when a temperature gradient is applied, and it follows that the pores are also aligned into a specific structure.^[103]

4.4.1. Recombinant Silks Processed into Mesoporous Foams

eADF4(C16) foams were prepared by salt-leaching and had a β -sheet content similar to samples of post-treated eADF4(C16) films (~42%).^[33c] Scaffolds made of eADF4(C16) were found to be in the range of soft tissue (elastic compressive moduli = 0.94–3.24 kPa) which is compared to rS1/9 foams which had about 100 \times the tensile strength at $18 \pm 5 \text{ N cm}^{-2}$ (180 kPa).^[49] This, combined with gravimetric analysis of eADF4(C16) foams determining a porosity of 92%, indicated these foams could be promising for tissue engineering applications. Therefore, foams made of eADF4(C16) with and without RGD domain were further evaluated for the adhesion and proliferation of Balb/3T3 mouse fibroblasts.

Cells cultured for 10 d on eADF4(C16)-RGD foams were homogeneously distributed and exhibited a spread morphology.^[33c] In spite of its high stiffness, a similar result was obtained testing 3T3 fibroblasts on 1F9 foams after 14 d in culture, as determined by confocal laser scanning microscopy (CLSM).^[61a] Moisenovich et al. showed 3T3 fibroblasts attached and proliferated in rS1/9 scaffolds, whereby a homogeneous cell distribution throughout the material was obtained after 14 d as found by CLSM.^[49,61b] Further, rS1/9 foams were compared to *B. mori* silk fibroin ones, which showed a similar result in terms of 3T3 fibroblast attachment and proliferation,^[61b,104] but allowed a 5 \times faster migration through the network, leading to the conclusion that rS1/9 foams yielded a reduced motility of 3T3 cells.^[61b] Freeze-dried L-RGDSx2 fibroin (LRF) scaffolds with a mean pore diameter of 80 μm showed promising results

for bone and cartilage tissue engineering, where primary chondrocytes from white rabbits produced more cartilage-like tissue on the surface of LRF than on native fibroin.^[53a]

The *Euprosthenoops australis* derivative 4RepCT and variants thereof were formed into foams with pore sizes between 30 and 200 μm .^[71,74,75b,76,90a] Unfortunately, the exact mechanism of foam preparation is not explained in any of these studies. Human primary fibroblasts seeded onto 4RepCT foams exhibited attachment, spreading, proliferation, and collagen I production over 11 d.^[71] In a follow up study, NSCs were shown to successfully differentiate to astrocytes using ciliary neurotrophic factor.^[90b] Further, for culture of human induced pluripotent stem cells (hiPSCs) and human embryonic stem cells (hESC) a xeno-free system was developed where 4RepCT modified with vitronectin (VN-4RepCT) was used. hiPSCs as well as hESCs maintained their pluripotency even after 30 passages on 4RepCT films, and successfully differentiated into cardiomyocytes and neuroectoderm on foams. They were then injected in severe combined immunodeficiency mice, where they formed teratoma generating cells from all three germ layers. Further, hiPSCs seeded on silk films were successfully differentiated into endoderm, cardiomyocytes, or neuroectoderm.^[75a] In a follow up study hiPSCs were cultivated over 10 passages and they were confirmed to be karyotypically normal and pluripotent.^[90b]

Two studies address pancreatic island engineering using either 4RepCT variants with N-terminal RGD, RGE, IKVAV, and YIGSR^[76] or N-terminal VN or fibronectin (FN) as well as RGD incorporated after the second or third Rep motif (2R- or 3R-4RepCT).^[75b] In Johansson et al., mouse and human pancreatic islands were seeded directly onto the scaffolds, and it was shown that the most effective adhesion took place on foams prepared from RGD-4RepCT. Even after a month in culture, the clusters maintained key functions such as insulin release upon glucose stimulation, and increase in $[\text{Ca}^{2+}]_i$ upon potassium or glucose stimulation. The cells on silk foams showed less necrosis compared to free floating clusters, and human islands were found to form sprouts and new islet like structures from donors less than 35 years old. Therefore, it was suggested to use this in vitro model for screening of potential therapeutic treatments and development of novel transplantation strategies. Islands from RGD-4RepCT and “free-floating” control samples were also transplanted into the anterior chamber of mice eyes. Islands from RGD-4RepCT were more stable in size, showed a better vascularization, lower cell death, and less insulin loss than observed in the control group.^[76] In a follow-up study, mouse and human pancreatic islands, as well as MIN6m9 mouse beta cell line, were investigated. Single cell suspensions were seeded onto the foams, and cluster formation was determined. RGD-4RepCT as well as 2R-4RepCT resulted in the best cluster formation, and these clusters also showed functionality in terms of insulin production and a change in $[\text{Ca}^{2+}]_i$ after depolarization (Figure 7). Further, the clusters from 4-RepCT and 2R-RepCT were transplanted into the anterior chamber of mice eye, and both groups facilitated insulin production and the formation of microvasculature, whereby larger vessels were found in 2R-4RepCT.^[75b]

In further studies, rS1/9 scaffolds were formed into bar shaped scaffolds and implanted into the midline dorsal subcutaneous area of BALB/c mice, where no toxicity or other tissue

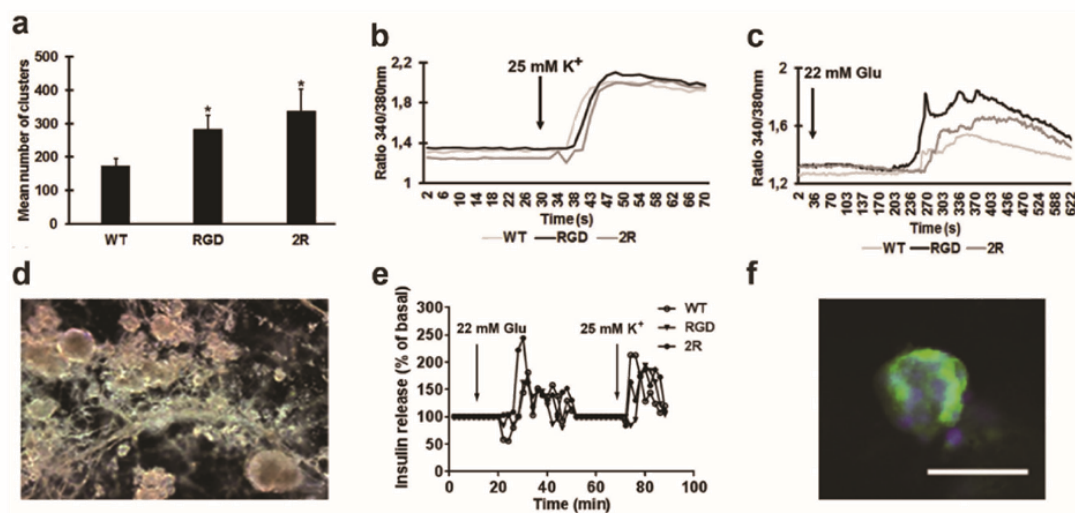


Figure 7. Human β -cells were cultured on silk protein foams and shown to form viable and functional islet-like clusters. a) Number of clusters obtained within foams after 7 d in culture on WT (4RepCT), RGD (RGD-4RepCT), and 2R (2R-4RepCT) ($n = 3$, triplicates, $^*p < 0.05$) and determination of change in internal calcium concentration upon b) depolarization with potassium or c) with glucose. These tests confirm the stimulatory effect and hence the viability and functionality of the islet-like clusters. The glucose stimulation (c) performed after 7 days in culture showed a slightly more pronounced increase in internal calcium concentration on RGD compared to WT foams. d) Representative micrographs of islet-like clusters on 2R foams. e) Dynamics in insulin release after depolarization with glucose or potassium of clusters on WT, RGD, and 2R foams. Therefore, cells were stimulated with glucose first, which showed expected level of insulin production. Afterwards, the release was brought back to a basal level by lowering the glucose concentration again. Subsequent potassium stimulation showed a successful depolarization. f) Micrograph of cluster stained for insulin (green) and nucleus (blue). It shows that most cells stain positive for insulin confirming the presence of β -cells; further some glucagon producing cells were found. Scale bar: 50 μm . Reproduced with permission.^[75b] Copyright 2016, Elsevier.

pathology was observed. Histology performed after eight weeks showed clear ingrowth of adipose and fibrous tissue as well as vascularization and nerve fibers.^[49] In a separate study, *B. mori* fibroin and rS1/9 foams were implanted into midline dorsal subcutaneous area or into femoral defects. The implants were well-tolerated, and histology after eight weeks of the subcutaneous implants showed the shape of the scaffold was conserved in both, in rS1/9 and in *B. mori* fibroin scaffolds; however, in-growth of connective and fat tissue, cell mediated erosion, and vessel and nerve fiber formation was more pronounced in rS1/9 than in *B. mori* fibroin scaffolds. For the bone implants, Roentgen and CT studies revealed that after four weeks a higher recovery took place in case of rS1/9 in terms of bone formation and maturation.^[61b] Further, scanning probe nanotomography confirmed a better regeneration of bone tissue in rats using rS1/9 compared to *B. mori* fibroin, probably due to higher nanoporosity thereof.^[104]

The performance of transgenic silkworm silk foams [(AGSGAG)₄E₈AS]₄ was also evaluated for its ability to promote bone regeneration. This silk contains additional glutamic acid residues, which should enhance calcium binding, and this was confirmed by X-ray photoelectron spectroscopy and Von Kossa staining. The sponges were analyzed in femoral defects in Japanese white rabbits and their performance was compared to that made of native silk fibroin. After four weeks, micro-CT revealed an enhanced bone formation in the transgenic silk fibroin, and further improvement was seen after eight weeks.^[54a]

In summary, salt leaching, phase-separation freeze drying, and an unknown foaming mechanism were used for foam preparation. The foams were in general very well characterized in terms of structure (SEM, CLSM), mechanical stability (compressive test), (secondary) structure content (FTIR + FSD, ¹³C crosspolarization magic angle spinning nuclear magnetic resonance), porosity (gravimetric analysis), cell attachment, and degradation (enzymatic, chemical). The only exceptions were foams prepared from 4RepCT and LRF scaffolds, which were unfortunately not as well-characterized, and therefore it is difficult to draw complete conclusions from these works. Further, foams were applied in attempts to form functional tissues including bone, peripheral nerve, and pancreas. Of these, particularly promising results were seen in terms of insulin production and calcification of foams, however many more studies must be conducted to enhance and fully characterize these tissue-like structures.

4.5. Hydrogels

Hydrogels can be most simply defined as polymer or proteins networks, induced by physical or chemical crosslinking in solution, which are primarily composed of water (>90%) but still retain their structure.^[105] Examples of physical crosslinking are chain entanglements, hydrophobic interactions, and hydrogen bonds.^[106] Physical crosslinking is normally a process which occurs spontaneously under certain

conditions, such as specific concentrations and temperatures.^[107] Chemical crosslinking is the use of a chemical agent to induce covalent bonds between polymer or protein chains, or salts for ionic bonding.^[106a,108]

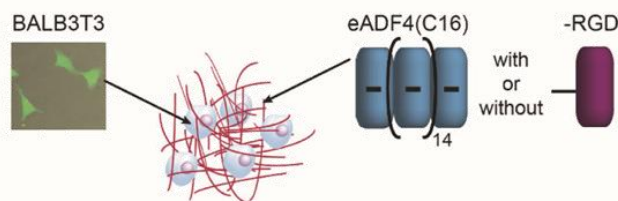
Compared to other morphologies, hydrogels are highly interesting in terms of 3D cell culture, as the cells are introduced to a truly 3D environment, as opposed to 2D or complex 2D surfaces.^[109] However, as implied from adding the 3rd dimension, significantly more protein or polymer is required to form hydrogels, as well as consumables used for evaluating the scaffolds, such as staining reagents. The diffusion of molecules (waste-nutrient exchange) is also significantly impeded. However, these disadvantages are usually out-weighed by the fact that hydrogels are the most physiologically accurate morphology. Further, they can be used as biomaterial component for 3D bioprinting, when they are able to flow under shear stress, and recover mechanical properties after the process is complete.^[110]

One of the reasons why spider silks are favorable materials for forming hydrogels for tissue engineering applications is that they can be formed without crosslinkers.^[107a,111] The formation of hydrogels through self-assembly is a thermodynamically driven process where the principle variables determining the rate of gelation are the concentration and the temperature. In the case of the investigated spider silk proteins, the nucleation phase is characterized by a structural change in the amino acid chain to more β -sheet rich structures, followed by the fibril elongation phase, followed by network formation.^[107a] To the best of the authors knowledge, there is only one case of recombinant spider silk hydrogels for tissue engineering, which is eADF4(C16), Table 1.

4.5.1. Recombinant Silk Hydrogels for Biofabrication

eADF4(C16) was shown to be effective for 3D bioprinting, Figure 8.^[112] In this study it was shown that the hydrogel was nontoxic to cells when encapsulated, and although there was a reduction in cell viability due to the encapsulation process, there was nearly 100% cell viability comparing before printing to after printing. Although there is room for improvement, this pilot study in general showed the promise for the use of eADF4(C16) for 3D bioprinting. In the future, these disadvantages should be improved, and again more specific cell types or growth factors should be used in an attempt to achieve a specific tissue function.

bioink preparation by encapsulation of cells in recombinant silk solution



bioink gelation

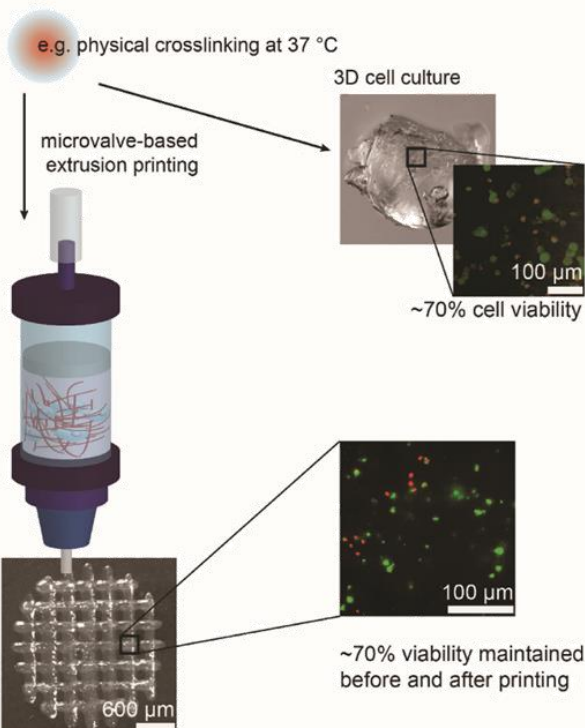


Figure 8. Biofabrication using eADF4(C16) as the biomaterial component of a bioink. Cells were encapsulated in highly concentrated eADF4(C16) solution and gelled by incubation at 37 °C. The bioink can either be used for 3D cell culture or for 3D bioprinting with reasonable cell viability.

5. Implant Coatings

When an implant is introduced into the human body there are several consequences, including high risk of infections at insertion site^[113] as well as several reactions of the body to the chemical, physical, and morphological characteristics of the implant surface. The foreign body response begins with protein adsorption followed by monocyte/macrophage adhesion, which will eventually fuse to form foreign body giant cells as they cannot digest the implant.^[114] These foreign body giant cells

then further initiate more complex inflammatory and wound healing responses, for example, scar tissue formation. Thereby, fibroblasts are attracted by the giant cells and begin synthesizing collagen, forming a complete avascular capsule around the implant.^[115] Thus, it is of great importance to understand the environment of and host response to certain biomaterials in order to use them in meaningful applications, referring to a review by Anderson et al. for more details.^[116]

5.1. Recombinant Silks Used as Implant Coatings

The number of methods used for coating hard and soft medical devices with recombinant silk proteins is limited to dip-coating or spray-coating or a combination of both. Aqueous solutions were used to avoid damaging the implant material as well as introducing residues of toxic solvents or salts in the body. In a pilot study by Zeplin et al., silicone implants were coated with a layer of eADF4(C16) $\approx 1 \mu\text{m}$ thick by dip-coating the implant into aqueous silk solution three times with the aim of reducing capsular fibrosis (Figure 9).^[25,117] In vivo studies in Sprague–Daley rats showed a decrease in fibroblast and histiocyte coverage as well as less collagen deposition on coated than on uncoated silicone samples. The reduction in capsule thickness and fibrosis factors was also confirmed by qPCR.^[25] Further, this implant coating was much more successful than others in current research. In a follow up study, eADF4(C16) was exploited to coat silicone catheters. Here, the material was prepared by oxygen plasma treatment followed by application of poly(ethyleneimine) (PEI: positive charged polymer) or eADF4(κ 16) (positively charged silk protein), to counterbalance the negative charge from plasma treatment, and finished by an eADF4(C16) (negatively charged silk protein) coating. The interaction with several cell lines (Balb/3T3 fibroblasts, B50 nerve cells, C2C12 myoblasts, and HaCaT keratinocytes) was investigated, and neither adhesion nor proliferation was observed. The coating was confirmed to be stable against delamination, even after bending.^[191] Harris et al.

also used dip-coating, spray-coating, and a combination of both to apply a 0.5–50 μm thick layer of rMaSp1/rMaSp2 onto silicon wafers, stainless steel, titanium chips, and PU or silicone catheters. A general smoothening effect of the surface was observed upon coating of catheters, which was confirmed by determining the friction coefficient. The best results for coating homogeneity were observed by using a combination of spray-coating and dip-coating. To see if this could also be used to reduce the formation of biofilms, thrombotic fouling, and protein accumulation, functional compounds or additives were added. In order to reduce the likelihood of an infection, antibiotics (kanamycin, gentamycin, tetracycline, ampicillin, or chloramphenicol), azole, and/or aminoglycosides were added. Furthermore, heparin was supplemented as a functional compound to prevent thrombosis. These silk/heparin coated silicone implants, which were incubated in blood that was induced to clot, showed a severe decrease in thrombotic fouling.^[62]

In order to functionalize implants with biologically active peptides, 4RepCT was modified with either cell-recognition peptide (FN-4RepCT) or an antimicrobial motif (Mag-4RepCT). The coating process was analyzed using quartz crystal microbalance and surface plasmon resonance, and it was shown that silk was adsorbed continuously and that the resulting layer was stable toward sodium hydroxide, hydrochloric acid (0.1/0.5 M), and ethanol treatment. The silk coating assembled into fibrils on the surface, and these nanofibrous coatings, especially FN-4RepCT, improved viability, spreading, and proliferation of HDMEC and human dermal fibroblasts. A decrease in *S. aureus* density was also observed on both 4RepCT and Mag-4RepCT.^[118]

In summary, it can be stated that recombinant silk coatings were successfully applied onto various surfaces and fulfilled the desired task in terms of tissue and cell response. For example, surfaces could be adjusted so that either cell attachment was decreased or increased. Almost all studies reported that silk coatings increased smoothness and rendered the surfaces more hydrophilic.^[25,62,91] Although

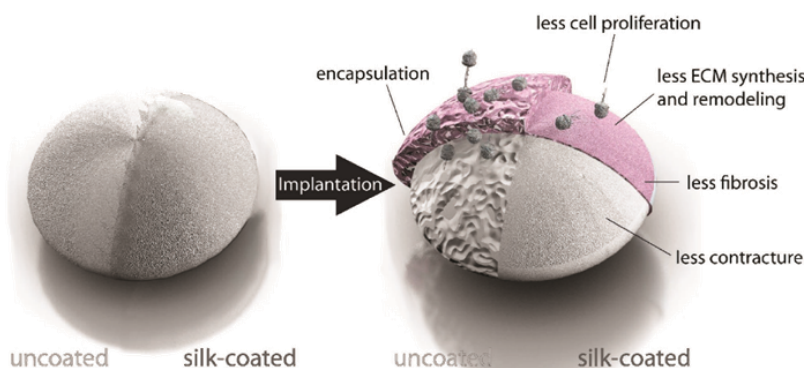


Figure 9. Scheme of bioshield function of silk coating on a silicone implant. Silicone, despite being resistant against enzymatic and hydrolytic degradation, displays a hydrophobic surface triggering adhesion of unspecific proteins and cells. This leads to a foreign body response, which might end in the formation of a fibrotic capsule, causing a deformation of the implant and pain and discomfort in patients. By applying a thin spider silk coating, which causes no immune reaction, the implant can be shielded and thereby capsule formation can be significantly reduced.^[25]

hydrophilic, it was found that 4RepCT coating formed a nanofibrillar structure.^[118] However, perhaps the most exciting result of this study was the nearly undetectable immune response as well as the slow biodegradation in vivo.

6. Drug Delivery

Drug delivery systems are designed for increasing the uptake efficiency and specificity of a drug for a target tissue.^[119] Usually the strategy is to target specific cells or characteristics of a diseased tissue, and to design the drug delivery vehicle such that it does not release its drug unless in that particular environment (Figure 10a). Other advantages of using drug delivery systems are to increase the loading efficiency of drugs which have low water solubility, and increase control over the release profile of the pharmaceutical agent.^[120] Simply stated, drug delivery systems allow for a reduction in the amount of drug administered, frequency of drug administration, as well as the potential side effects of a drug.^[121]

Drug delivery systems are often characterized as either stationary or mobile. Stationary systems act as a drug depot which are implanted in one location and slowly release drugs over a long period of time. Examples include implant coatings (films) or wound dressings (hydrogels).^[122] Biomaterial-based products are currently available in the market and are composed of polyanhydrides (Gliadel Wafer) and poly(lactic-co-glycolic acid) (Zoladex). Mobile systems on the other hand act as transporters carrying their drug load to the final destination, where it is released. Therefore, these systems are further characterized by how they target the site of interest, either actively or passively. Active target systems will attach recognition sequences for molecules such as nucleic acids, peptides, proteins, small molecules, or monoclonal antibodies which are unique to the target site. For example, ligands attached to the drug delivery system can bind to cell-specific membrane molecules on the target cell (Figure 10b).^[123]

There are many studies where *B. mori* silk fibroin was processed via different routes into microspheres and nanoparticles, and both were successfully loaded with different (model) drugs. However, *B. mori* fibroin suffers, like all naturally derived polymers, from batch-to-batch variations making quality control, necessary in biomedical applications, difficult,^[124] highlighting the use of recombinantly produced silk proteins.

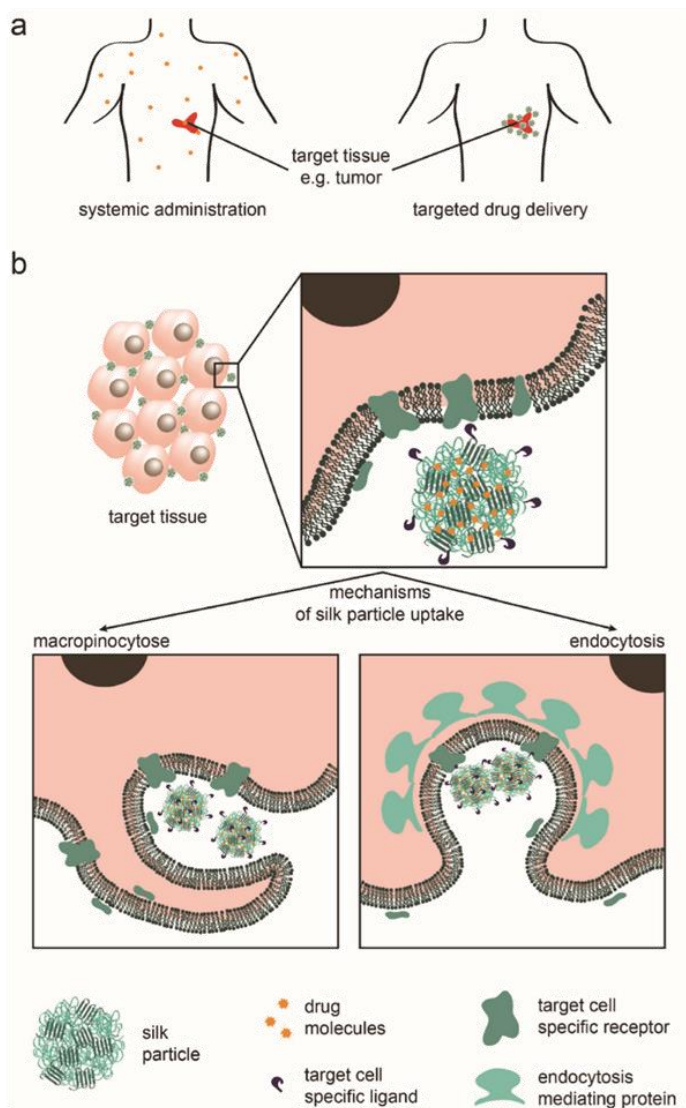


Figure 10. Drug delivery via silk particles. a) Comparison of systemic drug administration and targeted drug delivery. In systemic drug administration the whole body faces the medication, whereas in targeted drug delivery only desired cells are attacked. b) Cellular up-take of silk particles either via macropinocytosis or endocytosis. Silk particles were found to be mainly up-taken by different mechanisms, namely micropinocytosis and endocytosis, depending on the properties of the silk proteins used.

6.1. Hydrogels

Hydrogels are a particularly attractive choice for drug delivery because they can be easily loaded with relatively high amounts of water-soluble drugs by diffusion or by encapsulation.^[105,125] The drug release profile can be easily controlled

by hydrogel-specific characteristics, such as crosslinking density, environment-responsive swelling, or shrinkage. A further advantage is that preformed hydrogels are often injectable, or the hydrogel precursor solution can be injected as a liquid and gel on site. Therefore, hydrogels stay at the site of interest much more successfully than for example particles, which have a short residence time in the blood, especially at smaller size.^[126]

Challenges associated with using hydrogels as drug delivery carriers are that they often have an uncontrollable burst release, either immediately due to rapid diffusion time of small molecules, or later from a sudden, rapid degradation of the hydrogel.^[125b] However, most of these challenges are simple to overcome, for example by creating environmentally sensitive hydrogels,^[125a] or by making multimembrane hydrogels.^[127] Recombinant silk hydrogels are particularly interesting due to their slow biodegradation, however the only type examined so far is silk-elastinlike proteins (SELPs) (Table 1).

6.1.1. Recombinant Silk Hydrogels for Drug Delivery

One group focuses on the production of SELP hydrogels, in particular for cancer therapy. In the foundational publications, they investigated different variants of SELP, and showed that SELP-815K hydrogels (Table 1) had the best release of adenovirus.^[128]

In a paper by Poursaid et al. two variants of SELPs were tested as chemoembolization agents: SELP-47K and SELP-815K.^[55c] Chemoembolization is a cancer-treatment where the blood vessels to the tumor are blocked, resulting in tumor shrinkage, combined with chemotherapy drugs, to actually kill the tumor cells.^[129] First they conducted *in vitro* tests in microfluidic channels designed to imitate the hepatic vascular system, where they observed that the sol-gel transition occurred at an appropriate time point, which further resulted in clogging of the targeted channels only. It performed with similar success in rabbits, where it gelled in the site of interest and resulted in significant tumor shrinkage.^[55c]

Although these studies show these hydrogels to be promising for chemoembolization, there were a few points which were lacking conclusive comments from the researchers. For example, they reported reduction in tumor growth rate, however, they did not mention if there was complete regression of the tumor, or if this would be effective against metastatic forms of cancer. Overall, the hydrogels show highly interesting properties, and should be further investigated with more complex models and methods.

6.2. Films

Film-based and membrane-based scaffolds in drug delivery are often studied due to their simplicity and the possibility to obtain zeroth-order release kinetics allowing a constant drug administration.^[130] Hofmann et al. investigated silk fibroin films as drug delivery matrices by casting films from a protein-drug mixture. Indeed it was found that films with higher crystallinity showed no initial burst release. Further, the activity of protein drugs was evaluated and it was shown that horse radish peroxidase was still active after release from methanol treated films.^[131]

Long-term studies of enzymes entrapped in silk fibroin films showed a 40–100% activity of glucose oxidase, lipase, and horse radish peroxidase after 10 months of storage.^[132] It was further resolved that the entrapped enzyme was only released after proteolytic silk degradation, which was in turn dependent on the secondary structure of the silk matrix. Hence, controllable release kinetics of the films could be realized by adjusting the silk structure with different post-treatment techniques and/or the addition of a plasticizer like glycerol.^[133]

6.2.1. Recombinant Silk Films for Drug Delivery

The authors are only aware of two publications utilizing recombinant silk films for drug delivery. In both cases, films were formed from eADF4(C16) by film casting. In order to allow an easy removal, films were cast onto a polytetrafluorethylene surface either from organic HFIP^[134] or aqueous solution.^[121] In the study conducted by Hardy et al., eADF4(C16) was additionally blended with polycaprolactone and thermoplastic polyurethane at various ratios, and resulting films were about 100 μm thick.^[134] The films were well-characterized using differential scanning calorimetry and tensile testing (Young's moduli with 5500^[121] or 3300 MPa^[134]), as well as thermogravimetric analysis,^[134] isoelectric point,^[121] water absorption,^[121] and water contact angle^[134] measurements.

Low molecular weight drug models (methyl violet or ethacridine lactate) were loaded by incubation, and diffusion was determined in phosphate-buffered saline (PBS) via UV-vis spectrometry. The highest loading and the fastest release were observed in pure silk constructs, presumably due to the negative charge of eADF4(C16). The time of release could be further shortened by the addition of enzymes.^[134] In Agostini et al., pure and multilayered films as well as the impact of additives glycerol and 2-pyrrolidone on the release of loaded low molecular weight (etracaine HCl and paracetamol) and high molecular weight (fluorescein isothiocyanate (FITC)-bovine serum albumin (BSA) and FITC-dextran) model drugs were investigated. Paracetamol and FITC-dextran were released within one day only, and also FITC-BSA showed an initial burst followed by a steady release from the ≈ 30 μm thick monolayers. Multilayer films prepared by pressing a FITC-BSA and glycerol (glue) film between two pure silk films did not show any improvement in terms of release. Coating of FITC-BSA and 2-pyrrolidone (plasticizer) loaded films lead to a decrease in burst release to 20% followed by a steady release over 90 d.^[121]

In conclusion, films could be loaded with drugs, but not as effectively as particle systems. This could potentially be improved by using a system which allows for greater drug loading (e.g., hydrogels).

6.3. Capsules

Capsules allow the encapsulation and protection of larger molecules, small particles, or even small microorganisms.^[135] A capsule can be formed around a solid core, which is then removed afterwards. This technique was for example used to obtain LbL-capsules from modified *B. mori* fibroin by applying the silk onto

silica particles, which are subsequently dissolved.^[136] In the field of recombinant silks capsules were formed in an emulsion process, whereby an amphiphilic molecule lines the interface between water and oil thereby forming a capsule wall.^[48,137]

6.3.1. Recombinant Silk Processed into Drug Delivery Capsules

eADF4(C16) spider silk capsules were prepared in a water-in-oil emulsion using either toluene^[48,137a] or silicon oil.^[137b] Toluene has the advantage that it induces β -sheet formation and thus, no further post-treatment is necessary (Figure 11a); however, it also has the disadvantage that it is cytotoxic.^[48] Silicon oil on the other hand is FDA-approved, but an additional post-treatment step must be included after capsule formation. The capsule diameter as determined by light microscopy was 1–30 μm . Mass balance measurements showed that the membrane thickness was 50–70 nm. Compression tests performed with AFM gave a Young's modulus of 0.7–3.6 GPa. The capsules prepared in silicon had a molecular weight cut-off (MWCO) >40 kDa,^[137b] whereby the capsules prepared in toluene had a MWCO of about 27 kDa.^[48,137a] No rupture was observed under osmotic stress up to 10⁷ Pa, and the capsules were chemically stable in 2% sodium dodecyl sulfate and 8 M urea.

In further studies by Blüm et al., β -galactosidase was loaded into capsules.^[137b] It was shown that the enzyme could be entrapped in the capsule protecting it from proteolysis. Using such a closed reaction chamber with a semi-permeable membrane, inactive enzymes or their precursors could be encapsulated and then activated from outside by α -complementation of β -galactosidase.^[137b]

All three studies show that it is possible to prepare capsules from recombinant silk proteins with reasonable stability. This drug delivery system is still in the early stages of development, and further studies are required to determine its potential. The big advantage of this approach is the possibility to encapsulate not only large molecules, but even entire microorganisms, which makes it attractive for further research.

6.4. Particles

Previously it was shown that regenerated silk fibroin particles can be used as mobile drug delivery systems.^[138] Several different methods have been developed for preparation of silk fibroin particles as for example salting out, microfluidics, phase separation with polyvinyl alcohol, desolvation in an organic solution and liquid templating. The most commonly used approach for recombinant silk proteins is salting-out in phosphate buffer (Figure 11b), taking advantage of the fact that silk proteins are less soluble at high salt concentrations due to electrolyte–nonelectrolyte interactions.^[138a]

6.4.1. Recombinant Silks Processed into Drug Delivery Particles

In Lammel et al., particles were prepared by mixing an eADF4(C16) solution and phosphate buffer with a pipette, a micromixing device with laminar or turbulent flow, and by

dialysis of protein solution against phosphate buffer. Due to the importance of particle size, it was desired to establish the relationship between the concentration of the protein solution, the concentration of phosphate buffer, as well as the mixing time for determining particle size. Particle sizes were found to be between 250 nm (micromixing with turbulent flow) and 2.1 μm (dialysis) as determined by SEM and laser diffraction spectrometry (LDS).^[139] In general it was found that the lower the protein concentration, the higher the phosphate buffer concentration and the faster the mixing time the smaller the final particles will be.

Particles were also characterized in terms of heat, mechanical, colloidal, and chemical stability. Lucke et al. showed that eADF4(C16) particles prepared by micromixing (332 nm) or in an ultrasonic atomizer (6.7 μm) could be steam sterilized without any effect on size or secondary structure.^[140] A closer look on the interfacial properties of the particle was obtained by direct force measurements with a colloidal probe. Thereby it was found that eADF4(C16) particles are surrounded by a fuzzy protein layer protruding into the solution. This diffuse layer allows long-range interactions, which are based on electrostatic and steric forces (Figure 11c).^[141] Interestingly, an increase in physical crosslinking, for example, by increasing the molecular weight, had a severe impact on elastic modulus, whereby chemical crosslinking with ammonium persulfate (APS) and tris(2,2'-bipyridyl)dichlororuthenium(II) (Rupy) had only minor stiffening effects, as the initial β -sheet content in non-crosslinked particles was already high. Additionally, a continuous deformation behavior without buckling indicates a high homogeneity of silk particles.^[142] Interestingly crosslinking did have an effect on chemical stability; when incubated in 6 M guanidinium thiocyanate, formic acid, HFIP, 8 M guanidinium hydrochloride, and 10×10^{-3} M Tris(hydroxymethyl)aminomethane (Tris) buffer crosslinked particles were stable for 25 h, whereby non-crosslinked particles were only stable in guanidinium hydrochloride and Tris buffer.^[143]

Colloidal stability of eADF4(C16) particles and its variants was determined in several studies. It was found that eADF4(C16) particles are stable for six months in water, but a decrease in pH^[144] or the addition of kosmotropic salts^[145] leads to particle agglomeration. It is known that particles with a zeta potential below -20 mV show only little agglomeration.^[146] In a study by Elsner et al., particles made of eADF4(C16) hybridized with different motives (RGD, R₈G, Tat) and of eADF4(x16) were tested and the results remained consistent: particles of eADF4(C16) and the RGD variant had ≈ -25 mV (the lowest zeta potential) and showed low agglomeration, whereby Tat-eADF4(C16)Tat with -8 mV agglomerated.^[120b] Also Jastrzebska et al. found that MS2 particles showed a negative zeta potential ranging between -10 and -35 mV depending on the silk purification method, phosphate, and silk concentration, and on the pH.^[63] A later study detected that MS1 particles had a positive zeta potential of ≈ 9 mV, and interestingly a 8:2 mixture of MS1:MS2 gave an even higher value of ≈ 15 mV. Her2 binding peptides were genetically added to both variants (H2.1/2MS1/2), which had no influence on the zeta potential. The stability was tested by turbidity measurements and revealed that MS2 particles are more stable than MS1 particles, and the mixtures are found in between. Importantly, the Her2

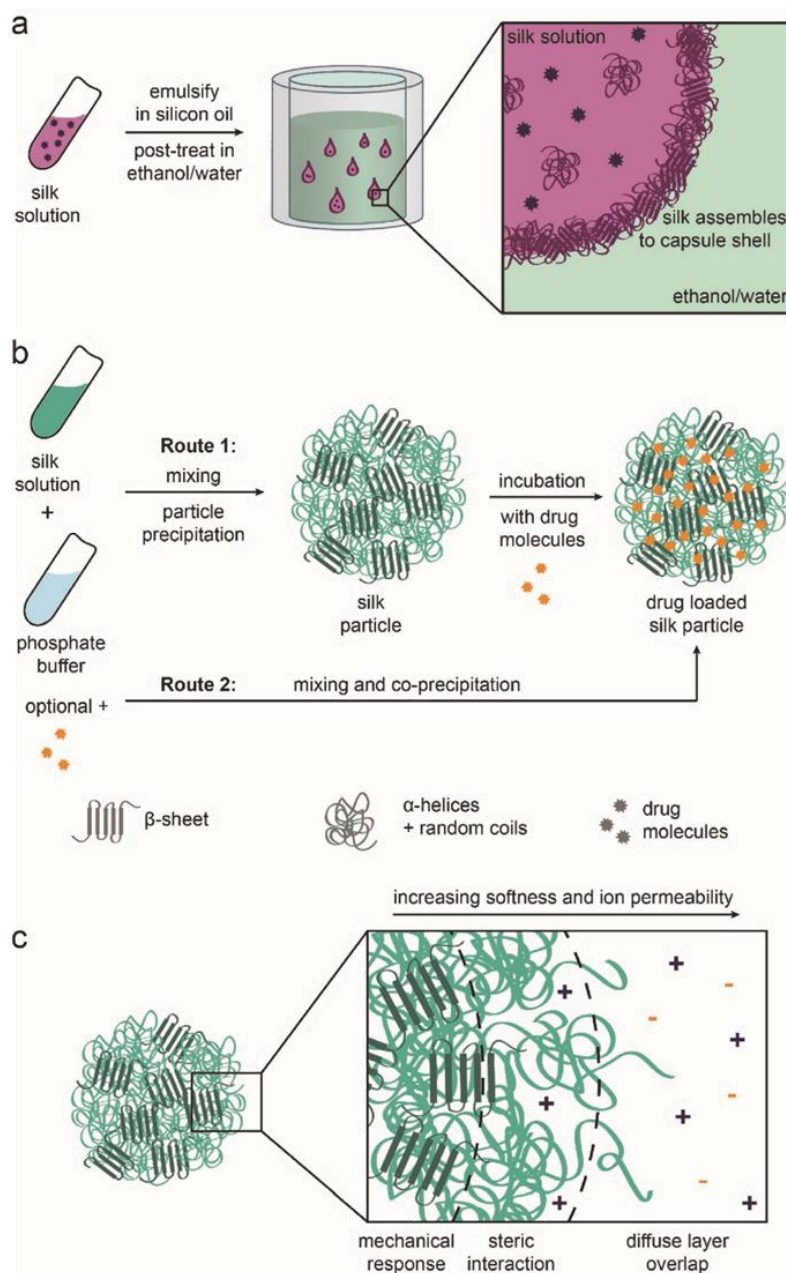


Figure 11. Preparation of mobile drug delivery systems made of silk proteins. a) Capsule formation: Silk solution is emulsified in silicon oil. The silk molecules adsorb at the water/silicon oil interface and form a film. This film is stabilized via a post-treatment step—here β -sheets are induced in an ethanol/water mixture. b) Particle formation by salting out: Route 1: the recombinant silk solution is mixed with phosphate buffer and then loaded with drug molecules by diffusion. Route 2: the recombinant silk solution is mixed with drug molecules before coprecipitation in phosphate buffer. c) Different layers in particles contributing to their properties: In the core elastic deformation takes place, which mainly determines the mechanical properties of the particles. On the particle surface brush-like structures (approximated by an Alexander–deGennes type of interaction) can be found, which determine the interaction with, e.g., drug molecules. A diffuse charged layer is located outside.

binding peptides did not influence the stability.^[147] With stable particles in solution, it is possible to consider particle loading.

In a study by Hofer et al., they could show using FITC-labeled proteins that neither uptake of uncharged FITC–dextran nor negatively charged FITC–bovine serum albumin into eADF4(C16) particles. The positively charged FITC–lysozyme could successfully be loaded, whereby again pH and ionic strength played a crucial role. Interestingly, the zeta-potential of the particles was the same before and after loading.^[144] A similar observation was also made by Schierling et al. where particles of several eADF4(C16) derivatives (negatively charged) were loaded with fluorescently labeled PEI (positively charged) or eADF4(κ 16) particles (positively charged) with labeled ssDNA (negatively charged or with a plasmid DNA doxorubicin (Dox) mixture) and this loading had no effect on the colloidal stability.^[148] Also negatively charged MS2 particles could be loaded with rhodamine B or Dox.^[63] In a later study it was shown that MS1 particles can be loaded with almost double the amount of Dox than MS2 particles (645 vs 372 ng per μ g silk), although MS1 and Dox are both positively charged. The reason might be a higher hydrophobicity as well as the looser packing of MS1 particles facilitating diffusion. Further, it was shown that Dox loading efficiency of a 8:2 mixture with or without Her2 binding peptide was between that of the pure silk particle variants.^[147] In the case of loading eADF4(C16), Lammel et al. proposed that loading is mainly driven by three parameters: (1) charge of the drug (determined by K_d), i.e., if the particle possesses a negative charge, only positively charged drugs can be loaded; (2) octanol water partition coefficient ($\log P_{o/w}$), hence the solubility of the molecule; (3) molecular weight of the drug, whereby (1) and (2) are the dominating factors.^[145]

Particle loading can also be accomplished by coprecipitation (Figure 11b). Coprecipitation was shown to efficiently load eADF4(C16) particles with the model drug rhodamine B or β -carotene.^[47,143] Similar results were observed for H2.1/2MS1, which could be successfully coprecipitated with Dox. Thereby \approx 355 ng of Dox were loaded per μ g of silk.^[46] Interestingly, this resembles only half the amount loaded via diffusion.

Release of drugs from particles was investigated in different buffer systems usually by UV–Vis spectroscopy.^[47,58b,145,147,148] Superhydrophobic β -carotene could only be released upon digestion of the silk particle. Here it was shown that the eADF4(C16) particles remained intact in artificial gastric fluid, whereby they were digested in artificial intestinal fluid.^[47] A decrease in pH caused a burst-release of lysozyme, methyl violet, or ethacridine lactate loaded eADF4(C16) particles, as well as of Dox-loaded H2.1MS1 and H2.2MS1 (H2.1/2MS1) particles. This could be explained by a change in charge due to the pH change, diminishing the electrostatic interactions between silk and drug and thereby promoting drug release.^[46,144,145] Only a small burst release of about 20% was reported by Florczak et al. in MS1, MS2, and their mixtures with or without binding peptide, and decreasing pH had less influence than in studies described before.^[147] Also an increase in ionic strength or character (i.e., kosmotropic or not) effected the kinetics.^[58b,144] Furthermore, it was found that in comparison to eADF4(C16) the lysine bearing eADF4(κ 16) revealed a burst release of small molecules like 6-carboxy-fluorescein under all tested conditions. This could be explained by the fact that lysine residues

found in eADF4(κ 16) are more hydrophilic and, hence, can be easier assessed by salts and solvents. A coating of eADF4(κ 16) particles with eADF4(C16) using a layer-by-layer technology was thought to slow down the release, but the opposite was true. Thus, the electrostatic repulsion of eADF4(C16) and the cargo overruled the desired closing effect of eADF4(C16).^[58b] In another approach crosslinking with APS and Rubpy was successfully used to slow down the release of the model drug rhodamine B. Further, it was shown that the mechanism of drug incorporation has a major influence on the release profile.^[143] The reason for this effect might be that drug release from silk particles can be described by second order kinetics. The drug molecules in the core of the particles bound via electrostatic and hydrophobic interactions first need to be transported to the surface due to a concentration gradient driven process. Then they can be slowly released from the surface, where they are bound via electrostatic interactions.^[143,145]

The last major step in evaluating drug delivery systems is the cellular uptake. Therefore, Elsner et al. investigated eADF4(C16) variants possessing different motifs, namely eADF4(C16)-RGD, eADF4(C16)-R₈G, eADF4(C16)-Tat, Tat-eADF4(C16), Tat-eADF4(C16)-Tat, and the positively charged eADF4(κ 16). First, it was confirmed that unloaded particles have no cytotoxic effect on HeLa^[120b] and Kelly neuroblastoma cell proliferation.^[148] Further uptake studies were performed using fluorescence activated cell sorting in which only 19% of HeLa cells took up eADF4(C16) particles after 72 h, but 97% internalized eADF4(κ 16) particles. The other variants were up-taken by 30–40% of HeLa cells.^[120b]

In a follow up study it was shown that even particles loaded with model drugs did not influence cell growth behavior. DNA/Dox loaded eADF4(κ 16) particles were also investigated in terms of cytotoxicity. Balb/3T3 fibroblasts, HeLa, and Kelly neuroblastoma cells were incubated with DNA/Dox loaded eADF4(κ 16) particles. All three cultures were terminated within 48 h when cultured with particle concentrations greater than 48 ng μ L⁻¹.^[148]

The up-take mechanism was found to be clathrin-mediated endocytosis in case of eADF4(C16)-RGD and eADF4(κ 16) particles, and macropinocytosis in case of eADF4(C16) and eADF4(C16)-R₈G particles (Figure 11b).^[148] CLSM confirmed that H2.1MS1 spheres not only targeted but also successfully entered Her2-overexpressing cancer cells exclusively, whereby the nucleus was not penetrated (Figure 12).^[46] A significant decrease in viability of Her2-overexpressing cancer cells was observed when H2.1/2MS1 particles loaded with Dox were added compared to MS1 control particles loaded with Dox. CLSM revealed that Dox effectively entered the nucleus. The Her2-negative control cell line on the other hand showed a general decrease in cell viability similar to the Her2-positive cells with MS1-Dox particles, but no difference between the different particles was observed.^[46] By combining MS1 with MS2 in a ratio of 8:2 the physical–chemical properties could be improved without losing these favorable drug delivering properties of MS1 particles. It was shown that the mixture containing the Her2 binding peptide successfully targeted Her2-positive cells and caused \approx 60% toxicity in these cells, whereby nonfunctionalized spheres reduced the viability by 10% only. Also Her2-negative control cells showed a rather high viability of 90%.^[147]

Besides loading of particles with drug molecules, recombinant silk can be complexed with plasmid DNA (pDNA) to

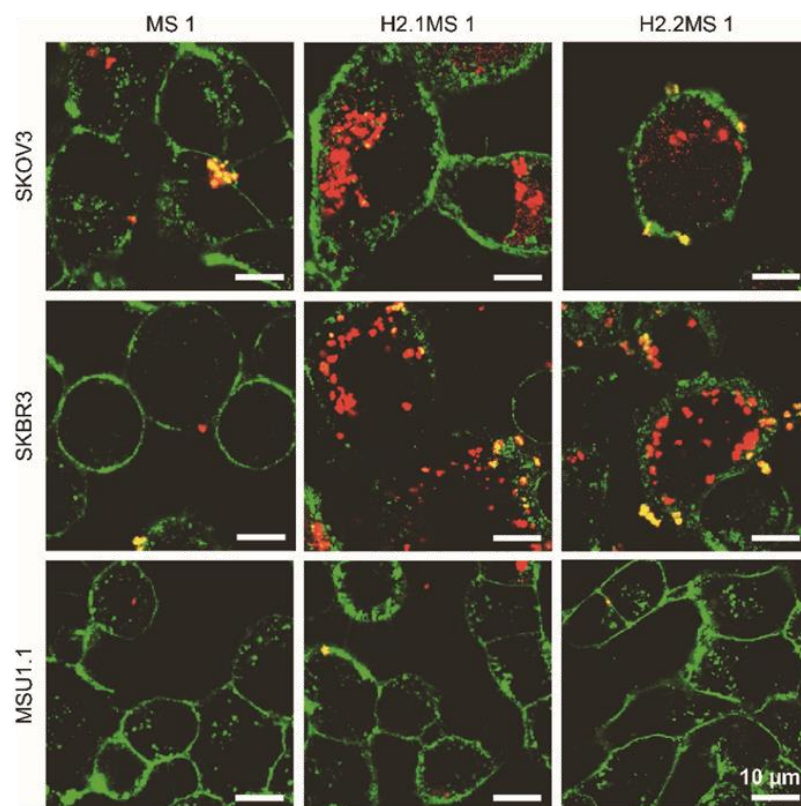


Figure 12. Interaction of Her2 positive (SKOV3 and SKBR3) and control (MSU1.1) cells with fluorescently labeled spider silk particles made of MS 1 (recombinant silk protein particles without the Her2 binding peptide) or H2.1/2MS 1 (recombinant silk protein particles with Her2 binding peptide). Cell membrane stained with ConA-FITC (green) and particles conjugated with ATTO 647N (red). The Her2/neu gene is overexpressed and/or amplified in 20–30% of invasive breast carcinomas and is thus an interesting target. Functionalized spheres (H2.1/2MS1) were effectively internalized into the cytoplasm of Her2 positive cells. Scale bar: 10 μ m. Reproduced with permission.^[46] Copyright 2014, American Chemical Society.

obtain a gene delivery system. Therefore, a silk-based block copolymer comprising 6mer and a poly(L-lysine) domain was developed. This protein formed ionic complexes with pDNA encoding GFP. The complex formation was analyzed with agarose gel electrophoresis, dynamic light scattering (DLS), and AFM, showing that the protein self-assembled into globules with pDNA possessing a solution diameter of about 380 nm. Human embryonic kidney (HEK) cells were transfected with an efficiency of 14% and no cytotoxicity was observed.^[149] Several follow-up studies were performed, all including different tags to increase transfection efficiency. A ppTG1 peptide was added, which is known to destabilize and penetrate cell membranes. Here, the protein was complexed with pDNA coding for GFP or Firefly Luciferase. Transfection efficiency of the complex to HEK cells and a melanoma cell line were comparable to Lipofectamine 2000, a golden standard gene vector. The cell viability was with 75% and 69% lower than in previous studies, but similar to that in presence of Lipofectamine 2000.^[150] Further, the cell binding motif RGD was added up to eleven times to the block

copolymer, which was then complexed with pDNA coding for Firefly Luciferase. Transfection was investigated with HeLa and HEK cells, whereby the transfection efficiency was clearly the highest with the protein complex with eleven RGD motifs, but approximately an order of magnitude lower than with Lipofectamine 2000. No significant effect on cell viability was observed.^[151] In a follow-up study, the tumor-homing peptides F3 and CGKRK were genetically added to the spider silk-poly(L-lysine) construct. Transfection experiments were performed with melanoma cells as well as highly metastatic human breast tumor cells, and nontumorigenic cells were used as control. Again, a Luciferase assay was used to determine successful transfection. All complexes preferably transfected the tumorigenic cell lines and showed almost no transfection of the nontumorigenic cells. Further, the constructs were shown to be noncytotoxic by an MTS cell proliferation assay. Additionally, an *in vivo* study in tumor-bearing mice was performed and showed that from day seven on Luciferase was significantly produced in the tumor.^[152] In the latest study by Numata et al. again tumor-homing peptides, namely

F3 and Lyp1, were investigated in combination with a shortened spider silk-poly(L-Lysine) construct (1mer + 15 Lysines). The goal here was to increase the molar percentage of the tumor-homing peptides. The same cells as in the previous study were tested and it could be shown that again a selective transfection of tumorigenic cells occurred. The F3 bearing complex with a size of about 100 nm was less cytotoxic and showed an overall better transfection efficiency and is therefore the more promising candidate.^[153]

In summary, it can be said that particulate drug delivery systems made of recombinant silk proteins have been thoroughly investigated using SEM,^[46,47,58b,63,120b,139,142–145,147,148] LDS,^[139,144,145] or DLS^[25,58b,120b,144] to determine particle size. Minor changes in the recombinant silk protein, the intrinsic properties of the (model) drug, the method of preparation and loading, as well as the release conditions have a major influence on loading efficiency and release kinetics. Further it was found that positively charged particles made of eADF4(κ16) are up-taken more efficiently, showing the usefulness of recombinant silks for mechanistic cellular-uptake studies.^[120b] Additionally, systems can be cell-targeted by the introduction of binding peptides as shown for H2.1/2MS1 particles.^[46] However, all recombinant silk particles systems have to be tested in vivo to see if these drug delivery systems are effective in a clinical setting.

7. Summary of Recombinant Silk in BME

In this review, the potential of recombinant silk proteins as a biomaterial was illustrated, **Figure 13**. They have been applied with particular success in tissue engineering and medical implant coatings, where it was found that cell behavior can be controlled by altering the charge,^[33e] by introducing cell-binding peptides^[74] and by changing the morphology of the scaffold.^[33a,71] Although there is no obvious, direct correlation between secondary structure content and cell behavior, it can have indirect effects due to changes in mechanical properties or hydrophobicity. However, the secondary structure content has a direct effect on properties such as chemical stability and drug loading. Although drug delivery systems have been shown to be functional in vitro, none of the systems developed so far have been tested in animal models. Although there are many advantages of using recombinant spider silk proteins for medical applications compared to other proteins, there are three in particular which the authors believe make this class of proteins exceptional.

The de novo production of recombinant proteins guarantees reproducible quality in the necessary quantities. This thereby also enables tailoring materials to have a special functionality,^[31c,154] for example by the introduction of different binding peptides.^[77c] The latter is particularly interesting, as most materials made of unmodified recombinant silk proteins are inert to cells, not allowing for attachment or differentiation, but also not causing any cytotoxicity. This is significant in that it makes it possible to culture cells on recombinant silk, and also provides a particularly powerful tool for mechanistically studying the effects of these binding peptides, or any other property such as topography.^[87,155] A step remaining for approving this material for cell culture is the regular removal of endotoxins, a

common byproduct from gram negative bacteria (e.g., *E. coli*).^[156] However, it is clear from the studies from one group, that it is possible to achieve a complete removal of these byproducts by using purification columns, as well as sterilize silk proteins.^[75a]

The second property of recombinant silk materials which makes them particularly outstanding as a biomaterial is the way the body responds to them. First demonstrated in 1710 as a wound dressing, spider silk could prevent bleeding and promote wound healing.^[28c] It has been recently shown in animal models that there is no significant fibrous capsule formation around recombinant silk-coated implants,^[25] as well as a significant reduction in the infiltration of inflammatory cells compared to controls.^[72] Further, spider silk implanted into pigs subcutaneously was locally tolerated.^[157] Problems with biocompatibility of silkworm silk only occurred due to sericins, which are glue-like proteins that encapsulate the raw fiber (also found in transgenic silkworm silk).^[28a] Hence, no immune response was observed with silk proteins, providing the perfect base for biomedical applications.

The third exceptional property of recombinant silks is that the biodegradability is slow, and it remains mechanically stable under physiological conditions for a significant amount of time. This is true even for fragile structures such as films or foams, which is unique compared to other naturally derived biomaterials; this is likely due to the low number of available sites for hydrolysis or active biodegradation of silk materials.^[24] On the other hand, degradation is still possible given the availability of matrix metalloproteinase (MMP) degradation sites in the primary structure, making it also more advantageous compared to stable, synthetic polymers which have no biodegradation sites.^[33d] However, it is important to note that the silk materials must be tested case-by-case because protein folding alters the availability of cleavage sites,^[51b] and sometimes it is necessary to introduce additional degradation sites into the recombinant silk protein.^[158]

The performance and success of a biomaterial is greatly determined by its stability in vivo, the rate of degradation, and the degradation products. Important hereby is that the biomaterial's degradation rate is similar compared to the rate that the cells are producing their own ECM. During the degradation, the biomaterial ideally keeps its mechanical stability to avoid collapsing of the newly formed tissue. Furthermore, the degradation products should not only be nontoxic, but in addition should not negatively influence the surrounding tissue as for example by lowering the pH, which is a common problem of polyesters. This is one of the reasons why naturally occurring or derived materials such as polysaccharides and proteins are gaining interest in the biomedical field; the body recognizes the degradation products and can clear them.^[96a]

In a foundational study on recombinant silk biodegradation, Lammel et al. investigated spider silk particle degradation using elastase and trypsin. It was found that elastase and trypsin first degrade the hydrophilic parts of the eADF4(C16) particle shell, and the hydrophobic particles then agglomerate. A rearrangement in the agglomerated particles leads to exposure of hydrophilic parts, which can then again be degraded.^[143] Further it was shown that eADF4(C16) particles can be completely digested using proteinase K or artificial intestinal fluid, but not in artificial gastric fluid.^[47] In a

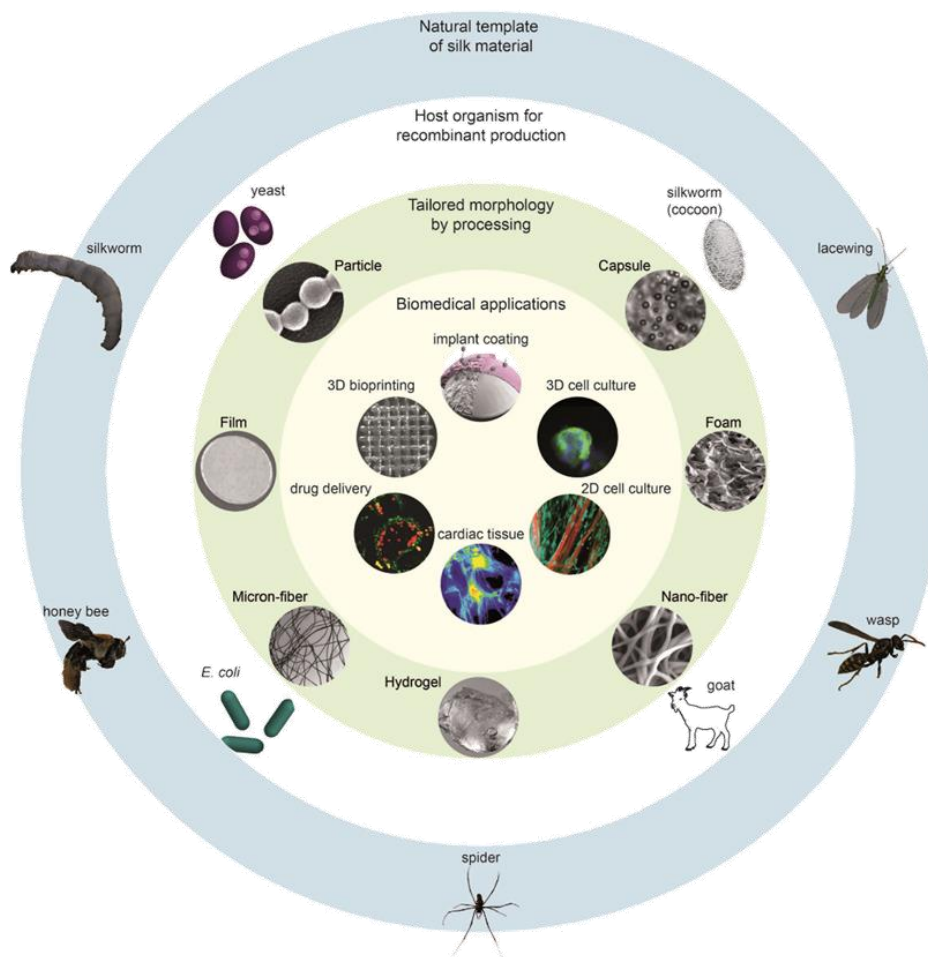


Figure 13. Recombinant silk proteins used as a biomaterial for biomedical engineering applications. Recombinant silk proteins were engineered and produced in host organisms, enabling the development of different morphologies and screening for putative applications. Silk worm, honey bee and wasp photos were taken and modified from open source images found on Pexels or Pixabay. 2D cell culture; Reproduced with permission.^[73] Copyright 2010, American Chemical Society. 3D cell culture; Reproduced with permission.^[75] Copyright 2016, Elsevier. Cardiac tissue.^[33d] Implant coating.^[25] Drug delivery; Reproduced with permission.^[46] Copyright 2014, American Chemical Society.

follow up study in vitro, the degradation of several different eADF4(C16) scaffolds was investigated. It was found that the soluble protein could be immediately degraded by the recombinant human proteases MMP-2 and polymorphonuclear (PMN) elastase within less than a minute. Further, the degradation of particles, films, and nonwoven meshes with and without crosslinking was investigated over 15 d in the presence of two bacterial model proteases, namely protease type XIV (PXIV) resembling a digestive model and collagenase type IA (CHC) resembling a wound environment, and was shown to be significantly slower than for soluble silk proteins.^[33d]

In general, all scaffolds were degraded faster by PXIV than by CHC, whereby crosslinking the scaffolds with APS and Rubpy

decreased the degradation rate. In absence of proteases almost no degradation was observed during the whole experiment. Also the morphology of the silk scaffold played a major role on the proteolytic stability, here particles degraded the fastest, followed by films and nonwoven meshes. No correlation was found between initial secondary structure contents of the scaffolds and its degradation rate. A 500× higher protease concentration than occurring in natural environment had to be used in order to measure degradation in a reasonable time frame. Therefore, degradation in vivo is supposed to be much slower.^[33d] This slow degradation in vivo, indirectly determined for eADF4(C16), was still found on coated silicone implants twelve months after implantation.^[25]

Spider silk implant coatings of polydimethylsiloxane (PDMS) resulted in a similar behavior, whereby the coating was rather stable against degradation by CHC, but was fully degraded in the presence of PXIV within 6 d.^[91] Furthermore, enzymatic degradation of eADF4(C16) foams was investigated using the same enzymes. A 1300× higher protease concentration than found in natural environment was used and led to a full degradation in the presence of PXIV within 4 d, whereby 75% of the scaffolds were still left after treatment with CHC for 15 d.^[33c] Moisenovich et al. performed two studies with rS1/9 silk foams, whereby the same degradation experiment was performed. Foams were incubated in PBS and Fenton's reagent (0.1×10^{-3} M FeSO₄, 1×10^{-3} M H₂O₂). It was shown that the foams are quite stable in PBS (20% loss), but degrade very fast in Fenton's reagent (>90% loss) over 11 weeks.^[49] Interestingly, a similar result was obtained in the follow up study already after 7 weeks.^[61b]

The degradation of recombinant honey bee silk AmelF3 was investigated using trypsin and α -chymotrypsin, both commonly found in the digestive system in the small intestine.^[159] As in the case of eADF4(C16), the protein was completely stable in buffer, and experienced rapid degradation only in presence of a protease. In a similar study, attachment of primary GFP-expressing fibroblasts from rabbits to AmelF3 nonwoven mats, and further degradation of the nonwoven meshes, was evaluated.^[51b]

Price et al. even introduced a sequence recognized by MMPs to SELP-815K in order to improve the degradability. In the presence of 40×10^{-9} M MMP-2, there was complete degradation of the protein in solution within 120 min, and hydrogels in vitro were significantly degraded after 14 d; and there was a corresponding increase in soluble protein found in solution. For in vivo testing, mice were infected with JHU-022 human head, and neck squamous cell carcinoma and the SELP-815K modified with the degradation sequence were assembled into hydrogels containing either saline or virus and were directly injected into the tumor. In vitro, hydrogels containing the degradation sequence could be degraded by MMP-2 completely after 60 min, whereas there was no degradation detected for those not containing the degradation sequence. By tailoring the hydrogel formulation, prolonged expression of the adenovirus could be achieved, and thereby there was a decreased growth rate of the tumor and an increase in the survival rate over a 50-day period, compared to the animals where adenovirus was injected alone.^[158]

8. Conclusion

In this review the use of recombinant silk proteins as a biomaterial assembled into different morphologies is summarized, and particularly promising results are highlighted. It can be stated that materials prepared from recombinant silk proteins show some clear advantages for BME compared to other biomaterials, such as their high-quality de novo production, low immunogenicity, and slow biodegradation. The next important step is to obtain FDA-approval for recombinant silk materials and then it is likely that these biomaterials will be used more frequently, and with great anticipation and hope for future success.

Acknowledgements

T.B.A. and E.D. contributed equally to this work. This work was financially supported by DFG grant SFB 840 TP A8 (to T.S.), European Union grant ETZ-EFRE 2014-2020, Freistaat Bayern-Tschechien, Project ID 123 (to T.S.), and the Bavarian Research Foundation (DOK-175-15, to T.B.A.). The authors would also like to thank Heike Herold and Adrian Golser for contributing advice and knowledge, which improved the content of this review.

Conflict of Interest

The authors declare no conflict of interest.

Keywords

biomaterials, biomedical engineering, drug delivery, recombinant silk, silk processing

Received: August 15, 2017

Revised: October 26, 2017

Published online:

- [1] BMES, BMES—FAQs about BME, <http://www.bmes.org/content.asp?contentid=140> (accessed: August 2017).
- [2] a) WHO, *World Health Statistics 2016: Monitoring Health for the SDGs*, WHO Press, Geneva, Switzerland 2016; b) V. Kontis, J. E. Bennett, C. D. Mathers, G. Li, K. Foreman, M. Ezzi, *Lancet* 2017, 389, 1323.
- [3] a) T. Niccoli, L. Partridge, *Curr. Biol.* 2012, 22, R741; b) M. C. Nevitt, S. R. Cummings, E. S. Hudes, *J. Gerontol.* 1991, 46, M164.
- [4] J. M. Quintana, I. Arostegui, A. Escobar, J. Azkarate, J. I. Goenaga, I. Lafuente, *Arch. Intern. Med.* 2008, 168, 1576.
- [5] NIH, Who Needs a Pacemaker?, <https://www.nhlbi.nih.gov/health/health-topics/topics/pace/whoneeds> (accessed: August 2017).
- [6] J. S. Miller, *PLoS Biol.* 2014, 12, e1001882.
- [7] M. J. Lysaght, J. A. O'Loughlin, *ASAIO J.* 2000, 46, 515.
- [8] Alzheimer's Association, *2016 Alzheimer's Disease Facts and Figures*, Chicago, Washington 2016.
- [9] CDC, Statistics Reported by Center for Disease Control and Prevention, <https://www.cdc.gov/> (accessed: August 2017).
- [10] *Stem Cells, Tissue Engineering and Regenerative Medicine* (Eds: D. Warburton), World Scientific Publishing Co. Pte. Ltd., Singapore 2015.
- [11] a) J. W. Michael, K. U. Schluter-Brust, P. Eysel, *Dtsch. Arztebl. Int.* 2010, 107, 152; b) E. A. Makris, A. H. Gomoll, K. N. Malizos, J. C. Hu, K. A. Athanasiou, *Nat. Rev. Rheumatol.* 2015, 11, 21.
- [12] S. S. Magill, J. R. Edwards, W. Bamberg, Z. G. Beldavs, G. Dumryati, M. A. Kainer, R. Lynfield, M. Maloney, L. McAllister-Hollod, J. Nadle, S. M. Ray, D. L. Thompson, L. E. Wilson, S. K. Fridkin, E. I. P. Healthcare, *N. Engl. J. Med.* 2014, 370, 1198.
- [13] D. M. Sievert, P. Ricks, J. R. Edwards, A. Schneider, J. Patel, A. Srinivasan, A. Kallen, B. Limbago, S. Fridkin, N. H. S. Network, P. N. Facilities, *Infect. Control Hosp. Epidemiol.* 2013, 34, 1.
- [14] S. B. Levy, B. Marshall, *Nat. Med.* 2004, 10, S122.
- [15] HELI, Health and Environment Linkages Initiative, <http://www.who.int/heli/en/> (accessed: August 2017).
- [16] M. M. Rodgers, V. M. Pai, R. S. Conroy, *IEEE Sens. J.* 2015, 15, 3119.

- [17] BRAIN-Initiative, Brain stimulation, <http://www.braininitiative.org/> (accessed: August 2017).
- [18] E. Strickland, 3 Squishy Medical Robots That Are as Soft as You Are, <http://spectrum.ieee.org/biomedical/devices/3-squishy-medical-robots-that-are-as-soft-as-you-are> (accessed: August 2017).
- [19] a) D. Huh, B. D. Matthews, A. Mammoto, M. Montoya-Zavala, H. Y. Hsin, D. E. Ingber, *Science* 2010, 328, 1662; b) A. M. Hopkins, E. DeSimone, K. Chwalek, D. L. Kaplan, *Prog. Neurobiol.* 2015, 125, 1.
- [20] D. Campoccia, L. Montanaro, C. R. Arciola, *Biomaterials* 2013, 34, 8533.
- [21] J. Groll, T. Boland, T. Blunk, J. A. Burdick, D. W. Cho, P. D. Dalton, B. Derby, G. Forgacs, Q. Li, V. A. Mironov, L. Moroni, M. Nakamura, W. Shu, S. Takeuchi, G. Vozzi, T. B. Woodfield, T. Xu, J. J. Yoo, J. Malda, *Biofabrication* 2016, 8, 013001.
- [22] J. P. Ioannidis, *PLoS Med.* 2005, 2, e124.
- [23] C. Wu, B. Wang, C. Zhang, R. A. Wysk, Y. W. Chen, *Crit. Rev. Biotechnol.* 2017, 37, 333.
- [24] L. S. Nair, C. T. Laurencin, *Prog. Polym. Sci.* 2007, 32, 762.
- [25] P. H. Zepelin, N. C. Maksimovikj, M. C. Jordan, J. Nickel, G. Lang, A. H. Leimer, L. Roemer, T. Scheibel, *Adv. Funct. Mater.* 2014, 24, 2658.
- [26] L. DeFrancesco, *Nat. Biotechnol.* 2017, 35, 496.
- [27] V. Elisseeff, in *The Silk Roads: Highways of Culture and Commerce* (Ed: V. Elisseeff), Berghahn Books, UNESCO Publishing, New York, USA 2000.
- [28] a) M. Bon, *Philos. Trans. R. Soc., B* 1710, 27, 2; b) M. Santin, A. Motta, G. Freddi, M. Cannas, *J. Biomed. Mater. Res.* 1999, 46, 382; c) G. H. Altman, F. Diaz, C. Jakuba, T. Calabro, R. L. Horan, J. S. Chen, H. Lu, J. Richmond, D. L. Kaplan, *Biomaterials* 2003, 24, 401.
- [29] C. L. Craig, *Annu. Rev. Entomol.* 1997, 42, 231.
- [30] T. D. Sutherland, J. H. Young, S. Weisman, C. Y. Hayashi, D. J. Merritt, *Annu. Rev. Entomol.* 2010, 55, 171.
- [31] a) E. Bini, C. W. P. Foo, J. Huang, V. Karageorgiou, B. Kitchel, D. L. Kaplan, *Biomacromolecules* 2006, 7, 3139; b) M. Hedhammar, A. Rising, S. Grip, A. S. Martinez, K. Nordling, C. Casals, M. Stark, J. Johansson, *Biochemistry* 2008, 47, 3407; c) S. Wohlrab, K. Spiess, T. Scheibel, *J. Mater. Chem.* 2012, 22, 22050; d) T. Asakura, Y. Suzuki, A. Nagano, D. Knight, M. Kamiya, M. Dernura, *Biomacromolecules* 2013, 14, 3731.
- [32] X. Hu, D. Kaplan, P. Cebe, *Macromolecules* 2006, 39, 6161.
- [33] a) A. Leal-Egana, G. Lang, C. Mauerer, J. Wickinghoff, M. Weber, S. Geimer, T. Scheibel, *Adv. Eng. Mater.* 2012, 14, B67; b) F. Bauer, S. Wohlrab, T. Scheibel, *Biomater. Sci.* 2013, 1, 1244; c) K. Schacht, J. Vogt, T. Scheibel, *ACS Biomater. Sci. Eng.* 2016, 2, 517; d) S. Müller-Herrmann, T. Scheibel, *ACS Biomater. Sci. Eng.* 2015, 1, 247; e) J. Petzold, T. B. Aigner, F. Tausch, K. Zimmermann, T. Scheibel, F. B. Engel, *Adv. Funct. Mater.* 2017, 27, 1701427.
- [34] R. Foelix, *Biology of Spiders*, 3rd ed., Oxford University Press, Oxford, UK 2011.
- [35] C. Thamm, T. Scheibel, *Biomacromolecules* 2017, 18, 1365.
- [36] a) O. Tokareva, V. A. Michalczewski-Lacerda, E. L. Rech, D. L. Kaplan, *Microb. Biotechnol.* 2013, 6, 651; b) X. Hu, K. Vasanthavada, K. Kohler, S. McNary, A. M. Moore, C. A. Vierra, *Cell. Mol. Life Sci.* 2006, 63, 1986; c) A. E. Brooks, H. B. Steinkraus, S. R. Nelson, R. V. Lewis, *Biomacromolecules* 2005, 6, 3095; d) C. Y. Hayashi, N. H. Shipley, R. V. Lewis, *Int. J. Biol. Macromol.* 1999, 24, 271.
- [37] J. M. Aarnodt, D. W. Grainger, *Biomaterials* 2016, 86, 68.
- [38] a) F. Vollrath, *Int. J. Biol. Macromol.* 1999, 24, 81; b) B. Madsen, Z. Z. Shao, F. Vollrath, *Int. J. Biol. Macromol.* 1999, 24, 301; c) A. Spönnner, W. Vater, S. Monajembashi, E. Unger, F. Grosse, K. Weisshart, *PLoS One* 2007, 2, e998; d) K. H. Guehrs, B. Schlott, F. Grosse, K. Weisshart, *Insect Mol. Biol.* 2008, 17, 553; e) L. Eisoldt, A. Smith, T. Scheibel, *Mater. Today* 2011, 14, 80.
- [39] C. Radtke, C. Allmeling, K. H. Waldmann, K. Reimers, K. Thies, H. C. Schenk, A. Hillrner, M. Guggenheirn, G. Brandes, P. M. Vogt, *PLoS One* 2011, 6, e16990.
- [40] M. Neuenfeldt, T. Scheibel, *Biomolecules* 2017, 7, 43.
- [41] J. A. M. Rarnshaw, J. A. Werkmeister, G. J. Durnsday, *Bioengineered* 2014, 5, 227.
- [42] S. Chattopadhyay, R. T. Raines, *Biopolymers* 2014, 101, 821.
- [43] a) H. M. Herold, T. Scheibel, *Z. Naturforsch. C. J. Biosci.* 2017, 72, 365; b) T. Asakura, T. Miller, in *The Power of Recombinant Spider Silk Proteins* (Eds: S. Wohlrab, C. Thamm, T. Scheibel), Springer Science+Business Media Dordrecht, Dordrecht: 2014; c) D. L. Kaplan, T. Scheibel, in *Reference Module in Materials Science and Materials Engineering* (Ed: S. Hashmi), Elsevier Inc., Amsterdam 2017; d) A. Heidebrecht, T. Scheibel, in *Advances in Applied Microbiology*, Vol. 82, (Eds: G. Gadd, S. Sariaslani), Elsevier Inc., Amsterdam, Netherlands 2013; e) T. Kato, M. Kajikawa, K. Maenaka, E. Y. Park, *Appl. Microbiol. Biotechnol.* 2010, 85, 459.
- [44] G. L. Rosano, E. A. Ceccarelli, *Front. Microbiol.* 2014, 5, 172.
- [45] D. Huennerich, T. Scheibel, F. Vollrath, S. Cohen, U. Gar, S. Ittah, *Curr. Biol.* 2004, 14, 2070.
- [46] A. Florczak, A. Mackiewicz, H. Dams-Kozłowska, *Biomacromolecules* 2014, 15, 2971.
- [47] B. Liebmann, D. Huennerich, T. Scheibel, M. Fehr, *Colloids Surf., A* 2008, 331, 126.
- [48] K. D. Herrmanson, D. Huennerich, T. Scheibel, A. R. Bausch, *Adv. Mater.* 2007, 19, 1810.
- [49] M. M. Moisenovich, O. L. Pustovalova, A. Y. Arhipova, T. V. Vasiljeva, O. S. Sokolova, V. G. Bogush, V. G. Debabov, V. I. Sevastianov, M. P. Kirpichnikov, I. I. Agapov, *J. Biomed. Mater. Res., Part A* 2011, 96A, 125.
- [50] A. Teplinin, A. Krashenninnikova, N. Agladze, K. Sidoruk, O. Agapova, I. Agapov, V. Bogush, K. Agladze, *PLoS One* 2015, 10, e0121155.
- [51] a) S. Weisman, V. S. Haritos, J. S. Church, M. G. Huson, S. T. Mudie, A. J. W. Rodgers, G. J. Durnsday, T. D. Sutherland, *Biomaterials* 2010, 31, 2695; b) C. R. Wittner, X. Hu, P. C. Gauthier, S. Weisman, D. L. Kaplan, T. D. Sutherland, *Acta Biomater.* 2011, 7, 3789.
- [52] a) T. Tamura, C. Thibert, C. Royer, T. Kanda, E. Abraham, M. Kamba, N. Kornoto, J. L. Thomas, B. Mauchamp, G. Chavancy, P. Shirk, M. Fraser, J. C. Prudhomme, P. Couble, *Nat. Biotechnol.* 2000, 18, 559; b) K. Kojima, Y. Kuwana, H. Sezutsu, I. Kobayashi, K. Uchino, T. Tamura, Y. Tamada, *Biosci., Biotechnol., Biochem.* 2007, 71, 2943; c) S. Yanagisawa, Z. H. Zhu, I. Kobayashi, K. Uchino, Y. Tamada, T. Tamura, T. Asakura, *Biomacromolecules* 2007, 8, 3487.
- [53] a) Y. Kambe, K. Yamamoto, K. Kojima, Y. Tamada, N. Torrita, *Biomaterials* 2010, 31, 7503; b) S. Inoue, K. Tanaka, F. Arisaka, S. Kimura, K. Ohtomo, S. Mizuno, *J. Biol. Chem.* 2000, 275, 40517.
- [54] a) A. Nagano, Y. Tanioka, N. Sakurai, H. Sezutsu, N. Kuboyama, H. Kiba, Y. Tanimoto, N. Nishiyama, T. Asakura, *Acta Biomater.* 2011, 7, 1192; b) A. Nagano, H. Sato, Y. Tanioka, Y. Nakazawa, D. Knight, T. Asakura, *Soft Matter* 2012, 8, 741.
- [55] a) J. Cappello, J. Crissman, M. Dorman, M. Mikolajczak, G. Textor, M. Marquet, F. Ferrari, *Biotechnol. Prog.* 1990, 6, 198; b) R. Dandu, A. Von Cresce, R. Briber, P. Dowell, J. Cappello, H. Ghandehari, *Polymer* 2009, 50, 366; c) A. Poursaid, R. Price, A. Tiede, E. Olson, E. Huo, L. McGill, H. Ghandehari, J. Cappello, *Biomaterials* 2015, 57, 142.
- [56] F. Bauer, T. Scheibel, *Angew. Chem., Int. Ed.* 2012, 51, 6521.
- [57] a) Y. Kambe, T. Kameda, *J. Silk Sci. Technol. Jpn.* 2014, 22, 47; b) Y. Kambe, T. D. Sutherland, T. Kameda, *Acta Biomater.* 2014, 10, 3590.

- [58] a) D. Huermerich, C. W. Helsen, S. Quedzuweit, J. Oschmann, R. Rudolph, T. Scheibel, *Biochemistry* 2004, 43, 13604; b) E. Doblhofer, T. Scheibel, *J. Pharm. Sci.* 2015, 104, 988.
- [59] M. Stark, S. Grip, A. Rising, M. Hedhammar, W. Engstrom, G. Hjalrn, J. Johansson, *Biomacromolecules* 2007, 8, 1695.
- [60] a) H. Darns-Kozłowska, A. Majer, P. Tornasiewicz, J. Lozinska, D. L. Kaplan, A. Mackiewicz, *J. Biomed. Mater. Res., Part A* 2013, 701, 456; b) S. C. Gornes, I. B. Leonor, J. F. Mano, R. L. Reis, D. L. Kaplan, *Biomaterials* 2011, 32, 4255.
- [61] a) I. I. Agapov, O. L. Pustovalova, M. M. Moisenovich, V. G. Bogush, O. S. Sokolova, V. I. Sevastyanov, V. G. Debabov, M. P. Kirpichnikov, *Dokl. Biochem. Biophys.* 2009, 426, 127; b) M. M. Moisenovich, O. Pustovalova, J. Shackelford, T. V. Vasiljeva, T. V. Druzhinina, Y. A. Karnenchuk, V. V. Guzeev, O. S. Sokolova, V. G. Bogush, V. G. Debabov, M. P. Kirpichnikov, I. I. Agapov, *Biomaterials* 2012, 33, 3887.
- [62] T. I. Harris, D. A. Gaztambide, B. A. Day, C. L. Brock, A. L. Ruben, J. A. Jones, R. V. Lewis, *Biomacromolecules* 2016, 17, 3761.
- [63] K. Jastrzebska, E. Felcyn, M. Kozak, M. Szybowicz, T. Buchwald, Z. Pietralik, T. Jesionowski, A. Mackiewicz, H. Darns-Kozłowska, *Sci. Rep.* 2016, 6, 28106.
- [64] a) C. Mason, P. Dunnill, *Regener. Med.* 2008, 3, 1; b) NIBIB, Tissue Engineering and Regenerative Medicine, <https://www.nibib.nih.gov/science-education/science-topics/tissue-engineering-and-regenerative-medicine> (accessed: August 2017).
- [65] a) A. Khadernhosseini, R. Langer, *Nat. Protoc.* 2016, 11, 1775; b) M. J. Webber, O. F. Khan, S. A. Sydlík, B. C. Tang, R. Langer, *Ann. Biomed. Eng.* 2015, 43, 641; c) H. Sadri-Ardekani, A. Atala, *Methods* 2016, 99, 1; d) D. F. Williams, *Biomaterials* 2014, 35, 10009.
- [66] J. W. Nichol, A. Khadernhosseini, *Soft Matter* 2009, 5, 1312.
- [67] NIH, *NIH Consensus Statement Online* 1982, 4, 19.
- [68] a) A. D. Doyle, F. W. Wang, K. Matsumoto, K. M. Yamada, *J. Cell Biol.* 2009, 184, 481; b) G. Charras, E. Sahai, *Nat. Rev. Mol. Cell Biol.* 2014, 15, 813.
- [69] a) A. Heidebrecht, L. Eisoldt, J. Diehl, A. Schmidt, M. Geffers, G. Lang, T. Scheibel, *Adv. Mater.* 2015, 27, 2189; b) M. Andersson, Q. P. Jia, A. Abella, X. Y. Lee, M. Landreh, P. Purhonen, H. Hebert, M. Tenje, C. V. Robinson, Q. Meng, G. R. Plaza, J. Johansson, A. Rising, *Nat. Chem. Biol.* 2017, 13, 262.
- [70] G. Li, Y. Li, G. Q. Chen, J. H. He, Y. F. Han, X. Q. Wang, D. L. Kaplan, *Adv. Healthcare Mater.* 2015, 4, 1134.
- [71] M. Widhe, H. Bysell, S. Nystedt, I. Schenning, M. Malmsten, J. Johansson, A. Rising, M. Hedhammar, *Biomaterials* 2010, 31, 9575.
- [72] C. Fredriksson, M. Hedhammar, R. Feinstein, K. Nordling, G. Kratz, J. Johansson, F. Huss, A. Rising, *Materials* 2009, 2, 1908.
- [73] M. Hedhammar, H. Brannfeldt, T. Baris, M. Widhe, G. Askarieh, K. Nordling, S. von Aulock, J. Johansson, *Biomacromolecules* 2010, 11, 953.
- [74] M. Widhe, U. Johansson, C. O. Hillerdahl, M. Hedhammar, *Biomaterials* 2013, 34, 8223.
- [75] a) S. Q. Wu, J. Johansson, P. Darnidropoulou, M. Shahsavani, A. Falk, O. Hovatta, A. Rising, *Biomaterials* 2014, 35, 8496; b) N. D. Shalaly, M. Ria, U. Johansson, K. Avall, P. O. Berggren, M. Hedhammar, *Biomaterials* 2016, 90, 50; c) D. Harvey, P. Bardelang, S. L. Goodacre, A. Cockayne, N. R. Thomas, *Adv. Mater.* 2017, 29, 1604245.
- [76] U. Johansson, M. Ria, K. Avall, N. D. Shalaly, S. V. Zaitsev, P. O. Berggren, M. Hedhammar, *PLoS One* 2015, 10, e0130169.
- [77] a) Y. Nakazawa, M. Sato, R. Takahashi, D. Ayernitz, C. Takabayashi, T. Tamura, S. Enomoto, M. Sata, T. Asakura, *J. Biomater. Sci., Polym. Ed.* 2011, 22, 195; b) T. Asakura, M. Isozaki, T. Saotome, K. I. Tatematsu, H. Sezutsu, N. Kuwabara, Y. Nakazawa, *J. Mater. Chem. B* 2014, 2, 7375; c) T. Saotome, H. Hayashi, R. Tanaka, A. Kinugasa, S. Uesugi, K. Tatematsu, H. Sezutsu, N. Kuwabara, T. Asakura, *J. Mater. Chem. B* 2015, 3, 7109.
- [78] R. Vasita, D. S. Katti, *Int. J. Nanomed.* 2006, 1, 15.
- [79] T. Fukunishi, C. A. Best, T. Sugiura, J. Opfermann, C. S. Ong, T. Shinoka, C. K. Breuer, A. Krieger, J. Johnson, N. Hibino, *J. Thorac. Cardiovasc. Surg.* 2017, 153, 924.
- [80] S. K. Seidlits, J. Y. Lee, C. E. Schmidt, *Nanomedicine (London, U. K.)* 2008, 3, 183.
- [81] a) Z. X. Cai, X. M. Mo, K. H. Zhang, L. P. Fan, A. L. Yin, C. L. He, H. S. Wang, *Int. J. Mol. Sci.* 2010, 11, 3529; b) J. P. Chen, G. Y. Chang, J. K. Chen, *Colloid Surf., A* 2008, 313, 183.
- [82] N. Bhardwaj, S. C. Kundu, *Biotechnol. Adv.* 2010, 28, 325.
- [83] G. Taylor, *Proc. R. Soc. London, Ser. A* 1964, 280, 383.
- [84] S. B. Cai, H. L. Xu, Q. R. Jiang, Y. Q. Yang, *Langmuir* 2013, 29, 2311.
- [85] A. Koski, K. Yirm, S. Shivkumar, *Mater. Lett.* 2004, 58, 493.
- [86] J. L. Lowery, N. Datta, G. C. Rutledge, *Biomaterials* 2010, 31, 491.
- [87] B. Zhu, W. Li, R. V. Lewis, C. U. Segre, R. Wang, *Biomacromolecules* 2015, 16, 202.
- [88] a) J. G. Hardy, A. Pfaff, A. Leal-Egana, A. H. E. Muller, T. R. Scheibel, *Macromol. Biosci.* 2014, 14, 936; b) B. An, M. D. Tang-Schorner, W. W. Huang, J. Y. He, J. A. Jones, R. V. Lewis, D. L. Kaplan, *Biomaterials* 2015, 48, 137.
- [89] a) S. Wohlrab, S. Muller, A. Schmidt, S. Neubauer, H. Kessler, A. Leal-Egana, T. Scheibel, *Biomaterials* 2012, 33, 6650; b) S. Gornes, K. Nurnata, I. B. Leonor, J. F. Mano, R. L. Reis, D. L. Kapan, *Biomacromolecules* 2011, 12, 1675; c) S. Gornes, I. B. Leonor, J. F. Mano, R. L. Reis, D. L. Kaplan, *Soft Matter* 2011, 7, 4964; d) S. Gornes, J. Gallego-Llamas, I. B. Leonor, J. F. Mano, R. L. Reis, D. L. Kaplan, *J. Tissue Eng. Regener. Med.* 2012, 6, 356.
- [90] a) M. Lewicka, O. Hermanson, A. U. Rising, *Biomaterials* 2012, 33, 7712; b) S. Wu, J. Johansson, O. Hovatta, A. Rising, *Cell. Mol. Life Sci.* 2016, 73, 1479.
- [91] C. B. Borkner, S. Wohlrab, E. Müller, G. Lang, T. Scheibel, *ACS Biomater. Sci. Eng.* 2017, 3, 767.
- [92] A. J. Mieszawska, L. D. Nadkarni, C. C. Perry, D. L. Kaplan, *Chem. Mater.* 2010, 22, 5780.
- [93] M. Widhe, N. D. Shalaly, M. Hedhammar, *Biomaterials* 2016, 74, 256.
- [94] J. Johansson, A. Rising, *Front. Bioeng. Biotechnol.* 2014, 2, 50.
- [95] A. K. Salem, R. Stevens, R. G. Pearson, M. C. Davies, S. J. B. Tendler, C. J. Roberts, P. M. Williams, K. M. Shakesheff, *J. Biomed. Mater. Res.* 2002, 61, 212.
- [96] a) H. Naderi, M. M. Matin, A. R. Bahrami, *J. Biomater. Appl.* 2011, 26, 383; b) E. A. Botchwey, M. A. Dupree, S. R. Pollack, E. M. Levine, C. T. Laurencin, *J. Biomed. Mater. Res., Part A* 2003, 67A, 357.
- [97] D. J. Mooney, D. F. Baldwin, N. P. Suh, L. P. Vacanti, R. Langer, *Biomaterials* 1996, 17, 1417.
- [98] A. G. Mikos, G. Sarakinos, S. M. Leite, J. P. Vacanti, R. Langer, *Biomaterials* 1993, 14, 323.
- [99] I. V. Yannas, J. F. Burke, P. L. Gordon, C. Huang, R. H. Rubenstein, *J. Biomed. Mater. Res.* 1980, 14, 107.
- [100] C. J. Doillon, C. F. Whyne, S. Brandwein, F. H. Silver, *J. Biomed. Mater. Res.* 1986, 20, 1219.
- [101] K. Whang, C. H. Thomas, K. E. Healy, G. Nuber, *Polymer* 1995, 36, 837.
- [102] N. Bolgen, F. Plieva, I. Y. Galaev, B. Mattiasson, E. Piskin, *J. Biomater. Sci., Polym. Ed.* 2007, 18, 1165.
- [103] J. Groll, U. Gbureck, K. Stuckensen, *Germany WO2013083844 A2*, 2013.
- [104] O. I. Agapova, A. E. Efirnov, M. M. Moisenovich, V. G. Bogush, I. I. Agapov, *Russ. J. Transplantol. Artif. Organs* 2015, 17, 37.

- [105] Y. Qiu, K. Park, *Adv. Drug Delivery Rev.* 2001, 53, 321.
- [106] a) J. Maitra, V. K. Shukla, *Am. J. Polym. Sci.* 2014, 4, 7; b) Q. Chai, Y. Jiao, X. Yu, *Gels* 2017, 3, 15.
- [107] a) K. Schacht, T. Scheibel, *Biomacromolecules* 2011, 12, 2488; b) M. R. Matanovic, J. Kristl, P. A. Grabnar, *Int. J. Pharm.* 2014, 472, 262.
- [108] E. DeSimone, K. Schacht, T. Scheibel, *Mater. Lett.* 2016, 183, 101.
- [109] J. Thiele, Y. J. Ma, S. M. C. Bruekers, S. H. Ma, W. T. S. Huck, *Adv. Mater.* 2014, 26, 125.
- [110] K. Hölzl, S. M. Lin, L. Tytgat, S. Van Vlierberghe, L. X. Gu, A. Ovsianikov, *Biofabrication* 2016, 8, 032002.
- [111] U. J. Kim, J. Y. Park, C. M. Li, H. J. Jin, R. Valluzzi, D. L. Kaplan, *Biomacromolecules* 2004, 5, 786.
- [112] K. Schacht, T. Jüngst, M. Schweinlin, A. Ewald, J. Groll, T. Scheibel, *Angew. Chem.* 2015, 54, 5.
- [113] G. Donelli, I. Francolini, *J. Chemother.* 2001, 13, 595.
- [114] a) M. C. Shen, I. Garcia, R. V. Maier, T. A. Horbett, *J. Biomed. Mater. Res., Part A* 2004, 70A, 533; b) A. K. McNally, J. M. Anderson, *Am. J. Pathol.* 1995, 147, 1487.
- [115] D. G. Castner, B. D. Ratner, *Surf. Sci.* 2002, 500, 28.
- [116] J. M. Anderson, A. Rodriguez, D. T. Chang, *Semin. Immunol.* 2008, 20, 86.
- [117] P. H. Zeplin, A. K. Beminger, N. C. Maksimovikj, P. van Gelder, T. Scheibel, H. Walles, *Handchir. Mikrochir. Plast. Chir.* 2014, 46, 336.
- [118] L. Nileback, J. Hedin, M. Widhe, L. S. Floderus, A. Krona, H. Bysell, M. Hedhammar, *Biomacromolecules* 2017, 18, 846.
- [119] Y. Wang, D. S. Kohane, *Nat. Rev. Mater.* 2017, 2, 17020.
- [120] a) R. Langer, *Science* 1990, 249, 1527; b) M. B. Elsner, H. M. Herold, S. Müller-Herrmann, H. Barge, T. Scheibel, *Biomater. Sci.* 2015, 3, 543.
- [121] E. Agostini, G. Winter, J. Engert, *J. Controlled Release* 2015, 213, 134.
- [122] R. Langer, N. A. Peppas, *AIChE J.* 2003, 49, 2990.
- [123] V. Sanna, N. Pala, M. Sechi, *Int. J. Nanomed.* 2014, 9, 467.
- [124] a) X. Q. Wang, E. Wenk, A. Matsumoto, L. Meinel, C. M. Li, D. L. Kaplan, *J. Controlled Release* 2007, 117, 360; b) E. Wenk, A. J. Wandrey, H. P. Merkle, L. Meinel, *J. Controlled Release* 2008, 132, 26; c) E. Wenk, H. P. Merkle, L. Meinel, *J. Controlled Release* 2011, 150, 128.
- [125] a) P. Gupta, K. Verrmani, S. Garg, *Drug Discovery Today* 2002, 7, 569; b) T. R. Hoare, D. S. Kohane, *Polymer* 2008, 49, 1993.
- [126] T. Banerjee, S. Mitra, A. K. Singh, R. K. Sharma, A. Maitra, *Int. J. Pharm.* 2002, 243, 93.
- [127] S. Ladet, L. David, A. Dornard, *Nature* 2008, 452, 76.
- [128] J. Gustafson, K. Greish, J. Frandsen, J. Cappello, H. Ghandehari, *J. Controlled Release* 2009, 140, 256.
- [129] a) J. M. Llovet, J. Bruix, B. C. L. C. Grp, *Hepatology* 2003, 37, 429; b) RSNA, Chemoembolization, <https://www.radiologyinfo.org/en/info.cfm?pg=chemoembol> (accessed: August 2017).
- [130] Y. F. Huang, K. Bailey, S. Wang, X. S. Feng, *React. Funct. Polym.* 2017, 116, 57.
- [131] S. Hofmann, C. T. W. P. Foo, F. Rossetti, M. Textor, G. Vunjak-Novakovic, D. L. Kaplan, H. P. Merkle, L. Meinel, *J. Controlled Release* 2006, 111, 219.
- [132] S. Z. Lu, X. Q. Wang, Q. Lu, X. Hu, N. Uppal, F. G. Omenetto, D. L. Kaplan, *Biomacromolecules* 2009, 10, 1032.
- [133] Q. Lu, X. Q. Wang, X. Hu, P. Cebe, F. Omenetto, D. L. Kaplan, *Macromol. Biosci.* 2010, 10, 359.
- [134] J. G. Hardy, A. Leal-Egana, T. R. Scheibel, *Macromol. Biosci.* 2013, 13, 1431.
- [135] T. M. S. Chang, *Nat. Rev. Drug Discovery* 2005, 4, 221.
- [136] a) O. Shchepelina, I. Drachuk, M. K. Gupta, J. Lin, V. V. Tsukruk, *Adv. Mater.* 2011, 23, 4655; b) C. H. Ye, O. Shchepelina, R. Calabrese, I. Drachuk, D. L. Kaplan, V. V. Tsukruk, *Biomacromolecules* 2011, 12, 4319; c) C. H. Ye, I. Drachuk, R. Calabrese, H. Q. Dai, D. L. Kaplan, V. V. Tsukruk, *Langmuir* 2012, 28, 12235.
- [137] a) K. D. Hermanson, M. B. Harasim, T. Scheibel, A. R. Bausch, *Phys. Chem. Chem. Phys.* 2007, 9, 6442; b) C. Blum, A. Nichtl, T. Scheibel, *Adv. Funct. Mater.* 2014, 24, 763.
- [138] a) A. S. Lammel, X. Hu, S. H. Park, D. L. Kaplan, T. R. Scheibel, *Biomaterials* 2010, 31, 4583; b) F. P. Seib, G. T. Jones, J. Rnjak-Kovacina, Y. N. Lin, D. L. Kaplan, *Adv. Healthcare Mater.* 2013, 2, 1606.
- [139] A. Lammell, M. Schwab, U. Slotta, G. Winter, T. Scheibel, *ChemSuschem* 2008, 1, 413.
- [140] M. Lucke, G. Winter, J. Engert, *Int. J. Pharm.* 2015, 481, 125.
- [141] N. Helfrich, M. Klug, A. Mark, V. Kuznetsov, C. Blum, T. Scheibel, G. Papastavrou, *Biomater. Sci.* 2013, 1, 1166.
- [142] M. P. Neubauer, C. Blum, E. Agostini, J. Engert, T. Scheibel, A. Fery, *Biomater. Sci.* 2013, 1, 1160.
- [143] C. Blüm, T. Scheibel, *BioNanoScience* 2012, 2, 67.
- [144] M. Hofer, G. Winter, J. Myschik, *Biomaterials* 2012, 33, 1554.
- [145] A. Lammel, M. Schwab, M. Hofer, G. Winter, T. Scheibel, *Biomaterials* 2011, 32, 2233.
- [146] R. H. Müller, *Zetapotential und Partikelladung in der Laborpraxis*, Wissenschaftlicher Verlagsgesellschaft mbH Stuttgart, Stuttgart, Germany 1996.
- [147] A. Florczak, K. Jastrzebska, A. Mackiewicz, H. Dams-Kozłowska, *J. Mater. Chem. B* 2017, 5, 3000.
- [148] M. B. Schierling, E. Doblhofer, T. Scheibel, *Biomater. Sci.* 2016, 4, 1515.
- [149] K. Numata, B. Subramanian, H. A. Currie, D. L. Kaplan, *Biomaterials* 2009, 30, 5775.
- [150] K. Numata, D. L. Kaplan, *Biomacromolecules* 2010, 11, 3189.
- [151] K. Numata, J. Hamasaki, B. Subramanian, D. L. Kaplan, *J. Controlled Release* 2010, 146, 136.
- [152] K. Numata, M. R. Reagan, R. H. Goldstein, M. Rosenblatt, D. L. Kaplan, *Biocorjugate Chem.* 2011, 22, 1605.
- [153] K. Numata, A. J. Mieszawska-Czajkowska, L. A. Kvenvold, D. L. Kaplan, *Macromol. Biosci.* 2012, 12, 75.
- [154] W. W. Huang, D. Ebrahimi, N. Dinjaski, A. Tarakanova, M. J. Buehler, J. Y. Wong, D. L. Kaplan, *Acc. Chem. Res.* 2017, 50, 866.
- [155] K. Y. Lee, D. J. Mooney, *Prog. Polym. Sci.* 2012, 37, 106.
- [156] M. B. Gorbet, M. V. Sefton, *Biomaterials* 2005, 26, 6811.
- [157] F. Vollrath, P. Barth, A. Basedow, W. Engstrom, H. List, *In Vivo* 2002, 16, 229.
- [158] R. Price, A. Poursaid, J. Cappello, H. Ghandehari, *J. Controlled Release* 2015, 213, 96.
- [159] E. Vandermarliere, M. Mueller, L. Martens, *Mass Spectrom. Rev.* 2013, 32, 453.

Part 6. Biofabrication of 3D Constructs: Fabrication Technologies and Spider Silk Proteins as Bioinks

DeSimone E.*, Schacht K.*, Jungst T., Groll J., Scheibel T.

Published in *Pure and Applied Chemistry*, **87**, 737-749
(2015)

Reprinted with kind permission from De Gruyter

Conference paper

Elise DeSimone^a, Kristin Schacht^a, Tomasz Jungst, Jürgen Groll and Thomas Scheibel*

Biofabrication of 3D constructs: fabrication technologies and spider silk proteins as bioinks

DOI 10.1515/pac-2015-0106

Abstract: Despite significant investment in tissue engineering over the past 20 years, few tissue engineered products have made it to market. One of the reasons is the poor control over the 3D arrangement of the scaffold's components. Biofabrication is a new field of research that exploits 3D printing technologies with high spatial resolution for the simultaneous processing of cells and biomaterials into 3D constructs suitable for tissue engineering. Cell-encapsulating biomaterials used in 3D bioprinting are referred to as bioinks. This review consists of: (1) an introduction of biofabrication, (2) an introduction of 3D bioprinting, (3) the requirements of bioinks, (4) existing bioinks, and (5) a specific example of a recombinant spider silk bioink. The recombinant spider silk bioink will be used as an example because its unmodified hydrogel format fits the basic requirements of bioinks: to be printable and at the same time cytocompatible. The bioink exhibited both cytocompatible (self-assembly, high cell viability) and printable (injectable, shear-thinning, high shape fidelity) qualities. Although improvements can be made, it is clear from this system that, with the appropriate bioink, many of the existing faults in tissue-like structures produced by 3D bioprinting can be minimized.

Keywords: biofabrication; bioink; biomaterials; biomedical applications; 3D bioprinting; biotechnology; NICE-2014; spider silk.

Biofabrication

In 1907, a protocol was first described for maintaining the viability of isolated tissue outside of an organism [1]. This technique, called *in vitro* tissue culture, catalyzed a boom of biologically-based technology and debate over the possibilities and implications of this development. One of the most exciting technologies which emerged is tissue engineering. Traditionally, tissue engineering is the modular assembly of biomateri-

Article note: A collection of invited papers based on presentations at the 2nd International Conference on Bioinspired and Biobased Chemistry and Materials: Nature Inspires Chemical Engineers (NICE-2014), Nice, France, 15–17 October 2014.

^aThe authors contributed equally to this work.

***Corresponding author: Thomas Scheibel,** Lehrstuhl Biomaterialien, Universität Bayreuth, Universitätsstraße 30, 95447 Bayreuth, Germany, e-mail: thomas.scheibel@bm.uni-bayreuth.de; Bayreuther Zentrum für Kolloide und Grenzflächen (BZKG), Universität Bayreuth, Universitätsstraße 30, 95440 Bayreuth, Germany; Institut für Bio-Makromoleküle (bio-mac), Universität Bayreuth, Universitätsstraße 30, 95440 Bayreuth, Germany; Bayreuther Zentrum für Molekulare Biowissenschaften (BZMB), Universität Bayreuth, Universitätsstraße 30, 95440 Bayreuth, Germany; and Bayreuther Materialzentrum (BayMAT), Universität Bayreuth, Universitätsstraße 30, 95440 Bayreuth, Germany

Elise DeSimone and Kristin Schacht: Lehrstuhl Biomaterialien, Universität Bayreuth, Universitätsstraße 30, 95447 Bayreuth, Germany

Tomasz Jungst and Jürgen Groll: Lehrstuhl für Funktionswerkstoffe der Medizin und der Zahnheilkunde, Universität Würzburg, Pleicherwall 2, 97070 Würzburg, Germany

© 2015 IUPAC & De Gruyter

Bereitgestellt von | De Gruyter / TCS
Angemeldet
Heruntergeladen am | 07.09.15 10:22

als, cells and biochemical factors into tissue-like constructs [2]. Most accept the premise that in order to do this successfully one must, to some degree, mimic the properties of the target tissue. These constructs are immediately implanted or incubated *in vitro* prior to implantation. Relevant applications of tissue engineering include, but are not limited to: implants for regenerative medicine [3], *in vitro* models [4], biobots [5], and alternative food-sources [6]. Although tissue engineering has shown promise towards these applications, few have been approved for consumer use.

The high attrition rates of tissue engineered products are often hypothesized to be due to the modularity of the approach. It results in high variability in the spatial arrangement of the different components (biomaterials, cells, soluble and insoluble biochemical entities). This is problematic for presentation of factors to cells, which direct their behavior, as well as the architecture-dependent mechanical properties of these materials [7]. Due to the intimate relationship between structure and function in biological systems, which is observed across size scales, the success of tissue engineering is thereby limited by this poor control over hierarchical structures and their assembly [8, 9]. To overcome these limits, novel technologies have been established: cell-sheet technology, embedding or molding, centrifuge casting, dielectrophoresis, magnetic-force driven cell-motion, micro-fluidics, biospraying and 3D bioprinting (Table 1). Of these, perhaps the most interesting is the process of 3D bioprinting (3DBP). In this context, biofabrication can be defined as the automated,

Table 1: Published techniques in biofabrication and their basic, generalized process.

Technique	Basic process	References
Embedding or molding	<ol style="list-style-type: none"> 1. Suspension of cells in polymer solution 2. Addition of crosslinker or induction of crosslinking conditions 3. Encapsulation of cells in crosslinked polymer solution, typically within a vessel which results in a defined 3D shape 4. Removal of construct from mold if necessary 	[10, 11]
Centrifuge casting	<ol style="list-style-type: none"> 1. Suspension of cells in polymer solution 2. Addition of crosslinker or induction of crosslinking conditions 3. Cell-polymer solution transferred to vessel with defined 3D shape 4. Centrifugation during polymerization of construct 5. Removal of construct from mold if necessary 	[12]
Dielectrophoresis	<ol style="list-style-type: none"> 1. Suspension of cells in a viscous polymer solution 2. Application of spatially non-uniform electric field 3. Movement of cells, depending on the set-up, towards low or high field intensities 4. Rapid polymerization of the solution, and encapsulation of cells 	[13]
Magnetic-force driven cell-motion	<ol style="list-style-type: none"> 1. Labeling of cells with magnetic nanoparticles 2. Cells cultured under magnetic field until monolayer formation 3. Repositioning of cell monolayer onto a magnetized, positive mold 4. Removal of cell-based constructs from mold 	[14]
Micro-fluidics	<ol style="list-style-type: none"> 1. Pre-fabrication of cell-laden constructs as 'building blocks' 2. Flowing of constructs through microfluidic channels to a collection site 3. Fusion of the constructs at the collection site 	[15, 16]
Cell sheet	<ol style="list-style-type: none"> 1. Culture cells on a 'smart polymer' surface until monolayer formation; many cultures are done in parallel 2. Release of an undisrupted monolayer from the polymer's surface upon external stimulus (e.g. UV) 3. Layering of monolayers to create 3D constructs 	[17]
Biospraying	<ol style="list-style-type: none"> 1. Suspension of cells in polymer solution 2. Placement of polymer solution into a chamber with a nozzle 3. Application of pressure resulting in a controlled spray of the material 	[18, 19]
3D bioprinting	<ol style="list-style-type: none"> 1. Generation of 3D image 2. Dissection of image into 2D layers 3. Translation of data to 3D printer 4. Layer-by-layer printing until construct completion 5. Post-processing if necessary 	[20–22]

additive assembly of a biological construct by 3D patterning of cells and biomaterials in one processing step [23, 24]. Although each of the named methods has unique advantages, 3DBP is often considered the most valuable technique for tissue engineering/biofabrication due to it having the best spatial control over specific components of the system.

The purpose of this review is to give the theoretical framework of 3DBP, and based on this framework to critically evaluate the recent success of the technology with a particular focus on its use in printing silk-based bioinks; bioinks are materials which are compatible with the 3DBP process.

3D bioprinting (3DBP)

3D printing, first patented by Charles W. Hull in 1986, is rapid fabrication of physical, three-dimensional morphologies [25]. The process can be divided into five steps: (1) generation of a 3D image, (2) re-definition of the 3D image into a stack of 2D layers by an user-demarcated thickness, (3) interfacing this data with the printer, (4) printing a layer of the previously defined thickness one-by-one until the construct is complete, and (5) any necessary post-processing of the material [26–29]. The last step, post-processing, will be discussed in greater detail in later sections, as this is dependent on the material which is used. Although this process applies to most of the existing 3D printers, it should be said that this is a general description: there are many types of 3D printing. As such, the nomenclature for this field is broad, and there is great variety depending on the subfield. For example, some are based on the use of solid or liquid materials in the printing process, while others are based on how the 3D object is created, for example, by adding material a layer at a time (additive manufacturing) [30].

3D printing fitting the definition of biofabrication is referred to as 3D bioprinting (3DBP). Its anatomical elements include: the print head, the material cartridge, the actuator, the nozzle, the working area, and the print stage. The print head is the part which connects precise, motor-controlled movement with actuation of the material. The material cartridge holds the biomaterial and the cells to be printed under user-specified conditions. The actuator is some element which applies pressure to cause material deposition. The nozzle is the orifice, frequently a blunt needle, from which material is ejected. The print stage is the surface which the 3D scaffold is printed onto, and in many set-ups also provides further motor-control. The working area is the volume of space available for the construct. 3D bioprinters are most commonly classified based on their mechanism of material deposition: extrusion, inkjet, or laser-assisted bioprinting (LAB).

Extrusion 3DBP, sometimes referred to as direct-write printing, is a set-up where the mechanical or pneumatic pressure is applied to a cartridge of material to extrude a continuous solution [31]. In the case of inkjet 3DBP, heat or acoustic energy is used to propel droplets of solution; the pressure in the cartridge is kept constant with compressed gas [32]. In LAB, a high energy density beam is directed through a glass slide onto an energy absorbing layer, typically gold or titanium, and the focused energy causes the formation of a concave pocket in the material layer, and subsequently droplets or a jet being propelled towards a collector [33, 34]. Generally, the final printed volume is composed of single droplets; therefore they are correspondingly depicted in Fig. 1. Each of these actuation mechanisms has direct and indirect effects. The direct, downstream effects are on the materials which can be printed and on the shape of the volume which is printed (Fig. 1).

In order to be suitable for biofabrication, the most critical characteristics of a 3DBP process are that it is (1) cell-friendly, (2) reproducible and practical, (3) it allows for printing complex physical and chemical gradients, and (4) geometric structures. The performance of printers is typically evaluated by cell density and viability (fulfills requirement 1), process speed, resolution and accuracy (fulfills requirement 2), and the range of printable materials (fulfills requirement 3 and 4). How well these different printer set-ups generally perform will now be discussed based on these requirements.

Extrusion printing

From this basic set-up there are many interesting variations, for example coaxial needle design [37] or complex robotic joints to increase the degree of geometric freedom [38]. In biofabrication the resolution of

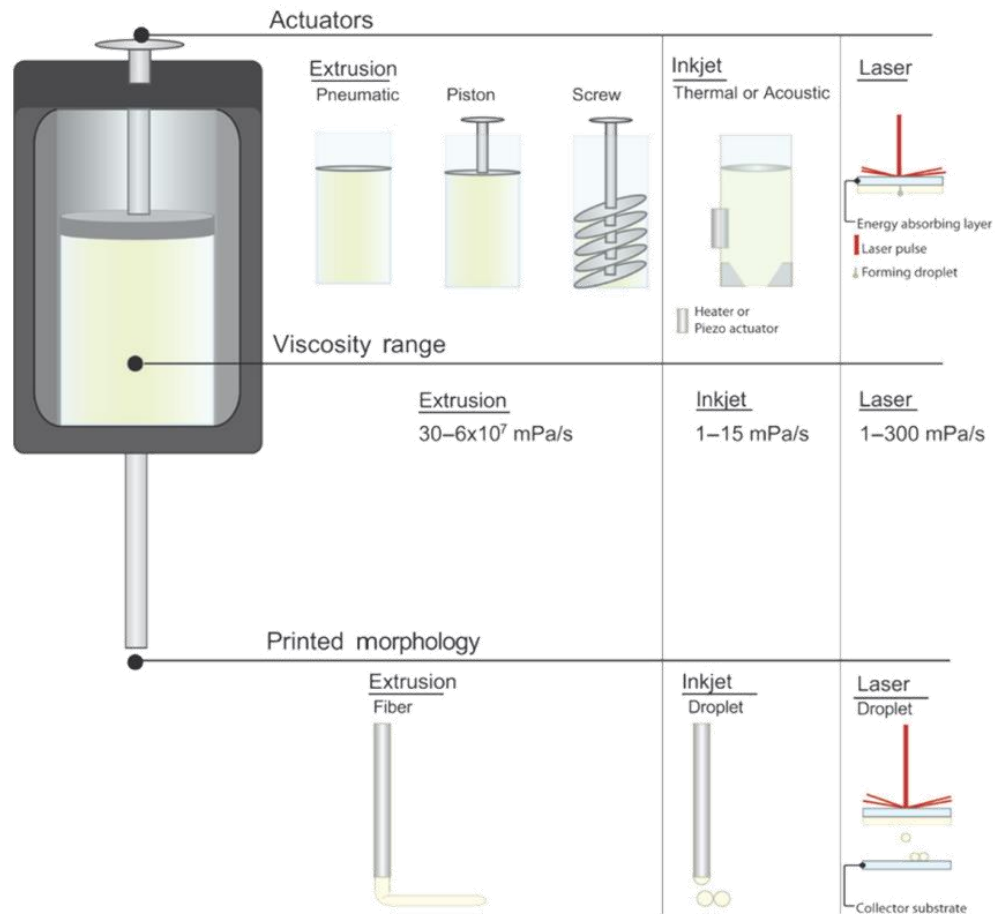


Fig. 1: The different types of 3D bioprinting set-ups. They are defined based on their mechanism of material deposition, the viscosity range of printable materials, and the morphology of the printed volume (i.e. fiber or droplet). These definitions are given in relation to a representation of a print head which shows the actuator, the housing, the material cartridge, and the nozzle (needle) [26, 32, 35, 36].

this technique is mainly limited by requirement 1 mentioned in the chapter above. Cell-free inks enable fiber diameters, and thus resolutions of this method, to be as small as $10\ \mu\text{m}$ [39]. Using cell-loaded bioinks limits the nozzle diameter and leads to a decrease in resolution to dimensions in the range of $200\ \mu\text{m}$. This limitation in resolution is accompanied by an increase in fabrication speed, as such extrusion printing enables generating 3D structures of clinically-relevant sizes in a reasonable period of time [29]. In terms of the effects on cells, cells can be printed at densities of several million/mL, and there is a wide potential for cell viability post-printing; the cell viability ranges from as low as 40 % to as high as 97 % post-printing [26, 40]. Based on this broad range, which is also compared across similar processing conditions (temperature and shear stress), it is reasonable to conclude that cell viability is significantly affected by the bioink which is used. Further, the attractiveness of this type of system is the wide-range of printable materials. In general, providing printable, biocompatible materials is a greater challenge in the field than the printing technology itself, as will be discussed in the later section, Bioinks.

Inkjet printing

Inkjet systems are the next most commonly used technique for 3DBP. The variables considered for the printed volume (size, shape, speed) are pressure in the material cartridge, rate of nozzle opening and nozzle size. Its performance allows cell viability of ~85 % and a resolution of 50 μm [26]. Compared to the other methods discussed in this review inkjet printing based on commercially available inkjet printers suffers from the lowest cell density (typically <1 million cells/mL) which can be printed [26]. Inkjet printing is also limited to a narrow range of low material viscosities to avoid nozzle clogging or application of cell-damaging forces. There have been, however, some adaptations used to prevent these problems, for example, nozzle-free ejection [26].

Laser-assisted bioprinting (LAB)

LAB is the least commonly used technique due to the complexity of the set-up, and the fabrication systems not being commercially available. However, this should not indicate that it is not a valuable technique. A distinct advantage of LAB is the absence of nozzle clogging, allowing a wide-range of rheological material properties, although the non-dynamic viscosity range is limited compared to extrusion printing [36]. LAB has exceptional resolution in the 10-micron range without affecting the cell viability as compared to the other techniques. The process reliably has cell viabilities above 95 %, and can be used with cell densities of up to 10^8 cells/mL [26]. Unfortunately, in spite of these attractive features from the technical point of view, LAB alone is unable to reach clinically-relevant construct volumes in a reasonable timeframe. This is because of the low volume of printing material in the donor layer as well as of printed droplets. Therefore, LAB might be limited in its practical applications in tissue engineering in the future.

Bioinks

In 3D bioprinting (3DBP) the term “bioinks” is used to describe cell-encapsulating material-matrices which combine printability with cytocompatibility. These demands are quite high and often result in contradicting requirements, making bioinks one great challenge in biofabrication. An ideal bioink can be printed, has high shape-fidelity upon printing, is cytocompatible, and is tailored to its target tissue. Amongst studied bioinks, hydrogels have had the greatest tendency towards success [29].

The major physicochemical parameters determining the printability of a hydrogel are their viscosity and their rheological properties. During 3DBP, the bioink should extrude smoothly and undergo a rapid gelation after printing. If the bioink is already pre-gelled, then the printing process should not result in irreversible damage of the polymer network. Adequate mechanical properties, which can be tailored by polymer concentration or crosslinking of the hydrogel, are necessary to retain the designed and fabricated shape up to clinically-relevant sizes [41]. As previously stated, the requirements imposed by the technique for the bioinks tend to conflict with the biological requirements imposed by the cellular components. The final constructs should allow migration, proliferation and support targeted differentiation of encapsulated cells, which typically calls for a soft substrate. Additionally, the gelation process should be mild and cell friendly [20]. Finally, once the hydrogel precursors have been printed and the cells have survived, the scaffold must degrade at a pre-determined rate when exposed to physiological conditions found in the target tissue [42]. Refer to Fig. 2 for representation of these requirements.

Established bioinks

Existing bioinks include natural (e.g. alginate, fibrin, collagen and gelatin) and synthetic [e.g. poly(ethyleneglycol) (PEG), polylactic acid (PLA)], polymers as well as modified versions of these polymers. The most commonly

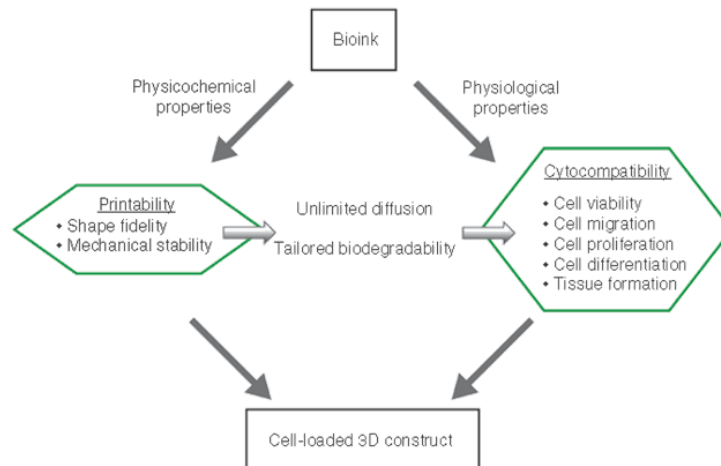


Fig. 2: Physicochemical and physiological requirements of the bioink. Physicochemical properties are related to the printability by the viscosity and macromolecular structure of the material. The printed construct should also allow for diffusion, relating the printed architecture to the cytocompatibility. The physiological activity is related to cytocompatibility by the degradation products, the behavior under physiological conditions, and the biological activity (e.g. cell binding motifs). The final product, the cell-loaded construct, should seamlessly combine these qualities.

used bioinks are the unmodified, natural polymers processed as hydrogels, and will therefore be the focus of this discussion; natural polymers are the only biomaterials whose fabrication process can be directly used for 3DBP [43, 44]. For more detailed information, refer to Table 2 and to Malda et al. [29].

Alginate is one of the most commonly used materials for 3DBP. As a biomaterial in general, alginate has been confirmed to be beneficial for cell viability and differentiation [42], as well as drug delivery [43, 45]. However, alginate-based bioinks also degrade rapidly, translate poorly when used with human-derived cells, and have a limited amount of bioactive binding sites [42, 43, 46]. The next most commonly used bioink is fibrin which has been used due to its success when cultured with neurons [22, 47] and the ability for autologous sourcing [48]. However, fibrin hydrogels possess poor mechanical properties for most applications and degrade before construct maturation [49, 50]. The last most commonly used hydrogel is collagen and its derivative, gelatin. Collagen possesses a major advantage in being biodegradable, biocompatible, easily available and highly versatile [32]. However, collagen-based bioinks show batch-to-batch variations, contraction of constructs, poor mechanical properties, are difficult to sterilize, and have poor water solubility [32, 51, 52]. In an attempt to maintain some of the positive biological activities while reducing these disadvantages, gelatin has also been developed as a bioink [53–55]. Although gelatin shows improvement of the water solubility and viscosity, the gel formation is solely based on physical intermolecular interaction of the gelatin molecules, and the resulting gels are not stable under physiological temperature. Additionally, these gels are also highly variable from batch-to-batch.

In order to expand the range of usable bioinks, there have been many modifications made to these polymers. The most common modifications are chemical ones or polymer blending [35]. Some examples of chemical functionalization include: methacrylation and acetylation of gelatin (modifies degradation) [54, 56], oxidation of alginate (modifies degradation) [42, 64], and synthesis of a block co-polymer comprised of poly(*N*-2-hydroxypropyl)methacrylamide lactate) [p(HPMAm-lactate)] and PEG (improves biodegradability) [62]. Some examples of blends include fibrin and alginate (improves biological activity) [22, 54, 61, 65, 66], alginate and gelatin, alginate and gelatin in modified and unmodified forms [55], alginate, gelatin and hydroxyapatite (optimized for bone tissue engineering) [58], thermoresponsive poly(*N*-isopropylacrylamide) grafted hyaluronan (HA-pNIPAAm) blended with methacrylated hyaluronan (HAMA) (to improve printability)

Table 2: Overview of existing bioinks, their gelation method, and their advantages and disadvantages.

Bioink	Gelation method	Advantages	Disadvantages	References
Alginate	Ionic	Biocompatible; supports cellular function and differentiation	Rapid degradation; lack of cell binding motifs	[42, 43, 45, 46]
Fibrin	Enzymatic	Biodegradable; rapid gelation; easy purification process	Poor mechanical properties; fast disintegration	[22, 47–50]
Collagen	Thermal	Biodegradable; biocompatible; availability; versatile	Limited sterilization techniques; batch-to-batch variations; poor mechanical properties	[32, 51, 52]
Gelatin	Thermal	Biodegradable; biocompatible; water soluble	Unstable at body temperature	[53–55]
Gelatin methacrylamide	Thermal/photo	Mechanically stable; biodegradable; biocompatible; water soluble	–	[54, 56]
Fibroin	Self-assembly	Biocompatible; biodegradable; robust mechanical properties	Lack of cell binding motifs or enzyme degradation sites; does not degrade under physiological conditions	[20, 57]
Recombinant spider silk	Self-assembly	Biocompatible; biodegradable; robust mechanical properties	Lack of enzyme degradation sites; does not degrade under physiological conditions	[40]
Bioinks optimized for specific applications by blending				
Alginate/gelatin/hydroxyapatite	Thermal/ionic/chemical	Biocompatible; biodegradable; robust mechanical properties	–	[58]
Gelatin methacrylamide/hyaluronic acid	Thermal/photo	Mechanically stable; biodegradable; biocompatible; water soluble	–	[55]
Gelatin methacrylamide/gellan gum	Ionic/thermal/photo	Mechanically stable; biodegradable; biocompatible; water soluble	–	[59, 60]
Fibroin/gelatin	Enzymatic/thermal	Biocompatible; biodegradable; robust mechanical properties	–	[20, 57]
Fully synthetic bioinks				
Poly(ethylene glycol) dimethacrylate	Photo	Mechanically stable; cartilage applications	Low cytocompatibility	[61]
p(HPMAm-lactate)-PEG	Thermal/photo	Biodegradable; mechanically stable	Low cytocompatibility	[62]
Glycosaminoglycan-based	Thermal	Chondrogenic	Low viscosity; slow gelation; poor printing properties	[63]
HA-pNIPAAm-HAMA	Thermal/photo	Cytocompatible; fast, reversible gelation; structural fidelity	–	[63]

[63], gelatin with hyaluronic acid or gellan gum (to improve cell behavior towards bone tissue engineering, mechanical properties and printability) [55, 59, 60, 67]. However, even with these modifications, there is an urgent need for further development of bioinks to improve the mechanical properties, gelation process, cytocompatibility, degradation rate, tissue specificity, and adaptability to clinical set-ups.

Silk materials are particularly interesting for technical and biomedical use since they show absence of toxicity, slow degradation, low or absence of immunogenicity, and extraordinary mechanical properties [40, 68–70]. Silk-based biomaterials have been used for medical sutures and breast implant coatings [70–72], biosensing applications [73], and enzyme immobilization [74–76]. Recently, a silk-gelatin blend was used as a bioink [20, 57]. This composite was cytocompatible, crosslinked, showed improved mechanical properties (to gelatin alone), improved cell viability and differentiation (to gelatin, alginate and silk alone), and improved degradation rates (to alginate and gelatin) [20, 43]. However, it was impossible to print silk fibroin without additives; deposition of plain silk fibroin solutions leads to frequent clogging due to shear-induced β -sheet crystallization [57]. In contrast, compared to silk fibroin scaffolds, spider silk bioink can flow through the nozzle without clogging facilitating scaffold manufacturing [40]. This is due to the fact that hydrogels made of recombinant spider silk proteins are physically crosslinked by β -sheet structures and hydrophobic interactions and entanglements, which allows for reversible gelation upon shear-thinning [40, 77]. Further, due to the biotechnological production of recombinant spider silk proteins they can be genetically modified, e.g. with the cell binding motif RGD improving cell attachment [40, 78]. The combination of these mechanical and biological properties raises the number of applications of recombinant spider silk as a novel bioink.

Post-processing and crosslinking

Without delving into complex macromolecular chemistry, it is important to briefly discuss some of the options for solidifying materials in 3DBP when materials do not self-assemble. The basic requirements for a crosslinking process are that it must be rapid for shape-fidelity as well as non-toxic to cells. There are two basic types of crosslinking which can be used: physical or chemical. In the case of physical crosslinking, the most common approach is to maintain the conditions which stabilize the liquid phase in the material cartridge and the conditions which push it towards gelation in the working volume or a tandem print head. An example of this principle is printing a temperature-sensitive hydrogel onto a heated print stage [55]. The advantage of physical crosslinking is that it is often cell-friendly; the disadvantage is that the networks formed are typically weak and their degradation difficult to control. Due to these disadvantages most physically crosslinked hydrogels must be post-processed by chemical crosslinking, and this results in newly formed covalent bonds [29]. This is particularly true for inkjet printing, where the necessity of a low viscosity material mandates some type of post-processing. Some interesting examples of chemical crosslinking techniques include the use of enzymes or UV light [31, 47]. An example of a versatile method for generating UV-crosslinkable hydrogels is by functionalizing 2-hydroxyethyl methacrylate (HEMA) with a photoinitiator. HEMA is a polymeric monomer which can be coupled at hydroxyl groups, making it compatible with many other polymers [79]. However, these types of crosslinking techniques often require synthetic chemistry, making them impractical. Wet-chemical crosslinking allows for predictable, stable network formation, however, the used crosslinking agents may be harmful to cells, and it requires a precise control of crosslinking kinetics to avoid nozzle clogging [29].

3D bioprinting with recombinant spider silk proteins

Recently, the recombinant spider silk protein eADF4(C16) and a variant containing an RGD-motif were established as bioinks. eADF4(C16) consists of 16 repeats of a module C mimicking the repetitive core sequence of dragline silk *Araneus diadematus* fibroin 4 (ADF4) of the European garden spider (Fig. 3a) [81, 82]. The

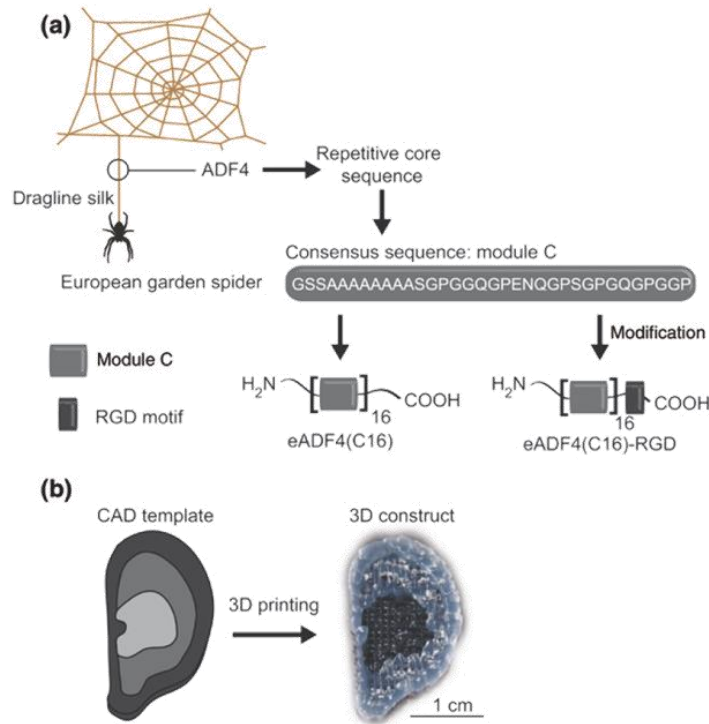


Fig. 3: (a) eADF4(C16) and eADF4(C16)-RGD are made of 16 C modules. The C-module reflects the consensus sequence of the repetitive core sequence of *Araneus diadematus* fibroin 4 (ADF4), one of the main components of the dragline silk of the European garden spider (*A. diadematus*). Dragline silk is the best characterized spider silk, constituting the outer frame of orb webs and serving as a lifeline for the spider [80]. (b) Going from a CAD template (left) to a 3DBP recombinant spider silk construct (right). Recombinant eADF4(C16) was printed by robotic dispensing. In the CAD template, the different shades of gray represent thickness with darker shades representing multiple layers. In the image of the construct it can be qualitatively observed that the construct has the same shape as the CAD file, and the printed strands made of spider silk also have high shape fidelity without the use of post-processing, crosslinking or thickeners.

recombinant spider silk proteins were assessed regarding their printability [40], and spider silk constructs could be printed by robotic dispensing using a print head with an electromagnetic valve. The hydrogels were process-compatible and had high shape fidelity (Fig. 3b). The printability is based on the β -sheet transformation of the proteins during gelation and shear thinning behavior of the hydrogels (Fig. 4).

It was shown that recombinant spider silk proteins can be used as bioink for 3D printing without the need of additional components or post-processing [40]. In contrast, alginate and fibroin need post-processing with crosslinkers or thickeners added to the solution to increase the printing fidelity [20, 58]. For more detailed information of other bioinks, refer to [29] and Table 2.

To produce cell-loaded 3D hydrogel constructs, cells were encapsulated within a highly concentrated silk solution before gelation. The addition of cells to the bioink did not influence the self-assembly into a hydrogel or the printability of the material [40]. The cells survived the printing process and were viable at least 7 days *in situ*. The viability within the spider silk hydrogel could be quantified with $70.1 \pm 7.6\%$. Although the cell viability in the spider silk constructs is lower when compared to established bioinks such as alginate ($\sim 90\%$) and gelatin ($\sim 98\%$), it could be shown that the printing procedure did not significantly affect viability, since after printing 97% of the cells survived [40, 42, 83].

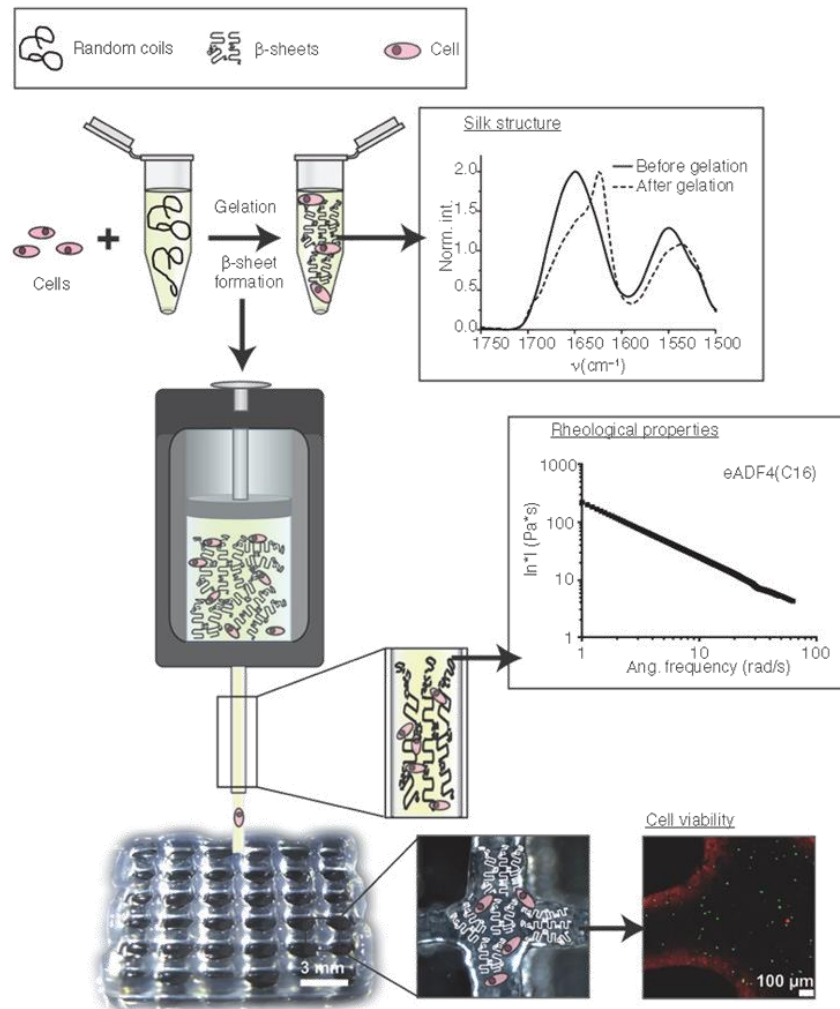


Fig. 4: Printing process for a physically crosslinked recombinant spider silk bioink. Cell-loaded spider silk constructs were printed by robotic dispensing, as mentioned in Fig. 3. The process begins with preparation of the hydrogel from a cell-loaded solution. The corresponding Fourier-transformed infrared spectroscopy (FTIR) structure data shows a peak shift corresponding to β -sheet formation which occurred during self-assembly of the hydrogel. The next step in the process represents the printing of the hydrogel accompanied by alignment of β -sheets under shear-stress, and this corresponds to the given rheological behavior with increasing angular frequency leading to a decrease in complex viscosity, which is called shear-thinning. The final construct is represented by a stereoscope image of the layered structure. The right-hand image represents the presence of viable cells (redlines reflect auto-fluorescence of spider silk; red stained cells are dead and green stained ones viable).

Conclusion and future perspectives

In conclusion, 3D bioprinting (3DBP) techniques hold potential to overcome the current, process-based challenges faced in tissue engineering; high variability and low control over the placement of different scaffold components. Of the different types of 3DBP, it seems as though extrusion printing will be one excellent option for the future of biofabrication, despite some of its drawbacks (nozzle clogging, resolution). Extrusion

printing allows for fabrication of clinically-relevant constructs (size, cell density) and greater ease in bioink development. Additionally, these advantages outweigh the disadvantages. For example, bioinks are critical in cell viability after printing (physicochemical properties) and cell behavior throughout construct maturation (physiological properties). Current bioinks tend to be better in either the “cell friendliness” (e.g. fibrin, gelatin) or printability (recombinant spider silk protein). Future work will most likely focus on polymer blends such that advantages are conserved or enhanced, and the disadvantages minimized or eliminated.

In terms of cell viability after printing, it is reasonable to hypothesize that cell viability is directly correlated with the mechanical stress that the cells are exposed to. In the optimal viscosity range for extrusion printing, there seems to be some protection to shear stress which is absent in inkjet printing; in LAB there are virtually no shear forces on the bioink, due to the nozzle-free set-up. However, LAB is incompatible with higher viscosity ranges, due to the incompatibility of cells with certain wavelengths and energy densities. Thereby, due to the greater flexibility in bioink development, it seems as though extrusion bioprinting will be the technology that shows the greatest potential in the future. However, it is also possible to imagine future developments will also focus on combining the different types of 3D bioprinting in order to further optimize the process.

Acknowledgments: This work was supported by the Deutsche Forschungsgemeinschaft (SCHE 603/9-1) and the European Union’s Seventh Framework Program (FP7/2007-2013) under grant agreement no. 309962 (project HydroZones).

References

- [1] R. G. Harrison, M. J. Greenman, F. P. Mall, C. M. Jackson. *Anat. Rec.* **1**, 116 (1907).
- [2] R. Langer, J. P. Vacanti. *Science* **260**, 920 (1993).
- [3] T. Aberle, K. Franke, E. Rist, K. Benz, B. Schlosshauer. *PLoS One* **9**, e86740 (2014).
- [4] M. A. Lancaster, J. A. Knoblich. *Nat. Protoc.* **9**, 2329 (2014).
- [5] A. Bozkurt, F. Gilmour R Jr., A. Lal. *IEEE Trans. Biomed. Eng.* **56**, 2304 (2009).
- [6] M. J. Post. *Meat Sci.* **92**, 297 (2012).
- [7] J. H. Shim, S. E. Kim, J. Y. Park, J. Kundu, S. W. Kim, S. S. Kang, D. W. Cho. *Tissue Eng. Part A* **20**, 1980 (2014).
- [8] J. J. Mancuso, J. Cheng, Z. Yin, J. C. Gilliam, X. Xia, X. Li, S. T. Wong. *Front. Neuroanat.* **8**, 130 (2014).
- [9] A. Wittinghofer, I. R. Vetter. *Annu. Rev. Biochem.* **80**, 943 (2011).
- [10] D. D. Allison, K. R. Braun, T. N. Wight, K. J. Grande-Allen. *Acta Biomater.* **5**, 1019 (2009).
- [11] M. D. Tang-Schomer, J. D. White, L. W. Tien, L. I. Schmitt, T. M. Valentin, D. J. Graziano, A. M. Hopkins, F. G. Omenetto, P. G. Haydon, D. L. Kaplan. *Proc. Natl. Acad. Sci. USA* **111**, 13811 (2014).
- [12] V. A. Kasyanov, J. Hodde, M. C. Hiles, C. Eisenberg, L. Eisenberg, L. E. De Castro, I. Ozolanta, M. Murovska, R. A. Draughn, G. D. Prestwich, R. R. Markwald, V. Mironov. *J. Mater. Sci. Mater. Med.* **20**, 329 (2009).
- [13] D. R. Albrecht, R. L. Sah, S. N. Bhatia. *Biophys. J.* **87**, 2131 (2004).
- [14] A. Ito, K. Ino, M. Hayashida, T. Kobayashi, H. Matsunuma, H. Kagami, M. Ueda, H. Honda. *Tissue Eng.* **11**, 1553 (2005).
- [15] G. Y. Huang, L. H. Zhou, Q. C. Zhang, Y. M. Chen, W. Sun, F. Xu, T. J. Lu. *Biofabrication* **3**, 012001 (2011).
- [16] Y. Ling, J. Rubin, Y. Deng, C. Huang, U. Demirci, J. M. Karp, A. Khademhosseini. *Lab. Chip.* **7**, 756 (2007).
- [17] I. Elloumi-Hannachi, M. Yamato, T. Okano. *J. Intern. Med.* **267**, 54 (2010).
- [18] A. Abeyewickreme, A. Kwok, J. R. McEwan, S. N. Jayasinghe. *Integr. Biol.* **1**, 260 (2009).
- [19] N. K. Pakes, S. N. Jayasinghe, R. S. Williams. *J. R. Soc., Interface* **8**, 1185 (2011).
- [20] S. Das, F. Pati, Y.-J. Choi, G. Rijal, J.-H. Shim, S. W. Kim, A. R. Ray, D.-W. Cho, S. Ghosh. *Acta Biomater.* **11**, 233 (2014).
- [21] L. Koch, M. Gruene, C. Unger, B. Chichkov. *Curr. Pharm. Biotechnol.* **14**, 91 (2013).
- [22] T. Xu, C. A. Gregory, P. Molnar, X. Cui, S. Jalota, S. B. Bhaduri, T. Boland. *Biomaterials* **27**, 3580 (2006).
- [23] P. Bajaj, R. M. Schweller, A. Khademhosseini, J. L. West, R. Bashir. *Annu. Rev. Biomed. Eng.* **16**, 247 (2014).
- [24] V. Mironov, T. Trusk, V. Kasyanov, S. Little, R. Swaja, R. Markwald. *Biofabrication* **1**, 022001 (2009).
- [25] C. J. Luo, S. D. Stoyanov, E. Stride, E. Pelan, M. Edirisinghe. *Chem. Soc. Rev.* **41**, 4708 (2012).
- [26] S. V. Murphy, A. Atala. *Nat. Biotechnol.* **32**, 773 (2014).
- [27] J. S. Miller. *PLoS Biol.* **12**, e1001882 (2014).
- [28] A. Pfister, R. Landers, A. Laib, U. Hubner, R. Schmelzeisen, R. Mulhaupt. *J. Polym. Sci., Part A: Polym. Chem.* **42**, 624 (2004).

- [29] J. Malda, J. Visser, F. P. Melchels, T. Jüngst, W. E. Hennink, W. J. A. Dhert, J. Groll, D. W. Hutmacher. *Adv. Mater.* **25**, 5011 (2013).
- [30] R. Nayanan, Ed. *Rapid Prototyping of Biomaterials: Principles and Applications*. Woodhead Publishing, Philadelphia (2014).
- [31] L. A. Hockaday, K. H. Kang, N. W. Colangelo, P. Y. Cheung, B. Duan, E. Malone, J. Wu, L. N. Girardi, L. J. Bonassar, H. Lipson, C. C. Chu, J. T. Butcher. *Biofabrication* **4**, 035005 (2012).
- [32] S. Moon, S. K. Hasan, Y. S. Song, F. Xu, H. O. Keles, F. Manzur, S. Mikkilineni, J. W. Hong, J. Nagatomi, E. Haeggstrom, A. Khademhosseini, U. Demirci. *Tissue Eng., Part C* **16**, 157 (2010).
- [33] M. Duocastella, J. M. Fernandez-Pradas, P. Serra, J. L. Morenza. *Appl. Phys. A: Mater. Sci. Process.* **93**, 453 (2008).
- [34] C. Mézel, L. Hallo, A. Souquet, J. Breil, D. Hebert, F. Guillemot. *Phys. Plasmas* **16**, 123112 (2009).
- [35] C. J. Ferris, K. G. Gilmore, G. G. Wallace, M. I. H. Panhuis. *Appl. Microbiol. Biotechnol.* **97**, 4243 (2013).
- [36] S. Catros, B. Guillotin, M. Bacakova, J. C. Fricain, F. Guillemot. *Appl. Surf. Sci.* **257**, 5142 (2011).
- [37] R. Cornock, S. Beirne, B. Thompson, G. G. Wallace. *Biofabrication* **6**, 025002 (2014).
- [38] I. T. Ozbolat, H. Chen, Y. Yu. *Robotics and Computer-Integrated Manufacturing* **30**, 295 (2014).
- [39] J. N. H. Shepherd, S. T. Parker, R. F. Shepherd, M. U. Gillette, J. A. Lewis, R. G. Nuzzo. *Adv. Funct. Mater.* **21**, 47 (2011).
- [40] K. Schacht, T. Jüngst, M. Schweinlin, A. Ewald, J. Groll, T. Scheibel. *Angew. Chem., Int. Ed.* **54**, 2816 (2015).
- [41] Q. L. Loh, C. Choong. *Tissue Eng. Part B, Rev.* **19**, 485 (2013).
- [42] J. Jia, D. J. Richards, S. Pollard, Y. Tan, J. Rodriguez, R. P. Visconti, T. C. Trusk, M. J. Yost, H. Yao, R. R. Markwald, Y. Mei. *Acta Biomater.* **10**, 4323 (2014).
- [43] N. E. Fedorovich, J. Alblas, J. R. de Wijn, W. E. Hennink, A. J. Verbout, W. J. A. Dhert. *Tissue Eng.* **13**, 1905 (2007).
- [44] B. Derby. *Science* **338**, 921 (2012).
- [45] B. S. Kim, D. J. Mooney. *Trends Biotechnol.* **16**, 224 (1998).
- [46] N. E. Fedorovich, W. Schuurman, H. M. Wijnberg, H. J. Prins, P. R. van Weeren, J. Malda, J. Alblas, W. J. A. Dhert. *Tissue Eng., Part C* **18**, 33 (2012).
- [47] J. C. Schense, J. A. Hubbell. *Bioconjug. Chem.* **10**, 75 (1999).
- [48] C. L. Cummings, D. Gawlitta, R. M. Nerem, J. P. Stegemann. *Biomaterials* **25**, 3699 (2004).
- [49] W. Xu, X. Wang, Y. Yan, W. Zheng, Z. Xiong, F. Lin, R. Wu, R. Zhang. *J. Bioact. Compat. Polym.* **22**, 363 (2007).
- [50] X. Wang, Y. Yan, R. Zhang. *Tissue Eng. Part B, Rev.* **16**, 189 (2010).
- [51] C. M. Smith, A. L. Stone, R. L. Parkhill, R. L. Stewart, M. W. Simpkins, A. M. Kachurin, W. L. Warren, S. K. Williams. *Tissue Eng.* **10**, 1566 (2004).
- [52] R. Parenteau-Bareil, R. Gauvin, F. Berthod. *Materials* **3**, 1863 (2010).
- [53] U. Hersel, C. Dahmen, H. Kessler. *Biomaterials* **24**, 4385 (2003).
- [54] E. Hoch, T. Hirth, G. E. M. Tovar, K. Borchers. *J. Mater. Chem. B* **1**, 5675 (2013).
- [55] W. Schuurman, P. A. Levett, M. W. Pot, P. R. van Weeren, W. J. A. Dhert, D. W. Hutmacher, F. P. W. Melchels, T. J. Klein, J. Malda. *Macromol. Biosci.* **13**, 551 (2013).
- [56] E. Hoch, C. Schuh, T. Hirth, G. E. M. Tovar, K. Borchers. *J. Mater. Sci. Mater. Med.* **23**, 2607 (2012).
- [57] S. Das, F. Pati, S. Chameettachal, S. Pahwa, A. R. Ray, S. Dhara, S. Ghosh. *Biomacromolecules* **14**, 311 (2013).
- [58] S. Wust, M. E. Godla, R. Muller, S. Hofmann. *Acta Biomater.* **10**, 630 (2014).
- [59] F. P. W. Melchels, W. J. A. Dhert, D. W. Hutmacher, J. Malda. *J. Mater. Chem. B* **2**, 2282 (2014).
- [60] R. Levato, J. Visser, J. A. Planell, E. Engel, J. Malda, M. A. Mateos-Timoneda. *Biofabrication* **6**, 035020 (2014).
- [61] X. F. Cui, K. Breitenkamp, M. G. Finn, M. Lotz, D. D. D'Lima. *Tissue Eng. Part A* **18**, 1304 (2012).
- [62] R. Censi, W. Schuurman, J. Malda, G. di Dato, P. E. Burgisser, W. J. A. Dhert, C. F. van Nostrum, P. di Martino, T. Vermonden, W. E. Hennink. *Adv. Funct. Mater.* **21**, 1833 (2011).
- [63] M. Kesti, M. Muller, J. Becher, M. Schnabelrauch, M. D'Este, D. Eglin, M. Zenobi-Wong. *Acta Biomater.* **11**, 162 (2015).
- [64] K. Y. Lee, D. J. Mooney. *Prog. Polym. Sci.* **37**, 106 (2012).
- [65] P. Kesari, T. Xu, T. Boland. *Mater. Res. Soc. Symp. Proc.* **845**, 111 (2005).
- [66] X. F. Cui, T. Boland. *Biomaterials* **30**, 6221 (2009).
- [67] J. Visser, B. Peters, T. J. Burger, J. Boomstra, W. J. A. Dhert, F. P. W. Melchels, J. Malda. *Biofabrication* **5**, 035007 (2013).
- [68] G. H. Altman, F. Diaz, C. Jakuba, T. Calabro, R. L. Horan, J. S. Chen, H. Lu, J. Richmond, D. L. Kaplan. *Biomaterials* **24**, 401 (2003).
- [69] A. Leal-Egaña, T. Scheibel. *Biotechnol. Appl. Biochem.* **55**, 155 (2010).
- [70] K. Schacht, T. Scheibel. *Curr. Opin. Biotechnol.* **29**, 62 (2014).
- [71] P. H. Zepelin, N. C. Maksimovikj, M. C. Jordan, J. Nickel, G. Lang, A. H. Leimer, L. Roemer, T. Scheibel. *Adv. Funct. Mater.* **24**, 2658 (2014).
- [72] P. H. Zepelin, A.-K. Berninger, N. C. Maksimovikj, P. van Gelder, T. Scheibel, H. Walles. *Handchir. Mikrochir. Plast. Chir.* **46**, 336 (2014).
- [73] H. Mori, M. Tsukada. *J. Biotechnol.* **74**, 95 (2000).
- [74] Y. Q. Zhang, W. D. Shen, R. A. Gu, J. Zhu, R. Y. Xue. *Anal. Chim. Acta* **369**, 123 (1998).
- [75] I. Drachuk, O. Shchepelina, S. Harbaugh, N. Kelley-Loughnane, M. Stone, V. V. Tsukruk. *Small* **9**, 3128 (2013).
- [76] C. Blum, A. Nichtl, T. Scheibel. *Adv. Funct. Mater.* **24**, 763 (2014).
- [77] K. Schacht, T. Scheibel. *Biomacromolecules* **12**, 2488 (2011).

- [78] S. Wohlrab, S. Muller, A. Schmidt, S. Neubauer, H. Kessler, A. Leal-Egana, T. Scheibel. *Biomaterials* **33**, 6650 (2012).
- [79] L. Pescosolido, W. Schuurman, J. Malda, P. Matricardi, F. Alhaique, T. Coviello, P. R. Weeren, W. J. Dhert, W. E. Hennink, T. D. Vermonden. *Biomacromolecules* **12**, 1831 (2011).
- [80] A. Aprhisiart, F. Vollrath. *Behav. Ecol.* **5**, 280 (1994).
- [81] D. Huemmerich, C. W. Helsen, S. Quedzuweit, J. Oschmann, R. Rudolph, T. Scheibel. *Biochemistry-US* **43**, 13604 (2004).
- [82] C. Vendrely, T. Scheibel. *Macromol. Biosci.* **7**, 401 (2007).
- [83] T. Billiet, E. Gevaert, T. De Schryver, M. Cornelissen, P. Dubruel. *Biomaterials* **35**, 49 (2014).

Acknowledgements

Throughout my PhD studies, I have had many helping hands and support to make it around, over or through roadblocks. Foremost, I would like to thank Prof. Dr. Thomas Scheibel for being my advisor and for supporting me throughout my research, and for helping me take the next steps in my career. I would also like to thank my PhD committee members Prof. Dr. Andreas Fery and Prof. Dr. Schmidt who gave me valuable advice at key milestones during my PhD and my defense chair Prof. Dr. Leonid Ionov.

I would also like to thank all of the people who read and gave input on my dissertation before its submission, Sahar Salehi, Martin Humenik, Eileen Lintz, Carolin Grill and Tamara Aigner. Further, for all persons who helped in my publications, as indicated in the acknowledgements of those papers, I am grateful for all of your contributions. To this end, I must also thank Tamara Aigner, who worked with me on the unpublished research presented in the dissertation, Martin Humenik who provided me with GFP, and Martin Humenik and Gregor Lang for their scientific discussions.

Thank you to all of my colleagues that I have worked with throughout my PhD. This is a great environment to be in, and I have really enjoyed doing my research at this department. I spent many long hours both in the lab and on the computer with Kristin Schacht and Tamara Aigner, sweating over compiling the perfect manuscript. Although the whole thing was incredibly exhausting, they are fond memories for me; we always seemed to have a laugh, no matter how high the pressure was. I would also like to thank the students that I have had throughout my PhD, Catrin Herprich, Saurav Ranjan Mohapatra, Thomas Frank and Max Reinhardt; I learned as much from you as you did from me.

To the heroes of the department, the technical assistants and the secretaries, thank you for tolerating how often I asked for your help. Especially Johannes Diehl, Claudia Stemmann, Alexandra Pellert and Andrea Bodner, I know that I contacted you frequently with various issues and questions, and you always helped me promptly and with great patience.

When I was not in the lab, I had my offices-mates, Kristin Schacht, Tamara Aigner, Kiran Pawar, Sahar Salehi, Indra Aspite, Carolin Grill, Kim Koeck, and Angela Arias-Jaramillo to motivate me to the next step, whether by blowing off steam or by engaging in scientific discussion. To this end, I would also like to thank Tamara Aigner, Gregor Lang, Sushma Kumari, Martin Humenik, Vanessa Neubauer and Christian Borkner for always taking the time to talk a problem through with me when I needed it.

I also wish to thank my core, the people who I have dedicated this thesis to: my family and my husband, Tom Liensdorf. They encouraged me through the finish line, and without them I would have never come this far.

(Eidesstattliche) Versicherungen und Erklärungen

(§ 9 Satz 2 Nr. 3 PromO BayNAT)

Hiermit versichere ich eidesstattlich, dass ich die Arbeit selbstständig verfasst und keine anderen als die von mir angegebenen Quellen und Hilfsmittel benutzt habe (vgl. Art. 64 Abs. 1 Satz 6 BayHSchG).

(§ 9 Satz 2 Nr. 3 PromO BayNAT)

Hiermit erkläre ich, dass ich die Dissertation nicht bereits zur Erlangung eines akademischen Grades eingereicht habe und dass ich nicht bereits diese oder eine gleichartige Doktorprüfung endgültig nicht bestanden habe.

(§ 9 Satz 2 Nr. 4 PromO BayNAT)

Hiermit erkläre ich, dass ich Hilfe von gewerblichen Promotionsberatern bzw. -vermittlern oder ähnlichen Dienstleistern weder bisher in Anspruch genommen habe noch künftig in Anspruch nehmen werde.

(§ 9 Satz 2 Nr. 7 PromO BayNAT)

Hiermit erkläre ich mein Einverständnis, dass die elektronische Fassung meiner Dissertation unter Wahrung meiner Urheberrechte und des Datenschutzes einer gesonderten Überprüfung unterzogen werden kann.

(§ 9 Satz 2 Nr. 8 PromO BayNAT)

Hiermit erkläre ich mein Einverständnis, dass bei Verdacht wissenschaftlichen Fehlverhaltens Ermittlungen durch universitätsinterne Organe der wissenschaftlichen Selbstkontrolle stattfinden können.

.....
Ort, Datum, Unterschrift

